Soil-derived branched tetraether membrane lipids in marine sediments: reconstruction of past continental climate and soil organic matter fluxes to the ocean

Johan W.H. Weijers

Soil-derived branched tetraether membrane lipids in marine sediments: reconstruction of past continental climate and soil organic matter fluxes to the ocean

Uit de bodem afkomstige vertakte tetraether membraanlipiden in mariene sedimenten: reconstructie van het vroegere continentale klimaat en van de aanvoer van organisch bodemmateriaal naar de oceaan

(met een samenvatting in het Nederlands)

Proefschrift

ter verkrijging van de graad van doctor aan de Universiteit Utrecht
op gezag van de rector magnificus, prof.dr. W.H. Gispen,
ingevolge het besluit van het college voor promoties in het openbaar te verdedigen
op donderdag 10 mei 2007 des middags te 2.30 uur

door

Johannes Wilhelmus Hendrikus Weijers

geboren op 27 oktober 1978 te Heemstede

Promotor: Prof. dr. ir. J.S. Sinninghe Damsté
Co-promotor: Dr. ir. S. Schouten

Aan mijn ouders

en ter nagedachtenis aan
mijn grootmoeders

M.C. Weijers-Seijsener
1919-2004

en

C.M. van Niel-Schipper
1921-2003

Table of contents

Part III   **Application: The MBT index**

Chapter 1

General introduction and outline

Johan Weijers

## 1.1. Marine sedimentary organic matter composition

The organic matter present in marine sediments is ultimately derived from either marine biomass, e.g. plankton, or terrestrial biomass transported mainly by rivers to the oceans, e.g. higher plant material. The bulk of marine biomass comprises polysaccharides and proteins and is quickly remineralised in the marine water column and at the sediment surface at the ocean floor. Typically, only a small fraction of marine organic matter (0.1 to 1%), mainly encompassing cell wall and cell membrane material, will ultimately be preserved in the marine sedimentary archive (e.g., de Leeuw et al., 1995) (Fig. 1.1). Terrestrial biomass comprises, amongst others, resistant biopolymers like lignin and sporopollenin which constitute the protective coating of plant stems and pollen (de Leeuw et al., 2006 and references therein). These type of compounds are relatively resistant against microbial and chemical attack and, thus, not easily degradable. Furthermore, terrestrial organic matter generally resides for some time in (partly) oxygenated soils and rivers and thus is likely to be in a more advanced state of degradation before entering the marine water column. These factors explain why terrestrial organic matter in marine sediments is generally found to be more refractory than marine organic matter (e.g., Prahl et al., 1997). Therefore, terrestrial organic matter might be preferentially buried in marine sediments relative to marine organic matter (e.g., Burdige, 2005 and references therein). For as yet unclear reasons, however, only a relatively small fraction of the organic matter in marine sediments seems to be of terrestrial origin (e.g., Hedges et al., 1997).

The extractable part of the sedimentary organic matter encompasses many kinds of biochemical compounds like pigments and membrane lipids. These molecular fossils often have a highly specific chemical structure. Such specific compounds are often derived from only a specific group of organisms and can, therefore, serve as a so-called 'biomarker' carrying detailed information about their source organisms. For example, 'dinosterol' and its diagenetic product 'dinosterane' is a typical marker of dinoflagellate algae (Nes and McKean,

1977), C_{37} alkenones are derived from haptophyte algae (Volkman et al., 1980) and the carotenoid isorenieratene is a pigment typically synthesised by photosynthetic green sulphur bacteria (*Chlorobiaceae*) (Liaaen-Jensen, 1978) (Fig. 1.2). In addition, the relative abundance and isotopic composition of such biomarkers provide information on the environmental conditions during the life span of the source organisms and can, thus, be used as a tool in palaeoenvironmental reconstruction studies (e.g., de Leeuw et al., 1995). For example, the abundance of taraxerol is used to estimate the extent of mangrove forests (Versteegh et al., 2004b), the presence of isorenieratene or its diagenetic products is used to indicate past photic zone anoxia (Summons and Powell, 1986; Koopmans et al., 1996) and the carbon isotopic composition of plant wax derived *n*-alkanes can be used to distinguish between vegetation types using the C_3 or C_4 pathway of carbon assimilation (e.g., Chikaraishi et al., 2004; Schefuß et al., 2005).
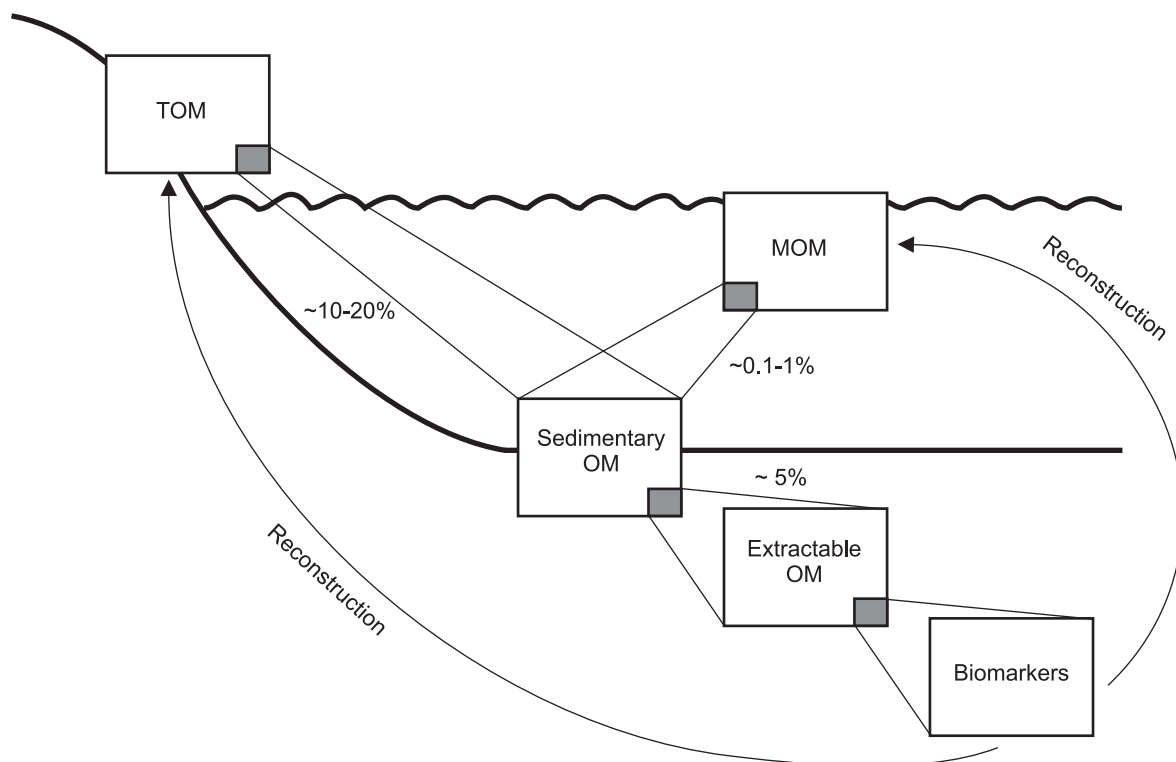
Figure 1.1: Schematic representation of the burial efficiency of TOM (Schlünz and Schneider, 2000; Burdige, 2005) and MOM (de Leeuw et al., 1995; Hedges et al., 1997 and references therein) and the extraction yield of sedimentary OM. Biomarkers derived from marine sedimentary organic matter are used to reconstruct the original composition of TOM and MOM and the contemporaneous environmental conditions. OM = organic matter, TOM = terrestrial OM, MOM = marine OM.
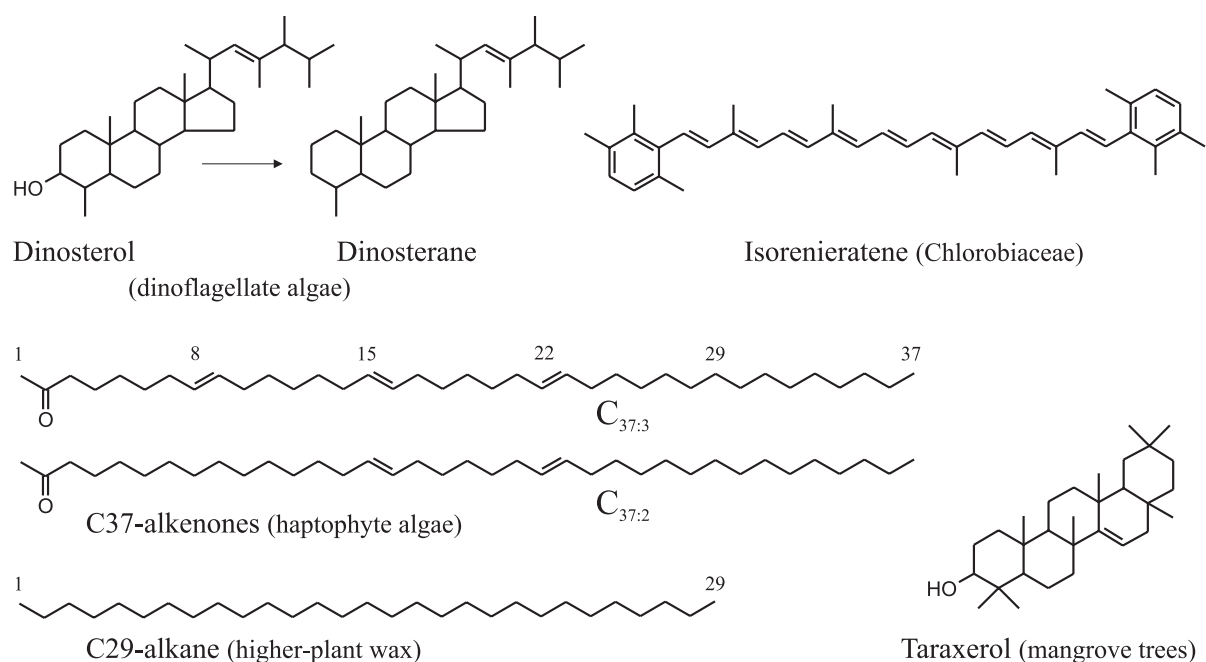
Figure 1.2: Examples of some chemical fossils which are used as biomarker. Their source is given between brackets.

1.2. Biomarkers as indicator of past climate conditions

Over the past century, global temperatures have risen contemporaneously with the increase in the atmospheric CO_2 concentration, which is generally assumed to be associated with massive combustion of fossil fuels by man since the Industrial Revolution. Global climate models are used to predict the extent of future climate change under these changing greenhouse gas conditions. These climate models are validated by simulating past climate changes. To test the model outcome of such retrospective exercises, data on past climates are needed. As the instrumental record of, for example, temperature goes back only a few hundred years, indirect measurements of these parameters are necessary, the so-called proxy data (from approximation). Besides several other approaches like sedimentology and geomorphology, microfossil analyses (e.g., foraminifera and pollen) and inorganic geochemistry (e.g., clay minerals, mineral isotopes), biomarker analysis has become a very important tool as well to reconstruct past climatic parameters.

For example, the degree of double bond saturation in haptophyte-derived C_{37} alkenones correlates with growth temperature (Brassell et al., 1986). Analysing these alkenones in marine sediment records, thus, provides a tool to reconstruct sea surface temperatures (Müller et al., 1998). Similarly, marine Crenarchaeota synthesise several types of isoprenoid tetraether membrane lipids containing different relative amounts of cyclopentyl moieties. The relative

abundance of these different membrane lipids in Crenarchaeota is shown to be strongly related to the temperature of growth (Wuchter et al., 2004). Consequently, determining their lipid distribution in the marine sedimentary archive can also be used to reconstruct past sea surface temperatures (Schouten et al., 2002). Another example is the hydrogen isotopic composition of plant wax *n*-alkanes isolated from marine sediments. Their isotopic composition is thought to be primarily controlled by the moisture balance at the time of growth (precipitation versus evapo-transpiration) (Sauer et al., 2001). Thus, analysing the hydrogen isotopic composition of fossil *n*-alkanes from a marine sediment record can provide information on past humidity conditions on the adjacent continent (e.g., Schefuß et al., 2005).

Besides their use in validating climate model simulations, these palaeoenvironmental reconstructions are also very important to improve our understanding of the complex atmosphere-ocean-biosphere interactions during times of climate change in the past. By reconstructing the timing and deciphering the driving forces and mechanisms behind past climate changes like the last deglaciation (the most recent period of global warming following the last ice age, ca. 15 ka BP) or the extreme warmth during the Palaeocene-Eocene thermal maximum (a period of extremely high atmospheric greenhouse gas concentrations, ca. 55 Ma ago), we gain knowledge which can be used to further improve climate prediction models. Ultimately, this will not only result in more precise predictions of future climate changes, but also in a better understanding of the possible consequences of these climate changes.

1.3. Membrane lipids and the Domains of Life

In microbiology, the view on relationships between microbes has changed considerably over the last decades. For long time, classifications of microbes were made mainly based on cell morphology. A few decades ago, however, it became clear that evolutionary relationships between organisms can be seen most clearly at the gene level (Woese et al., 1990 and references therein). With this in mind, Carl Woese and co-workers proposed the division of life on Earth into three Domains, the Archaea, Bacteria and Eucarya, based on the base pair sequences of their small subunit ribosomal RNA genes (Woese et al., 1990), a gene that all organisms have in common. In contrast to the previous classification, where the Archaea (at that time called Archaebacteria) and the Bacteria together formed the Prokaryotes, the Archaea are now recognised as a new, separate Domain. Thus, analysis of gene sequences has become one of the standard tools for defining and classifying microbes. Furthermore, environmental analysis of gene sequences, i.e. without prior cultivation and isolation of microbes, revealed that most of the microbes living in the environment had very different base pair compositions than those of cultured micro-organisms. This has led to the recognition that most of the microbial diversity in nature still remains to be discovered and of the so called 'rare-biosphere' (e.g., Sogin et al., 2006; Pedros-Alio, 2007).

One of the more spectacular findings of applying culture independent 16S rRNA sequencing techniques was the observation that the Archaea are far more widespread than previously assumed. Traditionally Archaea were seen as extremophiles, i.e. organisms thriving under more extreme conditions like anoxia, high temperatures, high salinity or strong alkaline or acidic conditions (Tindal, 1992). However, it is now clear that they also occur ubiquitously in temperate environments of both the marine and terrestrial realm (e.g., Fuhrman et al., 1992; Buckley et al., 1998; DeLong, 1998; Ochsenreiter et al., 2003).
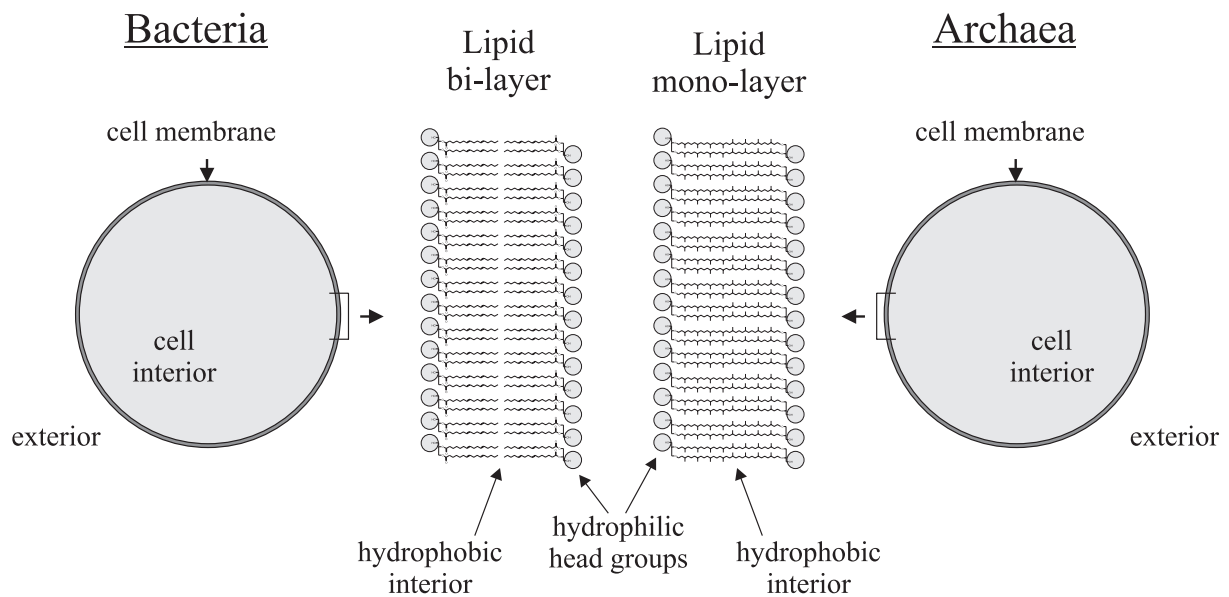
Figure 1.3: Bacteria generally possess a bi-layered cell membrane whereas Archaea generally possess a lipid mono-layer membrane. The alkyl chains of the membrane lipids form the hydrophobic interior of the cell membrane, which is enclosed between the hydrophilic head groups attached to the glycerol backbone of the membrane lipids.

Besides in the composition of their 16S rRNA genes, Bacteria and Archaea also differ remarkably in their general membrane lipid composition. The cells of both types of micro-organisms are enclosed by a membrane which acts as a barrier between the inner cell and its outside environment. These membranes are composed of membrane lipids, molecules consisting of a hydrophobic (= water repelling) interior enclosed between two hydrophilic (= water attracting) exteriors, and prevent fluids from flowing through the membrane into or out of the cell (Fig. 1.3). Typically the archaeal membrane consists of lipids composed of isoprenoid alkyl chains linked by ether bonds to the glycerol backbone to form glycerol dialkyl diether (Fig. 1.4a) and glycerol dialkyl glycerol tetraether (GDGT) (Fig. 1.4b) membrane lipids. Eucarya and Bacteria, in contrast, generally synthesise membrane lipids

composed of straight or branched alkyl chains linked by ester bonds to the glycerol backbone (Fig. 1.4c). A cell membrane predominantly composed of membrane-spanning GDGTs forms a monolayer which is thought to be more rigid than the bi-layered membrane composed of diethers or diesters (Fig. 1.3). This was thought to be necessary for organisms thriving in, for example, environments experiencing high temperatures to maintain their membrane stability, and in highly acidic environments to form a tight barrier to resist the high proton gradient over the cell membrane. Thus, GDGT membrane lipids seem to be perfectly suited for organisms thriving in more extreme conditions (van de Vossenberg et al., 1998). Some thermophilic bacteria are also found to synthesise membrane-spanning lipids like, for example, the thermophilic anaerobic *Thermotoga maritima* (Carballeira et al., 1997) and *Thermoanaerobacter ethanolicus* (Jung et al., 1994). In addition some thermophilic bacteria, like *Thermodesulfotobacterium commune* (Langworthy et al., 1983), *Aquifex pyrophylus* (Huber et al., 1992) and *Ammonifex degensii* (Huber et al., 1996), also synthesise glycerol dialkyl diether membrane lipids (Fig. 1.4d). However, most Bacteria and Eucarya seem to make glycerol dialkyl diesters.
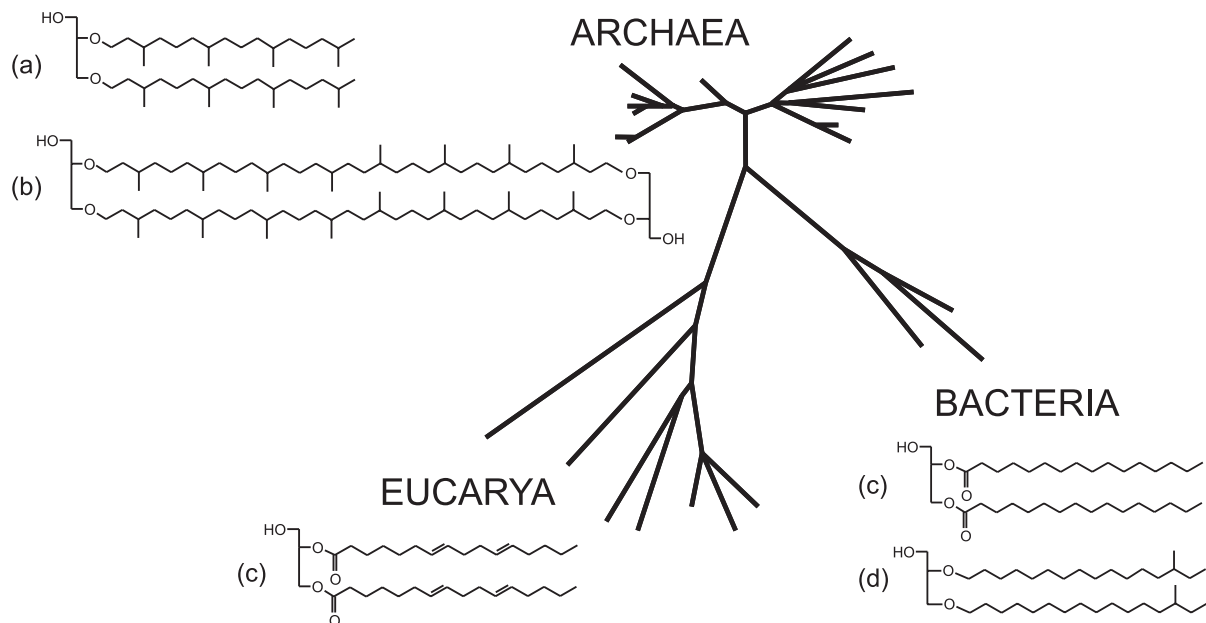
Figure 1.4: Shown is the Tree of Life which represents, by means of the length of the different branches, the evolutionary relations between organisms based on their small subunit rRNA genes and reveals the three Domains of Life. Chemical structures of some characteristic core membrane lipids synthesised by members of these Domains are shown; **(a)** glycerol diphytanyl diether, **(b)** glycerol dibiphytanyl glycerol tetraether, **(c)** glycerol dialkyl diester lipids, **(d)** glycerol dialkyl diether (in some thermophilic bacteria).

1.4. Environmental occurrence of GDGTs

Intact diether or diester core membrane lipids can be measured directly by means of gas chromatography / mass spectrometry (GC/MS) techniques, because the molecules are relatively volatile. Intact core GDGT membrane lipids as found in Archaea (e.g., Fig. 1.4b), however, are much larger and less volatile. As a consequence they are not amenable to GC/MS techniques, because they could not be retained in a gas phase at the temperatures used with this technique. The development of a high performance liquid chromatography / mass spectrometry (HPLC/MS) method enabled the analysis of the intact core GDGT membrane lipids by means of a polarity based separation in a liquid phase (Hopmans et al., 2000).

The development of this method allowed the detection of intact core GDGT membrane lipids in environmental samples (e.g., Schouten et al., 2000) (Fig. 1.5). In agreement with what molecular biologists found, i.e. the ubiquitous occurrence of archaeal sequences, archaeal GDGTs were also ubiquitous and abundant in temperate environments. One of the more common GDGTs, called crenarchaeol (Fig. 1.5), was unique as it contained an additional cyclohexyl moiety, something not found in (hyper)-thermophilic archaea. Based on environmental sequences it is thought that a specific Kingdom of the Archaea detected in these mesophilic environments, the Crenarchaeota, is synthesising this membrane lipid. The specific ring structure in crenarchaeol is thought to act as a 'kink' in the carbon chain preventing a too tight packing of the GDGT membrane in the relative cool environment (Sinninghe Damsté et al., 2002).

Besides the ubiquitous presence of isoprenoid GDGT membrane-spanning lipids derived from Archaea, another group of GDGTs was found in peat bogs. Nuclear magnetic resonance experiments revealed the peculiar structure of these compounds, containing branched instead of isoprenoid alkyl chains with a variable number of methyl branches on the alkyl chains (Sinninghe Damsté et al., 2000) (Fig. 1.5). As these compounds show a mixture of archaeal and bacterial characteristics, i.e. a tetraether configuration and branched alkyl chains, respectively, it was uncertain whether they have an archaeal or bacterial origin. Since non-isoprenoid lipids have not been encountered in Archaea and dialkyl glycerol diethers have been found in some thermophilic bacteria (Fig. 1.4d), a bacterial origin has been suggested (Sinninghe Damsté et al., 2000). These branched GDGTs were also detected in coastal and lake sediments (Schouten et al., 2000) (Fig. 1.5). The origin, source, distribution and the function of this new group of branched GDGTs, however, was unknown and has been subject of the studies presented in this thesis.
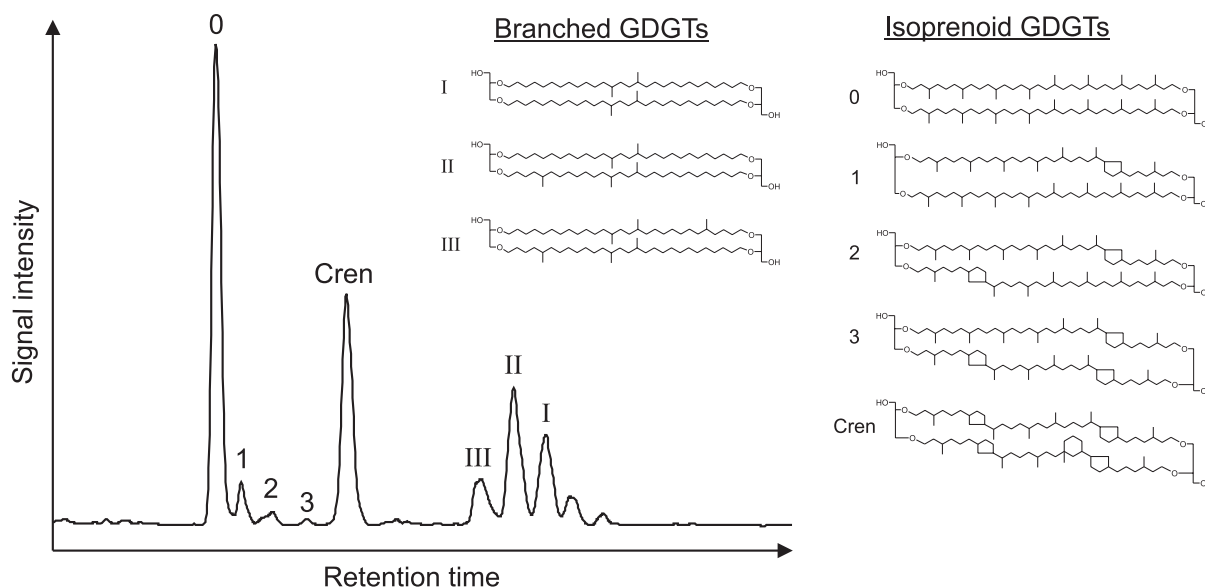
Figure 1.5: HPLC/MS base peak chromatogram of a sediment sample from the Mok Bay, the Netherlands, showing the presence of both isoprenoid and branched GDGT membrane lipids. Cren = crenarchaeol

1.5. Objective and outline of this thesis

This thesis aims at providing a more comprehensive picture on the occurrence, distribution, biological origin and function of these novel branched GDGT membrane lipids, and to explore their possible application as biomarker and palaeoenvironmental proxy.

   To this end, the thesis is divided into three parts. **Part I** (chapters 2, 3 and 4) focuses on the description and potential origin of the branched GDGTs. In **Part II** (chapters 5, 6, 7 and 8) the geographical distribution of the branched GDGTs is explored and, related to that, their potential to serve as a biomarker for the fluvial input of soil organic matter in marine sediments. The last part of this thesis, **Part III** (chapters 9, 10 and 11), describes the possible biological function of the branched GDGT membrane lipids and, based on that assessment, their potential to act as a proxy for past annual mean air temperatures and soil pH conditions on land.

Part I
In **Chapter 2** the distribution of branched GDGTs, including novel isomers that were not previously published, is reported together with a detailed description of their chemical structure based on the results of Nuclear Magnetic Resonance (NMR) analysis techniques. The NMR experiments provided for the first time unambiguous evidence for a bacterial origin for these membrane lipids. In addition, results of HPLC/MS analyses of two peat profiles are

presented showing that branched GDGTs are most abundant in the continuous water saturated and thus anoxic part of the peat bog and, therefore, most likely synthesised by anaerobic bacteria.

As the source organism(s) is (are) as yet still unknown, microbiological analyses were conducted on samples from a Swedish peat core, in order to establish the microbial sources of these compounds (**Chapter 3).** The results suggest that branched GDGT-producing bacteria may be part of the Kingdom of *Acidobacteria*.

In **Chapter 4** the isoprenoid GDGT content of this Swedish peat core has been determined. The depth profiles of these archaeal biomarkers indicated for the first time, besides the well known occurrence of methane producing Euryarchaeota, the presence of Crenarchaeota by means of the specific membrane lipid crenarchaeol.

Part II

In addition to peat bogs, branched GDGTs have also been detected in coastal sediments, but are essentially not detectable in open ocean sediments. This points to a largely terrestrial origin of these branched GDGTs and consequently their potential use as a biomarker for terrestrial (soil) organic matter in marine sediments. **Chapter 5** introduces the B̲ranched vs. I̲soprenoid T̲etraether (BIT) index, a measure for the relative fluvial input of terrestrial organic matter based on the abundance of branched GDGTs in marine sediments relative to the isoprenoid GDGT crenarchaeol which is predominantly derived from marine Crenarchaeota.

The results presented in chapter 5 suggested that branched GDGTs also occur in soils and that their occurrence is not restricted to peat bogs. In order to verify this assumption, soils derived from 27 various locations were analysed for their branched and isoprenoid GDGT content. The results of this study, presented in **Chapter 6**, revealed the ubiquitous occurrence of branched GDGTs in soils, supporting the concept of using the BIT index as a proxy for soil organic matter input. This survey also showed the occurrence in soils of the isoprenoid GDGTs, including crenarchaeol which was detected earlier on in a peat bog (chapter 4). As both the BIT index (chapter 5) and the TEX_{86} sea surface temperature (SST) proxy (Schouten et al., 2002) are assuming a pure marine origin of isoprenoid GDGTs, this terrestrial source slightly complicates the use of these proxies. This effect has also been explored in this chapter. The results indicate a rather negligible effect for the BIT index but point out that the TEX_{86} SST proxy should be used with care in front of large river outflows.

In **Chapter 7** the BIT index is applied in a marine sediment core in front of the Congo River outflow in order to determine the variability of past soil organic matter input in the Congo deep sea fan. By means of a three end-member mixing model, using the BIT index in conjunction with the stable carbon isotopic composition and carbon over nitrogen ratio of the total organic matter, it is shown that terrestrial organic matter accounts for ~45% of the total organic matter in these marine sediments over the period of the last deglaciation. The results

also indicate, however, that the accumulation of absolute amounts of terrestrial organic matter was likely not constant over glacial-interglacial times, but has varied considerably.

Another application of the BIT index is presented in **Chapter 8**. Here, the BIT index is determined in sediments from a marine core recovered from the Bay of Biscay in order to reconstruct the past activity of the palaeo Channel River outflow system. The BIT indices show that the Channel River discharge started to increase substantially at 21 ka BP in pace with global deglacial warming as evident from Greenland ice core records. Markedly, this river discharge declined abruptly at 17 ka BP, right at the start of Heinrich event 1. The release of large amounts of fresh and cold melt waters from floating icebergs (associated with Heinrich events), likely resulted in a freshwater lid on the Bay of Biscay, hindering sea water evaporation and cloud formation and resulting in a return to dryer conditions on the West European continent.

Part III

In the study on the occurrence of branched GDGTs in soils (chapter 6) a large variety in abundances of the different tetraethers was observed. This was further studied in **Chapter 9**, in which an even larger set of globally distributed soils is described that was analysed for the relative distribution of branched GDGTs. This revealed large variations in relative abundance of the various individual branched GDGTs in soils from different regions. By means of principal component analyses of the GDGT distribution and different environmental parameters, it is shown that the average amount of cyclopentyl moieties in the branched GDGT membrane lipids is related to soil pH values and that both the average amount of cyclopentyl moieties and methyl branches is related to the annual mean air temperature. Based on literature data, the observed relationships could be explained in terms of the biophysical function of the branched GDGT membrane lipids: organisms synthesising branched GDGTs use the differences in cyclisation and methylation to adjust their cell membrane to the ambient pH and temperature conditions in order to preserve a proper functioning of the membrane.

The relations between branched GDGT compositions and environmental parameters suggest that branched GDGTs could serve as a new proxy for reconstructing past soil pH values and terrestrial air temperatures. In **Chapter 10** a first application of these new proxies is shown in a marine sediment core recovered from the equatorial East Atlantic Ocean in front of the Congo River outflow. The obtained record provides a river basin integrated temperature and soil pH signal over the last deglaciation. It shows a gradual temperature increase of 4°C from ~21 to 25°C for central tropical Africa and the variations in soil pH values appear to be related to the variations in precipitation intensity in this region. Since the branched GDGTs were analysed in a marine core it was possible, in conjunction with an alkenone based SST record, to reconstruct a record of land-sea temperature differences over the last deglaciation. Strikingly, this record compared well with records of past humidity changes in central Africa,

including the reconstructed soil pH record, suggesting that this land-sea temperature difference exerts a strong control on central African precipitation patterns.

In **Chapter 11** a second application of this new temperature proxy is shown in a marine sediment core recovered from the Lomonosov Ridge in the Arctic Ocean covering the Palaeocene-Eocene Thermal Maximum (PETM), a period in Earth history characterised by extreme high temperatures and greenhouse gas concentrations. The estimated annual mean air temperatures indicate a temperature increase on the Arctic continents of as much as 8°C during the PETM reaching subtropical values of 25°C. These results are in line with earlier results obtained for the Arctic Ocean surface water temperatures and point to a reduced latitudinal thermal gradient during the PETM.

Membrane lipids of mesophilic anaerobic bacteria thriving in peats have typical archaeal traits

Johan W.H. Weijers, Stefan Schouten, Ellen C. Hopmans, Jan A.J. Geenevasen, Olivier R.P. David, Joanna M. Coleman, Rich D. Pancost and Jaap S. Sinninghe Damsté

Abstract

The 16S ribosomal DNA based distinction between the bacterial and archaeal Domains of Life is strongly supported by the membrane lipid composition of the two Domains; Bacteria generally contain dialkyl glycerol diester lipids, whereas Archaea produce isoprenoid dialkyl glycerol diether and membrane-spanning glycerol dialkyl glycerol tetraether (GDGT) lipids. Here we show that a new group of ecologically abundant membrane-spanning GDGT lipids, containing branched instead of isoprenoid carbon skeletons, are of a bacterial origin. This was revealed by examining the stereochemistry of the glycerol moieties of those branched tetraether membrane lipids, which was found to be the bacterial 1,2-di-*O*-alkyl-*sn*-glycerol stereoconfiguration and not the 2,3-di-*O*-alkyl-*sn*-glycerol stereoconfiguration as in archaeal membrane lipids. In addition, unequivocal evidence for the presence of cyclopentyl moieties in these bacterial membrane lipids was obtained by NMR. The biochemical traits of biosynthesis of tetraether membrane lipids and the formation of cyclopentyl moieties through internal cyclisation, which were thought to be specific for the archaeal lineage of descent, thus also occur in the bacterial Domain of Life.

2.1. Introduction

The phylogenetic distinction between Archaea and Bacteria (Woese et al., 1990) is supported by distinct differences in their core membrane lipid composition. Especially the chain architecture (isoprenoidal vs. *n*-alkyl) and the stereochemistry of the glycerol backbone (2,3- vs. 1,2-di-*O*-alkyl-*sn*-glycerol for Archaea and Bacteria, respectively; Kates, 1978) are strong lipid-taxonomic indicators, for which, to the best of our knowledge, no exceptions have been reported yet. Considering the stereochemistry of the glycerol backbone, it is known that only two enzymes are involved in introducing either of the stereoconfigurations (2,3- or 1,2-di-*O*-alkyl-*sn*-glycerol) in the glycerol moiety of membrane lipids. Those two stereospecific enzymes [G-1-P-dehydrogenase (Nishihara and Koga, 1995) for Archaea and G-3-P-dehydrogenase (Kito and Pizer, 1969) for Bacteria] are completely different in their amino acid sequence and are even thought to be one of the main reasons for the separate evolution of the Domains of Archaea and Bacteria (Koga et al., 1998).

Other lipid-taxonomic indicators which distinguish Archaea from Bacteria are the bond type (ether vs. ester bonds) and the membrane lipid structure (membrane spanning vs. bi-layered). However, some exceptions are known, especially in the case of thermophilic bacteria. Membrane lipids containing ether bound glycerols (e.g., **1**; see Appendix at the end of this chapter for structures) have, for example, been found in the hyperthermophilic bacteria *Thermodesulfotobacterium commune* (Langworthy et al., 1983), *Aquifex pyrophylus* (Huber et al., 1992) and *Ammonifex degensii* (Huber et al., 1996). Diether membrane lipids (e.g., **2**) were also found in yet unknown, non-thermophilic sulphate-reducing bacteria of a microbial consortium capable of anaerobic methane oxidation (Pancost et al., 2001) and recently in *Candidatus* 'K. stuttgartiensis' and *Candidatus* 'B. anammoxidans', two new members of the order *Planctomycetes* (Sinninghe Damsté et al., 2002b). These latter two strains and the sulphate-reducing bacteria *Desulfosarcina variabilis* and *Desulforhabdus amnigenus* (Rütters et al., 2001) also produce membrane lipids (e.g., **3**) with both an ester and ether bound alkyl chain within one glycerol membrane lipid. In the bacterial Domain, membrane-spanning lipids have also been inferred for some species. The thermophilic anaerobic *Thermotoga maritima*, for example, produces 13,14-dimethyloctacosane and 15,16-dimethyltriacontane carbon chains (Carballeira et al., 1997) of which the latter one is found to be ether bound to one glycerol unit (**4**) (De Rosa et al., 1988). Tetraester membrane lipids containing α,ω-13,16-dimethyloctacosane moieties (**5**) were identified in *Thermoanaerobacter ethanolicus* (Jung et al., 1994; Lee et al., 2002). Except for the monoether found in *Thermotoga maritima*, a combination of both ether bonds and membrane-spanning carbon chains has so far never been encountered in Bacteria, specifically not in a tetraether configuration like in Archaea (e.g., **6**). In addition to those distinguishing features, the presence of cyclopentyl moieties is another characteristic which is, to the best of our knowledge, only found in the alkyl chains of archaeal membrane lipids and are absent in those of Bacteria.

Over the last years, a new group of membrane lipids, branched glycerol dialkyl glycerol tetraethers (GDGTs) (**7**, **8**, **9**), has been found in peat bogs (Schouten et al., 2000; Pancost and Sinninghe Damsté, 2003; Hopmans et al., 2004) and soils (Weijers et al., 2006b) and unambiguously identified by NMR (Sinninghe Damsté et al., 2000). Strikingly, these new GDGTs differ from known archaeal tetraether lipids (e.g., **6**) in that the alkyl moieties are not comprised of isoprenoid units but of branched carbon chains. Branched GDGTs with cyclopentyl moieties were tentatively identified as well (**10**, **11**) (Schouten et al., 2000). Hence, these branched GDGTs contain a mixture of archaeal (membrane-spanning tetraether structure and cylcopentyl moieties) and bacterial (branched carbon chains) characteristics. It is thus uncertain to which Domain of Life the organism biosynthesizing these branched GDGT lipids belongs.

Application of molecular ecological tools to ascertain the origin of these enigmatic components is hampered by the huge phylogenetic diversity of micro-organisms in peats and soils (up to an estimated 10^4 different species in one small sample; Torsvik et al., 2002) and the bias of microbiological culture techniques. Examination of the stereochemical characteristics of the membrane lipids provides a good alternative to distinguish between an archaeal and bacterial origin. To this end, the stereochemistry of the glycerol backbone of a branched GDGT (**8**) was unambiguously established. Furthermore, the structure of a branched GDGT with the putative cyclopentyl moiety (**10**) was also determined. This shows the presence of distinct archaeal traits in anaerobic bacteria thriving in soils and peats. Finally, by analysing two peat depth profiles for their branched GDGT content, information is gained about the habitat of the source organisms.

2.2. Experimental procedures

2.2.1. Sites and sampling

Peat cores for GDGT analysis were taken from the Saxnäs Mosse in Sweden and the Bolton Fell Moss in England. The Saxnäs Mosse area (SW Sweden, 56 51' 20.78" N, 13 27' 39.62" E) is an ombrotrophic raised bog with vegetation mainly composed of *Sphagnum* species. The upper 25 cm constitute the acrotelm layer in which the water table fluctuates. Below 25 cm the peat bog is continuously water saturated and consequently anoxic. A 50 cm long core was taken with a Wardenaar peat profile sampler and sub-samples were taken at a two cm interval.

The Bolton Fell Moss (National Grid Reference NY 495695, Cumbria, England), is a large ombrotrophic mire with a raised central dome with an average depth of 6 m and vegetation currently dominated by Sphagnum species (Xie et al., 2004). The acrotelm/catotelm boundary was determined at about 30 cm depth. A 50 cm monolith was collected alongside a 5 m Russian core covering a depth range of 25-500 cm; these were then

subsectioned in 1 cm intervals and combined. A total of 50 sub-samples were taken from the upper 175 cm.

Bulk peat samples for isolation of GDGT **10** were taken from Étang de la Gruère in the Jura Mountains of Switzerland. Étang de la Gruère is a strongly domed, raised bog with a peat accumulation of more than 6 meters (Steinmann and Shotyk, 1997). About 2.5 kg of peat (wet weight) was collected with a Belorussian peat sampler from a depth of 4.75-5.25 m.

2.2.2. Sample preparation

Peat samples were freeze dried and powdered with a mortar prior to extraction by an accelerated solvent extractor (ASE 200, DIONEX), soxhlet or by sonication, with solvent mixtures composed of dichloromethane and methanol. The obtained total extracts were prepared further for GDGT analysis as described earlier (Hopmans et al. 2000)

2.2.3. Preparative HPLC

Isolation of GDGT **10** was achieved by semi-preparative high performance liquid chromatography (HPLC) followed by flow injection analysis according to Smittenberg et al. (2002) (Smittenberg et al., 2002). The columns used are a semi-preparative and an analytical Alltech Prevail Cyano column (250 mm × 10 mm; 5 μm; flow rate 3 ml min^{-1} and 250 mm × 4,6 mm; 5 μm; flow rate 1 ml min^{-1}, respectively).

2.2.4. HPLC/APCI-MS

GDGTs were analyzed and quantified by high performance liquid chromatography/ atmospheric pressure chemical ionization mass spectrometry (HPLC/APCI-MS), according to Hopmans et al. (2000) with minor modifications. Analyses were performed on an Agilent 1100 series/1100MSD series machine, equipped with auto-injector and HP Chemstation software. Separation was achieved on an Alltech Prevail Cyano column (150 mm × 2.1 mm; 3 μm). The flow rate of the hexane:propanol (99:1, v/v) eluent was 0.2 ml min^{-1}, isocratically for the first 5 min, thereafter with a linear gradient to 1.8% propanol in 45 min. Injection volume of the samples was 10 μl. Quantification of the GDGT compounds was achieved by integrating the peak areas in the $[M+H]^+$ and $[M+H]^+ +1$ ion traces (i.e., protonated molecule and first isotope peak) and comparing these to an external calibration curve prepared with known amounts of pure crenarchaeol (**17**). A correction was made for the branched GDGTs (**7-15**), as their molecular mass is lower than that of crenarchaeol.

2.2.5. HT-GC

Bolton Fell Moss samples were analyzed by high temperature-gas chromatography (HT-GC) performed on a Hewlett Packard 5890 Series II GC, equipped with a flame ionization detector. Samples were run over an SGE HT5 (5% phenyl equivalent, polycarborane siloxane), 6 m by 0.53 mm aluminium clad column. The following temperature program was

used for most analyses: 50 °C (1 min) to 140 °C at 20 °C/min followed by 140 °C to 420 °C (10 min) at 7 °C/min. GDGT peaks were identified based on comparisons with standards (2,3,2',3'-tetra-*O*-dibiphytanyl-di-*sn*-glycerol-1'-β-gulosyl-1-phosphoryl-3''-*sn*-glycerol sodium salt standard, subsequently converted into a GDGT; Universal Biologicals Ltd.), and GDGTs identified in cold seep samples using LC-MS (Zhang et al., 2003). Interpretations were then validated by comparison to GC-MS analyses of selected HI-LiAlH$_4$ treated samples.

2.2.6. Nuclear Magnetic Resonance

^{1}H- and ^{13}C-NMR spectroscopy was performed on a Bruker DMX-600 spectrometer as described previously (Sinninghe Damsté et al., 2002a). ^{19}F-NMR spectroscopy of the Mosher derivatives of GDGTs were performed on a Varian Unity Inova 500, as described previously (Sinninghe Damsté et al., 2004).

2.3. Results

2.3.1. Structural identification of GDGTs in peats

An HPLC base peak chromatogram of a sample from the Saxnäs Mosse bog (Sweden) shows high abundances of the branched GDGTs **7** and **8** and, to a lesser extent, GDGT **9** (Fig. 2.1). Concentrations of the ring-containing GDGTs (**10-15**) are generally 10% or less than those of GDGTs **7-9**. So far, only the structures of GDGTs **7** and **8** (Sinninghe Damsté et al., 2000) have been fully elucidated by NMR. It was, therefore, decided to attempt to fully characterize a GDGT containing a cyclopentyl moiety.

Preparative HPLC on the bulk peat sample from Étang de la Gruère bog (Switzerland) resulted in ca. 3 mg of isolate in which the ring-containing GDGT **10** accounts for ca. 88%, the remainder being minor amounts of GDGT **8** (9%), GDGT **7** (1%) and GDGT **12** (1%). The ^{1}H-NMR spectrum of this isolate is extremely complex even if measured at 600 MHz. In the 3.4-3.7 ppm region, multiplets accounting for 18 protons are observed (Table 2.1). These represent the protons of the two glycerol units and the first and ultimate methylene units of the alkyl moieties bound via the ether linkages. The same signals were observed in the ^{1}H-NMR spectra of GDGT **7** and **8** in an earlier study (Sinninghe Damsté et al., 2000). At ca. 2.2 ppm a broad singlet representing the two hydroxy groups is found. At 0.85 ppm two doublets occur, representing three methyl groups, whereas the spectra of GDGT **7** and **8** showed only one doublet representing four methyl groups. Another difference with these ^{1}H-NMR spectra is the presence of a multiplet between 1.7-1.8 ppm representing four protons.

The ^{13}C-NMR spectrum of GDGT **10** reveals 3 primary, 56 secondary, and 7 tertiary atoms (Table 2.1). APT, DEPT90 and DEPT135 experiments were used to assess the multiplicity of these carbon atoms. The ^{13}C-NMR spectrum did not show 66 resolved signals

because many carbon atoms are either strictly, or effectively, equivalent. Assignments of the carbon atoms is based on comparison with the ^{13}C-NMR data of GDGT **7**, **8** and **16** (Sinninghe Damsté et al., 2000; Sinninghe Damsté et al., 2002a), in combination with HMQC and HMBC experiments. Many shifts observed in the ^{13}C-NMR spectrum are identical to those reported for GDGT **7** (Sinninghe Damsté et al., 2000), confirming their close structural relationship. The major difference is that one methyl group (i.e., carbon atom B15) is absent and is part of a cyclopentyl moiety, as suggested previously on the basis of mass spectral analyses (Schouten et al., 2000). This results in characteristic shifts for carbon atoms B7-B15 and B13'-B15' that are different from the shifts observed for these carbon atoms in GDGT **7**. Both the ^{13}C and ^{1}H shifts for the atoms of the cyclopentyl moiety are consistent with literature data (Sinninghe Damsté et al., 2002a). The ultimate proof for this structural assignment is the observed correlation of the protons of carbon atom B15 with the carbon atoms B9, B10, B11 and B12, B13, and B14 in the HMBC spectrum. The structures of the other ring-containing GDGTs (**11-15**), all possessing 1 or 2 cyclopentyl moieties, were deduced from the characteristic $[M+H]^+$, $[M+H]^+$-18 (water loss) and $[M+H]^+$-74 (glycerol loss) pattern in their mass spectra, their retention time relative to their "parent" GDGTs (**7-9**) and the structure of GDGT **10**.
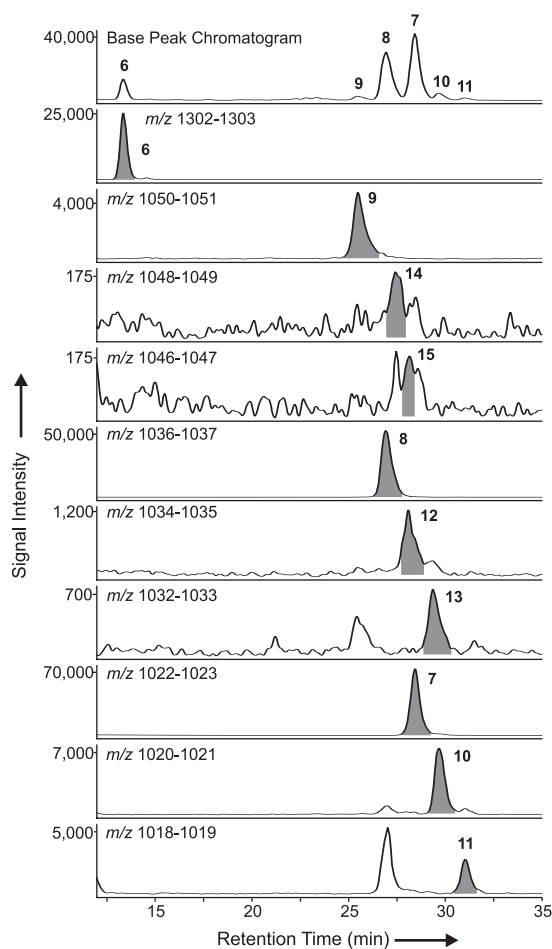
Figure 2.1: Partial HPLC/MS base peak chromatogram and mass chromatograms of the protonated molecule plus first isotope peak of the different GDGTs in a 43 cm deep sample from the Saxnäs Mosse peat bog. Numbers refer to the structures in the appendix. The highest peak at the m/z 1018 trace is a $[M+H]^+$-18 (H_2O) fragment from m/z 1036 (GDGT **8**). Similarly, the peak in the m/z 1032 trace in front of GDGT **13** represents the $[M+H]^+$-18 fragment of GDGT **9**.

Table 2.1: ^{13}C- and ^{1}H-NMR data used for structural identification of GDGT **10**

Carbon atom[a]	Carbon shift (ppm)[b]			Proton shift (ppm)[c]
	CH	CH$_2$	CH$_3$	
A1, B1'		71.77		3.41 (4H, m)
A1', B1		70.41		3.58 (2H, m), 3.51 (2H, m)
A2, B2'		29.40		1.53 (4H, m)
A2', B2		29.98		1.55 (4H, m)
A3, B3'		26.09		1.30
A3', B3		26.06		1.30
A4, A4', B4, B4'		c. 29.6		c. 1.24
A5, A5', B5, B5'		c. 29.6		c. 1.24
A6, A6', B6, B6'		c. 29.6		c. 1.24
A7, A7', B7'		c. 29.6		c. 1.24
B7		29.86		c. 1.24
A8, A8', B8'		c. 29.6		c. 1.24
B8		28.62		1.22
A9, A9', B9'		c. 29.6		c. 1.24
B9		36.77^{d}		1.23
A10, A10', B10'		30.05		1.21
B10			38.76^{e}	1.80
A11, A11'		27.05		1.23
B11		33.14^{f}		1.75 (eq), 1.03 (ax)
B11'		27.01		1.23
A12, A12'		37.15		1.06
B12		33.14		1.75 (eq), 1.03 (ax)
B12'		36.98		1.25
A13, A13'			33.05	1.31
B13			39.02^{g}	1.76
B13'			32.85	1.32
A14, A14'		34.35		1.07, 1.22
B14		34.00^{h}		1.23
B14'		35.85		1.05, 1.23
A15, A15'	19.79			0.858 (6H, d)
B15		38.67		1.30
B15'	19.86			0.854 (3H, d)
C1, C1'		71.11		3.49 (2H, m), 3.46 (2H, m)
C2, C2'			78.39	3.49 (2H, m)
C3, C3'		63.05		3.68 (2H, dd), 3.58 (2H, m)
OH				2.10 (2H, bs)

[a] numbering refers to GDGT **10** in the Appendix

[b] determined by APT, DEPT90 and DEPT135

[c] mainly obtained from the HMQC spectrum

[d] in good agreement with the $\delta= 36.83$ calculated from data of a cyclopentane-containing isoprenoidal GDGT (Sinninghe Damsté et al., 2002a) and the additivity principle

[e] in good agreement with the $\delta= 38.80$ calculated from data of a cyclopentane-containing isoprenoidal GDGT (Sinninghe Damsté et al., 2002a) and the additivity principle

[f] in good agreement with the $\delta= 33.08$ calculated from data of a cyclopentane-containing isoprenoidal GDGT (Sinninghe Damsté et al., 2002a) and the additivity principle

[g] in good agreement with the $\delta= 39.04$ calculated from the shift of carbon atom B10 and the additivity principle

[h] in agreement with the $\delta= 34.42$ calculated from the shift of carbon atom B9 and the additivity principle

Table 2.2: Chemical shift (in ppm relative to CFCl$_3$) of the CF$_3$ group of the Mosher products of the reaction of the branched GDGT **8**, 1,2-di-*O*-dihexadecyl-*rac*-glycerol, 1,2-di-*O*-dihexadecyl-*sn*-glycerol and the isoprenoid GDGT **16** with the S- and R-Mosher acid chlorides. Between brackets the relative abundance of the signal is given.

	GDGT **8**	1,2-di-*O*-dihexadecyl-*rac*-glycerol	1,2-di-*O*-dihexadecyl-*sn*-glycerol	GDGT **16**
S-Mosher acid chloride	-73.212 (100%)	-73.106 (50%) -73.170 (50%)	-73.170 (100%)	-73.048 (100%)
R-Mosher acid chloride	-73.129 (100%)	n.d.	-73.106 (100%)	-73.137 (100%)

n.d., not determined

2.3.2. Stereoconfiguration of the glycerol backbone of GDGTs in peats

The isolate of GDGT **8**, obtained previously from the Holocene Bargerveen peat bog (the Netherlands) (Sinninghe Damsté et al., 2000), was used here to determine the stereochemistry of the glycerol backbone. To this end, this GDGT was reacted with the S- and R- α-methoxy-α-(trifluoromethyl)phenylacetyl chlorides to give the so called Mosher ester (Dale and Mosher, 1973) and the chemical shift of the trifluoromethyl group was investigated with ^{19}F-NMR. The Mosher esters of this branched GDGT **8** gave comparable chemical shifts for the CF$_3$ group as the S- and R-Mosher acid derivatives of the commercially available 1,2-di-*O*-dihexadecyl-*sn*-glycerol, but opposite of those of the Mosher esters of the isoprenoid GDGT **16** isolated from *Sulfolobus acidocaldarius* (Sinninghe Damsté et al., 2002a) which possesses the 2,3-di-*O*-alkyl-*sn*-glycerol stereoconfiguration (Table 2.2). This shows that the branched GDGT **8,** found in peats and soils, possess the bacterial 1,2-di-*O*-alkyl-*sn*-glycerol and not the archaeal 2,3-di-*O*-alkyl-*sn*-glycerol stereoconfiguration.

2.3.3. GDGT profiles in peats

Two peat cores were analyzed for their branched GDGT content and for GDGT **6**, a commonly found isoprenoid GDGT (Figs. 2.2 and 2.3). Branched GDGTs **7-15** are all detected in the Saxnäs Mosse core (see also Fig. 2.1). In the Bolton Fell Moss core, only GDGTs **7**, **8** and **10-13** could be detected, whilst GDGTs **9**, **14** and **15** were below detection limit using high temperature – gas chromatography (HT-GC). Concentrations of the branched GDGTs in the Saxnäs Mosse are very low in the upper 8 cm (0.2 μg g^{-1} dry weight (wt) peat) and slightly higher, around 3 μg g^{-1} dry wt peat, between 8 and 28 cm depth. Branched GDGT concentrations are highest below 28 cm with an average concentration of 35 μg g^{-1} dry wt peat. The Bolton Fell Moss profile shows a similar pattern; branched GDGT concentrations are below detection limit in the upper 10 cm and are about 5 μg g^{-1} dry wt peat between 10

and 28 cm. Below 28 cm the average concentration is much higher at 37 µg g^{-1} dry wt peat. In the Bolton Fell Moss core, which extends to 175 cm depth, a trend to slightly lower concentrations can be observed from ca. 120 cm downward.

The concentrations of GDGT **6** in both cores are about two times lower compared to those of the branched GDGTs. In the Saxnäs Mosse, concentrations of GDGT **6** are 0.2 µg g^{-1} dry wt peat in the upper 8 cm, 1.2 µg g^{-1} dry wt peat between 8 and 28 cm and 13 µg g^{-1} dry wt peat between 28 and 50 cm. For the Bolton Fell Moss core, those concentrations are below detection limit for the upper 10 cm and 0.7 and 16 µg g^{-1} dry wt peat for the intervals 10 to 28 and 28 to 175 cm, respectively. As is observed for the branched GDGTs, GDGT **6** decreases in concentration in the lower 50 cm of the Bolton Fell Moss core.
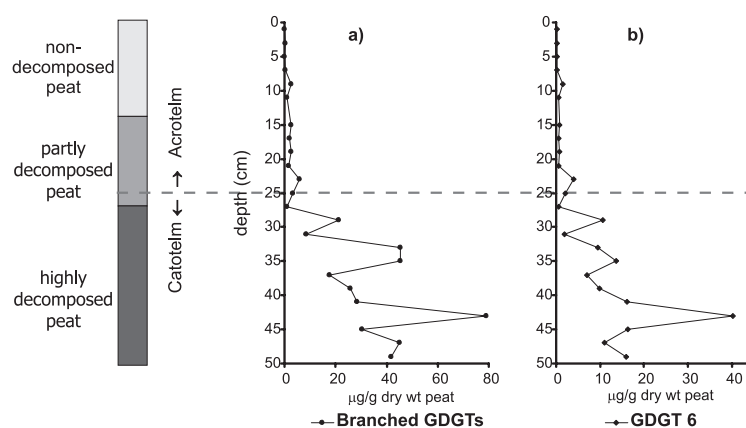
Figure 2.2: Concentrations of: **a)** the branched GDGTs **7-9** (average value) and **b)** GDGT **6** against depth in a peat core from the Saxnäs Mosse, Sweden, together with a schematic decomposition profile of the peat core. The acrotelm layer is the zone in which the water table fluctuates and the catotelm layer is the zone of permanent water saturation.
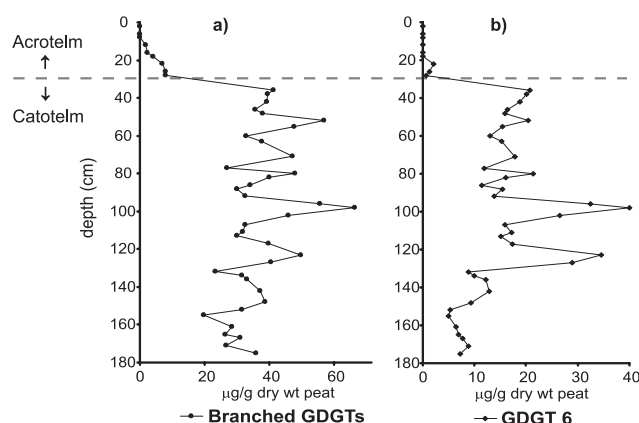
Figure 2.3: Concentrations of: **a)** the branched GDGTs **7** and **8** (average value) and **b)** GDGT **6** against depth in a peat core from the Bolton Fell Moss, Cumbria, England.

2.4. Discussion

2.4.1. A bacterial origin for branched GDGTs in peat
The elucidation of the stereochemistry of the glycerol backbone of GDGT **8** as the 1,2-di-*O*-alkyl-*sn*-glycerol stereoconfiguration strongly indicates that branched GDGTs encountered in peats are biosynthesized by members of the Domain of Bacteria. The stereochemical evidence is particularly strong since it is highly unlikely that Archaea would biosynthesize membrane lipids with a bacterial stereoconfiguration as the enzymes responsible for introducing the stereoconfiguration are thought to form the basis for the divergent evolution of the Bacteria and the Archaea (Koga et al., 1998). A possible archaeal origin would, therefore, mean a thorough reconsideration of the current ideas on early evolution and lateral gene transfer (LGT). A bacterial origin of the branched tetraethers is also consistent with the chain architecture (*n*-alkyl instead of isoprenoid). Furthermore, ether bonds as well as membrane spanning alkyl chains have previously been reported in some Bacteria (Langworthy et al., 1983; De Rosa et al., 1988; Lee et al., 2002). Considering the above stated arguments, the presence of cylcopentyl moieties in the alkyl chains, which, to the best of our knowledge, has so far never been reported before in core membrane lipids of Bacteria, should therefore be regarded as the first report of the occurrence of cyclopentyl moieties in Bacteria.

2.4.2. Biosynthetic pathway
The exact functional role of these branched GDGTs is as yet unclear, but they are likely membrane-spanning lipids just like archaeal GDGTs and may provide the cell membrane with a higher degree of stability. This assumption is supported by the calculated length of the branched GDGTs, which is ca. 34 Å versus 37 Å for the isoprenoid GDGT **6** (1 Å = 10^{-10} m; determined for an individual GDGT in a minimal energy mode between the chiral carbon atoms of the two glycerol moieties; CS ChemDraw Pro software, CambridgeSoftCorporation, MA, USA). This is of the same order of magnitude as the thickness of a black lipid monolayer membrane composed of tetraethers of the archaeon *Thermoplasma acidophilum*, which is, because stacked in a membrane and therefore smaller, determined at 25-30 Å (Stern et al., 1992). Due to the similarity in the overall molecular structure of the branched GDGTs and the archaeal isoprenoid GDGTs (e.g., **6**), a schematic biosynthetic pathway is postulated for the branched GDGTs, which to a certain extent resembles that of isoprenoid GDGTs (Boucher et al., 2004) (Fig. 2.4). The first step of this pathway involves the establishment of the *sn*-glycerol-3-phosphate backbone out of dihydroxyacetone phosphate (DHAP) by G-3-P dehydrogenase (Fig. 2.4). In this step Bacteria differentiate themselves from the Archaea, who use G-1-P dehydrogenase to form the opposite *sn*-glycerol-1-phosphate backbone out of DHAP. In step 2 and 3 two isopentadecane moieties are connected via an ether bond at the *sn*-1 and *sn*-2 positions of the glycerophosphate backbone, creating a diether. The existence of these steps seems to be plausible as similar diethers (e.g., **1**) are found in several bacteria,

such as *Thermodesulfotobacterium commune* (Langworthy et al., 1983), *Aquifex pyrophylus* (Huber et al., 1992) and *Ammonifex degensii* (Huber et al., 1996). The enzymes carrying out the ether bond formation in steps 2 and 3 are unknown and cannot be the same as those in the biosynthesis of diethers in Archaea as they have to cope with the opposite stereoconfiguration of the glycerophosphate backbone. The fourth step in the proposed pathway is similar to that of the biosynthesis of isoprenoid GDGTs and involves the head-to-head coupling of two glycerol di-alkyl diethers to form a glycerol di-alkyl glycerol tetraether. Although the details of this step as well as the enzyme(s) involved are as yet unknown for the Archaea as well, the existence of this step in the archaeal pathway has been proven indirectly by labelling experiments and by inhibiting this step with terbinafine (Nemoto et al., 2003; Eguchi et al., 2003). The responsible enzyme for this coupling process could be the same in both Archaea and Bacteria as the tails of both carbon chains are structurally identical (i.e., isoprenoid vs iso-branched). The next steps in the biosynthesis of both types of tetraethers comprise the formation of cyclopentyl moieties. In the archaeal tetraethers, formation of such a cyclopentyl moiety takes place via an internal cyclisation of a methyl branch with a δ-carbon (De Rosa et al., 1977). It is likely that the formation of cyclopentyl moieties in the branched GDGTs takes place in a similar fashion and based on the structural similarity, this cyclisation process might be carried out by similar enzymes as well. It might be possible that the bacteria producing the branched GDGTs acquired the enzymes for the head-to-head coupling and the formation of a cyclopentyl moiety via lateral gene transfer from Archaea, or vice versa, a process which has been shown to occur between thermophilic Archaea and Bacteria (Nelson et al., 1999).

2.4.3. Ecology

Analyses of two peat cores reveal that the branched GDGTs (**7-9**) are abundant in the continuously water saturated and consequently anoxic part of the peat bogs (Figs. 2.2 and 2.3). This suggests that anaerobic bacteria are the source of the branched GDGTs. The low abundances of GDGTs in the upper part of the profiles can probably be explained by alternating oxic and anoxic conditions, due to a moving water table. Concentrations of the branched GDGTs are about twice as high compared to the isoprenoid GDGT **6**, which in these settings is most likely derived from methane-producing, anaerobic archaea (Tornabene and Langworthy, 1979; Pancost et al., 2000). This is the same ratio as was found for biphytane and dimethyloctacosane in the Bargerveen peat bog (the Netherlands) after release of the alkyl moieties from the GDGTs by ether cleavage (Pancost and Sinninghe Damsté, 2003). Methanogenic archaea are known to play a major role in the carbon cycle in peat bogs and cell counts of Archaea in a Siberian peat bog showed that their relative abundance increases with depth up to 36% of the total microbial community (Kotsyurbenko et al., 2004). Therefore, the relatively high abundance of branched GDGTs indicates that the anaerobic bacteria producing them might also form an ecologically significant part of the microbial population. In both peat cores the pattern of the concentration profile of the branched GDGTs

(**7-9**) resembles to a great extent the concentration profile of the isoprenoid GDGT **6**. This suggests that both (groups of) organisms use the same substrates and/or catalyse the same processes. Until the bacteria which produce the branched GDGTs have been fully identified, however, any suggestion about their role in the biodegradation of organic matter remains speculative.
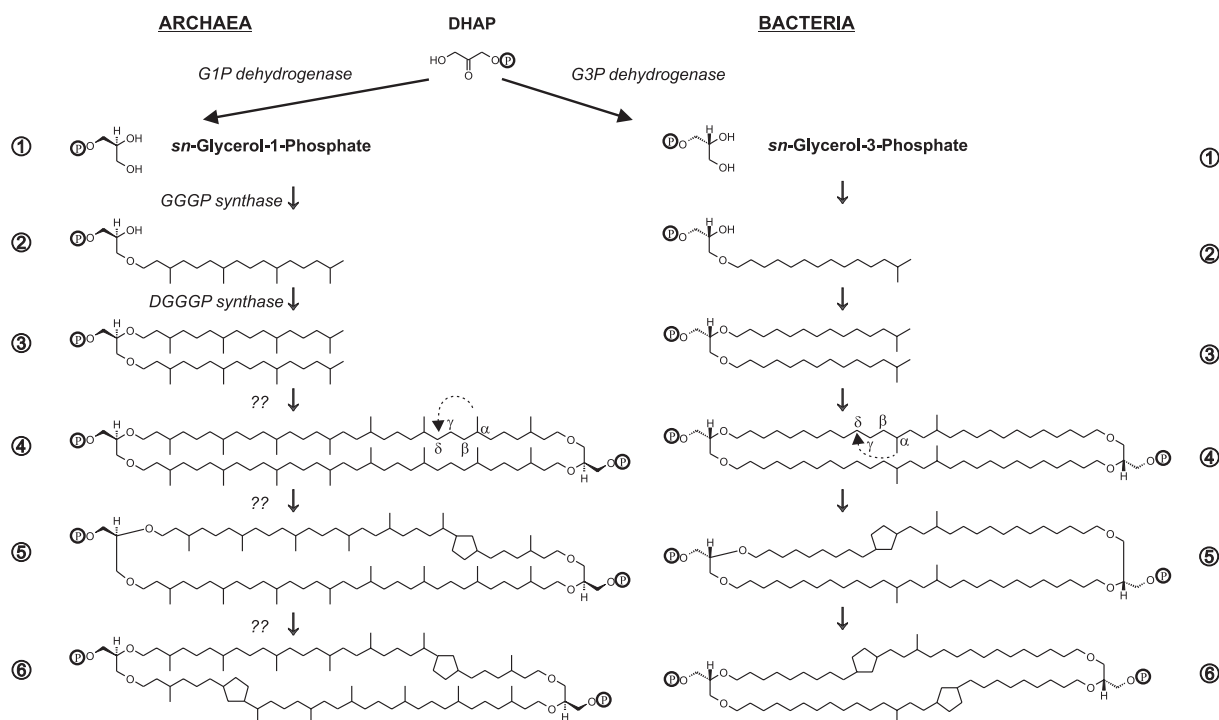
Figure 2.4: Schematic representation of the postulated biosynthetic pathway for the branched GDGTs compared with the biosynthetic pathway for isoprenoid GDGTs [modified after Boucher et al. (2004)]. P = Phosphate, DHAP = Dihydroxyacetone Phosphate, GGGP = geranylgeranylglyceryl phosphate, DGGGP = digeranylgeranylglyceryl phosphate. Double bonds, which are, at least in the isoprenoid pathway, present in all but the last stages, have been omitted for sake of simplification. For isoprenoid GDGTs the formation of cyclopentyl moieties can continue up to 8 rings.

2.4.4. Functional role of branched GDGTs

Besides being a relict from thermophilic ancestors, the presence of branched GDGTs in mesophilic bacteria could as well be an adaptation to the environment in which these organisms thrive. It is assumed that the formation of a monolayer cell membrane by membrane-spanning tetraethers is an adaptation of Archaea to more extreme conditions in order to maintain a certain degree of stability in the membrane (Van de Vossenberg et al., 1998). At first sight, the discovery of GDGTs in the ubiquitous mesophilic aquatic Crenarchaeota (Hoefs et al., 1997; DeLong et al., 1998; Schouten et al., 2000; Sinninghe

Damsté et al., 2002a) refutes this assumption. Those Crenarchaeota, however, have been shown to adapt their membrane to the cooler environment by the formation of an additional unique GDGT lipid, crenarchaeol (**17**), containing a cyclohexyl moiety (Sinninghe Damsté et al., 2002a). The presence of GDGT **6** in a peat also seems to refute the assumption that GDGTs are related to extreme environments. A peat environment, however, has pH values which are generally low, ranging from pH4-6. In *Sphagnum* moss peat those values are even known to reach as low as pH3-4. In this respect the presence in a peat bog of GDGT **6**, derived from methanogenic archaea, might be not surprising as monolayer membranes composed of isoprenoid GDGTs provide an excellent barrier against the high proton gradients present in acidic environments (Elferink et al., 1994; Van de Vossenberg et al., 1998). Indeed, Macalady et al. (2004) recently showed that there is a better correspondence between the occurrence of GDGT lipids and the degree of acidity than between the occurrence of GDGT lipids and temperature in a series of 49 archaeal species. Membrane lipids of acidophilic archaea were composed of up to 100% of GDGTs, whereas no GDGTs were detected in the three alkaliphilic archaea studied. Thus, although possessing branched instead of isoprenoid alkyl chains, the occurrence of branched tetraether lipids in anaerobic bacteria in peat bogs could well be related to the more acidic pH conditions in such an environment.

2.5. Conclusions

Branched GDGT membrane lipids (**7-15**) are shown to have an 1,2-di-*O*-alkyl-*sn*-glycerol stereoconfiguration. This feature, in combination with the characteristic branched alkyl chains, forms convincing evidence that branched GDGTs are biosynthesized by Bacteria. Furthermore, it has been unequivocally proven that branched GDGTs contain up to two cyclopentyl moieties. This is the first report of the occurrence of membrane-spanning tetraether lipids and the capability to form cyclopentyl moieties in core membrane lipids in the Domain of Bacteria. Although the exact source of the branched GDGT lipids remains, as yet, unknown, they are abundant in the anoxic parts of peat bogs. Since the abundance of branched GDGTs co-vary in two depth profiles with that of GDGT **6**, derived from anaerobic methanogens, a similar ecological niche for the methanogenic Archaea and the anaerobic, branched GDGT producing bacteria is expected. The biological function of branched GDGTs in the bacteria is unknown, but their presence could well be related to the acidic conditions in a peat bog.

Appendix
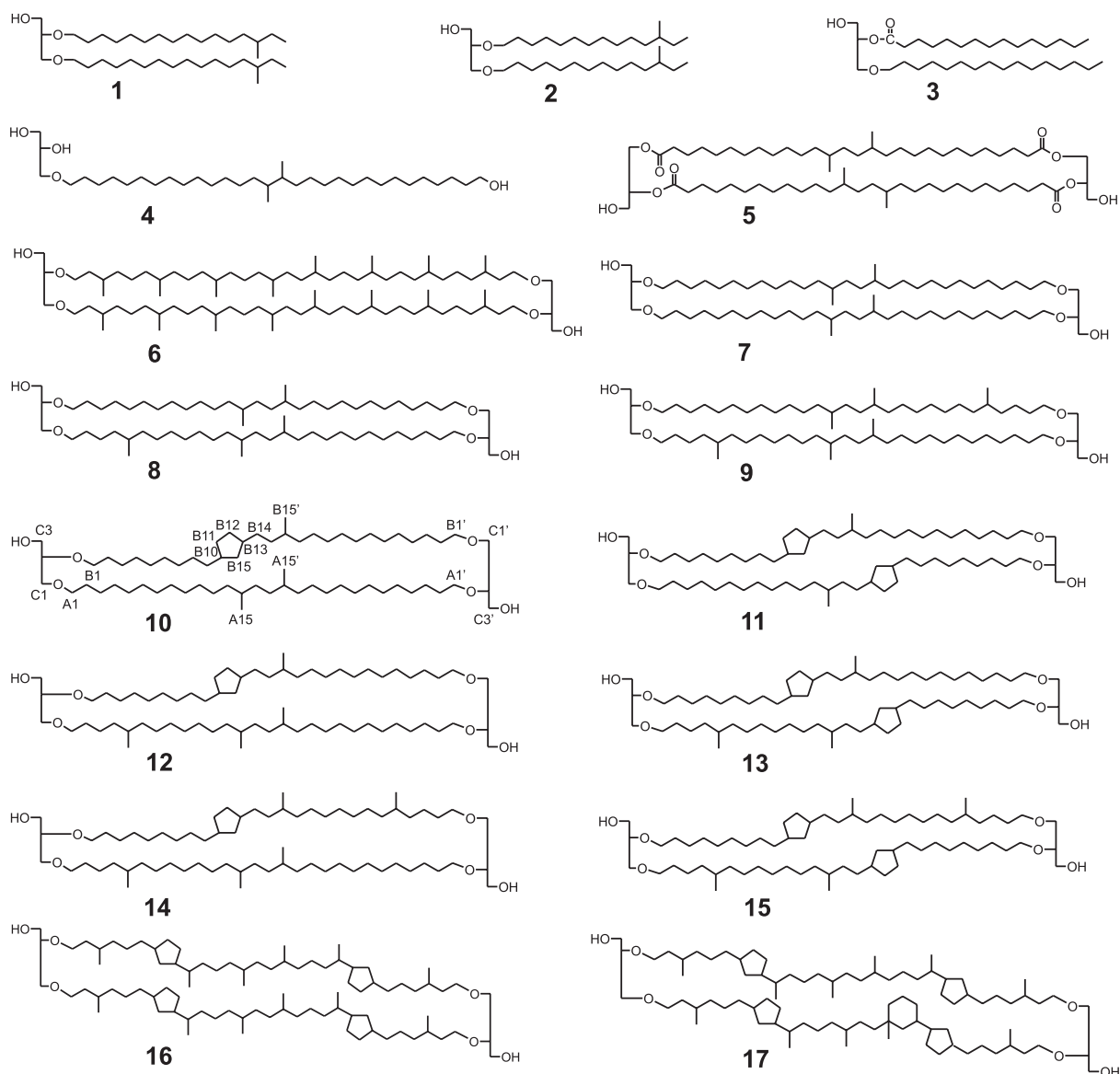
Chapter 3

Constraints on the biological source(s) of the orphan branched tetraether membrane lipids

Johan W.H. Weijers, Elda Panoto, Stefan Schouten, Melike Balk, Alfons J.M. Stams, W. Irene C. Rijpstra and Jaap S. Sinninghe Damsté

Abstract

Branched glycerol dialkyl glycerol tetraethers (GDGTs) are membrane lipids ubiquitous in soils and peat bogs. Based on their chemical structure and their abundant occurrence in the anoxic part of peat bogs, they were suggested to be derived from anaerobic bacteria (Weijers et al., 2006a). The exact biological origin, however, remains as yet unclear and is, due to the high microbiological diversity in soils and peat bogs, difficult to establish. In order to determine which phylogenetic group(s) of bacteria might encompass branched GDGT-synthesising species we conducted both core membrane lipid and 16S rDNA analyses of a Swedish peat bog. The results show a high abundance of branched GDGT lipids relative to methanogen-derived isoprenoid archaeol and archaeal GDGT-0 lipids. The molecular ecological results show that members of Rice Clusters IV and VI of the *Crenarchaeota* are the most dominant Archaea in the peat bog and that *Acidobacteria* comprise the dominant group of Bacteria present. This suggests that the phylum of *Acidobacteria* might include the biological source of the as yet orphan branched GDGT membrane lipids.

3.1. Introduction

Based on their distinct difference in 16S ribosomal RNA content, Bacteria and Archaea are identified as two separate Domains of Life (Woese et al., 1990). This distinction is supported by the different membrane lipid composition of Bacteria and Archaea. Where bacterial cell membranes generally comprise lipids with straight or branched alkyl chains ester-linked to a glycerol backbone and arranged in a bi-layer configuration, archaeal cell membranes generally comprise lipids with isoprenoidal alkyl chains connected by ether bonds to the glycerol backbones forming dialkyl glycerol diethers (DGDs) and membrane spanning glycerol dialkyl glycerol tetraethers (GDGTs). Additionally, the enantiomeric configuration of the glycerol backbone, 1,2- vs. 2,3-di-*O*-alkyl-*sn*-glycerol for Bacteria and Archaea, respectively, is a strong distinctive characteristic (Kates, 1978).

With the development of a high performance liquid chromatography / mass spectrometry (HPLC/MS) method for analysing intact core GDGT lipids (Hopmans et al., 2000), it appeared that GDGT membrane lipids occur widespread in the environment (Schouten et al., 2000). In the terrestrial realm, isoprenoid GDGTs (e.g., GDGT-0 in Fig. 3.1) were, together with DGDs (e.g., archaeol in Fig. 3.1) detected in peat bogs (Pancost et al., 2000; Schouten et al., 2000; Weijers et al., 2004). Based on their carbon isotopic composition and their occurrence in cultured methanogenic Archaea, both isoprenoid DGDs and GDGT-0 are used in peat bogs as tracers of methanogenic Archaea (Pauly and van Vleet, 1986; Pancost et al., 2000). A newly discovered group of tetraether membrane lipids, the branched GDGTs (Fig. 3.1), has been identified over the last years and found to be ubiquitous in peat bogs as well as in soils (Schouten et al., 2000; Sinninghe Damsté et al., 2000; Weijers et al., 2006b). Despite their membrane-spanning tetraether structure, which is thought to be a typical characteristic of the Archaea, they have been shown to have a bacterial origin. This is not only based on their branched instead of isoprenoid carbon skeleton but also on the bacterial 1,2-di-*O*-alkyl-*sn*-glycerol configuration of the glycerol backbone (Weijers et al., 2006a). Because of the high abundance of branched GDGT membrane lipids in the water saturated part of peat bogs relative to the non-saturated upper part, the bacteria producing them are assumed to be anaerobes or perhaps facultative aerobes (Weijers et al., 2006a). Based on these branched GDGTs, new proxies for the fluvial input of terrestrial organic matter in marine sediments (Hopmans et al., 2004) and for the reconstruction of annual mean air temperatures on land (Weijers et al., 2007b) have been developed. Although these membrane lipids have been found in every single soil and peat bog sample analysed so far (Weijers et al., 2006b, 2007a), the bacteria producing them are as yet unknown.

Microbial community structures in soils and peat bogs are complex and difficult to disentangle. The application of different culture-independent 16S rRNA sequencing techniques, however, enables the detection of many new bacterial and archaeal sequences in soils, wetlands and peat bogs. These culture-independent techniques have been applied in

several studies of bacterial community structures and diversity in soils (e.g., Bintrim et al., 1997; Dunbar et al., 2000; Hackl et al., 2004; Chan et al., 2006), in wetlands (e.g., Høj et al., 2005; Kraigher et al., 2006) and in peat bogs (e.g., McDonald et al., 1999; Sizova et al., 2003; Pankratov et al., 2005; Dedysh et al., 2006; Morales et al., 2006). Despite this, the physiology and function of the majority of bacterial and archaeal life in soils, wetlands and peat bogs are unknown as the majority of species seem hard to isolate in pure culture and many of them are inherently slow growers (Pace, 1997; Janssen, 2006 and references therein).

With this in mind and the fact that branched GDGTs are not easily, if at all, detected with standard techniques for lipid characterisation used in species description, it is not a surprise that the organism(s) synthesising branched GDGTs is (are) yet to be discovered. In order to constrain the biological source(s), we extracted prokaryotic 16S rDNA from samples at different depths in a peat core from the Saxnäs Mosse peat bog in Sweden. Subsequently, a qualitative comparison was made between the obtained bacterial and archaeal sequences and depth profiles of the concentrations of branched and isoprenoid GDGT membrane lipids and of the isoprenoid DGD lipid archaeol in this core.

3.2. Material and Methods

3.2.1. Study site and sampling

The Saxnäs Mosse is a raised bog composed of *Sphagnum* species near the village of Lidhult in south Sweden. The top 25 cm of the bog comprises the acrotelm layer, i.e., the layer experiencing alternating oxic and anoxic conditions due to the varying water table. The zone below 25 cm depth comprises the catotelm, the part of the bog which is continuously water saturated and consequently anoxic. Using a Wardenaar-corer, 50 cm long monoliths were obtained from the peat bog for GDGT and molecular ecological analyses. The top 14 cm of the bog consists of non-decomposed Sphagnum moss twigs with leaves (*Sphagnum magellanicum*) and is followed by a 13 cm thick interval of more decomposed *Sphagnum* twigs. The lower part of the bog consists of decomposed peat containing some *Ericaceae* and *Cyperaceae* remains between 30 and 40 cm depth and decomposed *Sphagnum papillosum* below 40 cm depth. Peat samples for organic geochemical analysis were taken at a 2 cm interval from the monolith back in the laboratory. The peat samples for microbiological analysis were taken with clean spatula at a 2 cm interval from the monolith directly in the field and put in sterile 16 ml containers (Greiner), transported in a mobile fridge at ~ 4°C within 24 h to the laboratory and stored frozen at -40°C until analysis.

3.2.2. Organic geochemistry

Lipid extraction. Peat samples for lipid analysis were freeze dried and powdered with mortar and pestle prior to extraction. The soluble organic matter was extracted from the peat samples

three times for 5 min by means of an accelerated solvent extractor at a pressure of ca. 7.6×10^6 Pa and a temperature of 100°C using a solvent mixture of dichloromethane (DCM):methanol 9:1 (v/v). The obtained extracts were rotary evaporated and further purified by separation into a relative apolar and polar fraction over an activated Al_2O_3 column using DCM:methanol 199:1 (v/v) and DCM:methanol 1:1 (v/v) solvent mixtures, respectively. After evaporation under a pure N_2 flow, the polar fraction, containing the GDGTs and archaeol, was ultrasonically dissolved in an hexane:propanol 99:1 (v/v) solution to a concentration of ca. 2 mg ml^{-1} and filtered over an 0.45 μm PTFE filter (ø 4 mm) prior to analysis with HPLC.
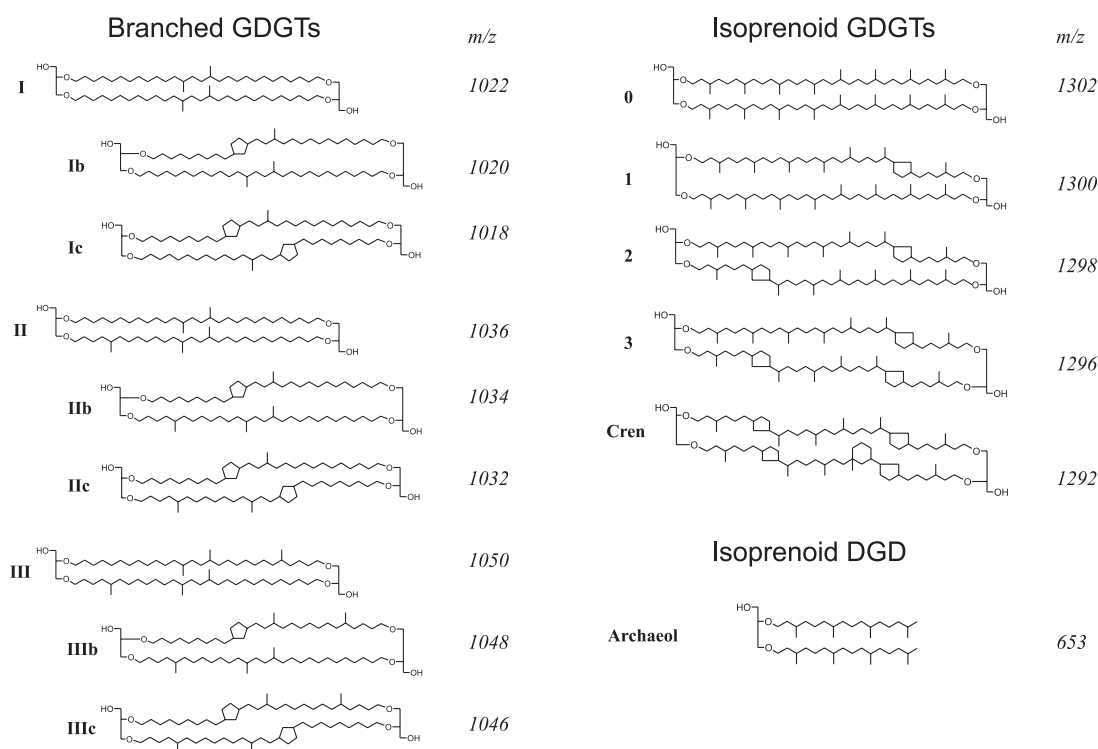
Figure 3.1: Chemical structures of the branched and isoprenoid GDGTs and the DGD archaeol. Cren = crenarchaeol

Lipid analysis. GDGTs and archaeol were analysed by high performance liquid chromatography/atmospheric pressure chemical ionisation – mass spectrometry (HPLC/APCI-MS) according to Hopmans et al. (2000) with minor modifications. Analyses were performed on an Agilent 1100 / Hewlett Packard 1100 MSD series machine equipped with automatic injector and HP-Chemstation software. Separation was achieved in normal phase on a Prevail Cyano column (150 mm × 2.1 mm; 3 μm) with a flow rate of the hexane:propanol 99:1 (v/v) eluent of 0.2 ml min^{-1}, isocratically for the first 5 min and thereafter with a linear gradient to 1.8% propanol after 45 min. Injection volume of the samples was 10 μl and quantification of the GDGTs was achieved by integrating the peak

areas in the $[M+H]^+$ and $[M+H]^+ + 1$ [i.e., protonated molecular ion (*m/z* values in Fig. 3.1) and first isotope peak] traces and comparing those with a standard curve prepared with known amounts of the isoprenoid GDGT-0. A correction was applied for the differences in mass between the branched GDGTs and GDGT-0. The DGD archaeol was analysed in a separate run, together with GDGT-0 in a single ion monitoring mode to increase sensitivity. Archaeol could not be quantified absolutely due to the absence of a DGD standard curve, but a relative quantification has been obtained by determining the ratio between archaeol and GDGT-0.

3.2.3. Molecular biology

Total DNA extraction. For molecular biological analysis 8 depth intervals were selected along the peat core (Figs. 3.4 and 3.6) covering the transition from the partly oxygenated acrotelm to the anoxic catotelm. About 2 g of peat material per sample was defrosted, centrifuged for 1 min at 1000 G to get rid of the excess liquid and subjected 3 times to a freeze-thaw cycle. DNA was extracted using the UltraClean Soil DNA Kit (Mobio laboratories Inc, Carlsbad, CA, USA) following the descriptions of the manufacturer.

PCR Amplification of archaeal and bacterial 16S rDNA. Partial archaeal 16S rDNA was amplified from the total DNA extract by polymerase chain reaction (PCR) using the forward primer Parch519f (Øvreås et al., 1997) and the reverse primer Arch-GC-915r (Stahl and Amann, 1991) including a 40-bp long GC-clamp (Muyzer et al., 1993) at the 5'-end. For the partial bacterial 16S rRNA amplification the forward eubacterial primer 341f including a 40-bp long GC-clamp (Muyzer et al., 1993) and the reverse primer 907R(a/c) (Amann et al., 1992) were used. All PCR amplifications were performed with a Geneamp PCR System 2400 (Perkin-Elmer, Connecticut, USA) using a mixture of the following components: 5 μl of 10X PCR-buffer (Pharmacia Biotechnology, Upsalla, Sweden), 10 mM of dNTP's, 20 μg of bovine serum albumine, 1 unit of Taq DNA polymerase (Pharmacia) and 0.5 μM of the respective archaeal and bacterial primers. PCR conditions included an initial denaturation step of 4 min at 96°C followed by 30 cycles including a denaturation step for 30 s at 94°C, a primer annealing step for 40 s at 57°C and a primer extension step for 40 s at 72°C. A final extension was performed for 10 min at 72°C.

DGGE analysis of 16S rDNA gene fragments. All PCR products were quantified by gel electrophoresis using a mass molecular DNA marker (Smartladder, Eurogentec) and subsequently separated by denaturing gradient gel electrophoresis (DGGE) (Schafer and Muyzer, 2001) carried out in a Bio-Rad D Gene system (Bio-Rad, München, Germany). About 100 ng PCR-product was loaded onto 6% (wt/vol) polyacrylamide gels [acrylamide/N,N'-methylene bisacrylamide ratio 37:1 (w/w)] in 1 × TAE buffer (pH 7.4). The archaeal gel contained a linear gradient from 30 to 60% denaturant [100% denaturant is 7 M urea plus 40% (v/v) formamide] and the bacterial gel contained a linear gradient from 20 to

70%. Electrophoresis of both gels proceeded for 5 h at 200 V and 60°C. Afterwards, gels were stained for 30 min in sterile double-distilled water containing ethidium bromide, de-stained for 60 min in sterile double-distilled water and photographed. DGGE-fragments were excised from the gel with sterile pipette points and the DNA of each fragment was eluted from the gel in sterile 10 mM Tris-HCL (pH 8.0) by incubation for 48 h at 4°C. The eluted DNA served as template DNA for re-amplification. Primers without GC-clamps were used for re-amplification.

Sequencing of DGGE bands. The amplified PCR products were purified using the QIAquick PCR Purification Spin Kit (Qiagen, Hilden, Germany) and quantified. Cycle sequencing reactions were performed with the ABI Prism Big Dye Terminator V3.0 kit (Applied Biosystems, CA, USA) using the forward or reverse primer (without GC clamp) at a final concentration of 0.2 μM and 10 ng of template DNA. The reaction volume was adjusted to a volume of 20 μl with molecular grade water (Sigma). The following reaction conditions were employed: 1 min initial denaturing at 96ºC followed by 25 cycles of 10 s at 96ºC, 5 s at 45ºC and 4 min at 60ºC. After an isopropanol mediated purification the pellets were dissolved in 15μl HiDi-formamide. Nucleotide positions were determined using an automated ABI-310 capillary sequencer (Applied Biosystems). Complementary sequences were aligned and manually edited using the AutoAssembler software package (Version 2.1.1; Applied Biosystems).

Phylogenetic analysis. Comparative analysis of the sequences was performed using ARB software (Ludwig et al., 2004). The partial sequences were aligned with sequences present in the database and with related full length 16S rDNA sequences obtained from NCBI using the BLAST-tool (http://www.ncbi.nlm.nih.gov/BLAST) (Benson et al., 2000). Phylogenetic trees were generated based on sequences of 1 kb and more using the maximum likelihood method. After applying a 50% variability filter, about 1400 columns of data were used for calculation of the tree. The specific sequences obtained by DGGE were added using the maximum parsimony option in ARB.

3.3. Results

3.3.1. Membrane lipids

In the upper part of the peat bog, which comprises non-decomposed peat and *Sphagnum* type vegetation, concentrations of the archaeal derived isoprenoid GDGT lipids were near the detection limit and the DGD lipid archaeol was not detected (Fig. 3.2). In this acrotelm layer, the average concentration of the summed isoprenoid GDGTs was 1 μg g^{-1} dry weight peat. In the water saturated part, the catotelm, this concentration increased considerably, with an

average value of 18 μg g^{-1} dry weight peat (Fig. 3.3). The acyclic isoprenoid GDGT-0 represented the majority of the detected isoprenoid GDGTs, i.e. ~60% in the acrotelm and ~80% in the catotelm. In the catotelm, archaeol was also detected and showed a constant abundance relative to the acyclic GDGT-0 (Fig. 3.3). A similar depth distribution was evident for the branched GDGTs although they were clearly more abundant in the peat core, by about a factor 5, than the isoprenoid GDGTs (Fig. 3.3). The average concentration of the summed branched GDGTs was only 5 μg g^{-1} dry weight peat in the upper part of the profile, but in the catotelm this concentration increased substantially to 115 μg g^{-1} dry weight peat on average (Fig. 3.3).
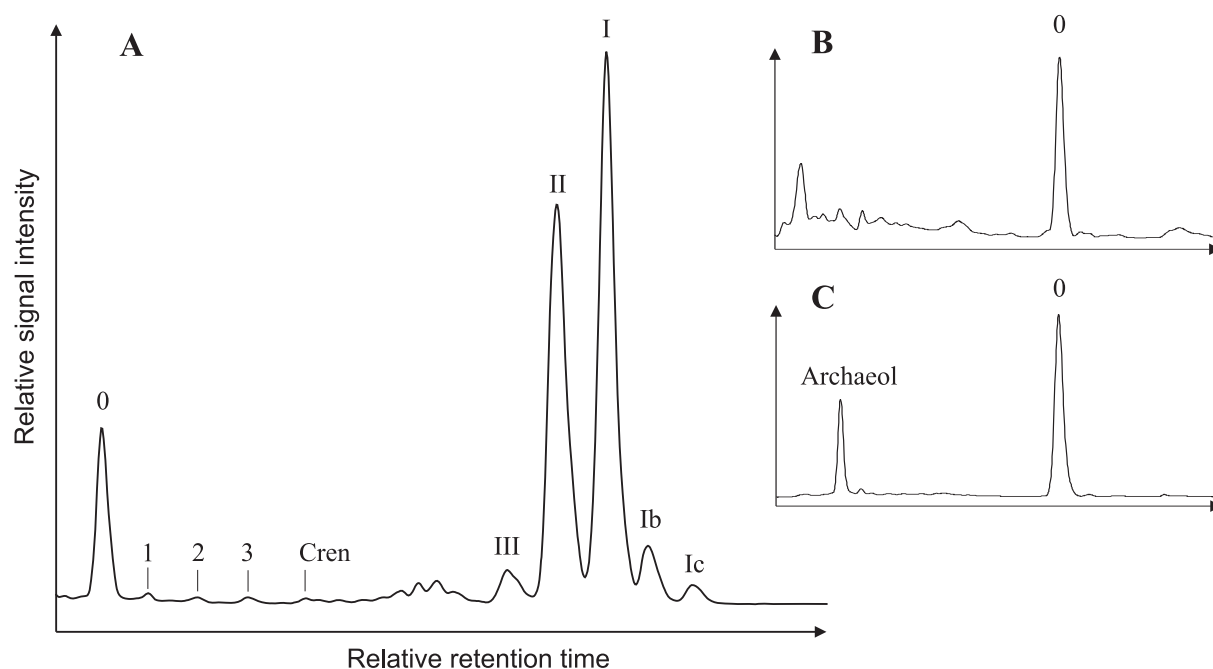
Figure 3.2: HPLC/MS base peak chromatograms of the Saxnäs Mosse peat bog. Panel A shows a typical base peak chromatogram with the relative abundances of isoprenoid and branched GDGTs. Panels B and C show the abundance of the DGD archaeol relative to GDGT-0 in the acrotelm (archaeol absent) and the catotelm of the peat bog, respectively. Numbers refer to the structures drawn in Fig. 3.1. Cren = crenarchaeol

3.3.2. Archaeal DNA sequences
Using the universal archaeal primer pair many different bands appeared on the DGGE gel containing the 8 selected depth intervals from the Saxnäs Mosse peat bog (Fig. 3.4). Of these, 31 bands could be successfully excised from the gel and sequenced (Fig. 3.4). One of the bands, band 22, appeared to be a bacterial sequence. A BLAST search revealed that the closest relative of this sequence (92% similarity) is an acidobacterial sequence from a Taiwanese forest soil. Phylogenetic analysis reveals that the majority of the obtained archaeal sequences fall within Rice Clusters (RC) IV and VI (Fig. 3.5), which are deep branching

clades in the Kingdom *Crenarchaeota* (Großkopf et al., 1998; Chin et al., 1999). Five sequences, band 10, bands 16 and 18 and bands 19 and 26, do not fall within these Rice Clusters and occupy rather isolated positions within the *Crenarchaeota*. Band 10 is only distantly related (<90%) to sequences obtained from a gold mine and a petroleum contaminated soil. The other four bands appear to be closest related (95-99%) to sequences derived from hot springs and a sulphurous lake. In general, there does not seem to be a trend towards a higher diversity of archaeal species in the deeper layers. Sequences obtained from the two deepest intervals in the peat core (38 and 40 cm) fall generally closely together within RC-VI. However, the DGGE method used does not exclude their presence in the shallower depth intervals.
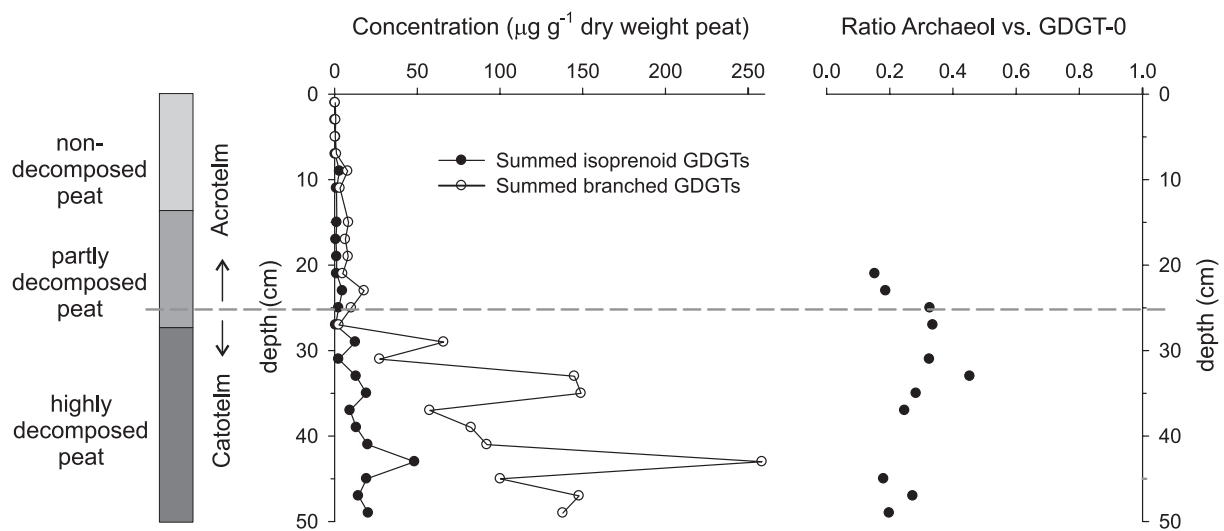
Figure 3.3: Depth profile of the Saxnäs Mosse peat core showing, on the left hand panel, the concentrations of the summed branched GDGT and summed isoprenoid GDGT (excluding crenarchaeol) membrane lipids and, on the right hand panel, the ratio between archaeol and GDGT-0. Also given are a schematic decomposition profile of the peat core and the boundary (grey striped line) between the acrotelm (zone in which the water table fluctuates) and catotelm (continuously water saturated and thus anoxic zone).

3.3.3. Bacterial DNA sequences

Using the universal bacterial primer pair several different bands were apparent on the DGGE gel. The number of bands in the gel increases from 2 in the two uppermost intervals to 9 in the deeper intervals, suggesting increased bacterial diversity although this might also be due to differences in sample concentrations (Fig. 3.6). A total of 14 different bands was successfully excised and sequenced (Fig. 3.6). Even though a universal bacterial primer was used, phylogenetic analysis revealed that 13 out of the 14 sequences belong to the phylum of *Acidobacteria* and only one sequence (band 9), detected in the 26 cm depth interval, falls within the *Syntrophobacteria* which is part of the large phylum of *δ-Proteobacteria* (Fig. 3.7).

The acidobacterial sequences are distributed along the subdivisions 1 (4 sequences), 3 (1 sequence) and 4 (3 sequences), following the classification proposed by Hugenholtz (1998), and one unknown subdivision (5 sequences).
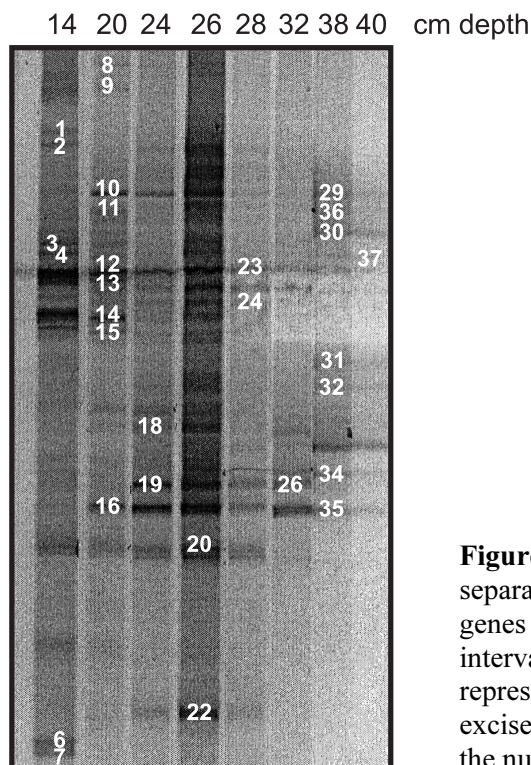
Figure 3.4: DGGE gel showing the separation of the archaeal 16S rDNA genes obtained from different depth intervals in the peat core. Numbers represent bands that were successfully excised and sequenced and correspond to the numbers in Fig. 3.5.

3.4. Discussion

3.4.1. Archaeal diversity

Although peat lands play an important role in global biogeochemical cycles via the microbe-mediated emission of CH_4 and CO_2 greenhouse gasses (Bartlett and Harriss, 1993), until recently, relatively little was known about the microbial communities present in these ecosystems. Only over the last years studies have been published aiming at the characterisation of microbial diversity and structures in peat bogs (e.g., Sizova et al., 2003; Kotsyurbenko et al., 2004; Pankratov et al., 2005; Juottonen et al., 2005; Dedysh et al., 2006; Morales et al., 2006). Microbial methanogenesis is an important process in the anaerobic degradation of organic matter in peat lands, carried out by methanogens comprising different species of *Euryarchaeota*. *Methanomicrobiales*, *Methanosarcinales*, *Methanobacteriales* and sequences belonging to Rice Cluster I (RC-I) are amongst the most regularly detected methanogen archaea in boreal peat lands (e.g., McDonald et al., 1999; Sizova et al., 2003; Horn et al., 2003; Kotsyurbenko et al., 2004; Høj et al., 2005; Juottonen et al., 2005; Brauer et al., 2006).
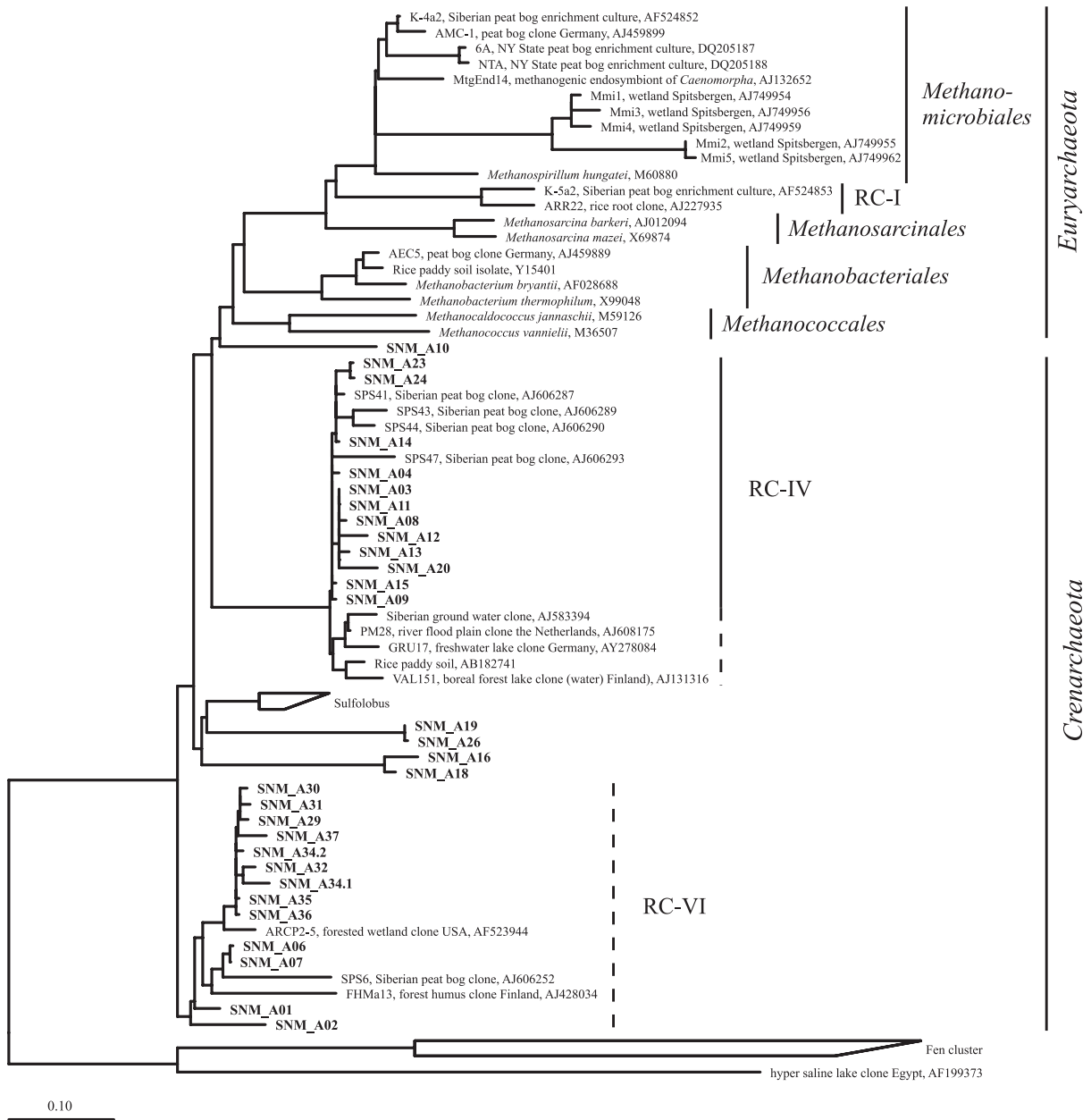
Figure 3.5: Maximum likelihood tree showing the phylogenetic position of the archaeal genes obtained from the Saxnäs Mosse peat core (SNM_A in bold). Numbers correspond to those in Fig. 3.4. RC = Rice Cluster

Strikingly, however, the archaeal sequences obtained from the Saxnäs Mosse bog belong to Rice Cluster IV (RC-IV) (Großkopf et al., 1998) and a cluster which most likely represents Rice Cluster VI (RC-VI) (Chin et al., 1999). These are no *Euryarchaeota* but deep branching members of the *Crenarchaeota*. Members of RC-IV have been detected on the roots of rice plants and were closely related to two earlier detected environmental sequences from a marsh environment and a freshwater sediment (Großkopf et al., 1998). RC-VI members have first

been described as such by Chin et al. (1999) in an anoxic rice field soil, but were earlier detected in an agricultural soil by Bintrim et al. (1997). Furthermore, Kemnitz et al. (2004) found, besides known methanogenic archaea, a high diversity of members of RC-IV and VI in a riparian flood plain in the Netherlands and Kotsyurbenko et al. (2004) detected these groups in an acidic west Siberian peat bog. The ecological niches and metabolic functions of members of RC-IV and VI are still unknown due to a lack of cultured relatives. It is unlikely that members of RC IV and VI are methanogens as this physiology has not been found yet in any crenarchaeotal species. The fact that we have not detected sequences closely related to methanogenic archaea might be due to the low specificity of the DGGE method, which only reveals the most abundant sequences. The diversity of methanogens in our peat could be high, but the abundance of individual methanogen species might be lower than that of the members belonging to RC IV and VI. Since with cloning and isolation studies RC IV and VI are usually detected together with methanogen communities, it might be assumed that methanogens are also present, though not detected with our methods, in the Saxnäs Mosse bog.
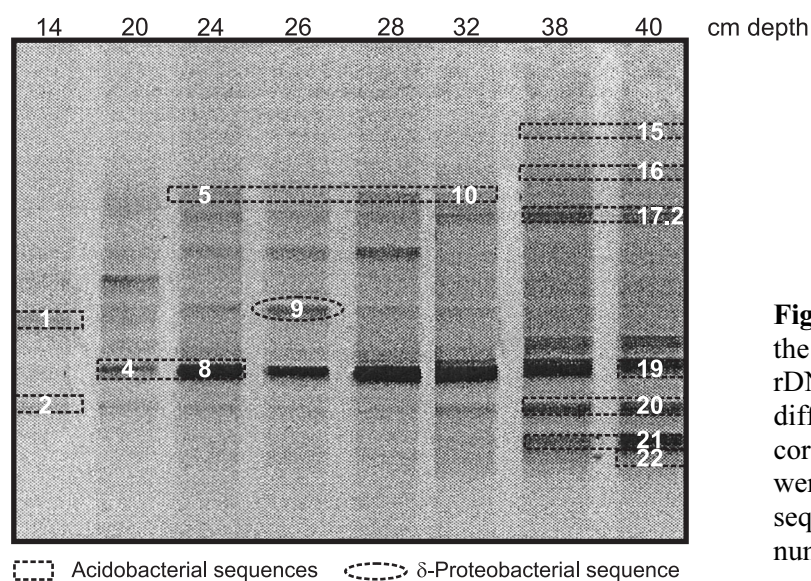

Figure 3.6: DGGE gel showing the separation of the bacterial 16S rDNA genes obtained from different depth intervals in the peat core. Numbers represent bands that were successfully excised and sequenced and correspond to the numbers in Fig. 3.7.

3.4.2. Bacterial diversity

Regarding the bacterial diversity, virtually all sequences obtained from our Swedish peat core fall within the phylogenetic cluster of *Acidobacteria*. Similar as with the Archaea, this seemingly low diversity is partially a result of the DGGE fingerprinting method used and creating a clone library may likely result in a somewhat higher diversity. However, the DGGE method screens for the most abundant sequences which in this case, clearly, belong to the *Acidobacteria*. The *Acidobacteria* are a relatively recently recognised phylogenetic cluster of

bacteria subdivided into at least eight groups (Kuske et al., 1997; Hugenholtz et al., 1998) together comprising a highly diverse phylum (Quaiser et al., 2003). Although they are found to be ubiquitous in environmental samples (Barns et al., 1999), this phylum is poorly represented by cultured organisms. Only 3 species are yet brought into culture; *Acidobacterium capsulatum*, an acidic, aerobic, mesophilic, gram-negative, non-spore forming bacterium (Kishimoto et al., 1991; Hiraishi et al., 1995) [belonging to subdivision 1; following the classification by Hugenholtz et al. (1998)]; *Holophaga foetida*, a strictly anaerobic, gram negative, homoacetogenic bacterium degrading methoxylated aromatic compounds (Liesack et al., 1994); and *Geothrix fermentans*, a strictly anaerobic, gram negative, Fe(III)-reducing bacterium (Lonergan et al., 1996; Coates et al., 1999) (both belonging to subdivision 8).

Our acidobacterial sequences are distributed over subdivisions 1, 3 and 4 and an unknown subdivision. The identity of this latter subdivision, containing 5 of the Saxnäs Mosse sequences, is rather difficult to establish as the German peat bog clone 'TM1', a closely related environmental sequence, is not classified in the original classification of Hugenholtz et al. (1998). Moreover, the soil clone 'DA052' that was originally classified in subdivision 2 (Hugenholtz et al., 1998), seems to cluster within subdivision 4, according to our phylogenetic analysis. It has to be mentioned, however, that the classification of the *Acidobacteria* by Hugenholtz et al. (1998) in some instances is only based on a few sequences combined with low bootstrap values.

Amongst the four subdivisions of *Acidobacteria* found in this study are different environmental sequences obtained from soils (e.g., Felske et al., 1998; Sait et al., 2002), a forested wetland (Brofft et al., 2002) and boreal peat bogs (e.g., Sizova et al., 2003; Juottonen et al., 2005; Dedysh et al., 2006). From the three cultured representatives of *Acidobacteria* only *Acidobacterium capsulatum* belongs to one of these subdivisions, i.e., subdivision 1, but differs by >5% sequence identity and is thus not closely related to the sequences obtained in this study (Fig. 3.7).

Molecular ecological studies of peat bog systems often reveal high abundances of *Acidobacteria*. A study of the bacterial community composition in 24 different peat bogs in New England, U.S.A., demonstrated a marked similarity in composition amongst the different bogs (Morales et al., 2006). Furthermore, 16S rDNA sequence analysis of one of these bogs showed that the *Acidobacteria* are, after the *Proteobacteria*, likely the most abundant bacteria in these bogs (11% of total number of clones) (Morales et al., 2006). Similar reports of *Acidobacteria* in peat bogs and fen soils have been made for a marsh in Slovenia (23% of total number of clones, second most abundant after *Proteobacteria*) (Kraigher et al., 2006), a Siberian peat bog (29% of total clone number, most abundant) (Dedysh et al., 2006) and four other peat bogs in Russia (*Acidobacteria* second or third most abundant after *Proteobacteria*) (Pankratov et al., 2005).
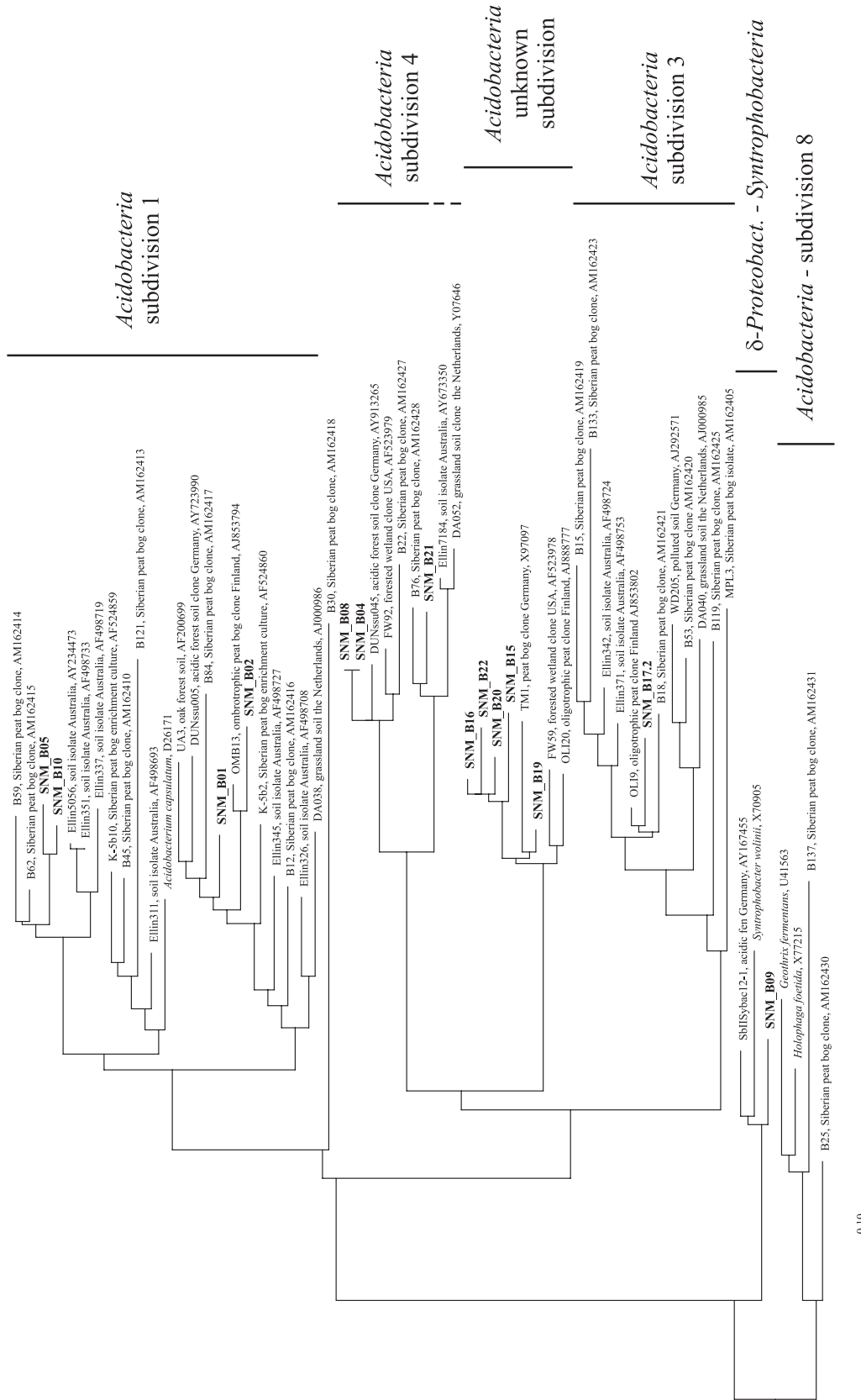
Figure 3.7: Maximum likelihood tree showing the phylogenetic position of the bacterial genes obtained from the Saxnäs Mosse peat core (SNM_B in bold). Numbers correspond to those in Fig. 3.6. Subdivisions of the *Acidobacteria* are according to the classification by Hugenholtz et al. (1998).

3.4.3. Membrane lipids

Considering non-thermophilic environments, GDGT-0 could be derived from either methanogenic *Euryarchaeota* (Kates et al., 1993; Pancost et al., 2000) or from mesophilic Group-1 *Crenarchaeota* (Schouten et al., 2000). These Group-1 *Crenarchaeota*, however, do also synthesise considerable amounts of crenarchaeol (Fig. 3.1) (Sinninghe Damsté et al., 2002a). It has been shown previously that crenarchaeol is only present in minor amounts relative to GDGT-0 in this Saxnäs Mosse peat bog (Weijers et al., 2004), which implies that Group-1 *Crenarchaeota* are not a likely source for the isoprenoid GDGTs found in this study. The Rice Cluster IV and VI *Crenarchaeota* may, however, also produce isoprenoid GDGTs. Yet, it is unlikely that they produce archaeol, which is typically found in methanogenic *Euryarchaeota* (Kates et al., 1993) and only in traces, if at all, in *Crenarchaeota*. The presence of archaeol, therefore, points to the presence of methanogens, and the relative constant ratio between archaeol and GDGT-0 in this core (Fig. 3.3) might suggest a same source for GDGT-0. The fact that no methanogen sequences were detected might be a methodological bias; crenarchaeol is present as well but no Group-1 crenarchaeotal sequences were detected either.

Strikingly, the abundance of branched GDGT membrane lipids in this core is clearly higher than that of the isoprenoid GDGTs by about a factor 5. Also in other peat bogs the average ratio of branched GDGTs versus isoprenoid GDGTs is high, i.e., the Netherlands (~2), England (~3) and Switzerland (~4) (J.W. et al., unpublished results). This suggests that the bacteria that synthesise branched GDGT lipids likely represent quite an abundant (group of) species. Based on the DGGE and subsequent 16S rDNA sequence analysis, the *Acidobacteria* are the most dominant species present in our peat bog and might represent a candidate phylum that could biosynthesise branched GDGTs. Additional evidence for this assumption is obtained from soils. In earlier studies, so far, we have detected branched GDGTs in all (>150) soils analysed, ranging from a tropical rainforest soil in Gabon to almost barren soils on Arctic Spitsbergen and at 4000 m altitude in the Andes (Weijers et al., 2006b, 2007a and J. Bendle, R. Pancost, J. Weijers and J. Sinninghe Damsté, unpublished results). Thus, branched GDGT-producing species must be very ubiquitous although we cannot fully exclude that these lipids are produced by many different species.

The *Acidobacteria* are, indeed, widespread occurring in a variety of environments like soils, swamps, fresh water lakes, hot springs and contaminated aquifers (Hugenholtz et al., 1998; Barns et al., 1999). This widespread occurrence suggests that *Acidobacteria* are significant constituents of many ecosystems (Hugenholtz et al., 1998). In soils, *Acidobacteria* are virtually always detected, ranging from Antarctic soils (Aislabie et al., 2006) to a hot desert soil in Tunisia (Chanal et al., 2006) and a tropical rainforest soil in China (Chan et al., 2006). In this latter soil, the relative abundance of *Acidobacteria*-affiliated sequences was as much as 80% (Chan et al., 2006). Based on comprehensive analysis of 32 libraries of 16S rRNA and 16S rRNA genes of members of the bacterial domain, prepared from a variety of

soils, Janssen (2006) estimated the average abundance of *Acidobacteria* in soils at 20%, which is second most abundant after the highly diverse phylum of *Proteobacteria*.

Based on the results of the microbiological analyses of the Saxnäs Mosse peat bog and the literature data, the *Acidobacterium capsulatum* (DSM 11244) and *Holophaga foetida* (DSM 6591) strains, two of the three strains available in culture from the phylum *Acidobacteria*, were analysed for the presence of branched GDGTs. Unfortunately, in both strains branched GDGTs were not detected. However, *Holophaga foetida* belongs to subdivision 8 and is rather distantly related to other environmental sequences. Secondly, although *Acidobacterium capsulatum* belongs to subdivision 1, in which more peat bog and soil clones are present, sequences obtained from our peat bog did not reveal very close relationships with this cultured strain (<95% sequence similarity). Nevertheless, the phylum of *Acidobacteria* is a highly diverse one with many subdivisions and clusters within these divisions, and the presence of branched GDGT-producing species can therefore not be excluded based on these results.

In addition, we analysed *Syntrophobacter fumaroxidans* (DSM 10017) for branched GDGT lipid content, as biomass of this species was readily available in our laboratory and the only bacterial sequences (SNM_B09) that did not fall in the *Acidobacteria* clustered within the *Syntrophobacteria*. *S. fumaroxidans* did not contain branched GDGTs either, but is also only distantly related to sequence SNM_B09, i.e., an insignificant relation based on a BLAST sequence alignment.

3.4.4. Alternative sources for branched GDGTs

An alternative approach to that described above is to examine phylogenetic relatives of bacterial species known to produce membrane lipids structurally related to that of branched GDGTs. The extreme thermophilic and strictly anaerobic bacterium *Ammonifex* is known to produce diether lipids (Huber et al., 1996) and the thermophilic *Thermoanaerobacter ethanolicus* is reported to produce membrane-spanning tetraester lipids containing α,ω-13,16-dimethyloctacosane carbon chains (Jung et al., 1994; Lee et al., 2002), which are alkyl chains identical to those found in some branched GDGTs. Possibly, low temperature relatives of these bacteria, which fall in the candidate phylum of the low G+C gram positive bacteria, might be biological sources for branched GDGTs. Therefore, from this phylum of low G+C gram positive bacteria, we analysed *Clostridium acidisoli* (DSM 12555) for the presence of branched GDGTs. This strain was chosen as it is an anaerobic acid tolerant species isolated from a German peat bog and because *Thermoanaerobacter* species show a 98-99% 16S rRNA similarity with the thermophilic and acid tolerant *Clostridium thermoamylolyticum* (Kuhner et al., 2000). Despite this seemingly close phylogenetic relation with species synthesising related types of alkyl chains, *Clostridium acidisoli* did not contain branched GDGT membrane lipids. It has to be mentioned, in addition, that these species (or relatives thereof) seem not to be ubiquitous among soils and peat bogs and that more ether bound and membrane-spanning

lipids have been reported in species belonging to other phyla, like the *Planctomycetes* (Sinninghe Damsté et al., 2002b) and the early branching *Aquificales* (Huber et al., 1992) and *Thermotogales* (Carballeira et al., 1997).

3.5. Conclusion

Branched GDGTs are present in high amounts relative to the ostensibly methanogen-derived isoprenoid GDGTs and archaeol in the Saxnäs Mosse peat bog. *Acidobacteria* seem to be the most dominant type of Bacteria present in this peat bog. As, in addition, both branched GDGTs and *Acidobacteria* are ubiquitous in globally distributed soils, we suggest that the phylum of *Acidobacteria* might encompass the organisms synthesising branched GDGT membrane lipids.

Chapter 4

Water table related variations in the abundance of intact archaeal membrane lipids in a Swedish peat bog

Johan W.H. Weijers, Stefan Schouten, Marjolein van der Linden, Bas van Geel
and Jaap S. Sinninghe Damsté

Abstract

The presence and distribution of isoprenoid glycerol dialkyl glycerol tetraethers (GDGTs), lipids that constitute the membranes of Archaea, have been investigated in a 50-cm long core from a Swedish peat bog. In the acrotelm, the periodically water saturated and thus oxic upper layer of the peat bog, only minor amounts of GDGTs were found. These amounts increase considerably in the catotelm, the continuously water saturated and consequently anoxic lower layer of the peat bog. Based on earlier analyses of GDGTs in different settings and on 16S rDNA results from literature, these lipids are likely derived from methanogenic Archaea. Crenarchaeol, previously only found in marine settings and in fresh water lakes, has also been found in this peat bog. Contrary to the other GDGTs, crenarchaeol concentrations remain relatively constant throughout the peat core, suggesting that they are produced by Crenarchaeota thriving in the oxic part of the peat bog and possibly also in the anoxic part.

4.1. Introduction

Archaea, one of the three Domains of life, consist of a wide diversity of micro-organisms genetically distinct from the other two domains of life, the Bacteria and the Eukarya (Woese et al., 1990). Initially, they were thought to only comprise extremophilic species. However, the use of culture-independent biological techniques has shown that they inhabit a wide variety of environments and are not restricted at all to extreme environments (DeLong, 1992; Fuhrman et al., 1992). Within the Archaea domain, three different phyla can be distinguished. First, the Euryarchaeota, of which cultured species exist capable of thriving at high temperatures or high salt concentrations. Uncultured Euryarchaeota are found in environments like deep marine anoxic waters, marshes, peat bogs, rice fields and even in the gut of a soil-feeding termite, and they are often involved in the methane cycle (e.g., Galand et al., 2002; Wakeham et al., 2003). A second phylum is formed by the Korarchaeota, which constitutes an as yet poorly characterised smaller branch of hyperthermophiles. Finally, the Crenarchaeota are the most diverse and abundant group within the Archaea kingdom (DeLong, 1998). Among cultured Crenarchaeota there are sulphur-oxidisers, most of which are (hyper)thermophiles (Woese et al., 1990). The uncultured Crenarchaeota mainly comprise non-thermophilic species, often referred to as 'Group 1' Archaea (see DeLong, 1998 for an overview) and they are found in diverse environmental settings. A part of this 'Group 1' Archaea are the non-thermophilic marine planktonic Crenarchaeota, which are ubiquitous in the world's oceans where they account for about 20% of all picoplankton (Karner et al., 2001). They are found in the marine water column (Fuhrman et al., 1992; DeLong et al., 1994; Karner et al., 2001) and in marine sediments (Vetriani et al., 1999). From this subgroup of marine planktonic Crenarchaeota, there is one 'culture' available: *Cenarchaeum symbiosum*, an archaeon living in symbiosis with the sponge *Axinella mexicana* (Preston et al., 1996). During the last years, a wealth of phylogenetic sequences belonging to this 'Group 1' Archaea has been discovered in forest soils and their rhizospheres, agricultural soils and palaeosoils (e.g., Buckley et al., 1998; Pesaro and Widmer, 2002; Ochsenreiter et al., 2003) and in fresh water lakes and sediments (e.g., MacGregor et al., 1997; Keough et al., 2003). However, compared to the marine environment, the amounts of Crenarchaeota found on land are much lower. Ochsenreiter et al. (2003) determined the relative amount of non-thermophilic Crenarchaeota in a bulk soil sample at 0.5 to 3% of bacterial rDNA and Buckley et al. (1998) calculated a relative abundance of 1.42% ± 0.42% of the total 16S rRNA in soils. This is in contrast with the marine water column where the amount of marine Crenarchaeota can reach as much as 39% of total DNA-containing picoplankton (20% on average) (Karner et al., 2001).

Besides their distinctive genetic composition, Archaea also possess a distinctive membrane, which is predominantly composed of glycerol dialkyl diether and glycerol dialkyl glycerol tetraether lipids (GDGTs; see Fig. 4.1 for structures). This contrasts with the ester-linked membrane lipids of Eukarya and most Bacteria (Kates et al., 1993). Membrane lipids

can, thus, provide an additional line of evidence for the widespread occurrence of Archaea in diverse environmental settings. GDGT lipids turned out to be abundant in marine water column particulate and sedimentary organic matter and have been proposed to derive from planktonic Crenarchaeota (e.g., Hoefs et al., 1997; King et al., 1998). They were also detected in *Cenarchaeum symbiosum* (DeLong et al., 1998) which confirms this hypothesis. With the development of a HPLC/MS technique for measuring intact GDGTs (Hopmans et al., 2000), new kinds of widespread occurring GDGTs were discovered in both oxic and anoxic marine waters and sediments and in lakes (e.g., Schouten et al., 2000; Wakeham et al., 2003). A newly discovered GDGT, 'crenarchaeol', which contains an additional cyclohexane moiety besides the usual pentane rings (Fig. 4.1), was found to be ubiquitous throughout marine sediments and turned out to be the most abundant lipid in *Cenarchaeum symbiosum* as well (Sinninghe Damsté et al., 2002). Recently, crenarchaeol was also found in fresh water lake sediments (Powers et al., 2004). Since crenarchaeol is only found in non-thermophilic, aquatic settings, it is thought to be an indicator for the presence of non-thermophilic Crenarchaeota.
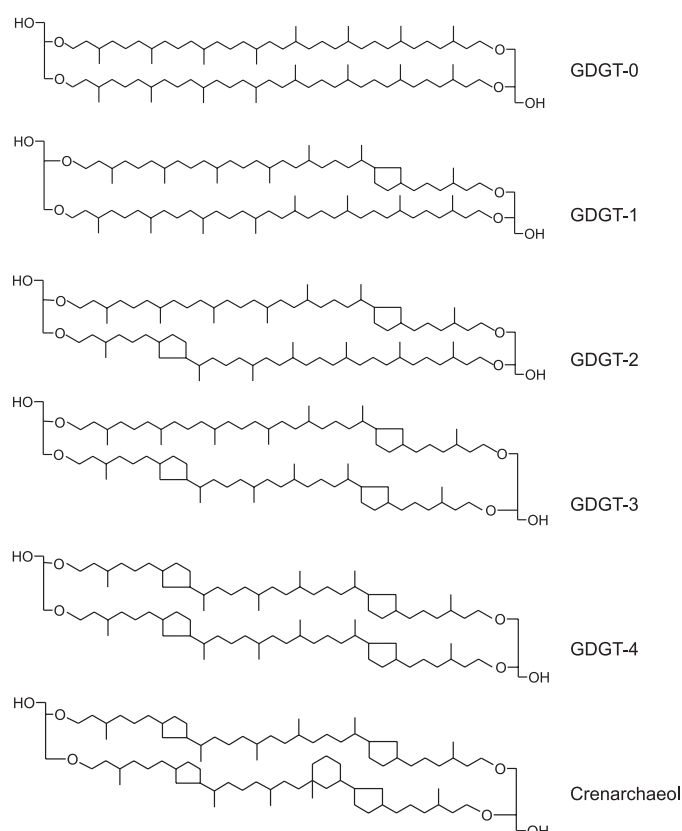
Figure 4.1: The different isoprenoid glycerol dialkyl glycerol tetraether (GDGT) structures discussed in the text. The numbers indicate the amount of cyclopentane moieties present.

So far, only a few studies have reported the presence of GDGTs in terrestrial settings and the characterisation of archaeal communities in soils and peat bogs based on their lipid content. Pancost et al. (2000) first reported the occurrence of GDGTs, as inferred from the presence of biphytanes released by ether bond cleavage, in two peat bogs and later Schouten et al. (2000) and Pancost et al. (2003) reported the presence of some intact GDGTs in two ancient peat bogs in Ireland and The Netherlands. Gattinger et al. (2003) demonstrated the use of GDGT lipid analysis for detecting archaeal communities in soils. To cover a broad diversity of archaeal lipids they used a bulk sample composed of different soil types. Although the analytical conditions did not allow for a clear separation of the GDGTs, they identified GDGTs 0 to 4. None of these studies reported the presence of crenarchaeol in their samples. Recently, however, traces of crenarchaeol were reported in a wetland from the USA, indicating that crenarchaeol is also more widespread than previously thought (C.H. Turich, E.C. Hopmans, S. Schouten, M.A. Bruns and K.H. Freeman, unpublished results).

In this study a *Sphagnum* peat core from southern Sweden was analysed for the presence of archaeal isoprenoid GDGT lipids. Since this peat core covers the aerated top part above the water table as well as the anaerobic part below the water table, two different ecological habitats are present. By analysing the changes in the lipid distribution along the depth profile, it was possible to distinguish between different archaeal communities inhabiting the two habitats.

4.2. Material and Methods

In summer 2003, samples were taken from the Saxnäs Mosse (56 51' 20.78" N, 13 27' 39.62" E), a raised bog area with vegetation mainly composed of *Sphagnum* species, near the village of Lidhult, SW Sweden. A 50 cm long peat core was taken with a Wardenaar corer and put into a metal box. The water table in the field was found at an average depth of 14 cm below surface. The upper 25 cm of the core constitutes the acrotelm layer and is followed by a 5 cm thick transition layer to a 5 cm thick layer of dark, brown/black, highly decomposed peat. After another 5 cm transition layer, a dark brown peat layer was found down to 50 cm depth. In the laboratory, during sampling, the upper 14 cm proved to consist of non-decomposed *Sphagnum magellanicum* stems with leaves, followed by a 13 cm thick layer of more decomposed but still visible *Sphagnum* branches. From 27 to 50 cm the core consists of decomposed peat, with between 30 and 40 cm also ericaceous and cyperaceous remains. The lowermost 10 cm consists of decomposed *Sphagnum papillosum*.

The core was sampled at two-centimetre intervals with a metal case of approximately 0.75 cm^3. Freeze-dried and ground samples were extracted 3 times for 5 minutes with an Accelerated Solvent Extractor (DIONEX ASE 200) using a mixture of dichloromethane (DCM):methanol 9:1 (v/v) at a temperature of 100°C and a pressure of 7.6 x 10^6 Pa. Extracts

were rotary evaporated under vacuum to near dryness. For GDGT analyses, the extracts were further purified by separation into two fractions over an activated Al_2O_3 column using DCM:methanol 199:1 (v/v) and DCM:methanol 1:1 (v/v), respectively. The latter fraction was evaporated under a continuous nitrogen flow, dissolved in a hexane:propanol 99:1 (v/v) solution by sonication and filtered through an Alltech 0.45 µm PTFE filter (ø 4mm). GDGTs were analysed by high performance liquid chromatography/atmospheric pressure chemical ionisation mass spectrometry (HPLC/APCI-MS), according to Hopmans et al. (2000) with minor modifications. Analyses were performed on an Agilent 1100 series/Hewlett Packard 1100MSD series machine, equipped with auto-injector and HP Chemstation software. Separation was achieved on an Alltech Prevail Cyano column (150 mm x 2.1 mm; 3 µm). Flow rate of the hexane:propanol 99:1 (v/v) eluent was 0.2 ml min^{-1}, isocratically for the first 5 minutes, thereafter with a linear gradient to 1.8% propanol in 45 minutes. Injection volume of the samples was usually 10 µl. Quantification of the GDGT compounds was achieved by integrating the peak areas in the $[M+H]^+$ and $[M+H]^+ + 1$ (i.e., protonated molecule and first isotope peak) traces and comparing these to a standard curve prepared with known amounts of GDGT-0.
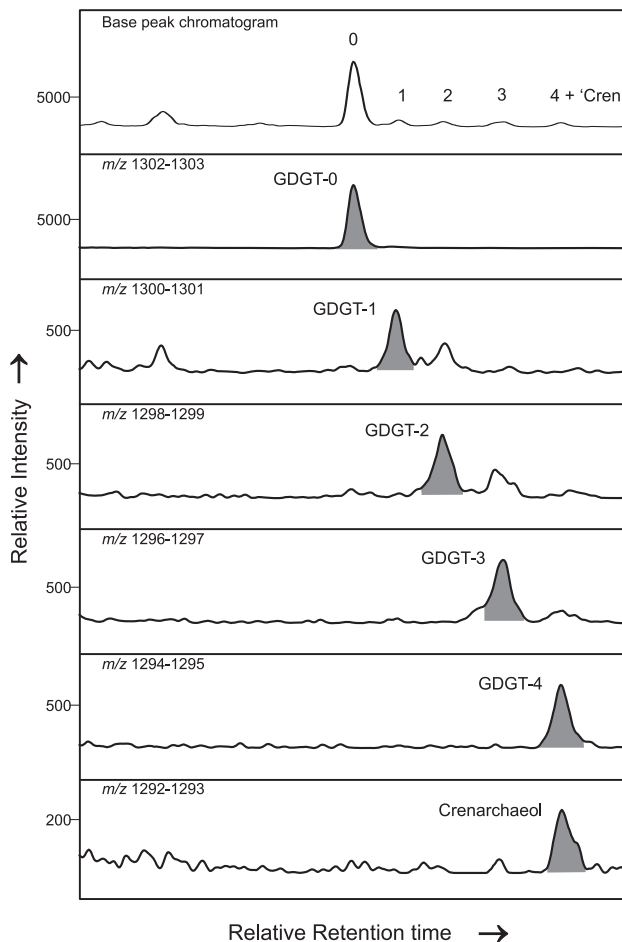
Figure 4.2: Partial base peak chromatogram and mass chromatograms of the protonated molecule plus first isotope peak of the different GDGTs in the peat sample from 35 cm depth. Numbers refer to the GDGT structures in Fig. 4.1. 'Cren' = crenarchaeol.

The relatively high abundance of the $[M+H]^{+}+2$ isotope peaks in the mass spectra of the GDGTs gives rise to signals in the mass chromatograms with a 2 Da higher mass (Hopmans et al., 2000) (see Fig. 4.2). Co-elution of GDGT-4 and crenarchaeol on the LC together with this overlap of isotope peaks in the mass spectra makes quantification of GDGT-4 by integration difficult. To overcome this, the average percentage of the $[M+H]^{+}+2$ isotope peak in the mass spectrum of crenarchaeol was calculated for several 'clean' marine samples from different places (i.e., samples containing only crenarchaeol). This percentage turned out to be about 33%. The GDGT-4 peak area in our samples was corrected by this percentage to obtain an estimate of the GDGT-4 concentration.
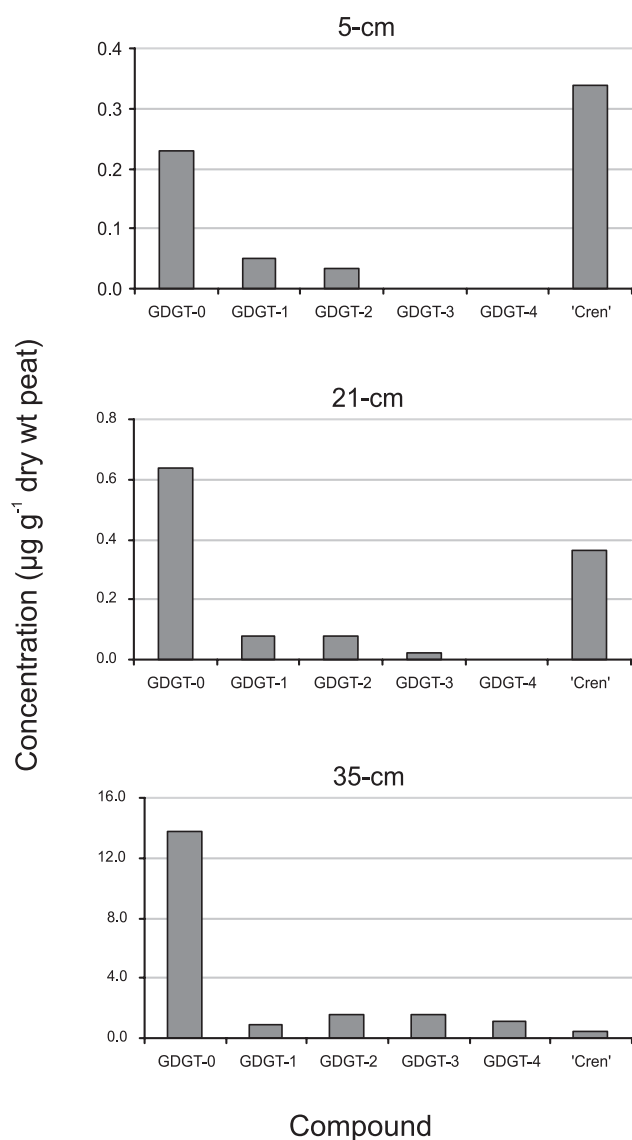
Figure 4.3: Relative distribution of GDGTs in samples from different depth intervals in the Saxnäs Mosse peat core. 'Cren' = crenarchaeol.

4.3. Results

HPLC/APCI-MS analyses of the peat core revealed the presence of 6 isoprenoid GDGTs (see Fig. 4.1 for structures). The most abundant is GDGT-0 followed by minor amounts of GDGTs containing 1 to 4 cyclopentane moieties and crenarchaeol. The last eluting peak in the HPLC chromatograms represents a mixture of GDGT-4 and crenarchaeol (Fig. 4.2).
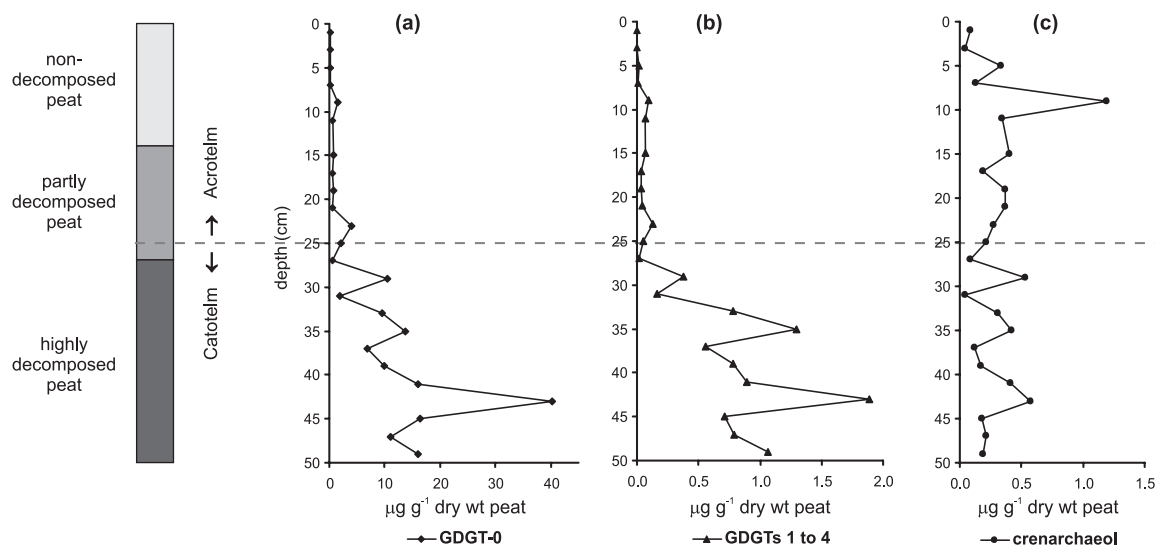
Figure 4.4: Concentrations of: (a) GDGT-0, (b) averaged GDGTs 1 to 4 and (c) crenarchaeol, versus depth in the Saxnäs Mosse peat (Sweden) accompanied with a schematic decomposition profile. The acrotelm is the zone in which the water table fluctuates and the catotelm is the zone of permanent water saturation. Note the difference in values on the x-axis.

If GDGT concentrations are plotted against depth, two separate trends can be distinguished (Figs. 4.3 and 4.4). First, GDGT-0 (Fig. 4.4a) and the cyclopentane containing GDGTs 1 to 4 (Fig. 4.4b) are present in low amounts in the upper part of the peat core and gradually increase in amount in the lower part. Concentrations of GDGT-0 increase from 0.3-0.4 μg g^{-1} dry wt peat to about 15 μg g^{-1} dry wt peat and concentrations of the cyclopentane containing GDGTs increase from near zero (ca. 0.05 μg g^{-1} dry wt peat) to concentrations around 1 μg g^{-1} dry wt peat. Not much variation is visible in the distribution of the cyclopentane containing GDGTs themselves, although there may be a very slight shift towards GDGTs with more pentane rings in the deeper samples (Fig. 4.3). A second, strikingly different trend is found in the crenarchaeol concentrations, which stay relatively constant throughout the whole core at about 0.3 μg g^{-1} dry wt peat (Fig. 4.4c). Those two different trends were further confirmed by a simple statistical test (Student's t-test) performed

on the data. Within a 99% confidence interval there is a significant change in concentrations of GDGT-0 and GDGTs 1 to 4 between the upper part (acrotelm) and the lower, continuously water saturated part of the profile, while there is no significant difference in the concentrations of crenarchaeol in these two parts of the peat core.

4.4. Discussion

The presence of an aerated top layer and an anoxic lower layer in the peat profile gives rise to two distinctive trends in GDGT abundance throughout the core. The crenarchaeol concentration remains approximately constant throughout both the oxic and the anoxic part of the profile (Fig. 4.4c). This GDGT is likely derived from Crenarchaeota, since crenarchaeol is considered as a diagnostic lipid for non-thermophilic Crenarchaeota present in marine and lacustrine environments (Sinninghe Damsté et al., 2002; Powers et al., 2004). Besides the oxic parts of the marine water column, crenarchaeol is also found in the anoxic water column of the Black Sea (Wakeham et al., 2003), suggesting that these aquatic Crenarchaeota may be facultative anaerobes. Thus, the relatively constant concentration of crenarchaeol in the peat profile can be explained by the presence of close relatives of the non-thermophilic aquatic Crenarchaeota, capable of thriving in both oxic and anoxic environments. Indeed, various phylogenetic studies have shown that new crenarchaeotal sequences from soils to some extent cluster together with marine planktonic Crenarchaeota (e.g., Buckley et al., 1998; Pesaro and Widmer, 2002; Ochsenreiter et al., 2003).

GDGT-0 and GDGTs 1 to 4 present in the oxygenated layer are most likely produced by non-thermophilic crenarchaeotal species as well, since their abundance relative to crenarchaeol in this part of the profile is comparable to the ratios found in aquatic Crenarchaeota (Schouten et al., 2000; Sinninghe Damsté et al., 2002). Those aquatic Crenarchaeota produce, depending on growth temperature (Schouten et al., 2002), about the same amounts of crenarchaeol and GDGT-0 and much smaller amounts of the cyclopentane containing GDGTs. However, the concentration of GDGT-0 in the anoxic lower part of the core increases substantially compared to crenarchaeol (Fig. 4.4a) and thus an additional source is expected here. As a number of methanogenic Euryarchaeota are known to biosynthesise GDGT-0 (Koga et al., 1993), they represent a likely source for the GDGT-0 found in this part of the peat core. In agreement with this, 16S rDNA of methanogenic Euryarchaeota is often found in the anoxic part of peat bogs (e.g., McDonald et al., 1999; Galand et al., 2002). Galand et al. (2002) found several sequences of methanogenic Euryarchaeota (related to members of Rice Cluster I) at 10 and 40 cm below the water table in a Finnish oligotrophic fen. Although a fen is by definition less acid than a bog, the water table level, the dominant *Sphagnum* moss vegetation and the oligotrophic character of the fen are comparable to our site.

The same interpretation may hold true for GDGTs 1 to 4, which are also predominantly found in the anoxic part of the core (Fig. 4.4b). It is very likely that the same group of organisms, methanogenic Euryarchaeota, produces both GDGT-0 and GDGTs 1 to 4, as the concentrations of these GDGTs co-vary. Analyses of the $\delta^{13}C$ values of the GDGTs can clarify if they derive from the same group of organisms or not, but unfortunately sample amounts were too low to perform such analyses on these samples. However, Pancost et al. (2003) determined the $\delta^{13}C$ values of the acyclic biphytane units, derived from GDGTs 0 and 1, and the monopentacyclic biphytane units, derived from GDGTs 1, 2 and 3, from an ancient peat bog after ether cleavage of the intact GDGTs. For the acyclic biphytane units, values vary between –24‰ and –31‰ and for the monopentacyclic biphytane units a more constant value between –35‰ and –36‰ was found. This suggested that at least two different (groups of) species within the methanogenic Euryarchaeota (probably utilising different substrates or slightly different metabolic pathways) are responsible for the production of GDGT-0 and GDGTs 1 to 4.

4.5. Conclusions

GDGT lipids provide a means to identify different archaeal communities in peat bogs. Non-thermophilic Crenarchaeota are suggested to be present in at least the oxygenated top part and possibly throughout the whole peat core, mainly producing GDGT-0 plus crenarchaeol and in lower amounts also cyclopentane-containing GDGTs. In the lower anoxic layer of the peat bog, these crenarchaeotal species are accompanied by groups of methanogenic Euryarchaeota, which produce predominantly GDGT-0, but also GDGTs 1 to 4.

Chapter 5

A novel proxy for terrestrial organic matter in sediments based on branched and isoprenoid tetraether lipids

Ellen C. Hopmans, Johan W.H. Weijers, Enno Schefuß, Lydie Herfort, Jaap S. Sinninghe Damsté and Stefan Schouten

Abstract

We propose a novel tracer for terrestrial organic carbon in sediments based on the analysis of tetraether lipids using HPLC/MS. Analysis of terrestrial soil and peats shows that branched tetraether lipids are predominant in terrestrial environments in contrast to crenarchaeol, the characteristic membrane lipid of non-thermophilic crenarchaeota, which is especially abundant in the marine and lacustrine environment. Based on these findings an index was developed, the so-called Branched and Isoprenoid Tetraether (BIT) index, based on the relative abundance of terrestrially derived tetraether lipids versus crenarchaeol. This BIT index was applied to surface sediments from the Angola Basin, where it was shown to trace the outflow of the Congo River. Furthermore, analyses of particulate organic matter from the North Sea showed relatively higher BIT indices in water column particulate organic matter near large river inputs. A survey of globally distributed marine and lacustrine surface sediments shows that the BIT index in these environments correlates with the relative fluvial input of terrestrial organic material making this index generally applicable. The new proxy allows the rapid assessment of the fluvial input of terrestrial organic material in immature sediments up to 100 Ma old.

5.1. Introduction

Large amounts of terrestrial organic carbon are annually transported from the continents to the oceans mainly by fluvial transport or, in lower amounts, by aeolian dust. They represent a large source for organic carbon in the marine environment (ca. 4×10^{14} g C/year, Schlesinger and Melack, 1981) and are thus an important part of the global carbon cycle. Information on the modes and distances of transport of terrestrial carbon allows the reconstruction of, for example, the proximity to continents and wind strengths. Hence, detailed knowledge on (past) variations in transport of terrestrial carbon to marine environments is of importance for reconstructing (past) carbon cycles.

Typically the relative amounts of terrestrial organic matter in marine sediments are determined by analyzing the ^{13}C content and C/N ratio of bulk organic matter (Hedges et al., 1997 and references cited therein). Present-day terrestrial organic matter tends to have a more ^{13}C-depleted content and a higher C/N ratio than marine phytoplanktonic organic matter. However, variations in ^{13}C contents of phytoplanktonic organic matter can be large (e.g., Deines, 1980) and terrestrial organic matter containing an important fraction of C_4-plants can have substantially enriched ^{13}C values (e.g., Deines, 1980). Furthermore, early diagenesis can significantly alter C/N ratios by, for example, selective loss of amino acids. Hence this approach can easily lead to erroneous interpretations of (changes in) the relative amounts of terrestrial organic matter in marine sediments.

An alternative approach is the analysis of specific molecular tracers for terrestrial organic matter and use them as a proxy for the terrestrial contribution to total sedimentary organic matter (Hedges et al., 1997). Long-chain odd-carbon-numbered *n*-alkanes are the most widely found terrestrial compounds in marine sediments and are derived from the surface waxes of terrestrial higher plant leaves (Eglinton and Hamilton, 1963). These compounds can be washed from the leaves by rain or eroded with soils and transported by rivers to the coastal marine environment. In addition, dust can ablate the waxes from leaves, thereby transporting them through the atmosphere to locations far from the coast (e.g., Gagosian et al., 1981; Poynter et al., 1989). Long-chain *n*-alkanes are therefore found in both coastal and open ocean sites (Hedges et al., 1997). The stable carbon isotopic composition of these *n*-alkanes allows to deconvolute sources of these *n*-alkanes and the reconstruction of vegetation belts on continents through time (e.g., Kuypers et al., 1999; Schefuß et al., 2003). Long-chain even-carbon-numbered fatty acids and *n*-alcohols are also derived from higher plants and are mainly fluvially transported (e.g., Meyers, 2003). Specific triterpenoids such as oleanene and taraxerol allow tracing specific plant inputs from gymnosperms and mangroves, respectively (e.g., Versteegh et al., 2004). Terrestrial organic components not directly amenable to gas chromatographic analysis are lignin and cutin, biopolymers which occur abundantly in vascular plant tissues (de Leeuw and Largeau, 1993) and are mainly fluvially transported (e.g., Goñi et al., 1997; Gordon and Goñi, 2003). Through cuprous oxide degradation reaction

products can be obtained from these biopolymers which are typical for different plants and tissues (see references in Hedges et al., 1997). By determining their stable carbon isotopic composition inferences can be made on the relative inputs of C_3 and C_4 plants in marine sediments (e.g., Goñi et al., 1997; Gordon and Goñi, 2003). Finally, reconstruction of terrestrial input is also often based on the relative abundance of C_{29} sterols compared to C_{27} and C_{28} sterols (Huang and Meinschein, 1976) since C_{29} sterols are dominant in terrestrial plants. However, C_{29} sterols have also shown to be ubiquitously occurring in marine algae (e.g., Volkman, 1986) and thus may not represent a pure terrestrial signal in marine sediments.

A large range of molecular proxies for terrestrial organic matter is thus available. However, quantification of the relative inputs of terrestrial carbon is difficult due to large variations in concentrations of compounds in the different plant materials. Also, terrestrially derived biomarkers have different degradation rates both compared to each other and to marine-derived compounds. For instance, we recently showed that preservation factors of long-chain *n*-alkanes, typical markers for terrestrial input, are substantially higher than those for long-chain alkenones, typical markers for prymnesiophyte algae (Hoefs et al., 2002; Sinninghe Damsté et al., 2002b). Hence, relative changes in the amounts of terrestrial *n*-alkanes compared to marine compounds may not only be due to changes in terrestrial contribution but also to changing oxygen exposure times.

An alternative approach to reconstruct terrestrial input into the marine environment is not to use a tracer derived from higher plants but from organisms thriving in soils and peats. For instance, Prahl et al. (1992) used diploptene in Washington coastal sediments as a tracer for soil organic carbon. Although this worked quite well in these sediments, general application of this tracer is made difficult by the fact that a number of marine bacteria also make diploptene or precursor compounds from which diploptene can be formed (e.g., Rohmer et al., 1984; Sinninghe Damsté et al., 2004).

The development of a HPLC/MS technique for the analysis of glycerol dialkyl glycerol tetraethers (GDGTs) (Hopmans et al., 2000) enabled us to recognize a group of non-isoprenoidal GDGTs (structures I, II, and III in Fig. 5.1) that was recently identified with 2D NMR techniques after isolation from a Dutch peat (Sinninghe Damsté et al., 2000). Its biological origin is as yet unclear but a survey of recent sediments indicates that it is derived from organisms living in the terrestrial environment (Schouten et al., 2000). In addition, we identified a structurally related isoprenoid GDGT of marine planktonic archaea, "crenarchaeol" (structure IV, Fig. 5.1, Sinninghe Damsté et al., 2002c). This compound occurs abundantly and ubiquitously in marine and lake sediments (e.g., Schouten et al., 2000; Schouten et al., 2002; Powers et al., 2004), the marine water column (e.g., Sinninghe Damsté et al., 2002a; Wakeham et al., 2003) and the only available uni-archaeal "culture" of the marine pelagic crenarchaeota, *Cenarchaeum symbiosum* (Sinninghe Damsté et al., 2002c). In marine sediments this biomarker is, together with GDGT V (a less specific GDGT but also

predominantly derived from planktonic archaea), probably the single most abundant component (Schouten et al., 2000).

Here we show that the amount of branched GDGTs compared to crenarchaeol in marine and lacustrine sediments, quantified in the so-called BIT index, is correlated with the relative amount of fluvial terrestrial input. This gives a new approach to reconstruct the fate of soil organic carbon, and thereby fluvial terrestrial input, in marine and lacustrine environments based on the analysis of GDGTs.
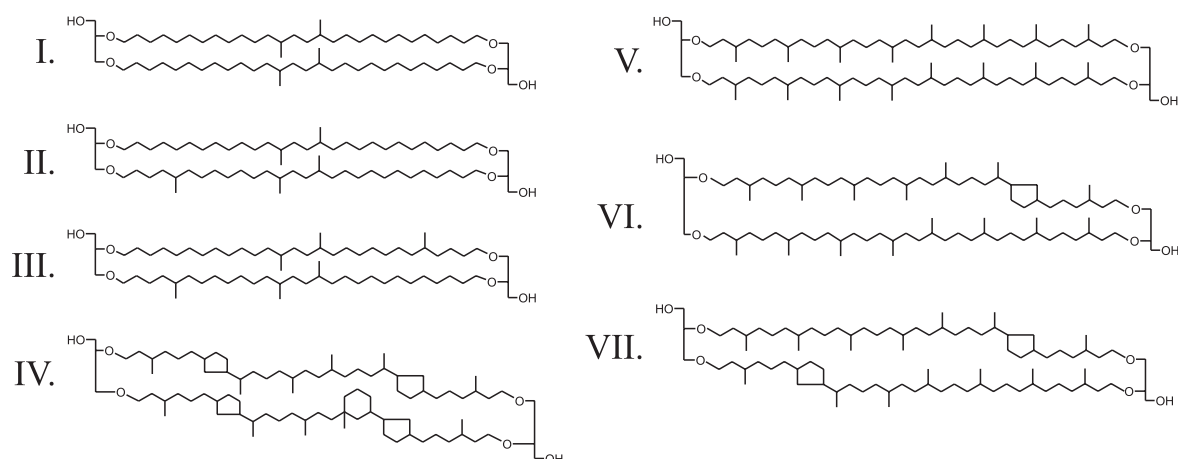
Figure 5.1: Structures of some GDGTs present in marine sediments, lakes and terrestrial soils and peats.

5.2. Methodology

5.2.1. Samples

Surface sediment samples representing the Congo river plume were collected during the RV Tyro cruise in the eastern South Atlantic during fall 1989 (Jansen et al., 1990). The box-cores were stored frozen at –20 °C and the uppermost 1-1.5 cm was used for analyses. The two samples from the estuary of the Congo River, 'Anker 24' and 'Anker 26', were taken as grab samples (Eisma et al., 1978) and stored as dried sediment in dark polyethylene containers at room temperature before analyses. Particulate organic matter from the southern North Sea was sampled during the CRENS cruise with the RV Pelagia in February 2003 by filtration of 40 l surface waters using 0.7-μm GFF filters. Particulate organic matter of the Wadden Sea water was sampled near the Mok Bay by filtration of 20 l surface waters using 0.7-μm GFF filters. Atmospheric dust was sampled off the coast of South-western Africa according to the procedure described by Schefuβ et al. (2003). Soil was collected from ca. 10 cm depth in a deciduous forest near De Koog on the island of Texel, The Netherlands.

5.2.2. GDGT analysis

Intact GDGTs were identified by high performance liquid chromatography/atmospheric pressure positive ion chemical ionization mass spectrometry (HPLC/APCI-MS) (Hopmans et al., 2000). Briefly, most sediments were ultrasonically extracted 3 times with methanol, 3 times with dichloromethane (DCM)/methanol (1:1, v/v), and 3 times with DCM and all extracts were combined to obtain a total extract. In most cases this total extract was subsequently separated using a column packed with Al_2O_3 to obtain an apolar and a polar fraction using hexane/dichloromethane (9:1, v/v) and dichloromethane/methanol (1:1, v/v) as eluents, respectively. An aliquot of either the dried total extract or the polar fraction was dissolved by sonication (10 min) in hexane/propanol (99:1, v/v). The resulting suspension was centrifuged (1 min, 3500 rpm) and the supernatant filtered through a 0.45-μm, 4-mm diameter PTFE filter prior to injection. Conditions for HPLC/MS analyses of the purified extracts were modified from Hopmans et al. (2000). Analyses were performed using an HP (Palo-Alto, CA, USA) 1100 series LC-MS equipped with an auto-injector and Chemstation chromatography manager software. Separation was achieved on a Prevail Cyano column (2.1 x 150 mm, 3 μm; Alltech, Deerfield, IL, USA), maintained at 30°C. Injection volumes varied from 1 to 5 μl. Tetraethers were eluted isocratically with 99% A and 1% B for 5 min, followed by a linear gradient to 1.8% B in 45 min, where A = hexane and B = propanol. Flow rate was 0.2 ml/min. After each analysis the column was cleaned by back-flushing hexane/propanol (9:1, v/v) at 0.2 ml/min for 10 min. Detection was achieved using atmospheric pressure positive ion chemical ionization mass spectrometry (APCI-MS) of the eluent. Conditions for APCI-MS were as follows: nebulizer pressure 60 psi, vaporizer temperature 400 °C, drying gas (N_2) flow 6 l/min and temperature 200 °C, capillary voltage -3 kV, corona 5 μA (~ 3.2 kV). Positive ion spectra were generated by scanning m/z 950-1450 in 1.9 s. Relative GDGT distributions were determined by integrating the summed peak areas in the respective $[M+H]^+$ and $[M+H+1]^+$ (protonated molecule and first isotope peak, respectively) traces of the GDGTs.

5.3. Results and discussion

5.3.1. Occurrence of branched GDGTs

All peat samples investigated contained, in addition to the ubiquitous and non-specific GDGT V, high amounts of branched GDGTs I-III. Interestingly, a soil sample obtained from a small deciduous forest located on the south-western part of Texel (the Netherlands) contained branched GDGTs I-II only (Fig. 5.2a). The absence of GDGT V in this soil suggests that the organisms that biosynthesize the branched GDGTs do not biosynthesize isoprenoid GDGTs such as GDGT V. Hence, in peats where GDGT V is found together with branched GDGTs I-III, the isoprenoid GDGT is likely derived from a different source, most likely methanogenic

archaea. This confirms the findings of Pancost et al. (2000) who found different stable carbon isotopic compositions for the branched and isoprenoid GDGTs. The presence of the branched GDGTs in the Texel soil suggests that this class of compounds can be used as a tracer for soil and peat organic matter.
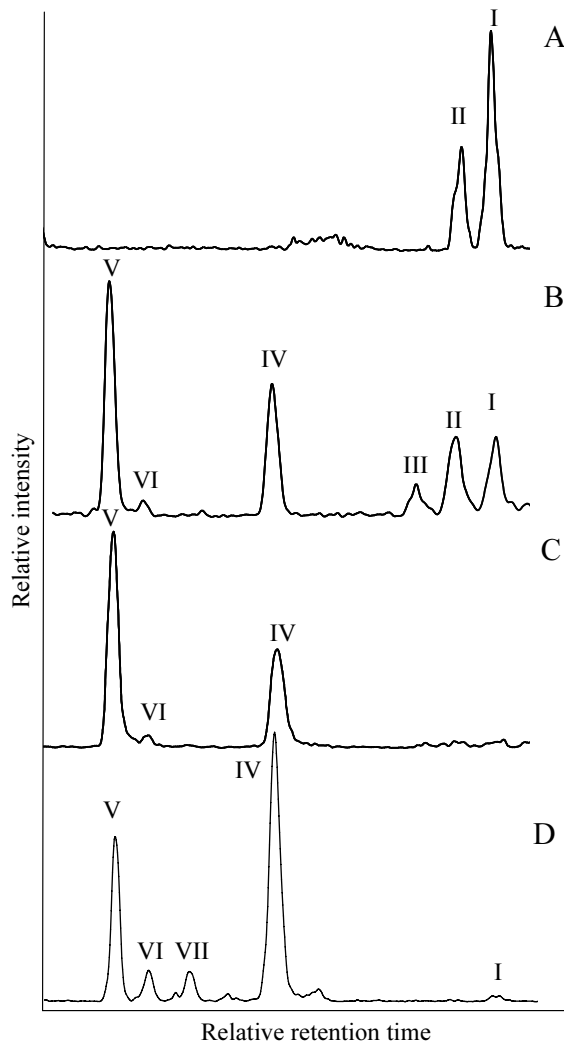
Figure 5.2: HPLC/MS base peak chromatograms of tetraether lipids in (a) soil from a deciduous tree forest, Texel, the Netherlands (b) surface sediment from the Mok Bay, Texel, the Netherlands (c) water column sample of the Wadden Sea and (d) core top sample from the Congo River basin. Roman numerals refer to structures in Fig. 5.1.

The branched GDGTs are also often found in coastal marine, open marine and lacustrine sediments. This could indicate that these compounds are not only produced by organisms living in soils and peats but also in marine and lake waters. However, analyses of water column samples in the Arabian Sea and the Black Sea distantly located from coasts and river input (Sinninghe Damsté et al., 2002a; Wakeham et al., 2003) did not reveal the presence of branched GDGTs. In addition, analysis of the GDGTs in surface sediment of the Mok Bay, a small inlet connected to the Wadden Sea, revealed high amounts of branched GDGTs I-III together with crenarchaeol (Fig. 5.2b). In contrast, analysis of water filtrates from the Wadden Sea revealed GDGT V and crenarchaeol as the dominant GDGTs (Fig. 5.2c). These results

strongly suggest that branched GDGTs are derived from organisms living in soils and peats and that they can be used as tracers for soil organic matter (Schouten et al., 2000; Sinninghe Damsté et al., 2000).

5.3.2. Branched and Isoprenoid Tetraether Index

Based on these observations, it is clear that the branched GDGTs present in marine and lacustrine sediments are derived from transport of terrestrial material. Crenarchaeol is the dominant compound in water column samples, in contrast to peats where crenarchaeol is only a minor compound, i.e., representing <1% of total GDGTs (Weijers et al., 2004). Thus, crenarchaeol in sediments is mainly derived from aquatic input. Hence, the two structurally similar types of GDGTs, branched GDGTs and crenarchaeol, represent terrestrial and marine organic matter sources, respectively. Based on this, we propose an index based on the relative abundance of these two types of GDGTs which is able to trace the relative amount of terrestrial organic carbon in open ocean, coastal marine and lake sediments. This Branched and Isoprenoid Tetraether (BIT) index is based on the relative abundance of branched GDGTs, representing terrestrial organic matter, and crenarchaeol, representing aquatic organic matter, and is defined as follows:

$$\mathbf{BIT} = \frac{[\mathbf{I} + \mathbf{II} + \mathbf{III}]}{[\mathbf{I} + \mathbf{II} + \mathbf{III}] + [\mathbf{IV}]} \qquad (1)$$

The roman numerals refer to the GDGTs indicated in Fig. 5.1. GDGT V was excluded from this novel index as it can originate from both marine and terrestrial sources (Schouten et al., 2000). In addition, GDGT V and some of its cyclisised derivatives are produced by methanogenic archaea (e.g., Koga et al., 1998) and anaerobic methane-oxidizing archaea (e.g., Pancost et al., 2001). This BIT-index, defined as above, can reach values ranging from 0, representing no branched GDGTs, to 1, representing no crenarchaeol.

To test the novel index, it was applied to core top sediments from the Angola Basin (eastern tropical Atlantic) near the mouth of the Congo River (Fig. 5.2d). Schefuβ et al. (2004) previously showed, based on organic carbon contents and bulk stable carbon isotopic composition (Fig. 5.3a), the extent of the fluvially transported terrestrial organic matter deposited by the Congo River in the Angola basin. A contour plot of the BIT index clearly follows the plume of the Congo River outflow into the Angola Basin (Fig. 5.3b), with BIT values ranging from 0 in open marine surface sediments to 0.91 for the sediments taken directly at the mouth of the Congo River. This plot is similar to the contour plot of the bulk stable carbon isotopic compositions of organic matter with ^{13}C depleted values near the Congo River mouth (Fig. 5.3b) (Schefuß et al., 2004). In contrast, the contour plot is quite different from that of the abundance of aeolian transported *n*-alkanes which shows a plume-like distribution below the main trade-wind trajectory originating from the coast of South-

western Africa (Fig. 5.3c) (Schefuß et al., 2004). This suggests that the BIT index does not trace aeolian transported terrestrial organic matter but that the index reflects primarily the fluvial transport of terrestrial organic matter. Further confirmation was obtained by the analysis of atmospheric dust obtained by air filtration near the West coast of Central Africa. HLPC/MS analysis revealed that GDGTs were below the detection level suggesting that they are not transported through the atmosphere.
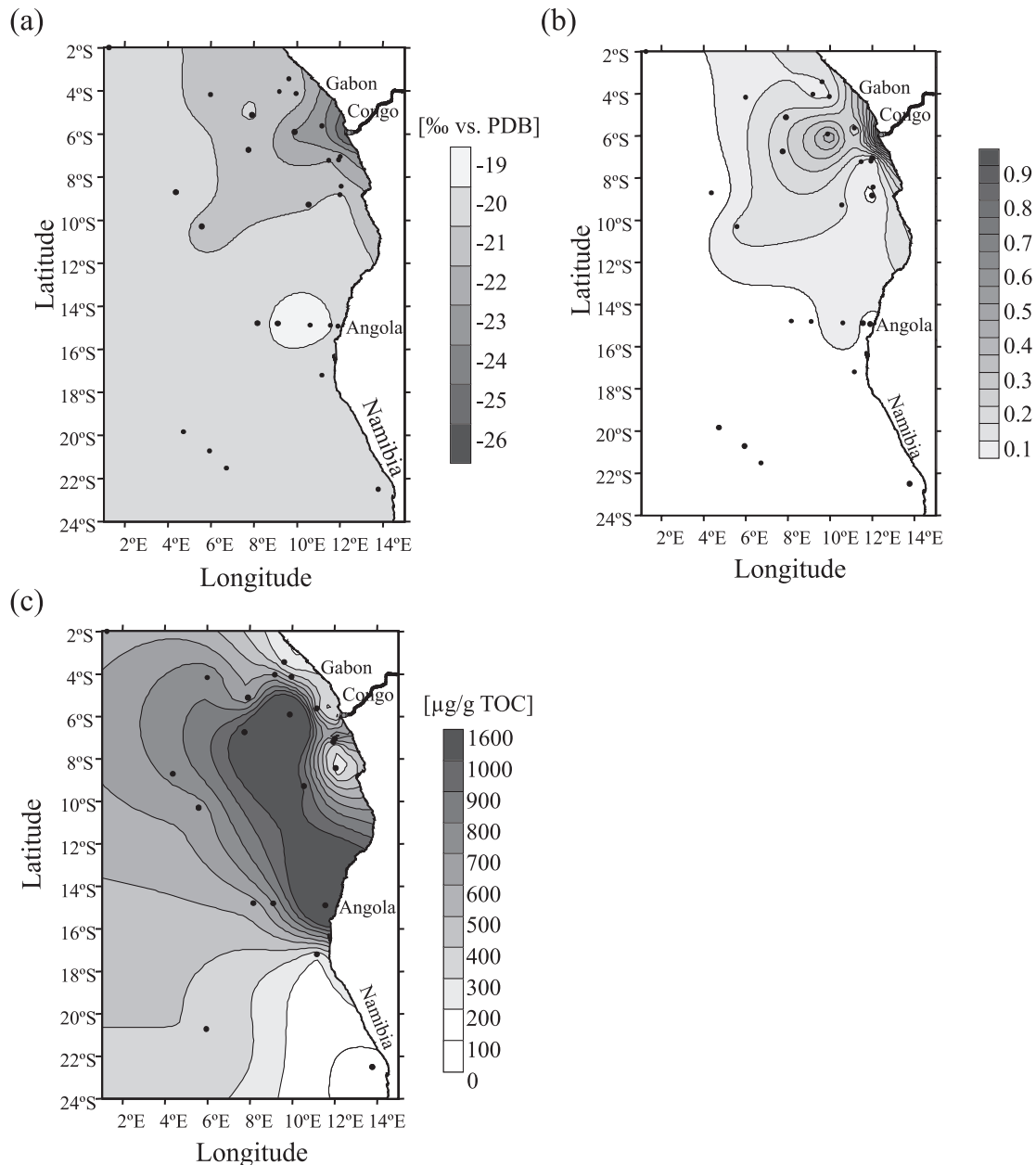
Figure 5.3: Contour plot of (a) $\delta^{13}C$ values of total organic carbon, (b) BIT index and (c) concentration of C_{25} to C_{33} odd-carbon-numbered *n*-alkanes from surface sediments of the eastern South Atlantic (north: Angola Basin with Congo River fan; south: Benguela upwelling system).

The BIT index was further tested by the analysis of particulate organic matter obtained from surface waters in the southern part of the North Sea. BIT values varied from 0 to 0.17 (Table 5.1). Interestingly, the highest BIT indices were found in surface waters at and south of the Frisian Front, an area where different water masses of the North Sea converge. These waters had significantly lower salinities testifying to a significant input of river water plume mainly from the rivers Thames and Humber (de Ruijter et al., 1987). Thus, in the southern North Sea the BIT index also traces fluvial input of terrestrial organic matter.

Table 5.1: BIT indices of particulate organic matter and salinities of surface waters in the southern North Sea

Location	Latitude	Longitude	Salinity (%)	BIT
Central Southern Bight	53° 00' N	03° 00' E	34.3	0.05
South of Frisian Front	53° 30' N	04° 30' E	30.7	0.17
Frisian Front	53° 42' N	04° 30' E	31.9	0.18
North of Frisian Front	54° 00' N	04° 30' E	34.2	0.00
Oyster Grounds	54° 30' N	04° 30' E	34.6	0.00
Dogger Bank	55° 00' N	03° 00' E	34.6	0.03

5.3.3. Global survey of BIT index

To test the general applicability of the BIT index we calculated BIT values for a range of Holocene marine and lake sediments, peats and a soil. The BIT values obtained (Fig. 5.4) span the whole range of possible values. The extreme situation is represented by sediments from the Peru Margin, the Aegean Sea and Ace Lake with a BIT value of 0, i.e., the branched GDGTs could not be detected. The results for the Peru margin sediments are in agreement with its location, which is far removed from any rivers and underlies a highly productive upwelling zone. Also, previous studies showed that the organic matter is completely dominated by organic matter of marine origin except for some terrestrial *n*-alkanes likely transported by aeolian dust (e.g., Farrington et al., 1988; McCaffrey et al., 1991). Similarly, the Aegean Sea is not located near major rivers. Several other sediments from open ocean settings contained only very low amounts of the terrestrial branched GDGTs, which resulted in low BIT values, ranging from 0.01 to 0.08. A relatively high BIT index of 0.22 was obtained for the Skagerrak (North Sea) sediment, but although this is a marine setting removed from the coast, van Dongen et al. (2000) also found relatively high amounts of fluvially transported terrestrial biomarkers. This suggests a relatively substantial influx of organic matter from rivers.

As expected, maximum BIT values of 0.98 to 1, i.e., no aquatic input, were found for the samples of terrestrial origin (samples 24-30; Fig. 5.4). The investigated lake sediments varied widely in BIT indices with values ranging from 0.01 to 0.93. The lowest BIT index was found

for Lake Issyk Kul, which is a high altitude lake in Kyrgyzstan surrounded by sparse vegetation and steep mountains. The other lakes had substantially higher BIT values, suggesting that the sedimentary organic matter contains a substantial allochtonous terrestrial component. For example, Lake Michigan sediment had a high BIT index of 0.60. Indeed, Meyers (2003) suggested based on organic geochemical parameters that sedimentary organic matter deposited during 1970-1980 in Green Bay, Lake Michigan, comprised a large fraction of allochtonous terrestrial organic matter. A BIT index of 0 was calculated for sediments from Antarctic Ace Lake due to the complete absence of terrestrial tetraether lipids. This suggests that the organisms producing GDGTs I-III may not live in Antarctic soils or that no soil organic matter is transported into the lake due to its near-permanent ice coverage. This is in agreement with the lack of any other terrestrial biomarker in Ace Lake sediments.
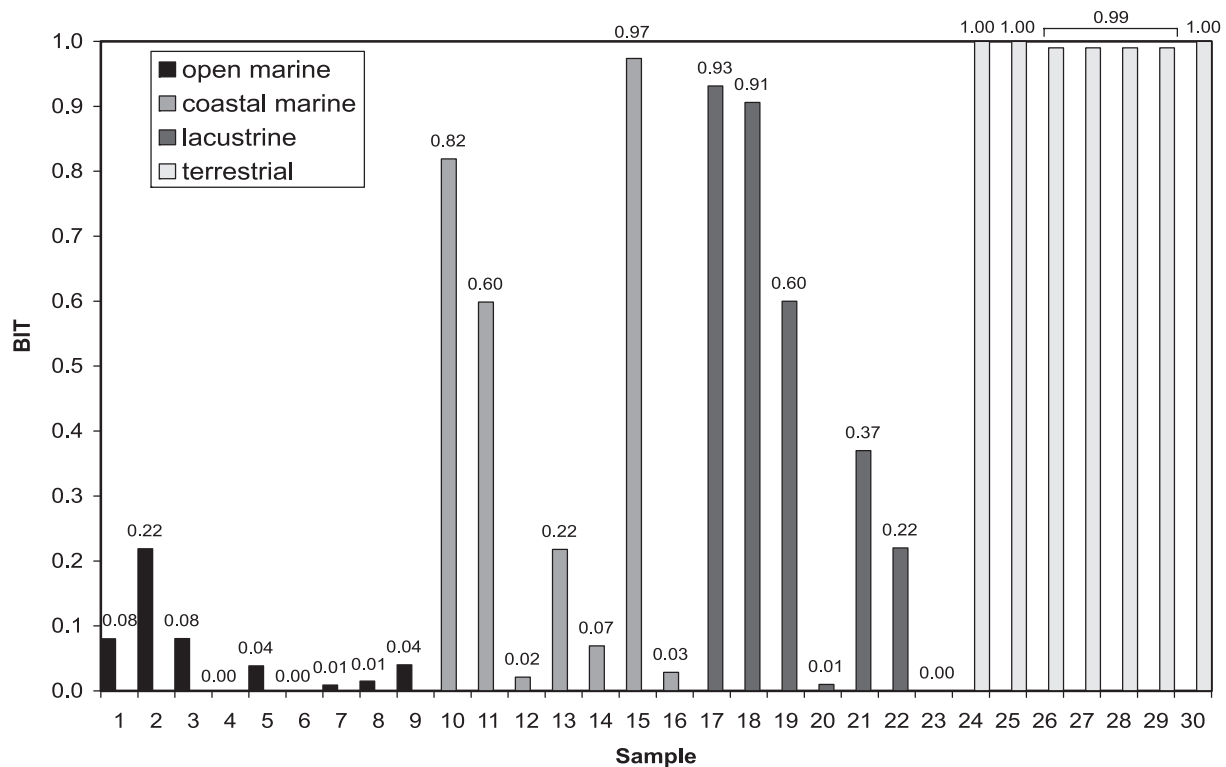
Figure 5.4: Bar graph showing the BIT index measured on Holocene sediments from a range of environments. Data points are from: 1. Black Sea, 2. Skagerrak (North Sea), 3. Arabian Sea, 4. Peru Margin, 5. Cariaco Basin, 6. Aegean Sea, 7. Goban Spur (North Atlantic), 8. and 9. Iberian Margin, 10. Wadden Sea (Netherlands), 11. Mok Bay (Texel), 12. Saanich Inlet (Canada), 13. Drammensfjord (Norway), 14. Skan Bay (Alaska), 15. Kyllaren Fjord (Norway), 16. Kau Bay (Indonesia), 17. Lake Paloma (Chili), 18. Siso Lake (Spain), 19. Lake Michigan (USA), 20. Lake Issyk Kul (Kyrgyzstan), 21.Lake Superior (USA), 22. Lake Malawi (Malawi), 23. Ace Lake (Antarctica), 24. Carbury peat (Ireland), 25. Meerstalblok peat (Netherlands), 26. Étang de la Gruère peat (Switzerland), 27. Bergvennen peat (Netherlands), 28 Saxnäs Mosse peat (Sweden), 29. Bear Meadows wetland (USA) 30. Texel forest soil (Netherlands).

In contrast to the investigated open marine settings, a larger variation was observed in the BIT index for the coastal marine settings, with values ranging from 0.02 to 0.97, probably reflecting the large differences in the delivery of terrestrial organic matter to these sediments. Especially the BIT values for the Saanich Inlet (0.02), Skan Bay (0.07), and Kau Bay (0.03) indicate low contributions of terrestrial organic matter. This is in agreement with previous investigations of the organic matter in these sediments (e.g., Middelburg et al., 1993; McQuoid et al., 2001). For example, McQuoid et al. (2001) reported, based on $^{13}C/^{12}C$ measurements, that the organic fraction in Holocene aged sediments of the Saanich Inlet is predominantly composed of marine material. Skan Bay is located in Alaska and due to the low temperatures, it is surrounded by little terrestrial vegetation and is covered by ice, similar to Antarctic Ace Lake. Finally, based on stable carbon isotopic compositions and biomarkers, Middelburg et al. (1993) concluded that organic matter in recent sediments in Kau Bay are predominantly of marine origin.

5.4. Implications

From these data it is clear that the BIT index is capable of estimating the relative amounts of terrestrial and aquatic organic matter in coastal marine, open ocean and lake sediments. There are several advantages to the use of tetraether lipids compared to other molecular and bulk proxies. Firstly, the terrestrial compounds have a similarly functionalized chemical structure as their isoprenoid counterparts and are therefore likely to be degraded at similar rates during sediment diagenesis. Secondly, the branched GDGTs are derived from seemingly ubiquitous organisms living in soils and peats and are thus not selective for particular vegetation types or climates. Similarly, crenarchaeol is ubiquitously present in the marine water column and marine and lake sediments (Schouten et al., 2000; Schouten et al., 2002; Powers et al., 2004). The BIT index is easily measured in a single GDGT analysis of sediment extracts and does not require specific chemical degradation procedures, as is the case for lignin analysis. Finally, we have found branched GDGTs in substantial amounts in sediments up to at least the Cretaceous, similar to crenarchaeol which has also been found up to the Cretaceous (Kuypers et al., 2001). Analysis of samples from the Cenomanian/Turonian at DSDP site 367 located near the coast of Morocco showed the presence of GDGTs I-III and with BIT values ranging from 0.03 to 0.27. Thus, reconstruction of terrestrial input in ancient immature marine sediments based on the BIT index may be possible at least up to the Cretaceous.

Chapter 6

Occurrence and distribution of tetraether membrane lipids in soils: Implications for the use of the TEX$_{86}$ proxy and the BIT index

Johan W.H. Weijers, Stefan Schouten, Otto C. Spaargaren and Jaap S. Sinninghe Damsté

Abstract

A diverse collection of globally distributed soil samples was analyzed for its glycerol dialkyl glycerol tetraether (GDGT) membrane lipid content. Branched GDGTs, derived from anaerobic soil bacteria, were the most dominant GDGTs present and were found in all soils. Isoprenoid GDGTs, membrane lipids of Archaea, were present as well, although in considerably lower concentrations. Crenarchaeol, a specific isoprenoid membrane lipid of the non-thermophilic Crenarchaeota, was also regularly detected and its abundance might be related to the pH of the soils. The detection of crenarchaeol in nearly all of the soil samples is the first report of this type of GDGT membrane lipid in soils and is in agreement with molecular ecological studies, confirming the widespread occurrence of non-thermophilic Crenarchaeota in the terrestrial realm. The fluvial transport of crenarchaeol and other isoprenoid GDGTs to marine and lacustrine environments could possibly bias the BIT-index, a ratio between branched GDGTs and crenarchaeol used to determine relative terrestrial organic matter (TOM) input. However, as crenarchaeol in soils is only present in low concentrations compared to branched GDGTs, no large effect is expected for the BIT-index. The fluvial input of terrestrial derived isoprenoid GDGTs could also bias the TEX$_{86}$, a proxy used to determine palaeosurface temperatures in marine and lacustrine settings and based on the ratio of cyclopentane-containing isoprenoid GDGTs in marine and lacustrine Crenarchaeota. Indeed, it is shown that a substantial bias of TEX$_{86}$ reconstructed sea and lake surface temperatures can occur if TOM input is high, e.g., near large river outflows.

6.1. Introduction

Culture independent molecular ecological techniques have shown that the Archaea, comprised of the Kingdoms of Crenarchaeota, Euryarchaeota and Korarchaeota, inhabit a widespread diversity of environments from extremophilic to mesophilic settings. In mesophilic environments, Archaea occupy diverse settings such as marine and lacustrine water columns and sediments (e.g., DeLong et al., 1994; MacGregor et al., 1997; Schleper et al., 1997; Vetriani et al., 1999; Jurgens et al., 2000; Karner et al., 2001; Keough et al., 2003), peat bogs, wetlands and soils (e.g., Buckley et al., 1998; Ochsenreiter et al., 2003; Sizova et al., 2003; Kotsyurbenko et al., 2004) and the deep subsurface (Takai et al., 2001). Despite being ubiquitous, only a limited number of archaeal cultures is available, mostly thermophiles and methanogens, one 'symbiont culture' of a mesophilic Crenarchaeota: *Cenarchaeum symbiosum*, an archaeon living in symbiosis with the marine sponge *Axinella mexicana* (Preston et al., 1996) and a nitrifying crenarchaeote isolated from a sea aquarium (Könneke et al., 2005).

From most of these cultures it is known that Archaea synthesize characteristic isoprenoid glycerol dialkyl glycerol tetraether (GDGT) membrane lipids. Archaeal GDGT membrane lipids can, therefore, provide additional information on the presence and diversity of the archaeal community. Archaeal GDGT membrane lipids have been found predominantly in wetland environments, like peat bogs (Pancost et al., 2000; Schouten et al., 2000; Pancost and Sinninghe Damsté, 2003; Weijers et al., 2004), where they are most likely derived from methanogenic Euryarchaeota (Pancost et al., 2000), and in marine environments, where they occur ubiquitously (Schouten et al., 2000). More recently, archaeal GDGT lipids have also been reported in sediments of some large lakes (Powers et al., 2004). In marine and lacustrine environments, the GDGT lipids are most likely derived from non-thermophilic pelagic Crenarchaeota (i.e., group 1.1 Crenarchaeota; DeLong, 1998), since they always comprise a unique GDGT lipid, crenarchaeol (**VI**; see appendix at the end of this chapter for structures), containing an additional cyclohexyl moiety. This compound is considered a biomarker for the group 1.1 Crenarchaeota as it has only been found in *Cenarchaeum symbiosum* (Sinninghe Damsté et al., 2002b) and not in thermophilic or methanogenic Archaea. Another recently discovered group of GDGT membrane lipids, containing branched instead of isoprenoid alkyl chains, is found mainly in peat bogs (Schouten et al., 2000; Sinninghe Damsté et al., 2000; Pancost and Sinninghe Damsté, 2003; Weijers et al., 2006a), but also in coastal marine sediments (Hopmans et al., 2004) and in lake sediments (Powers et al., 2004). Because of the branched alkyl chains and the bacterial 1,2-di-*O*-alkyl-*sn*-glycerol stereo configuration at the C-2 position of the glycerol backbone, those tetraethers are most likely of bacterial rather than archaeal origin (Weijers et al., 2006a).

Based on these GDGT membrane lipids, two proxies have recently been developed; the TEX_{86} sea surface temperature (SST) proxy (Schouten et al., 2002), recently also adapted for

application in lakes (Powers et al., 2004), and the Branched versus Isoprenoid Tetraether (BIT) index, a proxy for the relative fluvial input of terrestrial organic matter (TOM) in the marine environment (Hopmans et al., 2004). The TEX$_{86}$ SST proxy is based on the relative distribution of cyclopentane-containing isoprenoid GDGT lipids (**II-IV**, **VI'**) in the membranes of non-thermophilic pelagic Crenarchaeota. This distribution pattern has been shown to be primarily dependent on growth temperature (Wuchter et al., 2004). The BIT-index represents the ratio between crenarchaeol (**VI**) and three branched GDGT lipids (**VII-IX**) in marine and lacustrine sediments. Based on a rapid decrease in the concentration of branched GDGTs with increasing distance from the Congo River outflow (eastern tropical Atlantic Ocean) (Hopmans et al., 2004) and the detection of branched GDGTs in river water samples from the river Rhine, the Netherlands (Herfort et al., 2006), it is assumed that branched GDGTs are only terrestrially produced and fluvially transported to lakes and oceans. The fact that branched GDGTs are detected in many different coastal areas suggests that those compounds are ubiquitous in the terrestrial realm. Branched GDGTs on land, however, have so far only been reported in a few west-European peat bogs (Schouten et al., 2000; Sinninghe Damsté et al., 2000; Pancost and Sinninghe Damsté, 2003; Weijers et al., 2006a) and one Dutch soil (Hopmans et al., 2004). In fact, the occurrence of both branched and isoprenoid GDGT membrane lipids in soils has not been investigated in any detail yet. So far, Gattinger et al. (2003) have reported the presence of GDGTs **I-V** in one bulk soil sample composed of different soil types and Hopmans et al. (2004) have detected branched GDGTs **VIII** and **IX** in a forest soil from the Netherlands. The aim of the current study was, therefore, to investigate the distribution of GDGT membrane lipids in soils in more detail and to discuss their possible implications on the use of the BIT-index and TEX$_{86}$ proxy. To achieve this, a wide variety of globally distributed soils was investigated for their GDGT membrane lipid content.

6.2. Material and methods

6.2.1. Sample collection

To cover a wide diversity of soils, 58 samples from 26 globally distributed locations with different land use and vegetation patterns, and different organic contents (C$_{org}$) and pH values, were obtained (Table 6.1). Most soils were collected from the World Soil Database collection of the International Soil Research and Information Centre (ISRIC) in Wageningen, the Netherlands. They were obtained with hand auguring equipment during different field trips over the last decades. Although not sterilized, they have been stored dry and dark at room temperature and any biological activity since then, therefore, is assumed to be negligible. Samples of two soils from the island of Texel (the Netherlands) and one soil from Scotland were taken in summer 2000 and 2004, respectively, and freeze dried prior to further preparation.

Table 6.1: Land use, location, TOC and pH values of the soils analysed in this study

Sample	Landuse/vegetation	Latitude	Longitude	Altitude (m)	Depth (cm) [a]	C-org [b]	pH [b]
Alaska-17	alluvial terrace	64:52 N	147:50 W	ca. 200	0-28 (2)	4.0-3.1	7.1-7.3
Cameroon-1	coffee farm	4:14 N	9:20 E	1200	0-55 (2)	3.0-0.5	6.4-6.1
Canada-17	cropland (cleared forest)	49:57 N	98:11 W	256	0-70 (4)	n.d. [c]	n.d.
France-15	semi-natural grassland, grazed	45:03 N	2:33 E	1080	0-90 (4)	6.0 [d]	4.7-5.1
Gabon-1	tropical evergreen forest	0:31 N	12:48 E	530	0-65 (3)	3.3-0.6	3.3-4.2
Gabon-2	savannah with parts of forest	1:31 S	14:07 E	640	6-15 (1)	0.2	5.3
Gabon-3	herbs and grasses after burning	1:41 S	13:35 E	350	0-25 (2)	5.3-3.5	4.7-4.8
Gabon-4	grassland	2:13 S	11:32 E	215	0-19 (2)	2.7-1.0	5.3-5.2
Gabon-5	semi-deciduous shrub	2:21 S	11:23 E	150	0-20 (1)	2.2	5.1
Gabon-6	grassland	0:31 S	10:17 E	150	0-25 (2)	2.5-0.6	5.9-5.6
Ghana-2	coastal savannah grassland	5-7 N	ca. 0	27	0-24 (2)	0.3-0.2	6.0-5.7
Greece-13	deciduous forest	40:30 N	23:33 E	600	0-3 (1)	n.d.	5.4
Greenland-05	tundra	65:37 N	37:40 W	ca. 500	0-35 (2)	n.d.	n.d.
Hawaii-10	semi-natural grassland, grazed	22:4 N	159:24 W	180	0-64 (2)	4.0-2.2	5.1-5.4
Iceland-6	heath and mosses, grazed	65:21 N	20:53 W	ca. 100	5-30 (2)	6.6-5.7	6.1-6.5
Ireland-9	grazed shrubland	53:54 N	7:48 W	50	0-40 (2)	24.0-0.6	3.8-4.6
Italy-1	grazed woodland	39:40 N	16:09 E	500	0-10 (1)	2.9	6.2
Nigeria-15	grazed grassland in delta	5:18 N	6:38 E	2	0-55 (4)	3.1-0.1	4.4-5.0
Nigeria-19	semi deciduous forest	6:37 N	3:30 E	35	0-60 (2)	2.2-0.6	7.3-7.4
Scotland	grazed pasture grassland	55:0 N	3:6 W	0	0-10 (1)	n.d.	n.d.
South-Africa-7	grassland with acia trees	29:47 S	30:41 E	765	0-60 (3)	1.8-0.7	5.5
Spain-7	semi-natural grassland, grazed	38:59 N	6:20 W	260	0-15 (2)	3.9-0.7	5.5-5.1
Sweden-4	grassland, cultivated pasture	55:49 N	14:04 E	80	0-35 (2)	0.92	7.7
Texel-1	coniferous forest	53:04 N	4:44 E	5	0-10 (1)	n.d.	n.d.
Texel-2	deciduous forest	53:04 N	4:44 E	5	0-10 (1)	n.d.	n.d.
Zaire-1	evergreen forest	0:52 N	24:28 E	440	0-150 (5)	n.d.	3.9-4.3
Zaire-2	rubber plantation	0:46 N	24:26 E	460	0-30 (2)	1.26	4.1-4.4

[a] between brackets the number of depth intervals of which a sample is analysed

[b] range from uppermost to lowermost depth interval

[c] n.d., not determined

[d] value of the upper layer

6.2.2. Sample preparation

The samples were extracted with a solvent mixture of dichloromethane (DCM):methanol (9:1, v/v) three times for 5 min using an accelerated solvent extractor (ASE 200, Dionex) at 100 ºC and approximately $7.6 \; 10^6$ Pa. Each total extract was evaporated to near dryness using a rotary evaporator under near vacuum and separated over an activated Al_2O_3 column using hexane:DCM (1:1, v/v) and DCM:methanol (1:1, v/v) solvent mixtures. The latter fraction, containing the GDGTs, was dried under a continuous N_2 flow, ultrasonically dissolved in a hexane:propanol (99:1, v/v) solution at a concentration of ca. 2 mg ml^{-1} and filtered over a 0.45 μm PTFE filter (Alltech) prior to analysis.

6.2.3. Analysis

Samples were analyzed by high performance liquid chromatography / atmospheric pressure chemical ionization – mass spectrometry (HPLC/APCI-MS), according to Hopmans et al. (2000) with minor modifications. Analyses were performed on an Agilent 1100 series / 1100

MSD series machine, equipped with auto-injection system and HP-Chemstation software. Separation was achieved on a Prevail Cyano column (150 mm x 2.1 mm, 3 μm; Alltech). The flow rate of the hexane:propanol (99:1, v/v) eluent was 0.2 ml min^{-1}, isocratically for the first 5 min, thereafter with a linear gradient to 1.8% propanol in 45 min. Injection volume of the samples was 10 μl. In order to enable detection of low concentrations of GDGTs, MS-analyses were performed in a single ion monitoring (SIM) mode, which selectively scans for the masses of the compounds of interest. Quantification of the GDGT compounds was achieved by integrating the peak areas in the $[M+H]^{+}$ ion trace (i.e., protonated molecule) and comparing these to an external calibration curve prepared with known amounts of pure crenarchaeol (**VI**). A correction was made for the branched GDGTs (**VII-IX**), as their molecular mass is lower than that of crenarchaeol (**VI**). BIT indices were calculated following the equation by Hopmans et al. (2004):

$$\text{BIT-index} = \frac{[\mathbf{VII} + \mathbf{VIII} + \mathbf{IX}]}{[\mathbf{VII} + \mathbf{VIII} + \mathbf{IX}] + [\mathbf{VI}]} \tag{1}$$

The TEX$_{86}$ was calculated as follows (Schouten et al., 2002):

$$\text{TEX}_{86} = \frac{[\mathbf{III} + \mathbf{IV} + \mathbf{VI'}]}{[\mathbf{II} + \mathbf{III} + \mathbf{IV} + \mathbf{VI'}]} \tag{2}$$

The TEX$_{86}$ was converted into temperature according to the empirically derived formula given by Schouten et al. (2002):

$$\text{T (}^{\circ}\text{C)} = \frac{\text{TEX}_{86} - 0.28}{0.015} \tag{3}$$

An alternative TEX$_{86}$ proxy, the TEX$_{86}$', was applied by Sluijs et al. (2006) in order to reduce the influence of terrestrial derived isoprenoid GDGTs and is defined as:

$$\text{TEX}_{86}' = \frac{[\mathbf{III} + \mathbf{VI'}]}{[\mathbf{II} + \mathbf{III} + \mathbf{VI'}]} \tag{4}$$

The TEX$_{86}$' was converted into temperature with the formula given by Sluijs et al. (2006):

$$\text{T' (}^{\circ}\text{C)} = \frac{\text{TEX}_{86}' - 0.20}{0.016} \tag{5}$$

Table 6.2: Concentration (ng g^{-1} dry weight soil) of GDGT lipids with BIT-index

Sample	Depth (cm)	I	II	III	IV	VI	VI'	VII	VIII	IX	BIT-index
Alaska-17	0-20	22	9.1	7.0	2.7	34	1.1	17	33	15	0.66
	20-28	2.8	3.1	2.1	0.9	9.7	0.2	25	43	15	0.90
Cameroon-1	0-15	1.0	0.3	0.6	0.0	8.6	1.7	0.6	5.6	26	0.82
	38-55	1.8	1.8	3.5	2.9	0.2	0.0	0.0	0.6	6.1	0.98
Canada-17	0-15	10	3.1	3.9	2.7	25	2.9	19	35	13	0.73
	15-22	6.7	2.5	3.7	2.3	20	2.6	18	31	11	0.74
	44-64	2.3	1.3	2.0	1.5	10	1.2	26	44	17	0.89
	64-70	3.4	2.5	4.4	2.8	22	1.7	55	80	32	0.88
France-15	0-8	244	38	22	5.6	106	5.3	165	724	722	0.94
	8-32	57	24	29	7.6	35	1.9	29	169	188	0.92
	32-50	46	25	25	4.4	12	1.3	25	128	139	0.96
	50-90	30	18	23	4.5	3.8	0.6	4.7	28	46	0.95
Gabon-1	0-7	10	3.9	5.7	4.3	16	6.1	1.8	18	162	0.94
	7-20	3.4	1.2	1.5	1.4	3.6	1.4	0.3	4.3	53	0.95
	50-65	1.4	1.0	1.4	2.1	0.5	0.1	0.0	0.6	6.6	0.95
Gabon-2	6-15	0.4	0.1	0.1	0.1	0.3	0.0	0.0	0.1	6.1	0.96
Gabon-3	0-10	1.4	0.6	0.8	0.4	1.9	0.1	0.0	2.9	155	0.99
	10-25	1.3	0.7	0.9	0.6	0.9	0.1	0.0	0.5	32	0.98
Gabon-4	0-10	1.8	0.4	0.3	0.2	2.2	0.1	0.0	2.3	62	0.97
	10-19	0.7	0.3	0.2	0.2	0.1	0.0	0.0	0.5	19	1.00
Gabon-5	0-20	2.5	0.4	0.3	0.2	0.1	0.0	0.0	0.7	25	1.00
Gabon-6	0-5	2.2	1.7	2.3	2.0	26	1.5	0.5	6.4	51	0.74
	10-25	1.1	0.9	1.0	0.6	2.5	0.4	0.0	0.7	22	0.92
Ghana-2	0-10	0.6	0.2	0.7	0.3	5.4	0.3	0.0	0.2	17	0.80
	10-24	0.0	0.1	0.2	0.1	2.1	0.1	0.0	0.0	8.5	0.84
Greece-13	0-3	97	0.0	0.0	0.0	4.5	0.0	21	98	123	0.98
Greenland-05	0-5	0.0	0.0	0.0	0.0	0.9	0.0	16	45	35	0.99
	5-35	1.1	0.0	0.0	0.0	0.8	0.0	19	89	99	1.00
Hawaii-10	0-35	2.9	1.5	1.7	1.0	6.8	0.5	0.5	10	144	0.96
	35-64	5.4	4.6	7.4	5.3	1.2	0.1	0.4	6.9	60	0.98
Iceland-6	5-15	17	6.0	4.8	3.2	21	0.0	217	728	459	0.99
	17-30	79	8.8	13	2.7	51	1.2	471	1261	732	0.98
Ireland-9	0-7	99	10	15	13	7.0	0.0	102	971	1389	1.00
	7-40	16	1.4	1.4	0.9	0.9	0.0	3.4	42	79	0.99
Italy-1	0-10	5.1	1.2	1.0	0.2	0.9	0.1	5.0	23	24	0.98
Nigeria-15	0-12	4.1	1.9	2.2	2.4	0.4	0.0	0.0	1.9	92	1.00
	12-25	11	5.1	7.0	11	0.3	0.1	0.0	1.1	72	1.00
	25-37	2.1	1.5	2.1	3.0	0.2	0.0	0.0	0.3	19	0.99
	37-55	0.7	0.7	0.9	1.2	0.1	0.0	0.0	0.1	2.8	0.97
Nigeria-19	0-25	2.4	0.6	1.0	0.9	19	4.8	0.5	4.5	12	0.52
	25-60	0.5	0.1	0.2	0.3	3.0	0.5	0.0	0.7	5.9	0.74
Scotland	0-15	20	3.1	2.7	0.9	15	0.9	25	148	151	0.95
South Africa-7	0-10	2.2	0.0	0.0	0.0	0.8	0.1	0.0	2.1	16	0.97
	10-20	0.8	0.2	0.2	0.1	0.4	0.0	0.0	1.6	23	0.99
	25-60	0.8	0.4	0.6	0.2	0.3	0.0	0.0	0.4	4.6	0.95
Spain-7	0-2	4.0	0.4	0.4	0.0	2.7	0.2	4.8	28	21	0.95
	2-15	0.8	0.2	0.3	0.0	1.1	0.1	0.5	4.5	4.3	0.90
Sweden-4	0-15	12	1.0	1.2	0.9	9.5	0.9	3.3	5.8	2.5	0.55
	17-35	0.7	0.2	0.5	0.2	1.5	0.2	0.9	2.0	1.7	0.75
Texel-1	0-15	4.0	5.0	1.0	0.0	0.8	0.0	4.5	48	75	0.99
Texel-2	0-15	4.2	2.2	1.0	0.0	0.3	0.0	10	139	249	1.00
Zaire-1	0-15	7.0	1.9	2.6	1.7	8.4	2.2	0.7	10	112	0.95
	15-32	2.5	0.9	1.3	1.2	1.8	0.3	0.0	1.1	21	0.94
	40-70	1.6	0.9	1.4	1.7	0.6	0.1	0.0	0.3	7.7	0.94
	80-110	1.6	1.4	2.1	2.8	1.0	0.1	0.0	0.2	4.3	0.85
	120-150	3.5	1.8	2.9	2.9	1.7	0.1	0.0	0.4	5.3	0.81
Zaire-2	0-8	1.7	0.6	0.6	0.4	1.1	0.1	0.0	2.7	113	0.99
	10-30	0.6	0.3	0.4	0.4	0.4	0.1	0.0	0.7	16	0.98

See Appendix for structures.

6.3. Results

The isoprenoid and branched GDGT membrane lipid content of the soils was determined by HPLC/APCI-MS analysis (Table 6.2). Branched GDGTs dominate the soils, especially GDGT **IX** and to a lesser extent also **VIII** (e.g., Fig. 6.1), which are found in concentrations ranging from 10 to 1000 ng g^{-1} dry weight soil. Branched GDGT **VII,** however, is only present in considerable lower concentrations (0-100 ng g^{-1}). The isoprenoid GDGTs **I** and **VI** (crenarchaeol) are virtually always present in the soils and concentrations vary roughly from 1 to 100 ng g^{-1}. The cyclopentane-containing isoprenoid GDGTs **II-IV** are usually present in low amounts and sometimes below detection limit, with concentrations between 0 and 10 ng g^{-1}. GDGT **VI'**, a regio-isomer of **VI** (crenarchaeol), was detected in about half of the soils at concentrations generally below 2 ng g^{-1}. Only traces of GDGT **V** seem to be present and they could not be quantified as GDGT **VI** (crenarchaeol) co-elutes and the isotope peaks of crenarchaeol interfere in the quantification of GDGT **V**.
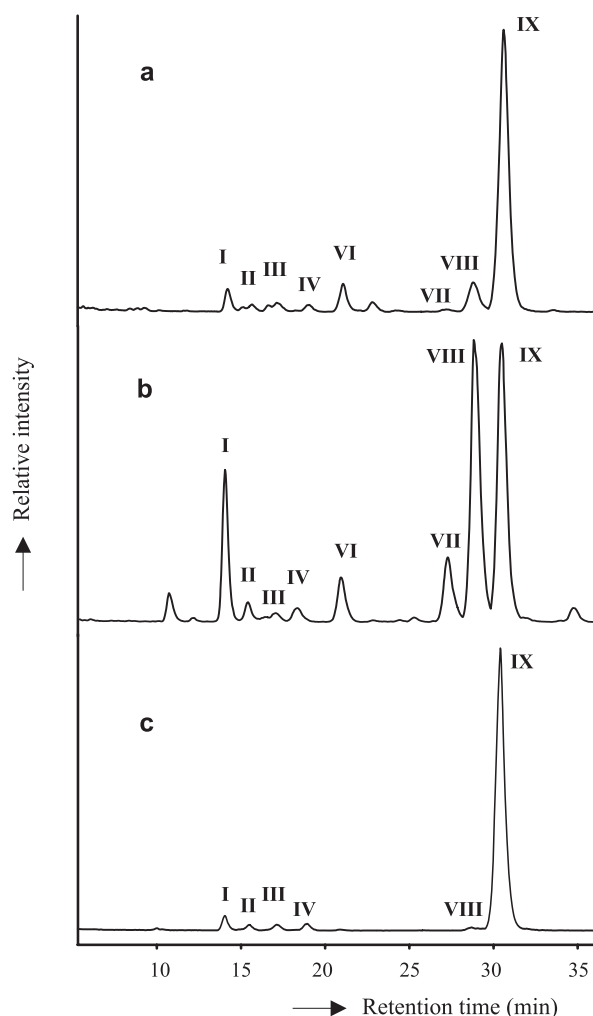
Figure 6.1: HPLC-MS base peak chromatograms of three soils (top sections) from (a) Gabon-1, (b) France-15 and (c) Nigeria-15, showing the relative GDGT distribution.
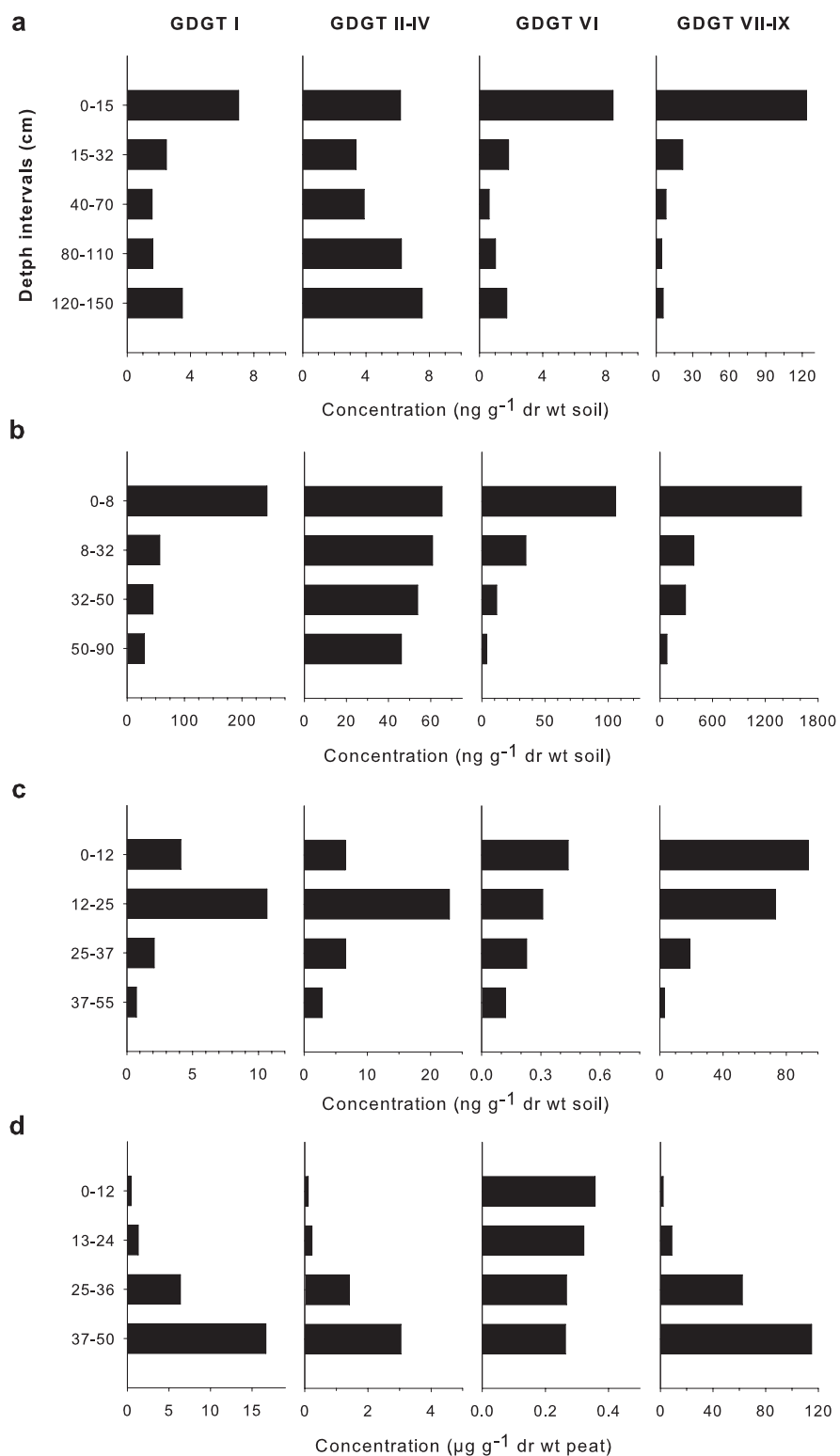
Figure 6.2: Depth profiles of the different GDGTs in soils from (a) Zaire-1, (b) France-15 and (c) Nigeria-15 and of (d) the Saxnäs Mosse peat bog, Sweden (data from Weijers et al., 2004; 2006a). Note the different unit used for the horizontal axis in profile (d).

At first sight, concentrations of GDGTs seem to be lower in soils from tropical areas (Table 6.2). It should be noticed, however, that GDGT concentrations are reported in ng g^{-1} dry weight soil. If concentrations are calculated as µg g^{-1} TOC, this difference is less apparent, as TOC contents of some of the non-tropical soils can be as high as 24% (e.g., Ireland), whereas that of tropical soils is lower (Table 6.1).

For three locations (Zaire-1, France-15 and Nigeria-15) a GDGT concentration profile with depth, down to 150, 90 and 55 cm, respectively, was obtained (Fig. 6.2a-c). Although there are differences in the absolute amounts of the different branched GDGTs (**VII-IX**), their distribution pattern is the same in each depth interval and therefore their concentrations are summed and plotted in one graph. Concentrations of the branched GDGTs (**VII-IX**) are clearly highest in the uppermost horizon and decrease rapidly with depth at all three locations. Also the profiles of GDGT **VI** (crenarchaeol) show a decrease from the top horizon downward, although in the Zairian profile (Fig. 6.2a) concentrations stabilize or even increase slightly again in the deeper intervals. Concentrations of GDGT **I** generally decrease with depth, although concentrations in the Zairian profile seem to increase slightly again in the deeper part (Fig. 6.2a) and in the Nigerian profile a clear peak in the second depth interval is visible (Fig. 6.2c). Similar to the branched GDGTs, concentrations of the cyclopentane-containing isoprenoid GDGTs (**II-IV**) are summed and plotted in one graph. These concentrations are rather invariable in the Zairian and French profile, although a slight increase (Zaire; Fig. 6.2a) or decrease (France; Fig. 6.2b) is noticeable. In the Nigerian profile (Fig. 6.2c) a clear maximum for GDGTs **II-IV** is present in the second depth interval, which resembles that of GDGT **I**.

6.4. Discussion

6.4.1. GDGTs in soils
6.4.1.1. Branched GDGTs *VII-IX*
Branched GDGTs (**VII-IX**) were found in every soil analyzed and appear to be the most abundant type of GDGT in soils (Fig. 6.1, Table 6.2). Their concentration is highest in the upper soil horizon and decreases rapidly with depth (Fig. 6.2a-c). This is in contrast with peat bogs, where concentrations of branched GDGTs increase with depth and clearly are highest in the anoxic part of the profile (Fig. 6.2d) (Weijers et al., 2006a). From this depth profile in peat bogs it was suggested that the bacteria producing the branched GDGTs are anaerobic micro-organisms, possibly involved in organic matter mineralization (Weijers et al., 2006a). In this deeper anoxic part of the peat bogs enough substrate is available for these microbes. In the deeper soil layers this might not be the case as TOC concentrations decrease substantially with depth (Table 6.1), which might reduce the abundance of branched GDGT-producing bacteria. The branched GDGT-producing bacteria in the upper soil layers and in the upper

zone of peat bogs might be facultative aerobes, but more likely thrive in anoxic micro habitats in (water filled) pores of the soils. A similar phenomenon has been observed for anaerobic methanogenic Euryarchaeota in a tundra soil. These Archaea became more abundant a few days after anoxic incubation of the soil, improving the conditions of growth (West and Schmidt, 2002). Concentrations of branched GDGTs normalized to TOC in soils are only slightly lower compared to those in the upper part (acrotelm) of peat bogs (Table 6.3), indicating that in the upper, better aerated part of soils and peat bogs the availability of anoxic micro habitats rather than available substrate might be the primary limiting factor for the abundance of branched GDGT-producing bacteria.

Table 6.3: Comparison of GDGT concentrations (μg g^{-1} TOC) in different environments

	GDGT **I**	GDGT **II-IV**	GDGT **VI**	GDGT **VII-IX**	
Soils					
Top layers	0.4 (± 0.9)	0.2 (± 0.3)	0.5 (± 0.7)	4.5 (± 6.1)	This study
All depth intervals	0.4 (± 0.8)	0.4 (± 0.6)	0.3 (± 0.5)	4.0 (± 5.1)	
Peat bogs					
SNM acrotelm	4 (±3)	0.5 (± 0.5)	0.8 (± 0.8)	13 (± 12)	Weijers et al. (2006a)
BFM acrotelm	n.d. [a]	n.d.	n.d.	11 (± 13)	
SNM catotelm	32 (± 25)	8 (± 5)	0.8 (± 0.5)	240 (± 160)	
BFM catotelm	38 (± 32)	n.d.	n.d.	180 (± 60)	
Marine surf.sed.					
Congo Fan	29	16	57	20	Unpublished results
Niger Fan	98	53	162	5	

For the peat bogs a TOC value of 40% was assumed for recalculating concentrations from μg g^{-1} dry weight peat to μg g^{-1} TOC. SNM, Saxnäs Mosse (Sweden); BFM, Bolton Fell Moss (Cumbria, UK); Acrotelm, zone in which the water table fluctuates; and Catotelm, permanent water saturated zone.
[a] n.d., not determined.

6.4.1.2. Crenarchaeol *VI*

GDGT **VI** (crenarchaeol), a specific biomarker for the group 1.1 Crenarchaeota (Sinninghe Damsté et al., 2002b), is nearly always detected in marine and often in lacustrine sediments (Schouten et al., 2000; Powers et al., 2004) and has only recently been shown to be present in peat bogs (Weijers et al., 2004) and even in some hot springs (Pearson et al., 2004). Although molecular ecological studies have revealed the presence of such non-thermophilic Crenarchaeota in soils (e.g., Bintrim et al., 1997; Jurgens et al., 1997; Buckley et al., 1998; Pesaro and Widmer, 2002; Ochsenreiter et al., 2003), their unique GDGT membrane lipid, crenarchaeol (**VI**), has so far never been reported in soils. This can partly be attributed to the amplification technique used in molecular biology studies, enabling the detection of genes at much lower concentrations than possible for lipid analysis. Nevertheless, the presence of crenarchaeol (**VI**) in nearly all soils analyzed in the current study, covering a large geographical range, confirms that crenarchaeol, and consequently its producers, members of the group 1.1 Crenarchaeota, are more widespread than previously thought.

The abundance of crenarchaeol (**VI**) relative to the total GDGT content in soils is higher than in peat samples, but still low compared to crenarchaeol in marine sediments, where it typically comprises about 50% of all GDGTs (Table 6.4). Concerning the microbial population, Ochsenreiter et al. (2003) have determined the abundance of Crenarchaeota in soils to be 0.5-3% relative to bacterial rDNA and Buckley et al. (1998) calculated an abundance of $1.42 \pm 0.42\%$ relative to total 16S rRNA. This is indeed much lower than in the marine water column where the abundance of pelagic Crenarchaeota can reach as much as 39% of total DNA-containing picoplankton (20% on average) (Karner et al., 2001).

**Table 6.4:** Relative abundances (%) of GDGTs in different environments

	GDGT **I**	GDGT **II-IV**	GDGT **VI**	GDGT **VII-IX**	
Soils					
top layers	7	3	9	81	This study
all depth intervals	7	9	7	77	
Saxnäs Mosse Bog					
acrotelm	20	3	4	73	Weijers et al. (2004, 2006a)
catotelm	11	3	0.3	86	
Marine surf.sed.					
North Sea	47	6	47	Not produced in situ	Herfort et al. (2006)
Congo Fan	30	16	55		Unpublished results
Niger Fan	32	16	52		Unpublished results

Interestingly, the abundance of crenarchaeol in soils is higher with increasing pH (Fig. 6.3). This relation seems to be stronger than that observed for other GDGTs (e.g., the branched GDGTs, Fig. 6.3), and, therefore, cannot be attributed solely to a change in the relative abundance of other GDGTs with increasing pH. Phylogenetic analyses of soil Crenarchaeota often reveal a close relation with the marine Crenarchaeota (e.g., Jurgens et al., 1997; Ochsenreiter et al., 2003). Considering that the average oceanic pH value is about 8.2, it might not be surprising that relatives living in soils also prefer alkaline conditions. This observation also fits with the results of Pearson et al. (2004), who found higher crenarchaeol abundances in neutral to alkaline hot water springs. 16S rRNA gene sequences from those springs, however, were related to thermophilic Crenarchaeota and no sequences related to the crenarchaeol producing non-thermophilic group 1.1 Crenarchaeota were found. This paradox might now be explained by our results, suggesting that the crenarchaeol detected in these hot springs might have been derived from surrounding alkaline soils instead from in-situ production.

6.4.1.3. Isoprenoid GDGTs *I-IV*

GDGT **I** is present in virtually all of the soils analyzed. Its abundance relative to total GDGT content, however, is lower in soils (7%) than in peat bogs (11-20%) and about equal to that of GDGT **VI** (crenarchaeol) in soils (7-9%; Table 6.4). This difference between soils and peat bogs might be the result of a much lower contribution of methanogenic Euryarchaeota, which

can contain GDGT **I** in high amounts (Koga et al., 1993), to the total microbial community in soils. In contrast with peat bogs, where methanogens (Euryarchaeota) can comprise up to 36% of the total microbial community (Kotsyurbenko et al., 2004), little data is available on the abundance of Euryarchaeota in soils. Molecular ecological studies on soils have mainly revealed sequences belonging to the non-thermophilic Crenarchaeota and rarely revealed clones belonging to the Euryarchaeota (e.g., Bintrim et al., 1997; Jurgens et al., 1997; Ochsenreiter et al., 2003). In British upland grassland soils for example, archaeal communities seem to be dominated by non-thermophilic Crenarchaeota and sequences of putative methanogenic Euryarchaeota could only be retrieved after enrichment experiments in an anaerobic microcosm (Nicol et al., 2003a; 2003b). A similar enrichment study was performed by West and Schimdt (2002) showing the presumably initial presence of small amounts of (methanogenic) Euryarchaeota in anaerobic micro sites in soils. Pesaro and Widmer (2002) could also detect only a few euryarchaeal sequences in a Swedish forest soil, which were related to Thermoplasmales. The thermophilic *Thermoplasmales acidophilicum* is also known to produce GDGT **I** (Langworthy, 1977). The GDGT membrane lipid data of soils reported here are thus in good agreement with this literature data; GDGT **I** is probably mainly produced by non-thermophilic soil Crenarchaeota and only for a smaller part by Euryarchaeota. Both non-thermophilic Crenarchaeota and methanogenic Euryarchaeota also produce small amounts of cyclopentane containing GDGTs, explaining the occurrence of GDGTs **II-IV** in soils. The fact that these GDGTs **II-IV** do not always follow the distribution pattern of either GDGT **I** or **VI** (e.g., Fig. 6.2) could be a result of this dual source. In addition, Pancost et al. (2000) found, after ether bond cleavage of the GDGTs of two peat bogs by HI treatment, different $\delta^{13}C$ values for the acyclic and the monocyclic biphytanes. This suggests that also within the methanogenic Euryarchaeota in peat bogs different groups occur, utilizing different metabolic pathways, which produce cyclopentane-containing GDGTs (**II-IV**) in different proportions relative to GDGT **I**.
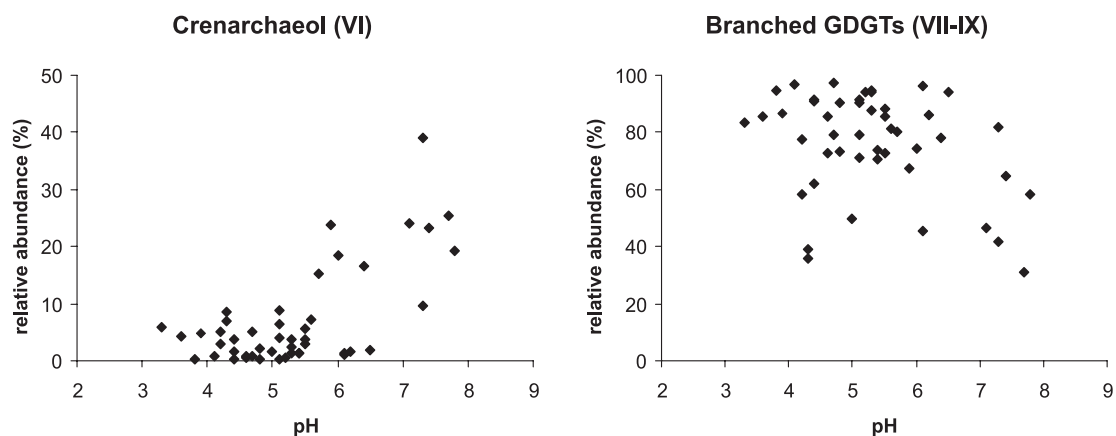

Figure 6.3: Plots showing the relation between pH of soils and relative abundance (to total GDGT content) of crenarchaeol (**VI**; left) and of branched GDGTs (**VII-IX**; right).
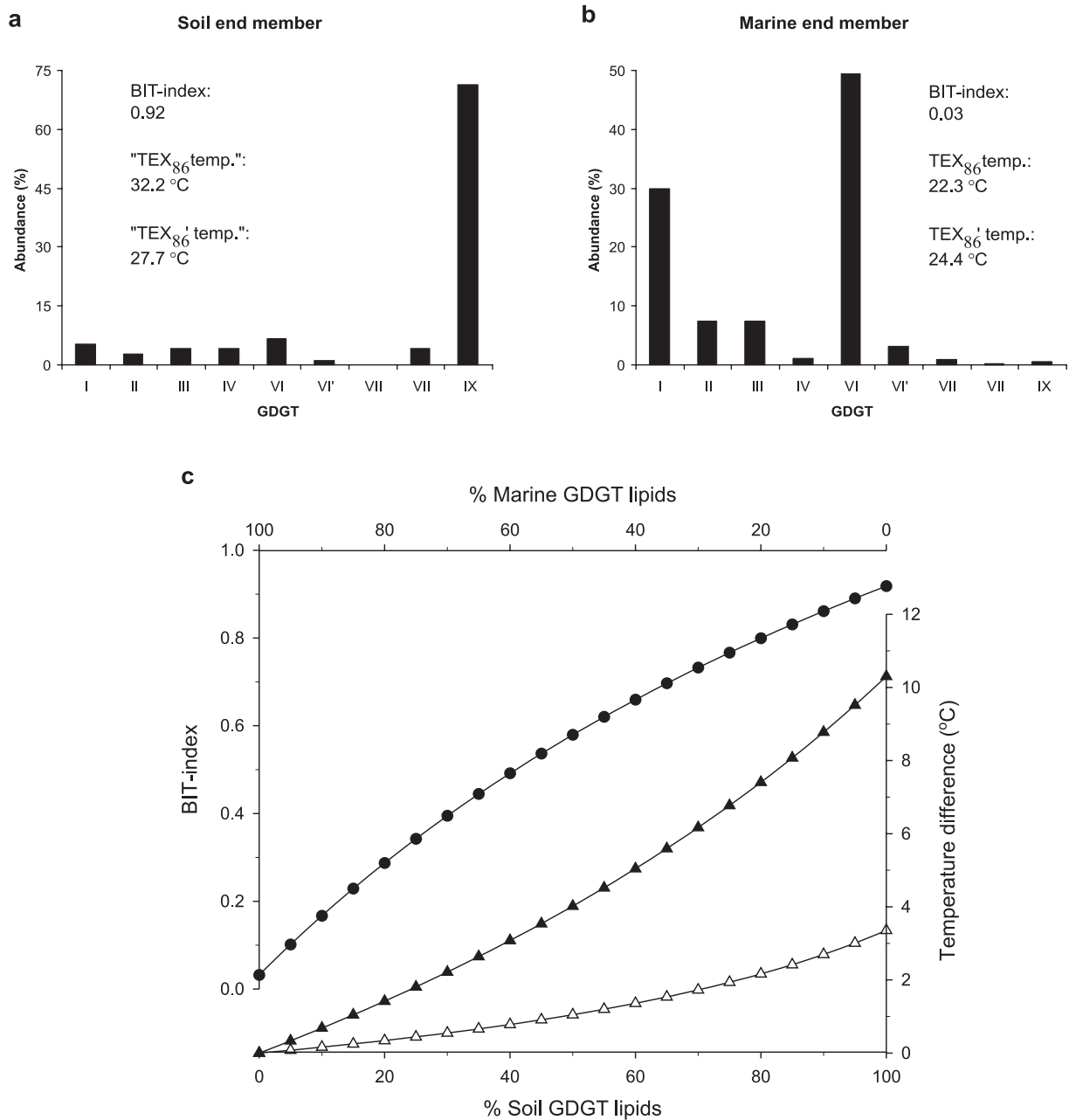
6.4.2. Geochemical implications

6.4.2.1. BIT-index

Although branched GDGTs are not present in such high concentrations as in peat bogs, soils are widespread and represent such a substantial part of the terrestrial realm that they likely form the major source of the branched GDGTs found in marine and lacustrine environments. This strongly supports the use of the BIT-index as a proxy for TOM input in the marine environment (Hopmans et al., 2004). The terrestrial end-member value of the BIT-index is assumed to be close to 1, meaning that no, or only insignificant amounts of crenarchaeol will be initially present in TOM. In that respect, it is important to note that, albeit in relatively low concentrations, GDGT **VI** (crenarchaeol) is unambiguously present in soils (Table 6.3) and that this could possibly complicate the use of this BIT-index. However, the BIT-index of the vast majority of soils is >0.90, although a few soils do show substantially lower values (Fig. 6.4). Those lowest values are found in the uppermost soil layers and are possibly the result of a good aeration of these layers. In soils, the relative abundance of non-thermophilic Crenarchaeota, which are suggested to be able to thrive in both oxic and anoxic environments (Sinninghe Damsté et al., 2002a; Weijers et al., 2004), is likely higher in these top soil layers, because of a lower abundance of branched GDGT-producing bacteria, who seem to be obligate anaerobes (Weijers et al., 2006a). Indeed, BIT indices in the subsequent lower depth interval are much higher again. The average BIT-index of all soils studied here is 0.91, which is still substantially higher than BIT-indices of open marine settings, which usually are close to 0 (Hopmans et al., 2004). Therefore, it can be concluded that despite the presence of GDGT **VI** (crenarchaeol) in soils, the BIT-index as proxy for TOM input in the marine environment is still applicable, although with a somewhat narrower range than previously suggested.
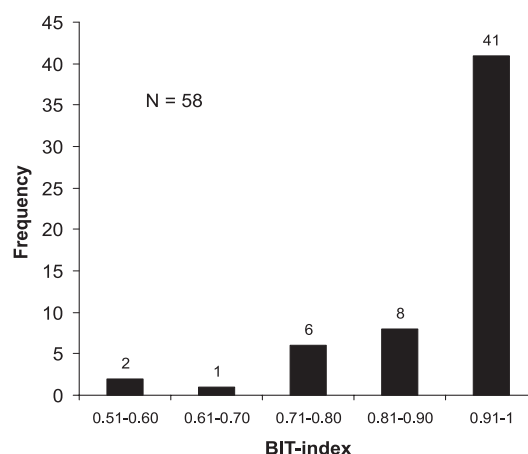
Figure 6.4: Frequency histogram of different BIT-ranges showing that the majority of the soils from this study has a BIT-index >0.90.

a   Soil end member

BIT-index:
0.92

"TEX$_{86}$temp.":
32.2 °C

"TEX$_{86}$' temp.":
27.7 °C

b   Marine end member

BIT-index:
0.03

TEX$_{86}$temp.:
22.3 °C

TEX$_{86}$' temp.:
24.4 °C

c

Figure 6.5: Hypothetical binary mixing model for the equatorial Atlantic region composed of (a) an end-member representing the average GDGT distribution in the African soils, and (b) an end-member representing the GDGT distribution in a marine sediment sample from core GeoB 4901 (Niger deep sea fan). Graph (c) shows with different mixing ratios the positive temperature difference from the original marine end-member value according to the TEX$_{86}$ proxy (black triangles) and the TEX$_{86}$' proxy (white triangles) with the accompanying BIT-indices (black dots).

6.4.2.2. TEX$_{86}$ SST proxy

The TEX$_{86}$ proxy is based on the relative distribution of the cyclopentane-containing isoprenoid GDGTs (**II-IV**) and the regio-isomer of crenarchaeol (GDGT **VI'**) in marine and lacustrine pelagic Crenarchaeota. The unambiguous presence of the cyclopentane-containing GDGTs (**II-IV**) and GDGT **VI'** in peat bogs and soils shown here and in previous studies (Gattinger et al. 2003; Weijers et al. 2004) suggests that when those GDGTs are fluvially transported to marine or lacustrine environments, they could bias the TEX$_{86}$ signal in those settings. It is important to consider, however, that the absolute concentrations of GDGTs **II-IV** and **VI'** in peat bogs and soils are about one to two orders of magnitude lower compared to those found in marine sediments (Table 6.3) and that consequently a substantial input of TOM is required to alter the marine TEX$_{86}$ value. However, especially near the outflow of large rivers, a bias of the TEX$_{86}$ might occur and could alter the reconstructed SSTs. This may also hold for reconstructing lake surface temperatures as proposed by Powers et al. (2004), because crenarchaeol abundances in lakes seems to be lower than in the marine environment (Powers et al., unpublished results) and lakes usually receive a relatively large amount of TOM.

An approximation for determining the relative amount of TOM input, and therefore a possible bias of the TEX$_{86}$ signal, can be derived from the BIT-index. As mentioned above, the BIT-index of soils is in most cases >0.90. In general, it can be assumed that if BIT-indices of marine or lacustrine sediments are low, i.e., a relatively low terrestrial GDGT input compared to marine GDGT production, the TEX$_{86}$ proxy can safely be used, as the vast majority of the isoprenoid GDGTs used for calculating this proxy will in these cases be of marine or lacustrine origin. If BIT-indices in these sediments are higher, however, the TEX$_{86}$ proxy might be altered to a certain degree by the input of terrestrially derived GDGTs.

To illustrate the potential effect of the terrestrially derived GDGTs on the TEX$_{86}$ proxy, a simple two end-member mixing model was used for the equatorial East Atlantic region. As terrestrial end-member, a GDGT lipid mixture was taken representing the average GDGT lipid distribution of the African soils, with a BIT-index of 0.92 and a TEX$_{86}$ derived 'temperature' of 32.2ºC (Fig. 6.5a). As marine end-member, a GDGT lipid mixture representing the GDGT distribution in a marine sediment sample from core GeoB-4901 from the Niger deep sea fan is taken, with a BIT-index of only 0.03 and a TEX$_{86}$ temperature of 22.3 ºC (Fig. 6.5b). For different mixing ratios of these end-members, i.e., a virtual transect from the open marine setting into the river mouth, the BIT-index and the TEX$_{86}$ SST were calculated. The temperature deviation from the original TEX$_{86}$ derived temperature of the marine GDGT lipid mixture is plotted together with the BIT-index (Fig. 6.5c). The curves clearly show that at higher BIT-indices the temperature deviation substantially increases in a non-linear way. In this particular example, a temperature deviation of +1ºC, which is the analytical error of the TEX$_{86}$ proxy, is reached at a BIT-index of 0.2–0.3, and a temperature deviation of >2 ºC is reached at a BIT-index of 0.4. These seem to be large deviations, but it

is important to recall that reaching a BIT-index of 0.4 represents a considerable TOM input, as concentrations of GDGTs in soils are much lower than in the marine environment (Table 6.3). In this particular example, with a BIT value of 0.4, >30% of the GDGTs is derived from soils and, consequently, >95% of the TOC is derived from TOM. Furthermore, the soil GDGT mixture taken here as terrestrial end-member will often be mixed with GDGTs derived from Crenarchaeota living in lakes and rivers, which will also be fluvially transported to the marine environment. The GDGT mixtures of those lake and river Crenarchaeota is not altered by methanogen-derived GDGTs and, therefore, contain a lower TEX_{86} value, which will consequently diminish the difference in GDGT distribution between the soil and marine environment.

Recently, an alternative TEX_{86}' proxy was applied by Sluijs et al. (2006) in a sediment core from the Arctic, covering the Palaeocene-Eocene thermal maximum interval, where exceptionally high levels of GDGT **IV** were found at intervals with a high BIT-index (0.5-0.7). The high abundance of GDGT **IV** was attributed to high levels of terrestrial input and therefore GDGT **IV** was left out of the TEX_{86} formula. Indeed, our results confirm that in soils the relative abundance of GDGT **IV** is often higher than in marine sediments (e.g., Fig. 6.5a-b). When the TEX_{86}' was calculated for our hypothetical binary mixing model, it indeed resulted in a much reduced temperature bias, and a +1ºC deviation is only reached at a BIT-index of about 0.6 (Fig. 6.5c). It should be noted, however, that this reduced bias will depend on the relative abundance of GDGT **IV** in soils, which can vary to a large degree. This variation will partly be due to differences in the abundance of different groups of methanogenic Euryarchaeota, as discussed earlier.

Regardless of using either the TEX_{86} or the TEX_{86}' proxy, the temperature deviation in the binary mixing model strongly depends on the TEX_{86} value of the end-members. The 'TEX_{86} signal' of soils might differ per region, as will the TEX_{86} signal of the marine end-member. The largest temperature deviations are likely to occur at places with cool ocean waters as soils generally contain a relatively warm TEX_{86} signal. If TEX_{86} SSTs in such cases are determined over a time interval in which BIT-indices remain constant, relative changes in TEX_{86} SSTs can, however, still be used, even though the absolute SST is biased. Overall, care should be taken in interpreting TEX_{86} derived absolute SSTs, and determination of the terrestrial GDGT input with the BIT-index is required in all lakes and near coastal areas, especially near large river outflows.
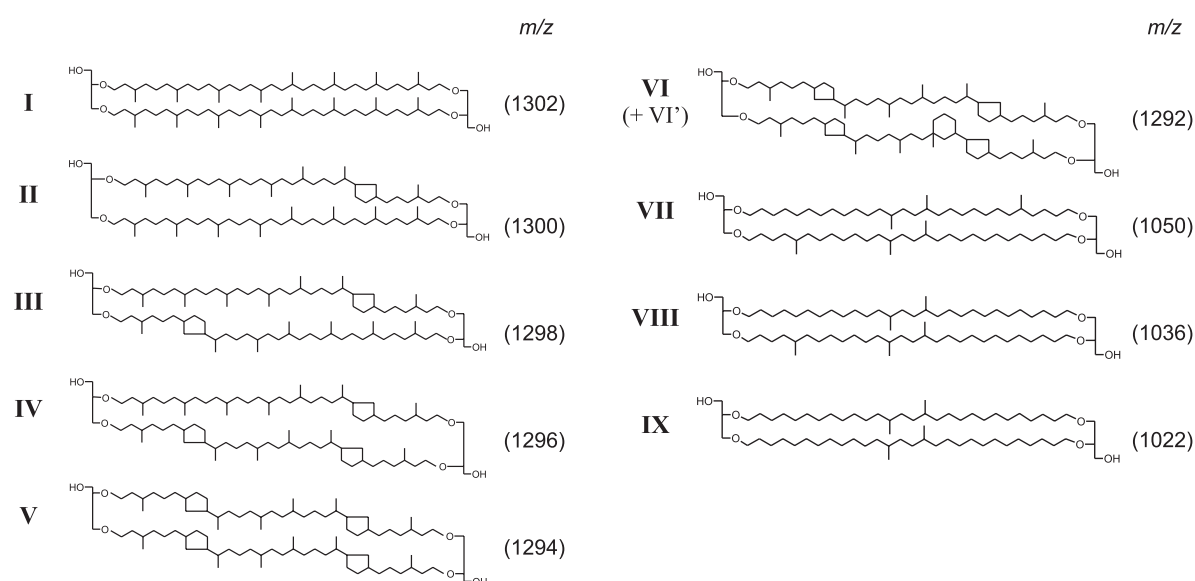
6.5. Conclusions

Branched GDGTs (**VII-IX**) are abundant in all soils investigated, confirming their widespread occurrence in the terrestrial environment. This shows that the BIT-index is a powerful tool to trace relative terrestrial organic matter input in the marine environment. Detection of GDGT

VI (crenarchaeol) in virtually all soils, a specific biomarker for the non-thermophilic (group 1.1) Crenarchaeota, confirms molecular ecological studies that have shown the occurrence of these organisms in soils. As the abundance of crenarchaeol (**VI**) in soils relative to the branched GDGTs (**VII-IX**) is very low compared to the marine environment, its presence does not have a large influence on the BIT-index used in marine settings. Cyclopentane-containing isoprenoid GDGTs (**II-IV**) were, although in low concentrations, also detected in soils. They could, when fluvially transported to the marine environment, bias TEX_{86} derived SSTs in near coastal areas and lakes, especially near large river outflows. At those places, therefore, quantification of the relative TOM input with the BIT-index is required to determine a possible bias in the TEX_{86} proxy.

Appendix

Chapter 7

A multi-proxy study of terrestrial organic matter input in the Congo deep sea fan over the past 20,000 years

Johan W.H. Weijers, Stefan Schouten, Enno Schefuß, Ralph R. Schneider and Jaap S. Sinninghe Damsté

Abstract

A marine sedimentary record from the equatorial East Atlantic Ocean near the Congo River outflow, spanning the past 20 kyr, was analysed for bulk and molecular properties, i.e., total organic carbon (TOC), organic carbon over total nitrogen (C/N) ratio, stable carbon isotopic composition of the organic matter ($^{13}C_{org}$), branched glycerol dialkyl glycerol tetraethers, crenarchaeol, odd-numbered long-chain *n*-alkanes and C_{37} alkenones, in order to reconstruct the terrestrial organic matter (TOM) input in the Congo deep sea fan. All proxies, generally, show lower relative TOM input at the end of the Last Glacial Maximum, during the Younger Dryas and during the late Holocene, and maximum input during the early Holocene. However, estimations of the proportion of TOM relative to marine organic matter (MOM) in the marine sediments by means of binary mixing models show considerable variations based on the different proxies. Most likely this is a consequence of the fact that end-member values for MOM and TOM can vary to a large extent and are not constant through time and, therefore, might not well enough represent MOM and TOM in these binary mixing models. Therefore, branched vs. isoprenoid tetraether (BIT) indices were used in conjunction with the C/N ratios and $\delta^{13}C_{org}$ values in a three end-member mixing model, representing a 'degraded' soil-derived fraction, a 'fresh' plant-derived fraction and a marine fraction, to characterise the organic matter composition. The results indicate a significant soil organic matter contribution (~ 45%) to the sediments of the Congo deep sea fan. Comparison of the three organic matter fractions with a record of Congo River discharge fluctuations shows that, as expected, TOM fluxes mirror past changes in river discharge, but that MOM fluxes also follow this pattern to a large extent. Estimations of TOM input suggest that only a minor amount (ca. 2.5%) of the fluvial TOM input is stored in marine sediments of the Congo deep sea fan and that the accumulation of TOM over the last deglaciation has varied considerably by up to a factor 5.

7.1. Introduction

The world's rivers deliver an estimated 430 Tg yr^{-1} of terrestrial organic matter (TOM) to the oceans (Schlünz and Schneider, 2000) and thus are an important factor in global carbon cycling. The fate of this TOM in the marine environment is still not fully understood (Hedges and Keil, 1995; Hedges et al., 1997; Burdige, 2005). TOM has been found to be more refractory than the relatively labile marine organic matter (MOM) (e.g., Prahl et al., 1997), probably because it has been exposed to oxygen for longer times before discharge and deposition. Therefore, TOM might be preferentially buried in marine sediments relative to MOM (e.g., Burdige, 2005 and references therein). Although the world's rivers deliver an amount of particulate TOM to the oceans theoretically enough to account for all of the organic matter (OM) eventually buried in marine sediments (Berner, 1989; Hedges and Keil, 1995), only a surprisingly low amount of the OM pool in marine sediments seems to be of terrestrial origin. Hedges et al. (1997) suggested the following reasons to explain what they called a 'geochemical conundrum': i) present estimations of the global carbon budget are significantly wrong, ii) the supposed refractory TOM turns out to be more sensitive to re-mineralization and MOM is more efficiently buried than expected, or iii) the methods for detection of TOM are not accurate enough. In order to estimate carbon budgets and TOM re-mineralization, an accurate determination of the proportion of sedimentary TOM is necessary. Such determinations, however, are severely hindered by the compositional heterogeneity of TOM and MOM.

Tracing relative TOM input in marine sediments is often performed using bulk chemical parameters like the organic carbon over total nitrogen (C/N) ratio and the ^{13}C content of bulk organic matter (Hedges et al., 1997 and references therein). Additionally, a wide range of source specific biomarkers is available like long-chain odd-numbered *n*-alkanes (e.g., Poynter et al., 1989) derived from plant waxes (Eglinton et al., 1962), lignin and cutin and their derivatives derived from vascular plants (e.g., Goñi et al., 1997), taraxerol derived from mangroves (Killops and Frewin, 1994; Versteegh et al., 2004) and sometimes also C_{29} sterols derived from terrestrial plants (Huang and Meinschein, 1976), although the latter compounds have also been shown to be produced by many species of marine algae (Volkman, 1986). In order to estimate TOM input to marine sediments, these biomarkers are often measured relative to biomarkers specific to marine organisms, like C_{37} alkenones derived from haptophyte algae (Volkman et al., 1980; de Leeuw et al., 1980) and C_{27} and C_{28} sterols, derived from different types of algae (Huang and Meinschein, 1976). Quantifications of TOM in marine sediments based on these bulk and molecular proxies is usually carried out by means of a simplified two end-member mixing model. The model output, however, depends on the end-member values used, which are not constant or difficult to assess due to changes in the abundance and properties of source materials, such as temporal and geographical differences in the vegetation composition. For example, shifts between ^{13}C-depleted C_3- vs.

^{13}C-enriched C$_4$-type terrestrial vegetation occur and large variability in the ^{13}C content of marine plankton exist (e.g., Deines, 1980), leading to inaccurate TOM estimates using a binary mixing model with fixed end-member ^{13}C values. Also selective degradation, like a preferential loss of amino acids (e.g., Cowie et al., 1992) or carbohydrates could lead to incorrect OM quantifications using fixed C/N end-member values.

An important additional caveat in discriminating between TOM and MOM in marine sediments is the lack of representation of soil organic matter (SOM). All terrestrial biomarkers, for example, are derived from higher plants and thus highly specific for plant organic matter, thereby largely ignoring SOM. SOM consists for a large part of decaying plant OM. OM degradation in soils, however, leads to different C/N and δ^{13}C$_{org}$ signatures of SOM relative to plant OM (e.g.,, Hedges and Oades, 1997 and references therein). By using an independent parameter for either 'fresh' or 'degraded' plant OM, one can thus assess SOM and plant OM fractions independently. For example, in sediments from the Gulf of Mexico, Gordon and Goñi (2003) compared a two end-member mixing model with a three end-member mixing model based on C/N ratios, δ^{13}C$_{org}$ values and lignin contents of MOM, SOM and vascular plant OM fractions, to quantify the terrigenous component of the deposited organic matter. Their results suggested a remarkable underestimation of TOM by 40 to 85% when using the two end-member instead of a three end-member model and thus showed that SOM needs to be represented in such mixing models (Gordon and Goñi, 2003).
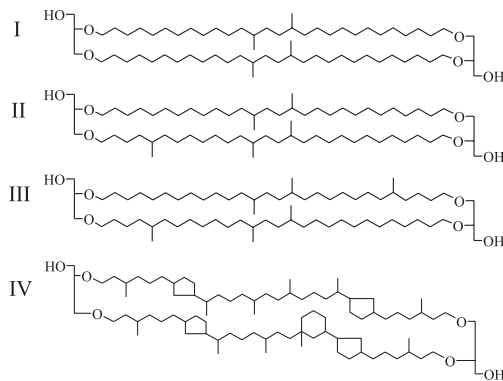
Figure 7.1: Chemical structures of the glycerol dialkyl glycerol tetraethers (GDGTs) used. I, II and III are the branched GDGTs and IV is the isoprenoid GDGT crenarchaeol.

A recently introduced novel proxy for relative fluvial input of soil-derived organic matter, the <u>B</u>ranched vs. <u>I</u>soprenoid <u>T</u>etraether (BIT) index (Hopmans et al., 2004), could be an alternative approach, as it is based on biomarkers not specific for the vegetation itself but derived from organisms living in the soils underneath, and thereby thus actually tracing fluvial SOM rather than TOM input. These biomarkers are branched glycerol dialkyl glycerol tetraethers (GDGTs) (see Fig. 7.1 for structures), which have been recognised in peat bogs and a wide variety of globally distributed soils (Sinninghe Damsté et al., 2000; Hopmans et al., 2004; Weijers et al., 2006b). Although the precise source organism of these compounds is as yet unknown, the branched GDGTs have been shown to be derived from bacteria thriving

in the anoxic parts of peat bogs and soils and to be fluvially transported to the marine environment (Hopmans et al., 2004; Weijers et al., 2006a). An aquatic, structurally related counterpart of these terrestrial branched GDGTs is the isoprenoid GDGT crenarchaeol (Fig. 7.1), a biomarker for the mesophilic pelagic Crenarchaeota (Schouten et al., 2000; Sinninghe Damsté et al., 2002) which occurs ubiquitously in large lakes (Keough et al., 2003) and in the world's oceans where they account for about 20% of the total marine picoplankton (Karner et al., 2001). Crenarchaeol has also been found in peat bogs and soils, but its concentration in these environments is generally very low relative to that of total GDGTs (Weijers et al., 2004; Kim et al., 2006). The BIT index is the ratio between these two groups of GDGTs and determines the proportion of fluvial derived SOM in marine sediments (Hopmans et al., 2004). Application of this index in marine surface sediments in the equatorial Atlantic Ocean close to the Congo River outflow demonstrated the ability of the BIT index to trace relative SOM input (Hopmans et al., 2004) (Fig. 7.2). Also in the Gulf of Lion and in the southern North Sea basin the BIT index was, in conjunction with other proxies, able to trace SOM input in both the water column and surface sediments (Kim et al., 2006; Herfort et al., 2006). The BIT index has so far been applied once to trace past changes in SOM input (Ménot et al., 2006), but was not used to quantify TOM input in marine sediments, which would be of interest for studying past changes in large-scale fluvial carbon fluxes.
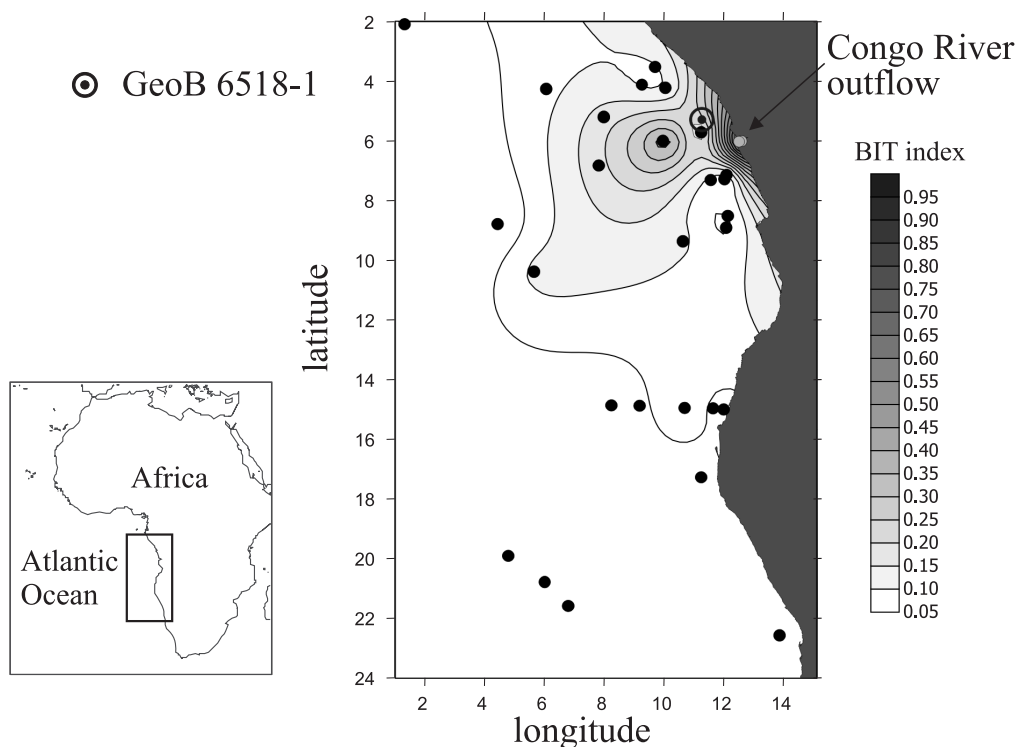
Figure 7.2: Map of the western equatorial Atlantic Ocean showing the location of core GeoB 6518-1 close to the Congo River outflow superimposed on a contour plot of the BIT index based on surface sediment samples (black dots) [figure adapted from Hopmans et al. (2004)].

In the current study we analysed the BIT index in conjunction with bulk geochemical (TOC, $\delta^{13}C_{org}$, C/N) and biomarker (summed odd-numbered long-chain *n*-alkanes vs. C_{37} alkenones) proxies in a marine core recovered from the Congo deep sea fan (GeoB 6518-1, Fig. 7.2) (Schefuß et al., 2005), spanning the past 20,000 years. Using both 'classical' binary mixing models and a three end-member mixing model, past variations in relative TOM input are reconstructed from the end of the Last Glacial Maximum (LGM) to the present. Furthermore, a comparison is made between the different OM fluxes and two proxy records representing changes in central African humidity and Congo River discharge to investigate to which extent TOM input, but also MOM input, in marine sediments is driven by river discharge fluctuations.

7.2. Methods

7.2.1. Sediment core

The 7.2 m long marine sediment core GeoB 6518-1 was recovered from the Congo Fan (05º 35.3'S, 11º 13.3'E) at a water depth of 962 m during the RV-METEOR cruise M47/3, June 2000 (Spiess and Cruise Participants, 2002) (Fig. 7.2). The Congo River is Africa's largest river system (ca. 3.7 x 10^6 km^2), draining large parts of equatorial tropical Africa (e.g., Laraque et al., 2001). The age model of this core is based on fifteen ^{14}C-AMS dates on mixed planktonic foraminifera fractions containing *Globigerinoides ruber* (white), *Globigerinoides sacculifer* and *Orbulina universa*. A conversion of these radiocarbon ages to calendar ages was made with the Calib 4.4 program (Stuiver et al., 1998) using the marine calibration and applying a reservoir age of 400 yr (Schefuß et al., 2005). Ages of intermediate samples were obtained by interpolation with a sixth power polynomial fit (R^2 = 0.998). From this core 112 sediment samples were taken at 5 cm intervals spanning the past 20 kyr.

7.2.2. Elemental analyses (TOC; C/N; $\delta^{13}Corg$)

For determination of total carbon and nitrogen contents, about 50 mg of samples were weighted and combusted at 1030 ºC in a Heraeus CHN-O-Rapid elemental analyser. Quantification of TOC contents was conducted using the same instrument after carbonate removal with hydrochloric acid. The C/N ratio was calculated as weight ratio of TOC and total nitrogen. Stable carbon isotope compositions of TOC were determined by combustion of de-carbonated samples at 1030 ºC in a Heraeus CHN-O-Rapid elemental analyzer connected to a Finnigan MAT Delta E mass-spectrometer. Analytical precision was better than ±0.1 ‰ VPDB.

7.2.3. n-Alkane and alkenone analyses

About 5 g dried and ground sediment samples were mixed with known amounts of standard mixtures and ultrasonically extracted (3×) using successively less polar solvent mixtures [Methanol (MeOH); MeOH/Dichloromethane (DCM) 1:1 (v/v); DCM]. Extracts of each sample were combined and rotary-evaporated to near dryness. Extracts were taken up in DCM, desalted with double-distilled H_2O, dried with anhydrous Na_2SO_4 and extracted again with DCM (3×). Elemental sulphur was removed by stirring overnight with activated copper in DCM. Extracts were then cleaned by elution with DCM over silica columns (Varian Bond elute cartridges). To remove wax esters, extracts were hydrolysed with 1 N KOH in MeOH [MeOH/H_2O 9:1 (v/v)] at 80ºC for 2 h. Lipids were extracted by partitioning into hexane and dried under N_2. Hydrocarbon fractions were separated by column-chromatography over activated Al_2O_3 eluted with hexane. Polar lipids were eluted with MeOH/DCM 1:1 (v/v). Saturated hydrocarbon fractions were obtained by column-chromatography over $AgNO_3$-impregnated silica eluted with hexane. Lipid fractions were analysed on a Hewlett Packard 5890 series II gas chromatograph using flame ionisation detection (FID). Quantification of compounds was performed by peak area integration in FID chromatograms relative to standards.

7.2.4. GDGT analyses

Freeze dried sediments (0.5 to 1 g) were extracted using an accelerated solvent extractor (ASE 2000, Dionex) at a pressure of 7.6×10^6 Pa and a temperature of 100 °C, three times for 5 min. The resulting total extract was rotary-evaporated under near vacuum and separated over an activated Al_2O_3 column, using hexane:DCM 1:1 (v/v) and DCM:MeOH 1:1 (v/v) solvent mixtures, respectively. The latter fraction, containing the GDGTs, was dried under a continuous N_2 flow, ultrasonically dissolved in a hexane:propanol 99:1 (v/v) solvent mixture to a concentration of ca. 2 mg ml^{-1} and filtered through an 0.45 μm mesh PTFE filter (ø 4mm; Alltech) prior to analysis.

GDGTs were analysed by high performance liquid chromatography – atmospheric pressure chemical ionisation / mass spectrometry (HPLC-APCI/MS) on an Agilent 1100 series / Hewlett-Packard 1100 MSD series machine equipped with automatic injector and HP Chemstation software according to Hopmans et al. (2000) with minor modifications. The injection volume of the samples was 10 μl. Separation of the compounds was achieved in normal phase on an Alltech Prevail Cyano column (150 mm x 2.1 mm; 3 μm) with hexane:propanol 99:1 (v/v) as eluent (flow rate 0.2 ml min^{-1}), isocratically for the first 5 min, thereafter with a linear gradient to 1.8% propanol in 45 min. In order to increase sensitivity and reproducibility, ion scanning was performed in a single ion monitoring mode adjusted to the masses of interest. Relative abundances were determined by integrating the peak areas of the $[M+H]^+$ (protonated mass) peaks and BIT indices were calculated as follows (Roman numerals refer to structures in Fig. 7.1):

$$\mathrm{BIT} = \frac{[\mathrm{I}] + [\mathrm{II}] + [\mathrm{III}]}{[\mathrm{I}] + [\mathrm{II}] + [\mathrm{III}] + [\mathrm{IV}]} \qquad\qquad (1)$$

This index ranges in value between 0, if only crenarchaeol is present and 1, if only branched GDGTs are present. Based on 34 duplicate HPLC/MS analyses of samples from this Congo fan core, the analytical reproducibility for the BIT index is ± 0.01 BIT units.

7.3. Results

7.3.1. Bulk parameters

The total organic carbon (TOC) content of the sediments from core GeoB 6518-1 varies between 2.5 % and 3.9 % (Fig. 7.3a). Values in sediments deposited at the end of the LGM were ca. 3.2 % and these decreased gradually to 2.5% just after 10 ka BP. During the Holocene TOC values increased gradually again towards values of ca. 3.6 %.

Accumulation rates (ARs) of TOC are low at the end of the LGM (~1.0 g m^{-2} yr^{-1}) and rapidly increase to values of ca. 5 g m^{-2} yr^{-1} around the YD. Highest ARs of TOC are reached during the early Holocene (8.5 g m^{-2} yr^{-1}), after which ARs rapidly drop again to values of ca. 3.0 g m^{-2} yr^{-1} during the late Holocene (Fig. 7.4a).

The C/N ratio of the organic matter was constant at the end of the LGM with values of ca. 11.5 and started to increase at 16 ka BP towards values of 12.4 (Fig. 7.3b). During the YD, C/N ratios clearly decreased, reaching a value of 10.8 just after the YD and immediately increased again towards values of ca. 12.2 at 9 ka BP. The last 9 ka of the record show a gradual decrease of the C/N ratio to values just below 10 at the end of the Holocene.

The OM was relatively enriched in ^{13}C at the end of the LGM (-21.2 ‰) and became more depleted in ^{13}C content from ca. 16 ka BP onwards, with a small interruption just after the YD (Fig. 7.3c). Most depleted values (-24.6 ‰) were reached around 8 ka BP. During the remainder of the Holocene, the carbon isotopic content became slightly more enriched again (-23.7 ‰), although for the last 1000 yrs of the record a more rapid enrichment in ^{13}C is observed with values of -22.4 ‰ for the youngest sediments.

7.3.2. Molecular markers
7.3.2.1. GDGTs and BIT index

Concentrations of the branched GDGTs throughout the record are on average 1.2 µg g^{-1} dry weight sediment (dws) with concentrations slightly higher during the early Holocene than at the end of the LGM and the late Holocene (Fig. 7.3e). Crenarchaeol concentrations are on average 2.1 µg g^{-1} dws, but with a distinct maximum around the YD where average
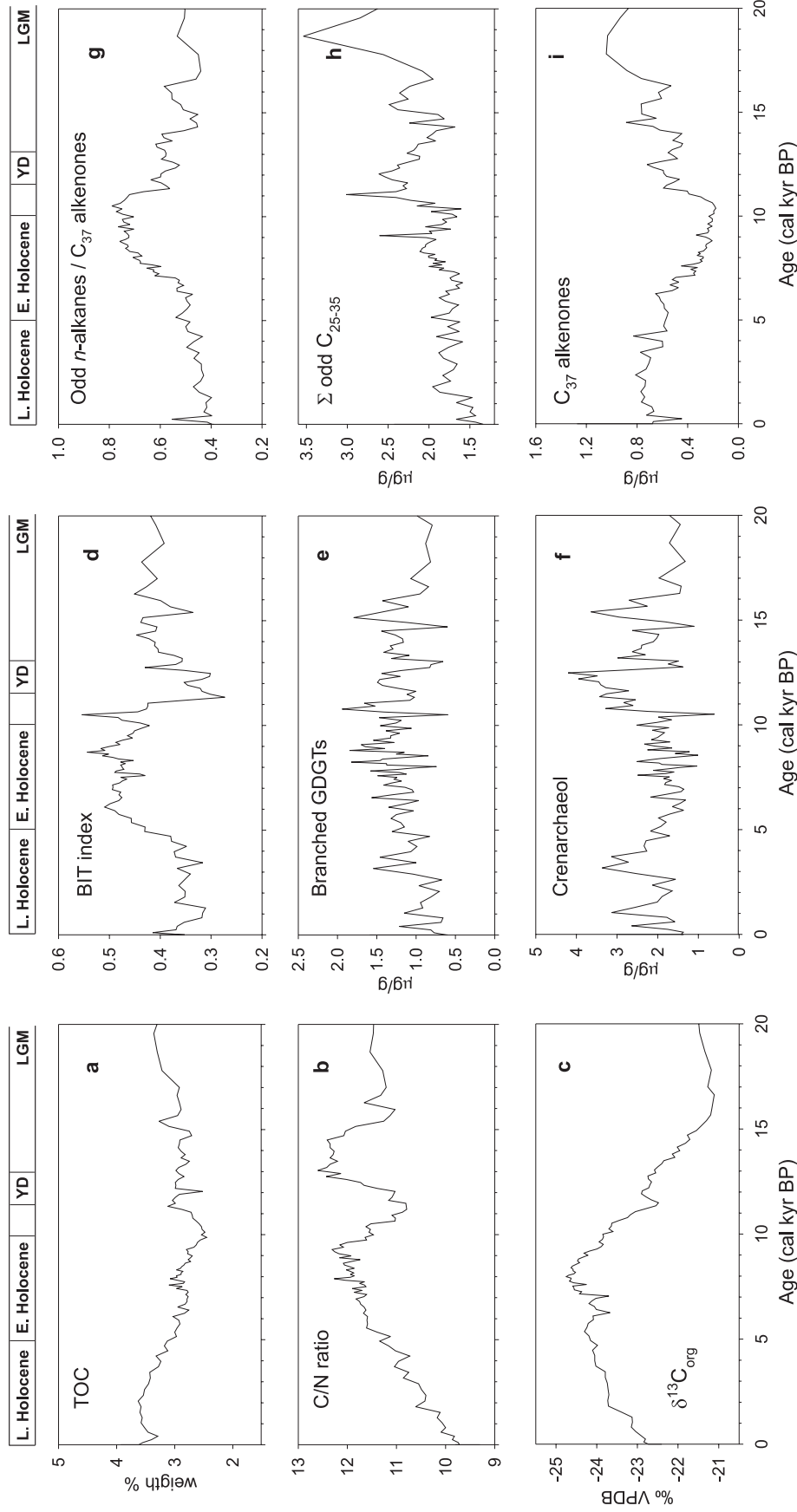
Figure 7.3: Records characterising the organic carbon content at site GeoB 6518-1: (a) total organic carbon (TOC); (b) organic carbon over total nitrogen ratio (C/N); (c) ^{13}C content of the organic matter ($\delta^{13}C_{org}$); (d) branched *vs.* isoprenoid tetraether index (BIT index); (e) concentrations of branched glycerol dialkyl glycerol tetraethers; (f) concentrations of crenarchaeol; (g) odd-numbered *n*-alkane/C_{37}-alkenone index; (h) concentrations of summed odd-numbered (C_{25} to C_{35}) *n*-alkanes; and (i) concentrations of C_{37} (37:2 and 37:3) alkenones. cal., calibrated

concentrations are 3.1 µg g^{-1} dws (Fig. 7.3f). Throughout the record, the ARs of branched GDGTs are lower than crenarchaeol ARs (Fig. 7.4b). Crenarchaeol ARs are relatively high around the YD and the early Holocene (up to 0.60 mg m^{-2} yr^{-1}) and relatively low during the late Holocene (~0.20 mg m^{-2} yr^{-1}). Branched GDGT ARs are relatively high during the early Holocene as well (up to 0.40 mg m^{-2} yr^{-1}), but, in contrast to crenarchaeol, values around the YD are relatively low (~0.20 mg m^{-2} yr^{-1}) (Fig. 7.4c). During the late Holocene, branched GDGT ARs decrease to values of ca. 0.10 mg m^{-2} yr^{-1}, which are only slightly higher than those at the end of the LGM (Fig. 7.4b).
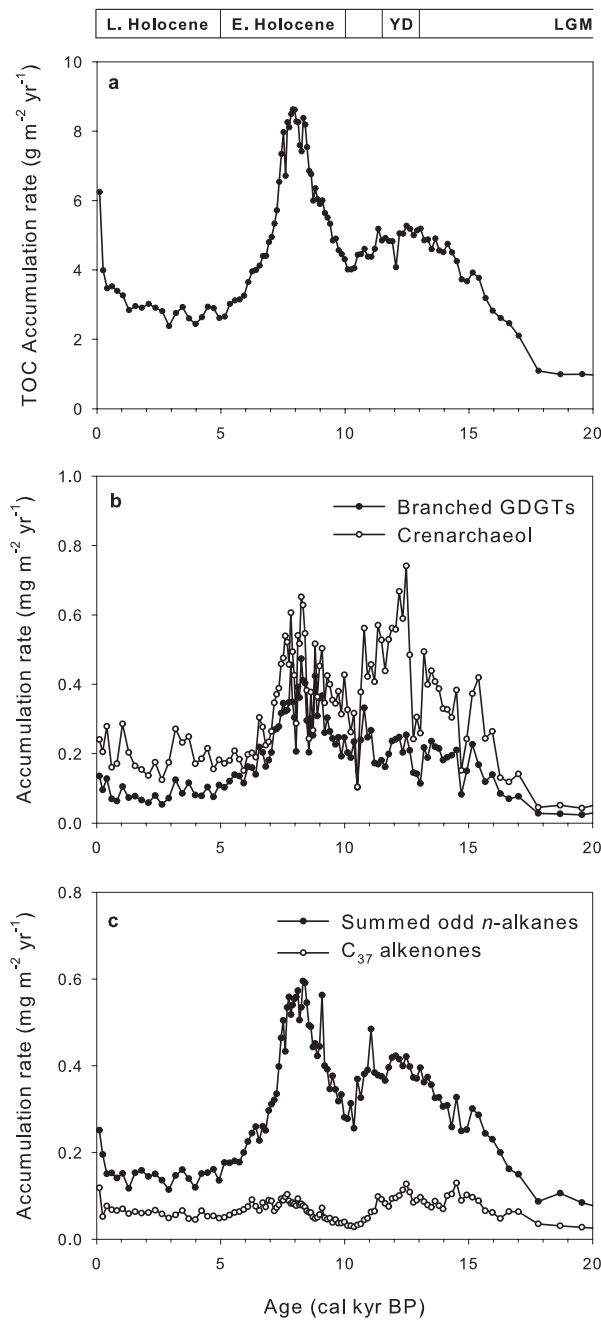
Figure 7.4: Accumulation rates in core GeoB 6518-1 of (a) total organic carbon (TOC); (b) branched GDGTs and crenarchaeol; and (c) summed odd-numbered *n*-alkanes and C$_{37}$ alkenones.

The BIT index, which reflects the relative difference between branched GDGTs and crenarchaeol, shows intermediate values of 0.41 ± 0.03 at the end of the LGM followed by lower values down to 0.27 around the YD (Fig. 7.3d). Highest BIT values occur during the early Holocene (0.48 ± 0.02) and intermediate values are obtained at the end of the Holocene (0.36 ± 0.03), which are slightly lower than the BIT values obtained for the end of the LGM.

7.3.2.2. n-Alkanes and alkenones

The average concentration of the odd-numbered long-chain *n*-alkanes (C_{25-35}) is highest at the end of the LGM and during the YD with 2.5 and 2.4 µg g^{-1} dws, respectively, and is lower during the early and late Holocene with 1.9 and 1.7 µg g^{-1} dws, respectively (Fig. 7.3h). The $C_{37:2} + C_{37:3}$ alkenone concentration is with 0.8 µg g^{-1} dws highest at the end of the LGM, is lower at the YD (0.6 µg g^{-1}) and reaches lowest values of around 0.4 µg g^{-1} during the early Holocene (Fig. 7.4i). Concentrations are higher again during the late Holocene with values of 0.7 µg g^{-1} dws. The ARs of the *n*-alkanes follow a rather similar pattern as those of the branched GDGTs, with increasing values from the end of the LGM (~0.10 mg m^{-2} yr^{-1}) to the YD (0.40 mg m^{-2} yr^{-1}) and highest values during the early Holocene (up to 0.60 mg m^{-2} yr^{-1}), followed by lower ARs during the late Holocene (~0.15 mg m^{-2} yr^{-1}) (Fig. 7.4c). Absolute ARs of C_{37} alkenones are, in contrast to crenarchaeol, the other marine biomarker, low throughout the record. Values of ~0.05 mg m^{-2} yr^{-1} are obtained for the end of the LGM and they slightly increase to ~0.10 mg m^{-2} yr^{-1} around the YD (Fig. 7.4c). Similar to crenarchaeol, lowest ARs are found at ca. 10 cal kyr BP (~0.03 mg m^{-2} yr^{-1}), increasing to ca. 0.10 mg m^{-2} yr^{-1} during the early Holocene, followed by lower ARs again during the late Holocene (0.06 mg m^{-2} yr^{-1}).

Marret et al. (2001) used the abundance of odd-numbered *n*-alkanes relative to alkenones as a measure for the relative strength of TOM input in marine sediments. We applied a similar index here, which is defined as:

$$n\text{-alkane/alkenone index} = \frac{[\text{odd-numbered } n\text{-alkanes}]}{[\text{odd-numbered } n\text{-alkanes}] + 3 \times [C_{37}\text{alkenones}]} \quad (2)$$

Since the odd-numbered *n*-alkanes comprise 6 compounds (C_{25}-C_{35}) and the C_{37} alkenones comprise 2 compounds ($C_{37:2}$ and $C_{37:3}$), the alkenone concentration has been multiplied by three. An *n*-alkane/alkenone index approaching 1 would indicate a predominant terrestrial source, whereas an index approaching 0 indicates a predominant marine input. This index gives an average value of 0.51 ± 0.05 at the end of the LGM, increasing to maximum values of ~0.75 at the start of the early Holocene (Fig. 7.3g). This is followed by a decrease towards average values of 0.44 ± 0.04 during the late Holocene with lowest values of 0.39 at the end of the record.

7.4. Discussion

7.4.1. Determining TOM in marine sediments using a binary mixing model

7.4.1.1. General trends

In order to compare the different proxies for TOM input with each other not only qualitatively but also in quantitative terms, the amount of TOM relative to total organic carbon in the Congo deep sea fan sediments has been calculated with a binary mixing model based on the C/N ratio, the ^{13}C content of TOC, the BIT index and the *n*-alkane/alkenone index. This two end-member mixing model of TOM and MOM is defined as follows:

$$f_{TOM} = \frac{(X_{SAMPLE} - X_{MOM})}{(X_{TOM} - X_{MOM})} \times 100\% \qquad (3)$$

Where f_{TOM} is the terrestrial organic matter fraction and X_{SAMPLE} is, depending on the proxy analysed, the BIT index, the *n*-alkane/alkenone index, the C/N ratio or the δ^{13}C value of the sample and X_{MOM} and X_{TOM} are the marine and terrestrial end-members, respectively, of the given proxy. The X_{MOM} and X_{TOM} values used in the calculations are given in Table 7.1. Notably, the ^{13}C value taken for X_{TOM} (-27‰) closely matches reported values of -26.7‰ for particulate organic matter in the Congo River (Mariotti et al., 1991).

All four different proxies ($\delta^{13}C_{org}$, C/N, BIT, *n*-alkanes/alkenones) show, in general, rather similar patterns in their records of relative TOM input to marine sediments (Fig. 7.5). Relative TOM input is low at the end of the LGM and after a small initial rise, either constant or decreasing between 13 and 11.5 ka BP. All proxies show highest proportions of TOM during the early Holocene. During the late Holocene, all estimates of TOM proportions are again lower, reaching values similar to those at the end of the LGM, except for the TOM estimates based on the δ^{13}C values. Judging from these four independent proxies as a whole, it is most likely that these general patterns indeed reflect the long-term changes in the proportion of TOM in the Congo deep sea fan. Nevertheless, dissimilarities are evidently present between the different individual TOM estimates, especially with regard to the absolute percentages of TOM. Possible causes will be discussed below.

Table 7.1: End member values used in the binary mixing models

Proxy	X_{MOM}	X_{TOM}	
C/N ratio	7	20	Hedges et al. (1986, 1997)
d13Corg	-20‰	-27‰	Fry and Sherr (1984); Hedges et al. (1986)
BIT index	0.00	0.91	Hopmans et al. (2004); Weijers et al. (2006b)
n-alkane/alkenone index	0.00	1.00	

7.4.1.2. C/N ratio

Generally, the C/N ratio indicates lower TOM proportions in the Congo fan sediments (20-40 %) than other proxies (35 to 75%) (except for the very low estimates after the LGM based on $\delta^{13}C$) (Fig. 7.5). The reason for these low estimates likely lies in the estimate of X_{TOM}. SOM tends to have a lower C/N ratio (8-14) than plant organic matter (~20) due to the retention of nitrogen by microbes during organic matter remineralisation in soils (e.g., Hedges and Oades, 1997), and hence X_{TOM} may be an overestimate. Decreasing X_{TOM} to a C/N value of for example 15 (average between soil and vascular plant values), would indeed result in higher estimates. However, as the ratio between SOM and plant organic matter is unknown and might have varied in time, it is impossible to accurately correct for this effect. The estimates of TOM input based on the C/N ratio, therefore, should be considered as minimum estimates. Notably, TOM estimates based on the C/N ratio during the last part of the Holocene are even lower than at the end of the LGM, a pattern which is also observed for the BIT index and the *n*-alkane/alkenone index. A possible explanation for the long term decrease of the C/N ratio during the Holocene might be an increased proportion of SOM relative to plant detritus, but it might also be that the younger sediments of the record contain, relative to the older sediments, higher proportions fresh labile MOM which has not yet been re-mineralised (e.g., Prahl et al., 1997).
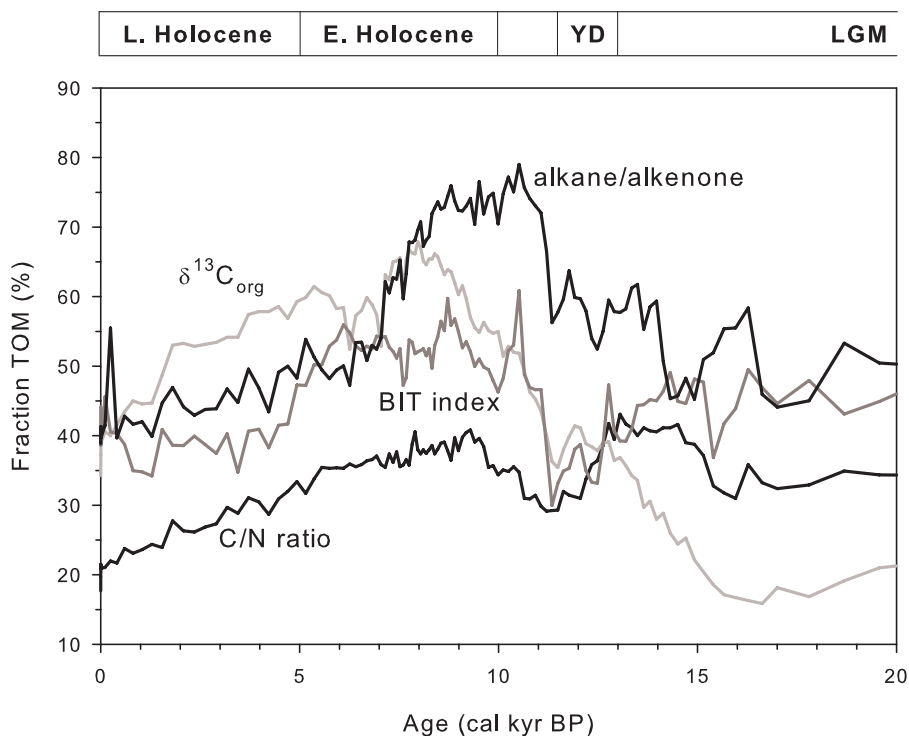
Figure 7.5: Estimates of the proportions of terrestrial organic matter (TOM) in the marine sediments at site GeoB 6518-1 over the past 20 kyr based on two end-member mixing models of the different proxies. See page 166 for colour figure.

7.4.1.3. $\delta^{13}C_{org}$

The most striking feature in TOM estimates based on $\delta^{13}C_{org}$ values is the high overall increase from slightly more than 15 % at the LGM to almost 70 % in the early Holocene, whilst the total range in TOM proportion change as revealed by the other proxies is only 20 to 40% (Fig. 7.5). Also the other proxies do not show such a long term, almost continuous increase in TOM proportions over this time interval from ca. 16 to 9 cal. kyr BP. Part of the explanation of this deviating pattern likely lies in the $\delta^{13}C$ value of X_{TOM}. The stable carbon isotopic composition for TOM differs between C_3-type vegetation (e.g., rainforest) and C_4-type vegetation (e.g., savannah grasses). C_3 plant-derived organic matter is characterised by bulk $\delta^{13}C$ values of ca. -27‰ (-25 to -29‰), whereas C_4 plant-derived organic matter is characterised by bulk $\delta^{13}C$ values of ca. -12‰ (-8 to -19‰) (Fry and Sherr, 1984; Tyson, 1995). The bulk carbon isotopic composition of MOM is ca. -20‰ (-19 to -22‰) (Fry and Sherr, 1984). Thus, admixture of C_4 plant-derived organic matter in the TOM fraction could lead to considerable 'heavier' carbon isotopic values more similar to MOM values and hence lead to an underestimation of TOM in marine sediments if only the C_3 plant $\delta^{13}C$ value is used as end-member for terrestrial bulk $\delta^{13}C$ values. This might explain the low estimates of TOM input during the LGM. However, based on analysis of the stable carbon isotopic composition of plant wax *n*-alkanes in this core, Schefuß et al. (2005) showed that the TOM in this core mainly consist of C_3 plant-derived organic matter with an admixture of C_4 plant-derived organic matter of ca. 17% from the YD to the present day and an only slightly higher admixture of ca. 23% during the LGM. Although TOM estimates for the end of the LGM, based on bulk $\delta^{13}C$ values, increase from ca. 15% to ca. 30% if corrected for this C_4 vegetation admixture, TOM estimates for the early Holocene also increases up to almost 90%, i.e., the large difference between the end of the LGM and the early Holocene remains. Admixture of C_4 plant-derived organic matter can, thus, not explain this large increase in TOM estimates.

As the large increase in TOM estimates takes place during the last deglaciation, another explanation might be a change in $\delta^{13}C$ values of X_{MOM} associated with the deglaciation. The carbon isotopic composition of phytoplankton, for example, is controlled by various factors like, amongst others, the availability of dissolved CO_2 in surface waters, nutrient availability and growth rate (Laws et al., 1995; Popp et al., 1998). Global CO_2 concentrations increased by ca. 40% from ~ 190 ppmv at the LGM to ~ 265 ppmv at the early Holocene (Monnin et al., 2001) and might have affected the carbon isotopic fractionation of marine plankton in such a way that bulk MOM gets slightly more depleted in ^{13}C. As this effect of increasing pCO_2 is only very small for terrestrial plant biomass (Arens et al., 2000; Tu et al., 2004), this process might be responsible for part of the observed shift in TOM input estimates based on this 2 end-member approach. However, also independent of $pCO2$, large differences in ^{13}C contents within MOM exist. For the eastern equatorial Atlantic Ocean, for example, Benthien et al.

(2005) showed that at least for the haptophyte algae it is mainly the surface water nutrient levels that control the $\delta^{13}C$ values of alkenones. They observed a shift of +1.8‰ in alkenone $\delta^{13}C$ values from the LGM to Holocene in front of the Congo River, likely due to lower haptophyte growth rates. If representative for MOM in general, this indicates that the $\delta^{13}C$ value of X_{MOM} during the LGM has been more depleted than in the Holocene. In our binary mixing model this might then result in estimates of MOM during the LGM that are higher and thus of estimates of TOM that are even lower than already observed in our record. It has to be noted, however, that this 1.8‰ shift in alkenones deviates from other locations in the Atlantic Ocean and that other marine plankton species (like diatoms) might have experienced an opposite change, due to enhanced fluvial silica input (Benthien et al., 2005). Nevertheless, these results suggest that LGM to Holocene plankton community changes and pCO_2 changes might be able to cause a shift in X_{MOM} values and thus in TOM input estimates based on the bulk $\delta^{13}C$ binary mixing model. Adjusting X_{MOM} experimentally with ± 1 to 2‰ shows that differences in LGM vs. Holocene estimates of TOM input might, indeed, be reduced by up to 20%, which brings this range back into the range observed for TOM estimates based on other proxies.

Finally, based on the $\delta^{13}C_{org}$ record, a sharp decrease in TOM proportions is apparent for the last 1,000 year of the record. Although plankton community shifts due to, for example, changes in Congo River discharge might be an explanation, this decrease could as well be a result of relative high amounts of fresh and labile MOM in the top sediment layers which has not yet been degraded, similar as suggested for the decrease observed with the C/N proxy.

7.4.1.4. n-alkane / C$_{37}$-alkenone index

TOM input estimates based on the *n*-alkanes / C$_{37}$-alkenone index range from 40 to75% (Fig. 7.5). In contrast to the other proxies, this proxy does not show decreased estimates of TOM proportions around the YD. An explanation for this difference might be different modes of transport. Besides fluvial transport, plant wax *n*-alkanes could, as a result of ablation of leave surfaces by wind and dust, also be predominantly transported by wind (Simoneit, 1977). Especially around the LGM and the YD, recognized in Africa as dry spells (e.g., Gasse, 2000), enhanced wind strength and dust transport could have caused an additional atmospheric delivery of *n*-alkanes and thus counteracted a reduced fluvial input of *n*-alkanes. In contrast to the branched GDGTs, during the YD both concentrations and ARs of *n*-alkanes, indeed, seem to be slightly higher (Figs. 7.3h and 7.4c). TOM proportion estimates with the *n*-alkane/alkenone index decrease over the Holocene, similar to the other proxies, and late Holocene estimates are slightly lower than estimates at the end of the LGM, a feature also apparent from the BIT index and the C/N ratio (Fig. 7.5).
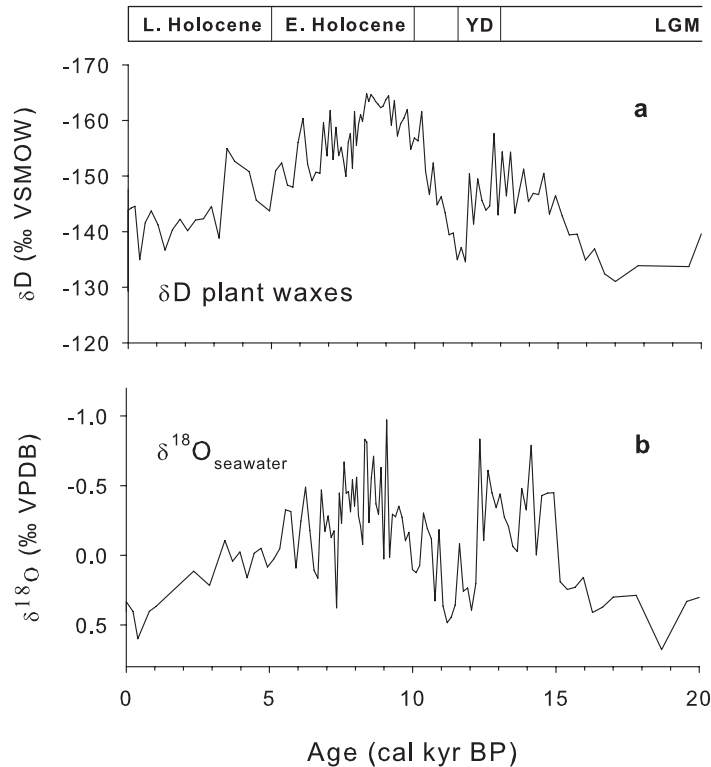
Figure 7.6: Records of humidity levels and Congo River discharge based on (a) δD values of plant wax C_{29}-alkanes and (b) residual $\delta^{18}O$ values of sea water obtained from planktonic foraminifera (Schefuß et al., 2005).

7.4.1.5. BIT index

Estimates of TOM proportions in the Congo fan sediments based on the BIT index range from 30 to 60 % (Fig. 7.5). The lowest estimates are recorded around the YD and are the result of increased crenarchaeol ARs, consistent with a decrease in TOM proportion estimates based on the C/N proxy. Highest ARs of branched GDGTs occur during the early Holocene, giving rise to the high estimates of TOM proportions in the sediments at this time interval. This period is contemporaneous with the African humidity optimum at around 9 cal kyr BP (Schefuß et al., 2005) (Fig. 7.6).

TOM quantifications based on biomarker proxies like the BIT index and the *n*-alkane/alkenone index implicitly assume similar and constant proportions of the organic biomarkers versus bulk organic matter. Unfortunately, only few proper quantifications of branched GDGTs in soils and crenarchaeol in open marine sediments are yet available, but based on data presented by Kim et al. (2006) and Weijers et al. (2006b), it seems that average concentrations of crenarchaeol vs. MOM might be slightly higher than average concentrations of branched GDGTs vs. TOM. This suggests that the TOM estimates based on the BIT index might be underestimates. However, large variability exists in biomarker concentrations, both

in terrestrial and marine settings. To properly correct for this type of bias, a detailed quantitative biomarker study both in the vast river catchment areas as in the marine sediments extending far beyond the river deep sea fan would be required.

7.4.2. Determining TOM in marine sediments using a three end-member model

Although some general trends are apparent from the two end-member model calculations, the quantifications of TOM input based on this approach vary considerably between the different proxies (Fig. 7.5). One of the reasons for these deviations is the notoriously heterogeneous nature of especially TOM, thereby making it difficult to obtain accurate and consistent values for X_{TOM}. Over the last years an increasing amount of data is being published showing this heterogeneous character of TOM and pointing to the need of at least defining SOM as a distinct organic carbon source in end-member mixing models (e.g., Bianchi et al., 2002; Gordon and Goñi, 2003; Holtvoeth et al., 2005; Goñi et al., 2006). Here we have the possibility to trace the relative contribution of SOM by means of the BIT index, which is a proxy for fluvial SOM input. Therefore, we used the BIT index data in conjunction with the ^{13}C content and C/N ratio of the OM in a three end-member model approach in a similar way as conducted by Gordon and Goñi (2003), separating the TOM fraction into a relatively degraded soil organic matter fraction and a more 'fresh' plant organic matter fraction. Where Gordon and Goñi (2003) used the lignin content of samples to characterise the 'fresh' fraction of TOM, we applied the BIT index as indicator of the 'degraded' SOM fraction of TOM. The three equations on which the three end-member mixing model is based are:

$$BIT_{SAMPLE} = (BIT_{MOM} \times f_{MOM}) + (BIT_{SOM} \times f_{SOM}) + (BIT_{POM} \times f_{POM}) \qquad (4a)$$

$$C/N_{SAMPLE} = (C/N_{MOM} \times f_{MOM}) + (C/N_{SOM} \times f_{SOM}) + (C/N_{POM} \times f_{POM}) \qquad (4b)$$

$$\delta^{13}C_{SAMPLE} = (\delta^{13}C_{MOM} \times f_{MOM}) + (\delta^{13}C_{SOM} \times f_{SOM}) + (\delta^{13}C_{POM} \times f_{POM}) \qquad (4c)$$

With an additional mass balance equation:

$$f_{MOM} + f_{SOM} + f_{POM} = 1 \qquad (5)$$

f_{MOM}, f_{SOM} and f_{POM} are the fractions of marine, soil and plant organic matter, respectively. The end-member values for the C/N ratio and $\delta^{13}C$ content were chosen from a large array of published data and fall within the ranges indicated by Goñi et al. (2006): $C/N_{MOM} = 7$ (Hedges et al., 1997), $C/N_{SOM} = 11$ (Williams et al., 2002) and $C/N_{POM} = 30$ (Gordon and Goñi, 2003); $\delta^{13}C_{MOM} = -20‰$ (Fry and Sherr, 1984), $\delta^{13}C_{SOM} = -26‰$ (Delègue et al., 2001; Powers and Schlesinger, 2002), and $\delta^{13}C_{POM} = -28‰$ (Hedges et al., 1986). This latter value is for every sample corrected for the relatively small admixture of C_4 plant-derived organic matter based on plant-wax $\delta^{13}C$ values (Schefuß et al., 2005). $BIT_{SOM} = 0.91$ and BIT_{MOM} and BIT_{POM} are zero (Hopmans et al., 2004; Weijers et al., 2006b).

Application of the three end-member mixing model to the sediment core GeoB 6518-1 shows that MOM contribution is lowest at the end of the LGM (34%) (Fig. 7.7 and Table 7.2). This contribution increases during the YD (51%) at the expense of SOM (36%) and POM (12%), likely due to increased marine primary production as suggested by the increase in crenarchaeol and alkenone ARs (Fig. 7.4b). At the early Holocene the estimated portion of SOM (51%) is higher relative to MOM (38%) whilst in the late Holocene the opposite situation exists with higher MOM (55%) and lower SOM (38%) estimates, more similar to the YD time interval. Fractions of the 'fresh' POM are generally low with maximum estimates of 16% from the end of the LGM until the YD and 11 and 6% for the early and late Holocene, respectively (Fig. 7.7).
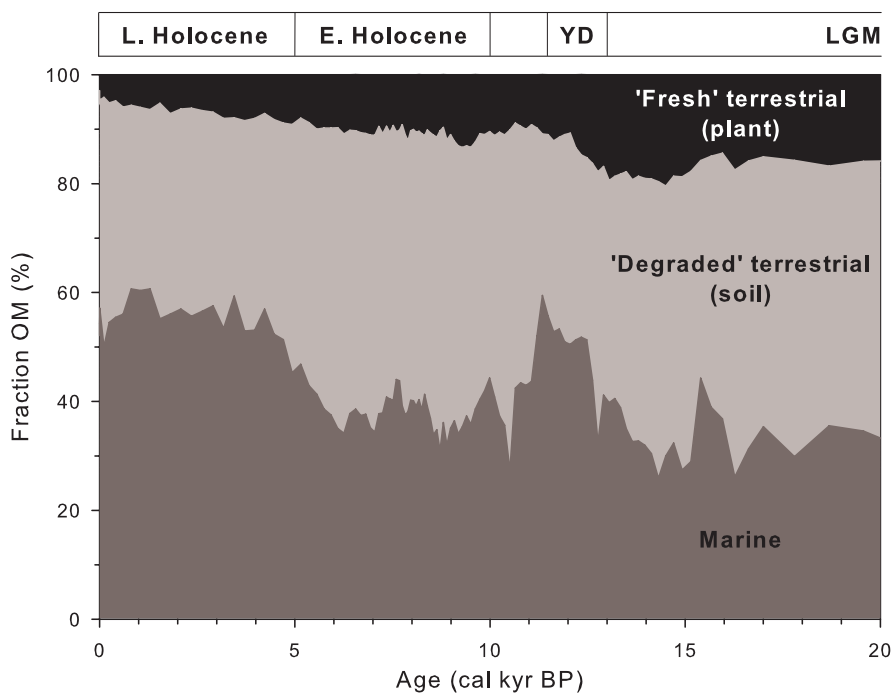
Figure 7.7: Estimates of the organic matter composition at location GeoB 6518-1 over the past 20 kyr based on the three end-member mixing model composed of the C/N ratios and $\delta^{13}C_{org}$ values of TOC and the BIT index.

Comparing these results with the results obtained from the binary mixing models shows that in the three end-member approach the estimated fraction of TOM (= SOM + POM) is higher by about 4 to 8% from the YD to the late Holocene (Tables 7.1 and 7.2). For the time interval from the end of the LGM to the YD, the three end-member model gives an estimate for TOM input of 66%, whereas the average estimate obtained from the binary mixing models is only 37%. Part of this 29% difference might be explained by the problems accompanying TOM estimates with the binary mixing model based on $\delta^{13}C$ values of the bulk OM (see section 4.1.3.), but even if that estimate is left out, the difference is still 23%.

Table 7.2: Contribution (%) of different sources to the organic matter in marine sediments at GeoB 6518-1 integrated over different time intervals using the three end-member mixing model. Number between brackets is standard deviation.

OM fraction	Holocene		Younger Dryas	End of LGM
	Late	Early		
'Fresh' terrestrial (plant) OM	6 (±2)	11 (±1)	12 (±2)	16 (±1)
'Degraded' terrestrial (soil) OM	38 (±4)	51 (±3)	36 (±4)	50 (±5)
Marine OM	55 (±4)	38 (±3)	51 (±4)	34 (±5)

The chosen end-member values in the three end-member model are still generalisations and a wide range of scatter might be present, especially for the C/N ratios and δ^{13}C values, as many different geological, climatological and biological factors can affect these values (see also discussion in section 4.1.3.). A sensitivity test for this model, i.e., changing $\delta^{13}C_{MOM}$ to -19 or -21.5‰, $\delta^{13}C_{SOM}$ to -24‰ or C/N$_{SOM}$ to 9, resulted in maximum differences in contribution of 5% per OM fraction. Overall, these three end-member model results, thus, suggest that about half of the total sedimentary organic carbon deposited in the Congo deep sea fan since the LGM consist of SOM (~ 45%). This result is consistent with the suggestion put forward by Holtvoeth et al. (2005) that SOM is an important contributor to the organic matter in marine sediments of the Congo and Niger deep sea fans during the Late Quaternary. It also is in accordance with global estimates of TOM flux and burial rates showing that the amount of TOM buried off rivers is roughly equal to the amount of MOM buried (Schlünz and Schneider, 2000 and references therein). Although Gordon and Goñi (2003) applied their three end-member model to sediments from a transect from an estuary to the open ocean instead of in a sediment core, they also showed that SOM always remained a significant fraction of the total organic carbon deposited in the marine sediments.

7.4.3. Organic matter fluxes in the Congo deep sea fan

As SOM is predominantly fluvially transported to the marine environment, our SOM input estimates from the three end-member model can be compared with records of African humidity level changes and river discharge fluctuations. Central African humidity changes are obtained from the deuterium content of plant wax *n*-alkanes from core 6518-1 (Fig. 7.6a) and river discharge fluctuations have been reconstructed based on the residual δ^{18}O values of planktonic foraminifera in this core after correction for ice volume and sea-surface temperature changes based on the U$^{K'}_{37}$ record (Fig. 7.6b) (Schefuß et al., 2005). In order to compare absolute OM fluxes rather than trends of relative OM input with river discharge variations, OM fluxes have been calculated by multiplying the estimates of the MOM, the 'degraded' SOM and the 'fresh' POM fractions derived from the three end-member mixing model with the TOC ARs (Fig. 7.8).
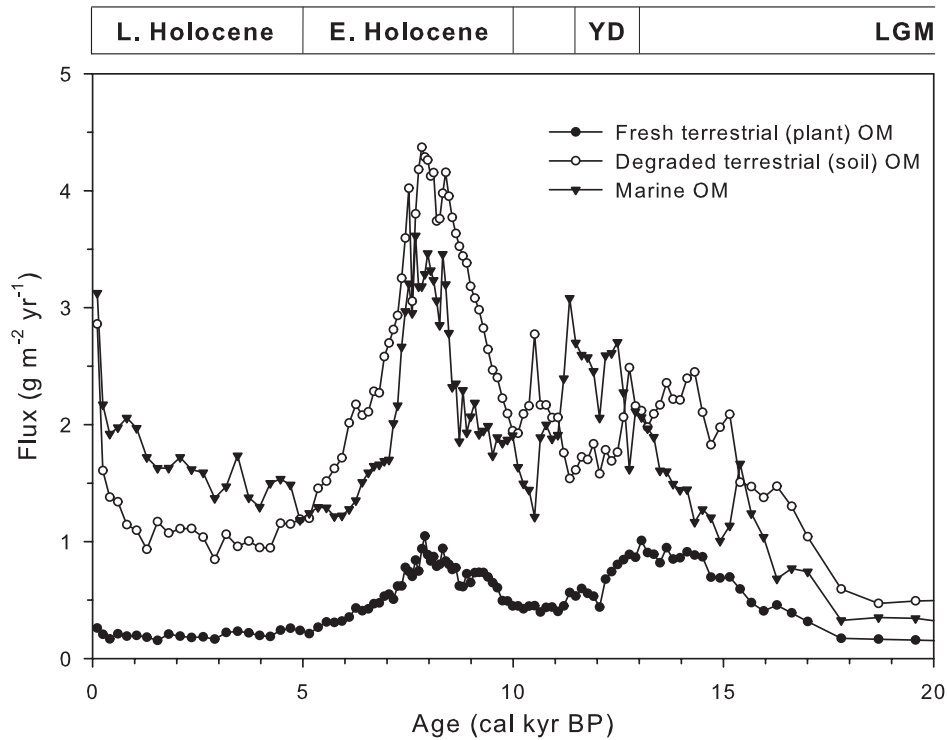
Figure 7.8: Fluxes of the 'fresh' terrestrial (plant) organic matter, the 'degraded' terrestrial (soil) organic matter and the marine organic matter fractions at site GeoB 6518-1 over the past 20 kyr.

With the increase of central African humidity and river discharge at ~17 kyr BP (Fig. 7.6) also the OM fluxes start to increase. The terrestrial SOM and POM fluxes reach a first maximum centred at ~13 to 14 kyr BP, similar to the river discharge and humidity records. During the YD, Congo River discharge clearly declined. This decline is mirrored by both terrestrial organic matter fluxes. The flux of MOM, in contrast, shows a peak around the YD (~12 cal kyr BP). Contemporaneous with highest humidity levels and Congo River discharge, OM fluxes peak at the early Holocene, with the SOM flux showing the strongest increase relative to pre-Holocene values. Towards the end of the early Holocene both terrestrial (SOM and POM) and marine OM fluxes sharply decrease, which is in contrast to the more gradual decrease in Congo River discharge. During the late Holocene, fluxes of all OM fractions are relatively low and MOM fluxes are higher than the SOM fluxes, a situation similar to the time interval around the YD. The increasing OM fluxes during the last 500 yr of the record seem to have no relation with changes in Congo River discharge. Possibly, this is the result of imprecise age-depth correlation for the top part of this core or incomplete diagenesis of the organic matter in the fresh top sediments. Alternatively, due to human activities in the Congo River Basin, the sediment load of the river might have increased dramatically.

Overall, the records of both the degraded (soil) and fresh (plant) terrestrial organic matter fluxes reflect rather well the trends in African humidity and Congo River discharge over the past 20 kyr. Though to a lesser extent, also the record of MOM fluxes mirrors these general trends, probably as a result of higher rates of primary production at times of increased river discharge and thus of increased nutrient delivery to the ocean.

7.4.4. Terrestrial organic matter burial budgets

Our data might allow estimating TOM burial budgets in the Congo deep sea fan. The aerial extent of the Congo deep sea fan is approximately 3×10^{11} m^2 (Anka and Seranne, 2004). The average late Holocene AR of TOC is ~2.8 g m^{-2} yr^{-1} (Fig. 7.4a). For the late Holocene, this TOC consists for 44% of TOM (Table 7.2), giving a TOM AR of ~ 1.2 g m^{-2} yr^{-1}. Multiplying with the Congo deep sea fan area results in a TOM burial flux of ca. 3.7×10^{11} g yr^{-1} for the late Holocene period. It has to be noted that these calculated TOM burial fluxes rely on the assumption that the TOC ARs at the location of core GeoB 6518-1 are representative for the whole Congo deep sea fan. Based on published data from core top sediments of the Congo deep sea fan (Schefuß et al., 2004) TOC ARs have been determined showing a large range between 0.03 and 7.38 gTOC m^{-2} yr^{-1}. Due to dating uncertainties in the top part of the sediment core, unfortunately, we were not able to reliably calculate present day TOC ARs for this core, but given its location and the late Holocene TOC ARs relative to the data of Schefuß et al. (2004) it seems that ARs in this core are likely somewhat higher than on average for the whole deep sea fan and thus that our TOM burial fluxes might represent an overestimation.

Despite this uncertainty, a comparison of our estimated TOM burial flux for the late Holocene to the present day organic matter discharge of the Congo River of ca. 14.4×10^{12} g yr^{-1} (Coynel et al., 2005), shows that only ~ 2.5% of the fluvial TOM input is buried in the marine sediments of the Congo deep sea fan. This burial efficiency might be doubled as TOC AR, and thus TOM burial fluxes, seem to be higher during the last 500 yrs of our record (Fig. 7.4a). With 2.5 to 5%, this burial efficiency is at the lower range of what is found for the Amazon fan (6 to 10%) (Showers and Angle, 1986) and the globally estimated amount of 10% (Schlünz and Schneider, 2000). Nevertheless, considering the number of assumptions made, our estimates seem quite reasonable.

TOM burial flux calculations for the older parts of our record give values of ca. 10.2×10^{11} g yr^{-1} for the early Holocene, 7.1×10^{11} g yr^{-1} for the time interval around the YD and 2.0×10^{11} g yr^{-1} for the end of the LGM (Table 7.3). Thus, TOM burial fluxes have varied considerably over the past 20 kyr (by up to a factor 5) in accord with palaeoriver discharge variations (Fig. 7.6b). This pattern differs from results obtained for the Amazon deep sea fan where a similar budgeting exercise revealed no significant change between last glacial and modern time TOM burial fluxes (3.7 vs. 3.1×10^{12} g yr^{-1}, respectively) (Schlünz et al., 1999), but it has to be noticed that the settings of the Congo deep sea fan and Amazon deep sea fan

differ. Past burial efficiencies of TOM are difficult to estimate as past fluvial TOM discharges are unknown. However, given that Congo River discharge was higher during the early Holocene, the higher TOM burial flux estimated for this time interval is likely the result of higher TOM discharge and not the result of a considerable higher burial efficiency. Thus, the estimated 2.5 to 5% TOM burial efficiency might have been relatively constant over the last deglaciation, implying that the vast majority of TOM input is rather quickly remineralised and/or further dispersed in the ocean (e.g., Opsahl and Benner, 1997).

Table 7.3: TOC accumulation rates, TOM fractions, TOM accumulation rates and TOM burial fluxes averaged over different time intervals in core GeoB 6518-1.

	Holocene		Younger Dryas	End of LGM
	Late	Early		
TOC AR (g m^{-2} yr^{-1})	2.8	5.5	4.9	1.0
Fraction TOM (%)	44	62	48	66
TOM AR (g m^{-2} yr^{-1})	1.2	3.4	2.4	0.7
TOM burial flux ($\times 10^{11}$ g yr^{-1})	3.7	10.2	7.1	2

7.5. Conclusions

(1) Analysis of a 20 kyr sedimentary record from the Congo deep sea fan (core GeoB 6518-1) shows that the different individual proxies for relative TOM input in marine sediments do not show similar patterns due to the notoriously heterogeneous nature of the OM. On a glacial-interglacial time scale, however, this multi-proxy approach indicates general trends in relative TOM input, such as a higher input during the early Holocene.

(2) With regard to proportions of TOM input, estimates obtained from binary mixing models vary by up to 40%. Application of a three end-member mixing model, distinguishing a 'degraded' soil OM and a 'fresh' plant OM fraction, suggests that SOM accounts for about half (~ 45% on average) of the OM present in the marine sediments of the Congo deep sea fan over the past 20 kyr.

(3) The combined fluxes of the 'fresh' plant organic matter and the 'degraded' soil organic matter fractions over the past 20 kyr show an increase of TOM accumulation since ca. 17 kyr BP, a decline during the YD, peak accumulation during the early Holocene and relative low accumulation in the late Holocene. This is a similar pattern as revealed by reconstructions of past central African humidity and Congo River discharge. TOM accumulation, thus, seems to follow long-term palaeodischarge fluctuations of the Congo River rather well. Except for the YD, also MOM

accumulation shows this general pattern, likely due to increased primary production at times of high river discharge.

(4) Tentative TOM budget calculations for the Congo deep sea fan suggest that 2.5 to 5% of the fluvial TOM input by the Congo River is buried in fan sediments and that TOM accumulation in these sediments probably has varied by up to a factor 5 over the last deglaciation.

Acknowledgements

Chapter 8

Early reactivation of European rivers during the last deglaciation

Guillemette Ménot, Edouard Bard, Frauke Rostek, Johan W.H. Weijers, Ellen C. Hopmans, Stefan Schouten and Jaap S. Sinninghe Damsté

Abstract

During the Last Glacial Maximum, the sea-level low stand combined with the large extent of the Fennoscandian and British ice sheets led to the funneling of European continental runoff, resulting in the largest river system that ever drained the European continent. Here we show an abrupt and early reactivation of the European hydrological cycle at the onset of the last deglaciation, leading to intense discharge of the Channel River into the Bay of Biscay. This freshwater influx, probably combined with inputs from proglacial or ice-dammed lakes, dramatically affected the hydrology of the region, both on land and in the ocean.

Despite the recognized sensitivity of oceanic circulation to changes in the freshwater budget at high latitudes (Broecker et al., 1989; Stocker and Wright, 1991; Manabe and Stouffer, 1997; Ganopolski and Rahmstorf, 2001), river runoff studies have so far mainly been focused on low-latitude palaeorecords (Adegbie et al., 2003; Jennerjahn et al., 2004; Schefuß et al., 2005). Furthermore, except for a few continental archives such as speleothems and wetlands that reflect local conditions, little is known about hydrological and water drainage changes in Europe during the last deglaciation. During the Last Glacial Maximum (LGM), a large ice sheet (known as the Fennoscandian ice sheet) was established on the Eurasian continent. Both the sea-level low stand and the extent of the ice sheet deeply influenced the drainage basins of European rivers that flowed into the Channel River, thus generating one of the largest rivers ever to have extended across the European continent (Fig. 8.1). Because this river transported much of the meltwaters coming from the European glaciers as well as from the Fennoscandian and British-Irish ice sheets (Scourse et al., 2000; Antoine et al., 2003), its runoff is expected to have reacted strongly to the retreat and growth of the Eurasian ice sheets and of the alpine glaciers. Therefore, a record of the activity of this palaeoriver could provide a detailed account of the effect of European deglaciation on the hydrological cycle.

Core MD952002 (47°27'N, 8°32'W, 2174 m water depth) was recovered on the northwestern slope of the Bay of Biscay in the direct axis of the English Channel during the IMAGES 101 cruise of the research vessel Marion Dufresne (Fig. 8.1). The chronology of this core is based on calibrated ^{14}C ages (see supporting material for methods at the end of this chapter). This core covers a critical period including the last deglaciation, as well as abrupt climatic changes such as Heinrich events 1 and 2 (H1 and H2), which are clearly identified by two discrete peaks in the abundance of lithic grains and the magnetic susceptibility at 16 and 24 thousand years before the present (kyr B.P.) (Fig. 8.2B) (Zaragosi et al., 2001). Total organic carbon (TOC) content varies between 0.2 and 1.2%, with minima during both H1 and H2 events (green circles in Fig. 8.2C). The $C_{37:4}$ alkenone, a biomarker derived from haptophyte algae and thought to be a proxy for low-salinity water associated with icebergs (Bard et al., 2000), is absent during the Holocene but exhibits high values between 11 and 18 kyr B.P., with a prominent maximum reached during H1, corresponding to 30% $C_{37:4}$ among the total of C_{37} alkenones (black diamonds in Fig. 8.2C). This is a characteristic feature for H1 in this area and has been related to the advection of low-salinity water associated with icebergs (Bard et al., 2000).

Figure 8.1: The palaeoenvironment of the LGM on the Eurasian continent was radically different from today. The Fennoscandian ice sheet was established on the northern part of Europe, extending west into the Norwegian Sea, south across the north German Plain into Poland, and eastward into North Poland and Russia (Bowen et al., 2002; Mangerud et al., 2004). A smaller dome was installed on the British Isles (Bowen et al., 2002). Recent geomorphological evidence indicates that the British-Irish ice sheet (BIS) and Fennoscandian ice sheet coalesced, and a huge ice dam extended over the present-day North Sea (Mangerud et al., 2004; Svendsen et al., 2004). The Alps were almost entirely covered by an ice dome formed by valley glaciers (Denton and Hughes, 1981). The maximum extent of ice sheets at the LGM is illustrated by the blue contours. A final ice-age sea-level lowstand led to emersion of the channel between England and France, with the coastlines at 14 and 21 kyr B.P. illustrated by the dashed lines (after Lambeck, 1997). A palaeoriver, known as the Channel River (in orange), extended across the emerged continental margin (Bourillet et al., 2003). It drained most of the major rivers in northwestern Europe, that is, the Rhine, Maas, Seine, Solent and Thames (yellow arrows on the map). In addition to these rivers, the Irish Sea drained a large part of the BIS meltwaters (McCabe and Clark, 1998). Furthermore, damming by the Fennoscandian ice sheet favored the development of southward-flowing meltwater valleys and ice-margin spillways running westward. These spillways collected proglacial waters from rivers even farther east than the Elbe basin and allowed drainage to the Channel River (Marks, 2002; Mangerud et al., 2004). Core MD952002 (red dot) was taken at a water depth of 2174 m in the axis of the English Channel, close to the LGM position of the Channel River outlet. See page 167 for color figure.
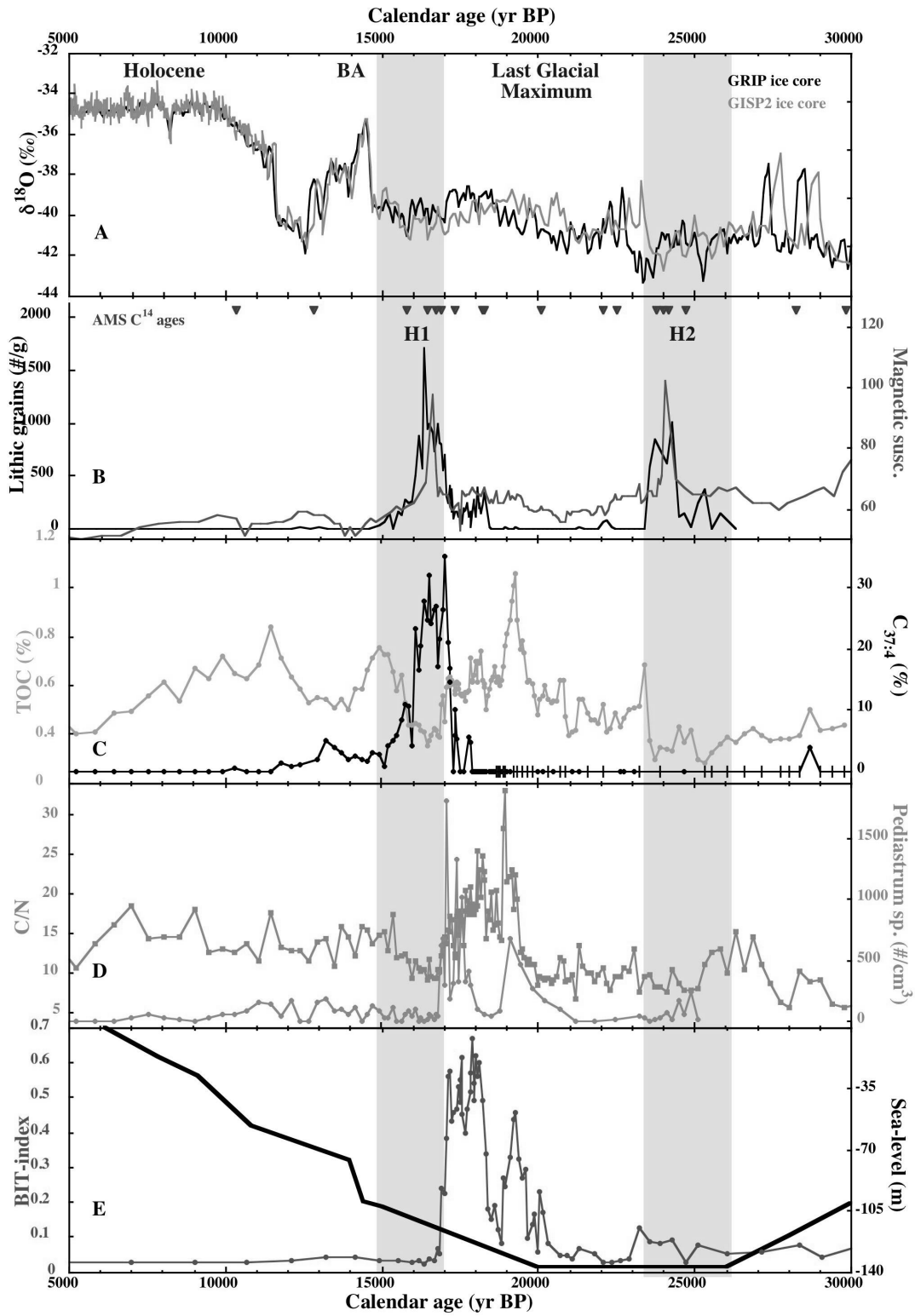
We applied the branched and isoprenoid tetraether (BIT) index to reconstruct terrestrial organic matter fluvially transported to the ocean (Hopmans et al., 2004). This proxy uses the relative abundance of membrane lipids (i.e., non-isoprenoid glycerol dialkyl glycerol tetraethers) (Sinninghe Damsté et al., 2000) derived from anaerobic bacteria thriving in soils and peats (Weijers et al., 2006a), compared with crenarchaeol, a structurally related isoprenoid molecule characteristic of ubiquitous marine planktonic and lacustrine crenarchaeaota (Sinninghe Damsté et al., 2002). BIT-values for suspended particulate matter in river waters are typically >0.9 (Herfort et al., 2006). A survey of Holocene sediments showed that the BIT index can be directly correlated to the relative amount of fluvial terrestrial organic matter input. BIT index values of <0.1 are typical for open marine settings receiving only small amounts of terrestrial organic matter, while values >0.4 are typical for river fans and fjord systems (Hopmans et al., 2004). The BIT index values throughout the core MD952002 remain below 0.1, except for two well-defined peaks with values as high as 0.7 centered at 19.5 kyr B.P. and between 19 and 17 kyr B.P. (red circles in Fig. 8.2E). The two maxima in the BIT-index profile, therefore, reveal periods during which large amounts of terrestrial organic matter must have been transported to this site in the Bay of Biscay. These maxima are consistent with those obtained from the abundance of remains of freshwater algae (*Pediastrum sp.*) (blue curve on Fig. 8.2D) (Zaragosi et al., 2001). The total organic carbon-to-nitrogen ratio (C/N) varies between 5 and 30, with minimum values typical of the marine environment end-member during H1 and H2 events, and higher values in the intervening period, also indicative of a larger terrestrial contribution (Fig. 8.2D).

Figure 8.2 (opposite page)**:** Deglaciation-Holocene records of the past activity of the Channel River as a function of palaeoclimatic changes. The chronology is based on calibrated ^{14}C ages measured on planktonic foraminifera [shown as triangles in (B)] (see supporting material at the end of this chapter). Climatic events are abbreviated as follows: B-A, Bølling-Allerød; H1, Heinrich 1; and H2, Heinrich 2. The grey areas underline the H1 and H2 events. (**A**) δ^{18}O GRIP (black line) (Johnsen et al., 2001) and δ^{18}O GISP2 (light blue line) (Stuiver and Grootes, 2000) records reflecting Greenland air temperatures. (**B**) Black line shows the counting of grains identified as ice-rafted debris (IRD) per 10 g for the size fraction coarser than 150 μm, and the grey curve shows the magnetic susceptibility (MS) record measured on board Marion Dufresne (Auffret et al., 2002). (**C**) Green circles represent the total organic carbon contents, and the black diamonds the percentage of $C_{37:4}$ among C_{37} alkenones, i.e., %$C_{37:4}$ = 100 × [$C_{37:4}$]/[$C_{37:2}$ + $C_{37:3}$ + $C_{37:4}$]. Beyond 19 kyr B.P., the relative percentage of $C_{37:4}$ could not be quantified because alkenones are very scarce in the sediments corresponding to the last glacial period (black ticks in Fig. 8.2C). (**D**) Orange squares indicate the total organic carbon-to-nitrogen ratios (C/N), and the blue symbols show the abundance of freshwater algae, *Pediastrum sp.* (counts from Zaragosi et al., 2001). (**E**) The BIT index is defined as follows: BIT = (I+II+III)/[(I+II+III)+(IV)] (the roman numbers refer to the glycerol dialkyl glycerol tetraethers in Figure 5.1, Hopmans et al., 2004), and is represented here by red dots. The black curve shows the sea-level curve (Lambeck et al., 2002). See page 168 for color figure.

During H2 and the LGM, cold and dry conditions prevailed on the European continent (Allen et al., 1999). At that time, ice sheets reached their maximum extent (Fig. 8.1) and sedimentation at the Channel River outlet was typical of a marine environment with low values of the BIT index and TOC as well as low C/N ratios (Fig. 8.2, C to E). At the end of the LGM, between 21 and 17 kyr B.P., an early warming is observed in the Greenland air-temperature record (Fig. 8.2A). This temperature increase is also clearly detected in several North Atlantic records (e.g., Jones and Keigwin, 1988; Bard et al., 2000; Pailler and Bard, 2002; Alley et al., 2002) as well as in continental reconstructions inferred from pollen in lacustrine and peat sequences over Europe (e.g., Sanchez Goñi et al., 2000; Combourieu Nebout et al., 2002). This warming was accompanied by enhanced precipitation, as is also evident from the pollen assemblages. Despite this climatic warming, soils remained partly frozen and hence impermeable (Renssen and Vandenberghe, 2003). Furthermore, the vegetation cover was scarce and spatially discontinuous, mainly composed of peat with only few woody species (Tzedakis et al., 2002). This situation led to the development of large fluvial systems, intense soil erosion, and enhanced river discharge. This transient period is coincident with an abrupt maximum in the BIT index in core MD952002 (Fig. 8.2E), indicative of an early and drastic reactivation of European rivers.

Associated with this reactivation of the hydrological cycle, meltwaters might well have played a role in the runoff increase. In fact, when the Fennoscandian ice sheet started to retreat from its maximum position at ~22 kyr B.P., a new series of short-lived glacial lakes formed at its southern margin, more particularly in the Polish basins and German lowlands (Marks, 2002; Bowen et al., 2002). Because of the position of the ice margin, the meltwaters first drained through the southern Peribaltic area toward central Poland, to the Elbe River, and then to the Channel River (Mangerud et al., 2004). The retreat was not continuous, and readvances of the Fennoscandian ice sheet have been recognized based on geomorphological and lithostratigraphic evidences as well as by cosmonuclide and thermoluminescence dating (Marks, 2002; Bowen et al., 2002). Two major deglaciation phases have been reported in Poland during the low sea-level stand: the Poznan and the Pomeranian phases at 22.0 and 18.6 kyr B.P. (Marks, 2002). Similar pulsations have also been described for the British-Irish ice sheet over the same period (Bowen et al., 2002). On the southeastern sector, the Scandinavian ice sheet begins to retreat around 19 kyr B.P. after a phase of maximum extent at 20.9 kyr B.P. (Rinterknecht et al., 2006). A massive and early breakdown of the LGM system of ice domes in the Alps is reported to occur simultaneously (e.g., Ivy-Ochs et al., 2006).

A peculiar geographic setting reinforced the effect of this increased water runoff from the European continent, leading to increased discharge of the River Channel into the Bay of Biscay. In fact, the low sea level during the LGM (Fig. 8.2E) means that the river mouth was located very close to the core location [the dashed line in Fig. 8.1 represents the palaeocoastline at 21 kyr B.P., reconstructed after Lambeck (1997)]. Moreover, due to the topography of the catchment basin, the Channel River drained a large area with inputs from

the Rhine, Seine, Maas and Thames basins (Antoine et al., 2003). This topographic funneling effect was reinforced by the location of the British-Irish ice sheet, which reached its maximum extent at 16.7 kyr B.P. (McCabe and Clark, 1998). A simultaneous readvance of the Scandinavian ice sheet is recorded on the southeastern sector (Rinterknecht et al., 2006).

The onset of the H1 event, at 17 kyr B.P., is characterized by the sudden drop in the BIT index (Fig. 8.2E). As already observed for Heinrich events (Pailler and Bard, 2002), the biological productivity is low, but the BIT index indicates a predominant marine origin for the sedimentary organic matter (Fig. 8.2). Consistently, the C/N record exhibits a clear minimum over this time interval. Furthermore, a prominent $C_{37:4}$ alkenone peak is synchronous with the maximum abundance in lithic grains. A similar maximum of $C_{37:4}$ linked to H1 has already been described at other sites (Rosell-Melé, 1998; Bard et al., 2000). The fall in BIT index is clearly simultaneous with the rise in lithic grain abundance and percentage of $C_{37:4}$ alkenone, indicating that this switch was probably due to the impact on marine hydrology of icebergs coming from the Fennoscandian and the Laurentide ice sheets (Grousset et al., 2000). In parallel, the return to dry and cold conditions on the continent during H1 probably led to a regime with less fluvial runoff.

There was no recurrence of high BIT index values when warmer and wetter conditions returned during the Bølling-Allerød and the Holocene period (Fig. 8.2E). This is probably due to the sea-level rise of about 60 m compared with the LGM lowstand, which caused a northward displacement of the river mouth by about 300 km and thus a more attenuated influence of the Channel River at the core site (Fig. 8.1). Furthermore, due to the position of the Fennoscandian ice margins during the Bølling-Allerød, the meltwaters of the Peribaltic area drained into the southern part of the Baltic Basin and no longer through Poland and the Elbe Basin (Mangerud et al., 2004).

The abrupt runoff event that occurred at the onset of the last deglaciation on the European continent is unique in magnitude and timing and reflects an early reactivation of the European hydrological cycle leading to an intense discharge of terrestrial organic matter on the Celtic Margin and Bay of Biscay. The intensity of this event is due to a peculiar combination of topographic and palaeoclimatic factors: the large extent of the Fennoscandian and the British ice sheets, which coalesced over the North Sea, forced the drainage of rivers into the Channel River, thus creating one of the largest river systems ever existing on the European continent. The reactivation of European river runoff has also probably been fuelled by proglacial lakes developing at the southern margin of the ice sheets. Indeed, high abundances of remains of freshwater algae are found simultaneous with the large increase in BIT index (Fig. 8.2).

Interestingly, although the freshening of the surface waters starting at 21.5 kyr B.P. is progressive and parallel to the temperature increase after the LGM, the return to fully marine conditions is sharp and occurs in about a century at the start of the H1 event. As a result of sea-level rise, after 17 kyr B.P., conditions never became suitable again for recording events of the Channel River of such a magnitude in the Bay of Biscay.

Our results reveal large changes in the magnitude of the discharge of cold fresh water into the North Atlantic during the last deglaciation. This situation is similar to that reconstructed for the Laurentide ice sheet meltwater outflow which probably affected the meridional overturning circulation (Broecker et al., 1989; Manabe and Stouffer, 1997). Modeling experiments could help to evaluate the effect of the European river reactivation on the millennium-scale climatic events that punctuated the last deglaciation.

Acknowledgments

Supporting Material

Analytical methods

After freeze-drying and grinding, sediments were analyzed at CEREGE for their nitrogen and organic carbon contents with a Fisons NA-1500 Elemental Analyzer [Carlo Erba NA-1500 Elemental Analyzer; see Pailler and Bard (2002) for details]. For lipid analysis, 1 to 5 g of sediment was extracted for biomarkers by the accelerated solvent extraction method (ASE 200 system, Dionex, California, USA) at 120°C and 100 bars with dichloromethane/methanol (9:1 v/v). The total lipid extract was analyzed at CEREGE for alkenone concentrations by gas chromatography (GC8000 Series Fisons) with flame ionization detection (GC-FID) [using analytical conditions similar to Sonzogni et al. (1997)]. % $C_{37:4}$ expresses the percentage of the tetra-unsaturated C_{37} alkenone among the total of C_{37} alkenones. Identification of alkenones is based on GC mass spectrometry (GC-MS; GC8000 MD800 Fisons) and quantities are based on the chromatographic peak areas. The total lipid extract was subsequently separated into polar and apolar fractions using a column packed with Al_2O_3 using hexane/dichloromethane (9:1, v/v) and dichloromethane/methanol (1:1, v/v) as eluents, respectively. The polar fraction was then filtered through a 0.45-μm, 4-mm diameter PTFE filter prior to injection. Glycerol dialkyl glycerol tetraethers were then identified and quantified at NIOZ by high-performance liquid chromatography/atmospheric pressure chemical ionization mass spectrometry using a HPLC/MS 1100 Series as described by Hopmans et al. (2004).

The age/depth scale is based on tie points shown as triangles on Figure 8.2A, which rely on ^{14}C ages (Auffret et al., 2002; Zaragosi et al., 2006) measured by accelerator mass spectrometry on monospecific samples of planktonic foraminifera *Neogloboquadrina pachyderma* (s.) or *Globigerina bulloïdes*. We calibrated these ^{14}C ages by using the Calib 5.0 radiocarbon calibration program (Stuiver and Reimer, 1993) with the Marine04 curve (Hughen et al., 2004), and an extension (Bard et al., 1998; Bard et al., 2004) for the three oldest ^{14}C ages. The age/depth model is then derived by a fifth order polynomial. The chronology is therefore fully independent of the GRIP and GISP2 records for the time span between 0 and 30 kyr B.P..

Chapter 9

Environmental controls on bacterial tetraether membrane lipid distribution in soils

Johan W.H. Weijers, Stefan Schouten, Jurgen C. van den Donker, Ellen C. Hopmans and Jaap S. Sinninghe Damsté

Abstract

Over the last years a novel group of branched glycerol dialkyl glycerol tetraether (GDGT) membrane lipids has been discovered in peat bogs and soils. They consist of components with 4 to 6 methyl groups attached to the *n*-alkyl chains and 0 to 2 cyclopentyl moieties in the alkyl chain. These branched membrane lipids are produced by an as yet unknown group of anaerobic soil bacteria. In this study we analysed the branched membrane lipid content of 134 soil samples from 90 globally distributed locations to study the environmental factors controlling the relative distribution of the different branched GDGT isomers. Our results show that the relative amount of cyclopentyl moieties, expressed in the cyclisation ratio of branched tetraethers (CBT), is primarily related to the pH of the soil ($R^2 = 0.70$) and not to temperature ($R^2 = 0.03$). The relative amount of methyl branches, expressed in the methylation index of branched tetraethers (MBT), is positively correlated with the annual mean air temperature (MAT) ($R^2 = 0.62$) and, to a lesser extent, negatively correlated with the pH of the soil ($R^2 = 0.37$). If both parameters are combined, however, it appears that the variation in the MBT is largely explained by both MAT and pH ($R^2 = 0.82$). These results suggest that the relative distribution of soil-derived GDGT membrane lipids can be used in palaeoenvironmental studies to estimate past annual MAT and soil pH.

9.1. Introduction

The presence, distribution and isotopic composition of organic compounds in sediments and soils are widely used to reveal changes in past environmental conditions. Plant wax *n*-alkanes, for example, are indicative of higher plant vegetation and their carbon and hydrogen isotopic compositions provide information about the abundance of C_4- versus C_3-type vegetation and continental humidity, respectively (Eglinton et al., 1962; Schefuß et al., 2004; Chikaraishi et al., 2004; Schefuß et al., 2005). Derivatives of the characteristic pigment isorenieratene are indicative of euxinic (i.e., anoxic and sulfidic) conditions within the photic zone of the water column (Sinninghe Damsté et al., 1993; Koopmans et al., 1996) and the relative distribution of long chain unsaturated ketones, derived from haptophyte microalgae is used in the U^{k}_{37}' ratio to estimate sea surface temperature (SST) (Brassell et al., 1986; Prahl and Wakeham, 1987). An additional, more recently developed organic proxy that is used for SST reconstructions is the TEX_{86} (Schouten et al., 2002). The TEX_{86} is an index representing the relative distribution of cyclopentyl containing isoprenoid glycerol dialkyl glycerol tetraethers (GDGTs) (Schouten et al., 2002), which are the core membrane lipids of mesophilic Crenarchaeota, an ubiquitous and abundant group of pico-plankton in marine and lacustrine waters (Karner et al., 2001; Keough et al., 2003). It has been shown that the relative distribution of these GDGTs in pelagic Crenarchaeota is highly correlated to growth temperatures (Wuchter et al., 2004) and, hence, that these distributions throughout the sedimentary record can be used to estimate past SST (Schouten et al., 2002; Powers et al., 2004).

A related group of core membrane lipids, with respect to their chemical structure, constitute the branched GDGTs, which have been detected in peat bogs and soils (Sinninghe Damsté et al., 2000; Weijers et al., 2006a, 2006b). Despite their membrane-spanning nature and the presence of ether bonds, they have been proven, based on their straight alkyl chain and stereo configuration at the C-2 position of the glycerol backbone, to be of bacterial origin, presumably produced by anaerobic bacteria thriving in soils and peat bogs (Weijers et al., 2006a). The various branched GDGT lipids differ both in the amount of methyl groups attached to their alkyl chains and in the amount of cyclopentyl moieties (Sinninghe Damsté et al., 2000; Weijers et al., 2006a) (see the Appendix for structures). However, the controlling factors on the relative distribution of these peculiar membrane lipids are currently unknown. Unfortunately, the bacteria producing these branched GDGTs are as yet unknown and consequently not available in culture, preventing any cultivation experiments. To circumvent this problem, we analysed a set of 134 soils from 90 different locations from a wide variety of settings for their branched GDGT composition and performed a principal component analysis (PCA) in order to obtain information on the environmental parameters potentially controlling the distribution of these branched GDGTs in soils.

9.2. Materials and methods

9.2.1. Soil collection

The soils used for this study (Table A9.1 at the end of this chapter) are predominantly obtained from the soil sample repository of the International Soil Reference and Information Centre (ISRIC) in Wageningen, the Netherlands. In addition to the soils from the ISRIC sample collection, which were obtained in the period 1960-1990, a number of soils were sampled in the field. Generally, samples from each soil are derived from one or two depth intervals between ca. 0-30 cm depth.

9.2.2. Determination of environmental parameters

If available, pH values, concentrations of summed cations (Ca, Mg, Na and K; in meq/100g) and the electronic conductivity (in mS/cm) of the soils were obtained from the ISRIC Soil Information System database (ISIS version 5.0). The pH values of the remaining soils were measured according to standard methods, i.e., in a soil/water mixture of 1:2.5 (v/v), with a pH measuring instrument (pH315i/SET, WTW Weilheim, Germany). Re-measurement of some soils from the ISRIC collection showed that our lab measurements are within $\pm$ 0.1 pH unit from those reported in the ISIS database.

The annual mean air temperatures and annual mean precipitation at climate stations nearest to the sample locations were obtained from the World Climate Information database (KNMI, 1997) of the Royal Dutch Meteorological Institute (KNMI) and represent a 30 year average over the period 1961-1990. If necessary, a temperature correction was made for differences in altitude between the sample location and the weather station by linearly interpolating the temperature between two nearby stations at different altitudes. In cases where insufficient climate stations were present in the World Climate Information database, data were obtained from either the database of the ISRIC or from websites of local weather stations.

9.2.3. Sample preparation for GDGT analysis

If necessary, samples were freeze dried and powdered with mortar and pestle prior to extraction. Extraction was performed 3 times with an accelerated solvent extractor (ASE; DIONEX2000) with a solvent mixture of dichloromethane (DCM):methanol 9:1 (v/v) at a temperature of 100 ºC and a pressure of 7.6 x 10^6 Pa for 5 min. The obtained total extracts were rotary evaporated under near vacuum and separated over an activated Al_2O_3 column, using DCM and DCM:methanol 1:1 (v/v), into an apolar and polar fraction, respectively. The polar fraction, containing the branched GDGTs, was then dried under a continuous N_2 flow, ultrasonically dissolved in a hexane:propanol 99:1 (v/v) mixture at a concentration of 2 mg ml^{-1} and filtered through an 0.45 μm PTFE filter (ø 4 mm) prior to analysis.

9.2.4. HPLC/APCI-MS

The samples were analysed by high performance liquid chromatography / atmospheric pressure chemical ionisation – mass spectrometry (HPLC/APCI-MS) on an Agilent 1100 series / Hewlett-Packard 1100 MSD series machine equipped with automatic injector and HP Chemstation software according to Hopmans et al. (2000) with minor modifications. Separation was achieved in normal phase on an Alltech Prevail Cyano column (150 mm x 2.1 mm; 3 μm). The flow rate of the hexane:propanol 99:1 (v/v) eluent was 0.2 ml min^{-1}, isocratically for the first 5 min, thereafter with a linear gradient to 1.8% propanol in 45 min. Injection volume of the samples was 10 μl. In order to increase sensitivity and therefore reproducibility, ion scanning was performed in a single ion monitoring (SIM) mode. Quantification of the compounds was achieved by integrating the areas of the [M+H]$^{+}$ (protonated molecular ion) peaks and comparing these with an external standard curve composed of known amounts of crenarchaeol (an isoprenoid GDGT).

9.2.5. Principal component analysis

Principal component analysis (PCA) was performed to independently identify the interrelations and the directions of these relations between the branched GDGT composition and the different soil parameters and to determine the amount of variance in the data set that is explained by these interrelations. The method (Morrison, 1976) assigns a loading to each variable, i.e. soil parameter, on each principal component, representing the degree (and direction) by which this parameter is influenced by that factor. A commonly employed sub-routine is VARIMAX-rotation of the calculated factor loading. This calculation method involves the rotation of the factor-axes in a multi-dimensional space, resulting in the simplest composition of factors, with either minimum or maximum loading of each variable on the extracted factors while preserving trends. The SYSTAT software package (Systat 11.0) was used for all PCA calculations.

9.3. Results and discussion

9.3.1. Distribution of branched GDGTs in soils and PCA results

A total of 134 soils from 90 globally distributed locations (Table A9.1 and Fig. 9.1) was analysed for their branched GDGT membrane lipid content (see Fig. A9.1 in the Appendix for GDGT structures). Branched GDGT membrane lipids were present in every soil analyzed, supporting an earlier report on the widespread occurrence of these membrane lipids in soils (Weijers et al., 2006b). However, large differences in the abundance of the different branched GDGTs occur throughout the sample set. The first observation apparent from the chromatograms is the large difference in the distribution of branched GDGTs **I**, **II** and **III**, containing none, one or two additional methyl branches on the positions 5 and 5' of their

carbon chain, respectively (see the Appendix), in the different soils (Fig. 9.2). Occasionally, GDGT **III** abundances are below detection limit, whereas in other soils it is one of the more abundant compounds. Branched GDGTs containing one or two cyclopentyl moieties (**Ib-IIIb** and **Ic-IIIc**) (Weijers et al., 2006a) are clearly less abundant than the branched GDGTs not containing cyclopentyl moieties (**I-III**) (Fig. 9.3). GDGTs **IIIb**, **IIc** and **IIIc** were sometimes even not detected. However, their abundance relative to the non-cyclopentyl-containing branched GDGTs varies considerably between the different soils.

Figure 9.1: World map giving a general overview of the different locations of soil samples used in this study.
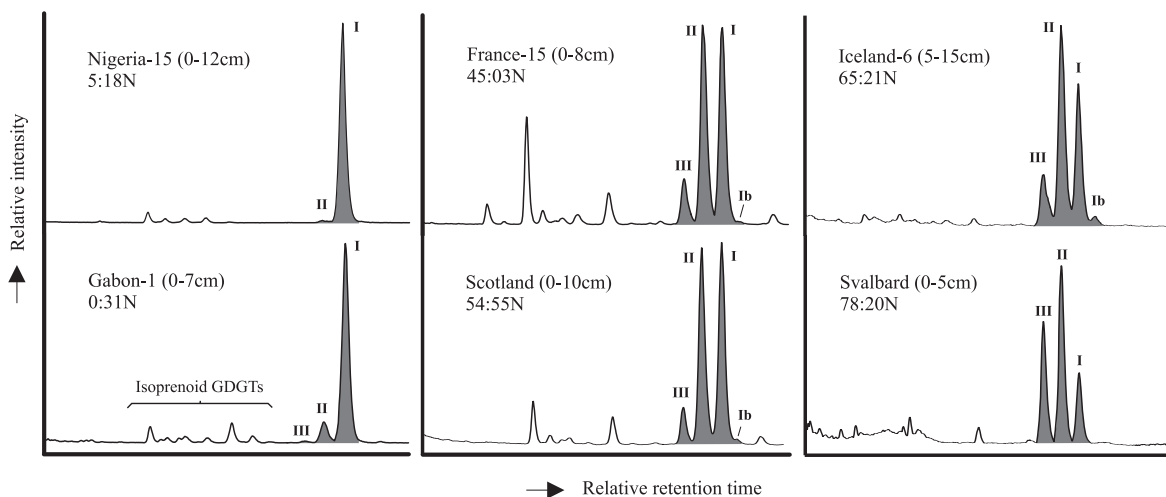
Figure 9.2: HPLC/MS base peak chromatograms of soils from 6 different locations showing the differences in branched glycerol dialkyl glycerol tetraether (GDGT) distribution. Roman numerals refer to the structures drawn in Fig. A9.1 in the Appendix.

Absolute concentrations of individual branched GDGTs vary to a large extent from 1 to 1000 ng g^{-1} TOC. Generally, higher concentrations of branched GDGTs are found in soils with a lower pH (Fig. 9.4). This suggests that growth conditions for the branched GDGT-producing bacteria are more optimal at low (<6) pH ranges.
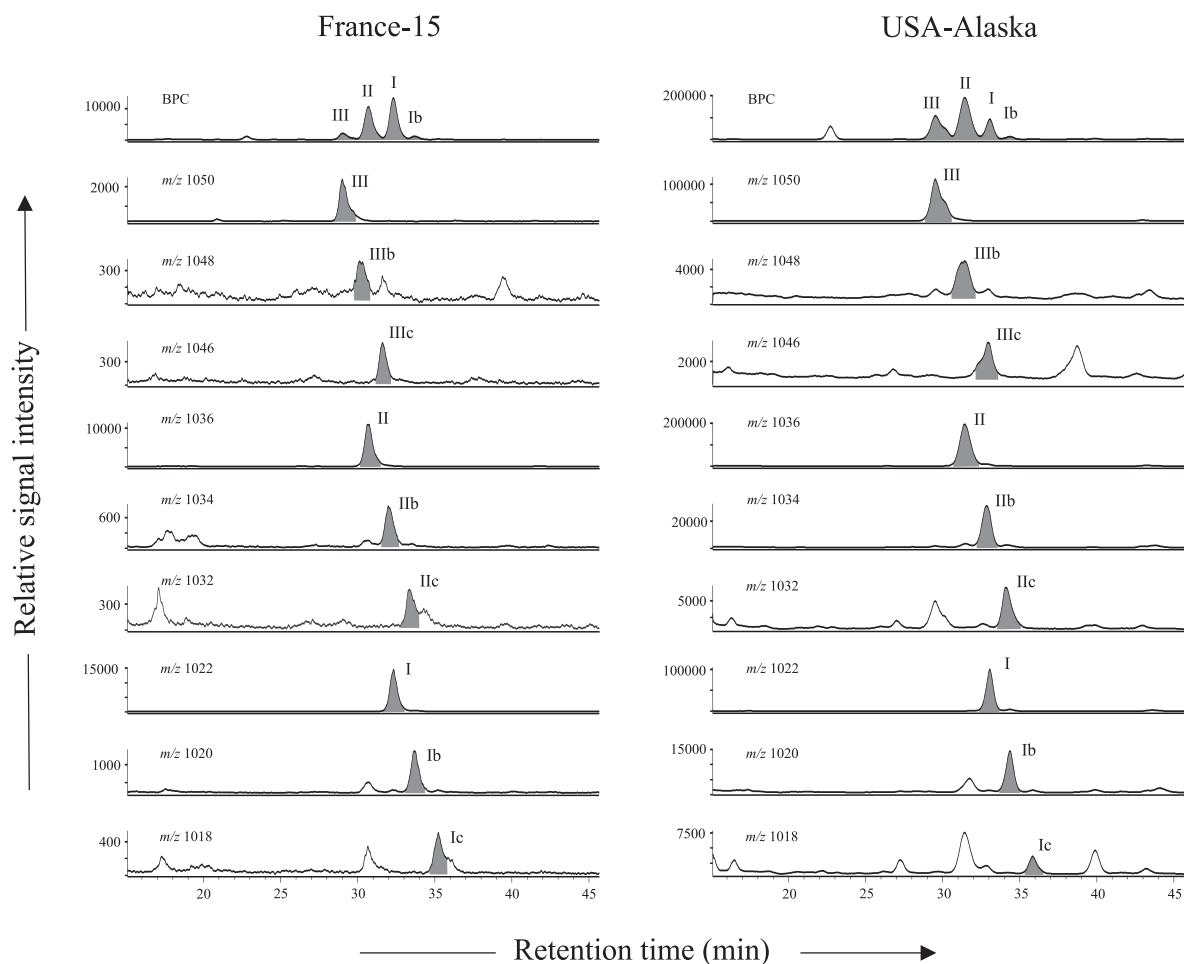
Figure 9.3: HPLC/MS base peak chromatograms plus mass chromatograms of the different branched GDGTs found in two soils of different pH. Soil 'France-15' has a pH value of 4.3 and the soil 'USA-Alaska' has a pH of 7.1. Roman numerals refer to the structures in Fig. A9.1 in the Appendix.

The average amounts of methyl branches and cyclopentyl moieties, thus, seem to be highly variable in the soil dataset. In order to quantify these differences in GDGT distributions and to use them in a principal component analysis, two ratios were defined. The first one, the Methylation index of Branched Tetraethers (MBT) represents the degree of methylation at position C-5 and C-5' of the branched GDGTs and is defined as follows:

$$MBT = \frac{[I + Ib + Ic]}{[I + Ib + Ic] + [II + IIb + IIc] + [III + IIIb + IIIc]} \qquad (1)$$

with a high MBT value being representative of a low degree of methylation and vice versa. The cyclopentyl containing GDGTs are included, since cyclopentyl moieties most likely are synthesised by an internal cyclisation (Weijers et al., 2006a) in a similar way as is proposed for archaeal isoprenoid lipids (De Rosa et al., 1977). The MBT values of the soils analysed in this study vary between 0.16 and 0.99 (e.g., soils Spitsbergen-2 and Gabon-3; Table A9.1).

In addition to the MBT index, we defined the cyclisation ratio as a measure for the relative amount of cyclopentyl moieties in branched GDGTs:

$$\text{Cyclisation ratio} = \frac{[\textbf{Ib}] + [\textbf{IIb}]}{[\textbf{I}] + [\textbf{II}]} \tag{2}$$

Due to the often low abundance of branched GDGTs **IIIb**, **IIc** and **IIIc**, hindering proper quantification, these isomers and consequently also GDGTs **Ic** and **III** were excluded from this ratio. Cyclisation ratios of the soils analysed in this study range from 0.01 to 0.50 (e.g., soils Finland-2 and Netherlands-Bunde; Table A9.1), where higher values are indicative of relatively high abundances of cyclopentyl containing branched GDGTs. Based on duplicate HPLC/MS-analyses, the analytical error of both the MBT index and the cyclisation ratio was determined at ± 0.01 units.
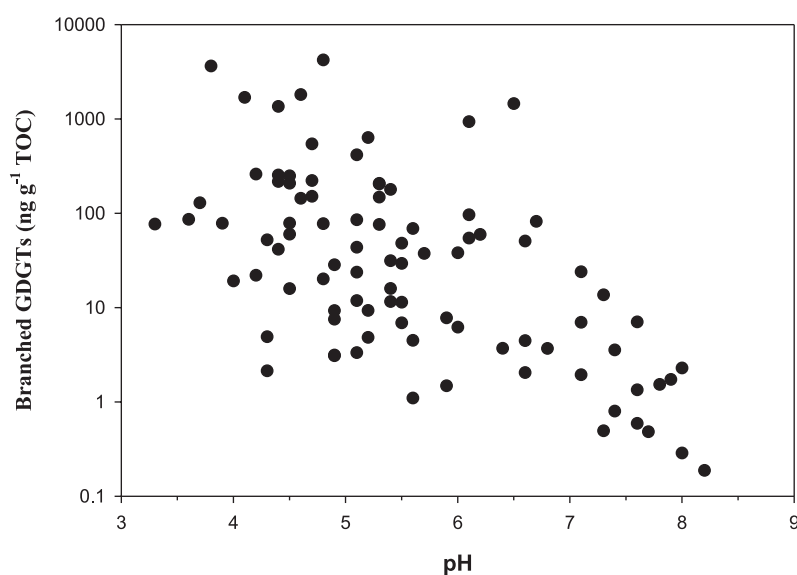
Figure 9.4: Branched GDGT concentrations in soils plotted against the soil pH, showing higher abundances of branched GDGTs in the more acidic soils.

To test whether the differences in the degree of methylation or cyclisation of branched GDGTs in soils are related to changes in environmental parameters, the MBT index and cyclisation ratio were subjected to a PCA together with the soil pH, the summed cation concentration in soils, electronic conductivity (a measure of salinity) of the soil, annual precipitation and annual mean air temperature (MAT) at the respective sampling sites. It would have been more desirable to use soil temperature rather than MAT as an environmental

parameter, however, global soil temperatures are not documented at high spatial and temporal resolution. As soil temperatures are largely governed by air temperatures, nevertheless, the annual MAT is assumed to be a good approximation for annual mean soil-surface temperature. The PCA yields two dominant factors (i.e., with eigenvalues >1) together explaining 73% of the variance in the data (Table 9.1). Nearly all parameters used have a clear maximum loading on either of the two factors. This might indicate the presence of interrelationships between parameters showing high loadings on the same factor. The electronic conductivity, however, has low loadings on both factors, suggesting that this parameter is not closely associated with any of the other parameters. Below we discuss these interrelationships in more detail.

Table 9.1: PCA results. Shown are the loadings on the two principal components, which together explain 73% of the total variance.

Factor	1	2
Latent roots (eigenvalues)	3.45	1.67
"Variance" explained by rotated components	2.69	2.43
Percent of total variance explained	38.4	34.7
Parameter	Varimax -rotated loading matrix	
pH	**0.890***	-0.129
Sum cations	**0.853**	-0.212
Electronic conductivity	0.410	-0.220
MAT	-0.072	**0.937**
Precipitation	-0.058	**0.905**
MBT	**-0.534**	**0.788**
cyclisation ratio	**0.841**	0.056

* Values >0.5 in bold for comparison.

9.3.2. Cyclisation ratio and pH

In the PCA the cyclisation ratio clearly has the highest loading on principal component 1 and no loading on principal component 2. The pH and the summed cation concentrations have similar loadings as the cyclisation ratio, i.e., same magnitude and direction, on component 1 and low loadings on component 2 as well. This suggests that there may be a relation between the relative amount of cyclopentyl containing branched GDGTs in soils and these parameters. If the branched GDGT cyclisation ratio is plotted against the pH value of the soils, there is an exponential correlation between the two ($R^2 = 0.70$) (Fig. 9.5a). This correlation suggests a causal relation between membrane lipid composition and pH which may not be surprising as the existence of a proton gradient over the cell membrane is of vital importance for the energy supply of a cell (Mitchell, 1966). Once an electrochemical proton gradient (pH gradient) over

the cell membrane is established, the proton motive force transduces this potential energy to other energy requiring processes (e.g., formation of ATP) (e.g., Booth, 1985). The proton permeability of the cell membrane plays a crucial role in maintaining this pH gradient and is most likely determined by the amount of water molecules getting trapped in the lipid core of the membranes. These trapped water molecules act as a short living conduit in the membrane along which protons can be transported (Nagle and Morowitz, 1978; Driessen et al., 1996). It might be possible that alterations of the alkyl chain of membrane lipids by, for instance, introduction of cyclopentyl moieties would result in a loosening of the packing of the membrane lipids enabling more water molecules to get trapped and consequently increasing the membrane proton permeability. The observation of a decreasing cyclisation ratio at successively lower pH seems to support this hypothesis. A steeper proton gradient is then counteracted by a more impermeable membrane. The exponential nature of the empirically derived correlation between the cyclisation ratio and pH also supports this hypothesis, because the proton gradient over the cell membrane of these soil bacteria is mainly determined by the ambient proton concentrations and pH is defined as the negative logarithm of these proton concentrations. In addition, changes in the membrane lipid fatty acid composition in response to changing pH have been observed in cultured bacteria, where a decrease in ambient pH was associated with an increase in the proportion of saturated vs. unsaturated fatty acids and in the amount of cyclopropane fatty acids (Beales, 2004; Yuk and Marshall, 2004). These changes in membrane composition are suggested to cause a decrease in membrane fluidity through a better membrane packing, resulting in a less permeable membrane and enabling survival in more acidic environments. Thus, in a similar way, the decrease in the amount of cyclopentyl moieties in the branched GDGTs at lower pH likely results in a more rigid membrane.

The summed cation concentrations have a similar loading as the cyclisation index on factor 1 in the PCA. If plotted together, however, the cyclisation ratio and the summed cation concentration show only a moderate correlation ($R^2 = 0.41$; Fig. 9.5b). A possible explanation for this correlation may be the counteractive intake of cations by cells at lower ambient pH. In order to maintain the internal pH at acceptable levels in a low pH environment, a cell actively pumps out protons. This results in a strong electrochemical potential over the cell membrane which might eventually prevent further excretion of protons. This increasing electrochemical potential is, however, compensated by the active intake of cations, such as potassium ions (Beales, 2004). Indeed, the correlation between the summed cations and soil pH is higher ($R^2 = 0.52$; Fig. 9.5c) than the correlation between the summed cations and the cyclisation ratio. Thus, the correlation of summed cations with the cyclisation ratio is most likely a result of covariance with pH and does not necessarily point to a direct causal relationship.
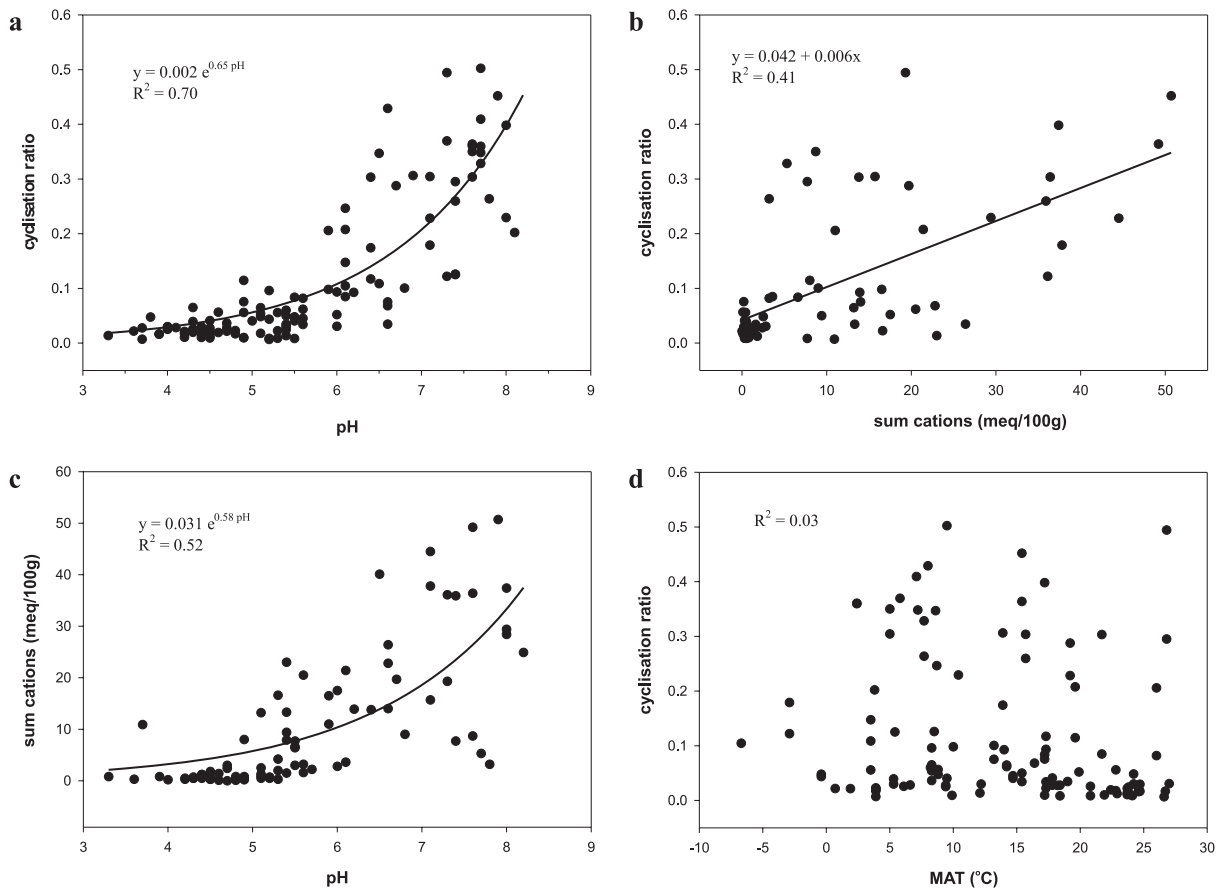
Figure 9.5: Various cross plots with respect to the cyclisation ratio in soils, showing (a) the cyclisation ratio vs. soil pH; (b) the cyclisation ratio vs. summed cation concentrations; (c) the summed cation concentrations vs. soil pH; (d) cyclisation ratio vs. annual mean air temperature (MAT).

Strikingly, in isoprenoid GDGT membrane lipids of Crenarchaeota the number of cyclopentyl moieties is strongly related to ambient temperature (e.g., Gliozzi et al., 1983; Schouten et al., 2002). It is surprising, therefore, that a relation between the cyclisation ratio of branched GDGTs and annual MAT is lacking (R^2 = 0.03; Fig. 9.5d). As far as membrane-spanning GDGT lipids are concerned, no reports have been made, to the best of our knowledge, on changes in GDGT membrane lipid composition in response to pH changes, except for the presence of higher proportions of membrane-spanning tetraether lipids versus non-membrane-spanning diethers in Archaea growing at low pH (Macalady et al., 2004). Our results, however, strongly suggest that these soil bacteria adjust their cell membrane to changes in ambient pH by changing the amount of cyclopentyl moieties in their branched GDGT membrane lipids.
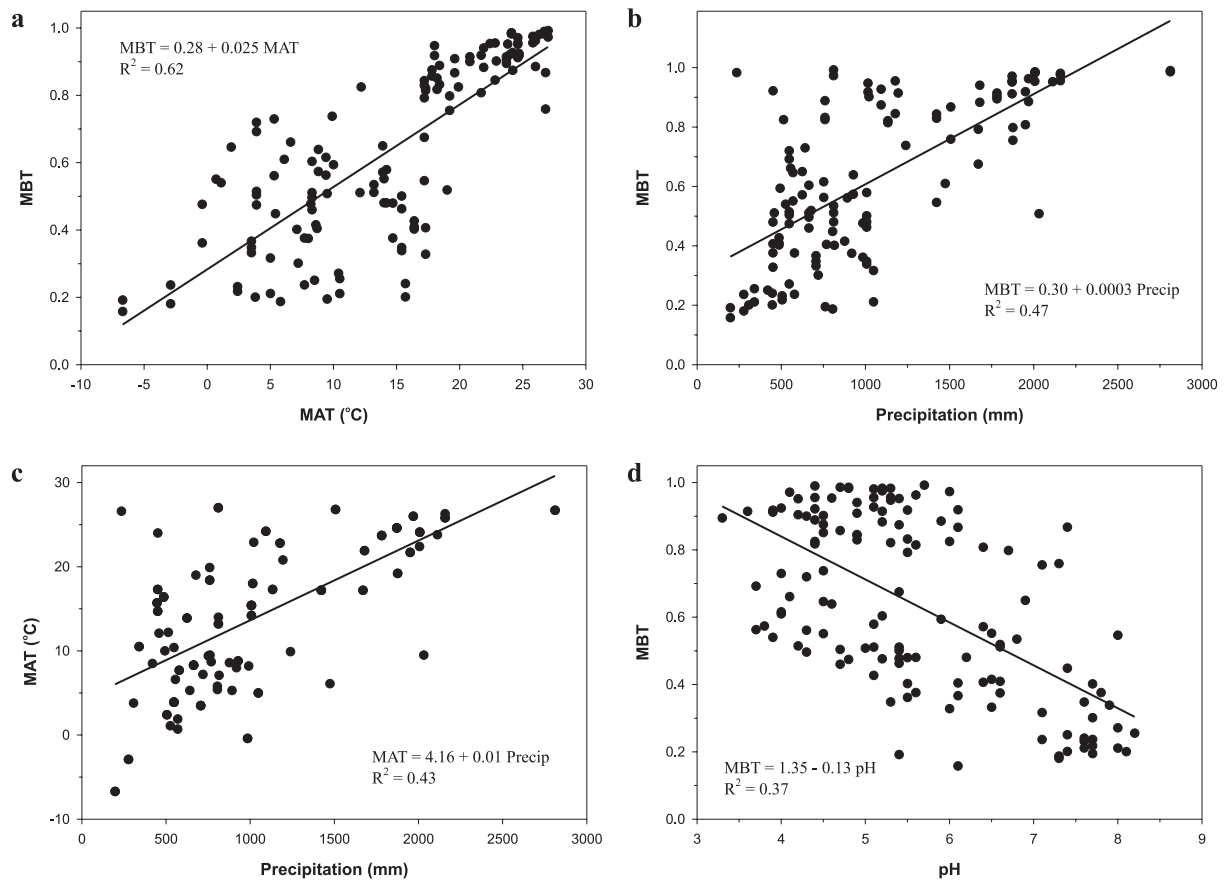
Figure 9.6: Various cross plots with respect to the methylation index of branched tetraethers (MBT) in soils, showing (a) the MBT vs. annual mean air temperature (MAT); (b) MBT vs. annual mean precipitation; (c) annual MAT vs. annual mean precipitation; (d) MBT vs. soil pH.

9.3.3. Methylation index and temperature

The MBT index has most of its loading on factor 2, together with MAT and precipitation which have loadings of similar magnitude and direction, pointing to a possible relation between the degree of methylation of branched GDGTs and temperature and precipitation (Table 9.1). A scatter plot of the MBT index of the soils against annual MAT indeed shows a linear correlation ($R^2 = 0.62$; Fig. 9.6a), with a higher degree of methylation found in soils at lower temperatures. It is well known that micro-organisms adapt the composition of their cytoplasmic cell membrane to changing growth temperatures. In order for the cell to function optimally, it has to maintain an acceptable degree of fluidity of the membrane at changing temperatures, a process called 'homeoviscous adaptation' (Sinensky, 1974; Russell and Fukunaga, 1990), and for this they alter their membrane lipid composition. Archaea change the number of cyclopentyl moieties in their carbon chains (Gliozzi et al., 1983; Uda et al., 2001), whilst Bacteria change the chain length, the degree of saturation or the degree of

branching of the fatty acid alkyl chains (e.g., Reizer et al., 1985; Prado et al., 1988; Suutari and Laakso, 1992). Reizer et al. (1985), for example, found in a thermophilic *Bacillus sp.* an 8-fold increase in the amount of branched chain fatty acids relative to saturated straight chain fatty acids with a decrease in growth temperature from 65 ºC to 45 ºC. Our results suggest that the branched GDGT-producing bacteria adapt their membrane lipid composition to temperature in a similar way by varying the amount of methyl groups on the carbon chains. In soils from warm, tropical areas, branched GDGT distributions containing predominantly GDGT **I** are found and in soils from successively colder regions more GDGTs with additional methyl branches (**II** and **III**) are detected, up to a dominance of these GDGTs in soils from the Arctic region (Fig. 9.2). Biosynthesising membrane lipids with additional methyl groups on the carbon chain is likely to result in a more loose packing which enables the membrane to remain in a liquid crystalline state at lower temperatures. We assume that in case of these fully saturated membrane-spanning tetraether lipids this process of temperature adaptation is energetically more favourable than increasing the alkyl chain length or introducing double bonds.

The correlation found between MBT and annual MAT, however, still has a relatively high degree of scatter (Fig. 9.6a). To examine whether seasonal variations in temperature are the cause of this scatter, the MBT index was also plotted against summer and winter MAT as well as against the temperature of the month of sampling. However, this did not result in better correlations than the correlation with annual MAT. Thus, additional environmental parameters might also influence the relative distribution of the branched GDGTs **I**, **II** and **III**. Like MAT, precipitation also has a high loading on principal component 2 and a relation with the MBT index could be expected. Although a moderate linear correlation is observed between the MBT index and precipitation ($R^2 = 0.47$) (Fig. 9.6b), it is doubtful if this means that precipitation really has an influence on the MBT index. Annual mean precipitation in the tropics can be up to an order of magnitude higher than at the higher and thus colder latitudes. Indeed, in our dataset the scatter plot between annual MAT and annual mean precipitation ($R^2 = 0.43$) (Fig. 9.6c) shows a similar pattern to that between MBT and precipitation. This suggests that the co-variation between annual MAT and annual mean precipitation gives rise to an apparent correlation between the MBT index and precipitation. As the correlation of the MBT index with MAT is stronger than with precipitation, and in contrast to precipitation membrane lipid adaptation to temperature change is a well known feature, the correlation between the MBT index and annual MAT is suggested to represent the causal relation which gives rise to the observed variation in branched GDGT distribution. In addition, a causal relation between the MBT index and precipitation is difficult to envisage as unicellular micro-organisms can only thrive in an aqueous solution and thus addition of water by means of increased precipitation is unlikely to affect the functioning of the cell and subsequently the membrane lipid composition.

MBT = 0.867 - 0.096 pH + 0.021 MAT
$R^2 = 0.82$
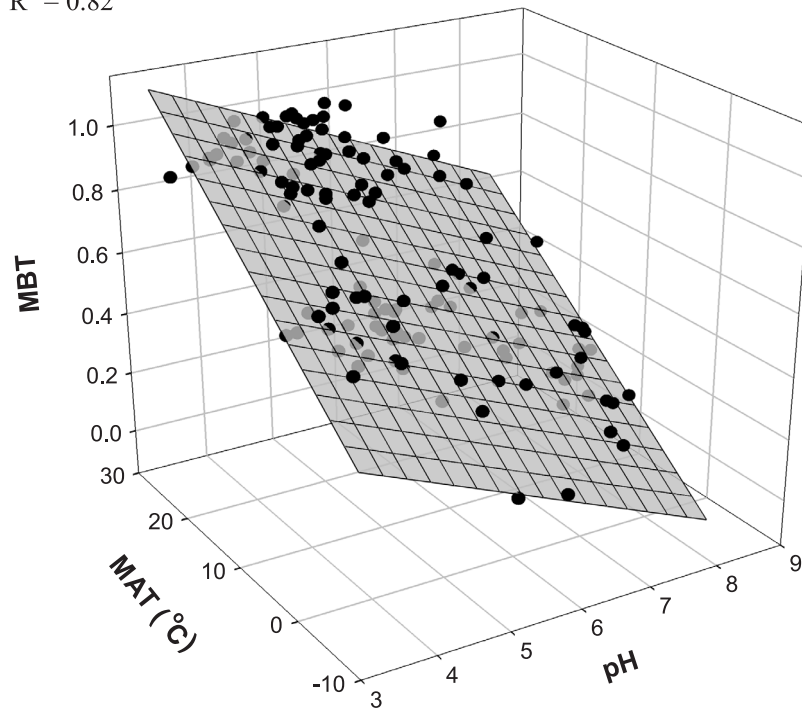
Figure 9.7: 3-D calibration plot of the methylation index of branched tetraethers (MBT) in soils vs. soil pH and annual mean air temperature (MAT).

9.3.4. Methylation index and pH

The PCA results show that the MBT index also has a considerable loading on factor 1, in opposite direction of pH. Thus, annual MAT and soil pH together might determine largely the distribution of the methylated branched membrane lipids (**I-III**) in soils. Plotting MBT against soil pH only results in a weak negative linear correlation ($R^2 = 0.37$) (Fig. 9.6d). However, if the annual MAT and soil pH are plotted against the MBT index in a 3-dimensional scatter plot a strong correlation between these three parameters becomes apparent (Fig. 9.7):

$$MBT = 0.867 - 0.096 \times pH + 0.021 \times MAT \quad (R^2 = 0.82) \tag{3}$$

A reason for the influence of pH next to MAT on the MBT could be that the addition of methyl branches on the carbon chain results in a similar change in membrane properties as with the cyclopentyl moieties, i.e., an increase in the permeability of the membrane. It has been shown by van de Vossenberg et al. (1995) that with increasing temperature the basal ion permeation across the membrane also increases. Within the range of growth temperature, membranes are in a liquid crystalline phase, but the fluidity of the membrane can still change

within this phase. The proton permeability of bacterial membranes at their growth temperature, however, is maintained within a narrow window by adjusting the membrane lipid composition, i.e., homeo-proton permeability adaptation (van de Vossenberg et al., 1999). Thus, the growth temperature dependent alterations in the structure of the alkyl chains are suggested to be mainly aimed at maintaining the proton permeability of the cytoplasmic membrane at a rather low and constant level (van de Vossenberg et al., 1999). This explains why, next to temperature, pH is an important parameter determining the membrane lipid composition of Bacteria, and thus why pH also has an impact on the composition of branched GDGTs.

9.3.5. Geochemical implications

The correlation found between branched GDGT membrane lipid distributions in soils and soil pH and annual MAT is surprisingly strong (R^2 = 0.82), but quite some scatter remains. A similar empirical study in the marine realm showed a stronger correlation between the membrane lipid distributions of mesophilic pelagic Crenarchaeota and temperature (R^2 = 0.92) (Schouten et al., 2002). However, oceans are a much more homogeneous entity compared to soils and, as a consequence, both temporal and spatial differences in environmental parameters such as temperature and pH are much smaller in the oceans than on land. Uncertainties with respect to the assessment of the pH of heterogeneous soils and with the exact determination of annual MAT at these local sites might, thus, account for a large proportion of the remaining scatter. Furthermore, there is likely to be a slight mismatch between the used annual MAT averaged over the last few decades (1961-1990) and the signal reflected by the membrane lipids in the top soils which is likely to reflect several centuries. It is also possible that decreased metabolic activity of the bacteria during periods of dryness or freezing conditions will result in recorded temperatures which slightly deviate from the real annual MAT. The effects of cation concentrations, electric conductivity and precipitation cannot be completely excluded as potentially influencing factors, though based on this study they seem to be of minor importance. Finally, the scatter may have been caused by other environmental parameters not included in this study. Although the detection and subsequent cultivation of the bacterial species producing the branched GDGT membrane lipids is required in order to fully prove and further investigate the relationships found, our results strongly suggest that membrane lipid distributions of these soil bacteria are governed mainly by pH and temperature.

By combining the correlation between the cyclisation ratio and pH with the correlation between MBT, pH and MAT, and substitution of pH with the cyclisation ratio, we can obtain a direct relation of annual MAT with the distribution of branched GDGTs. The non-linear relation between the cyclisation ratio and pH is, however, a complicating factor. Given the exponential relation between pH and the cyclisation ratio (Fig. 9.5a) and the definition of pH as the negative logarithm of the proton concentration, it is possible to obtain a linear relation between the two by defining an alternative ratio:

$$CBT = - LOG \left(\frac{([Ib]+[IIb])}{([I]+[II])} \right) \tag{4}$$

This <u>C</u>yclisation ratio of <u>B</u>ranched <u>T</u>etraethers (CBT) ranges from just below 0 to 2.17 in the soil dataset and its analytical accuracy was determined at $\pm$ 0.03 CBT units. Plotting this CBT against the pH of the soils resulted in the following linear correlation (Fig. 9.8):

$$CBT = 3.33 - 0.38 \times pH \quad (R^2 = 0.70) \tag{5}$$

This linear relation now simplifies the substitution of pH with CBT in the original 3-dimensional calibration plot of MBT, pH and MAT. Although slightly lower, this new calibration plot still yields a strong correlation (Fig. 9.9):

$$MBT = 0.122 + 0.187 \times CBT + 0.020 \times MAT \quad (R^2 = 0.77) \tag{6}$$

The advantage of these two calibrations (equations 5 and 6) is that they raise the possibility of reconstructing both soil pH and annual MAT based on branched GDGT membrane lipid distributions in sedimentary archives. In addition, branched GDGTs have been found in a range of coastal sediments with large river influx (Schouten et al., 2000; Hopmans et al., 2004) with ages up to the Cretaceous, suggesting the potential application of the MBT index and CBT ratio on long geological timescales.
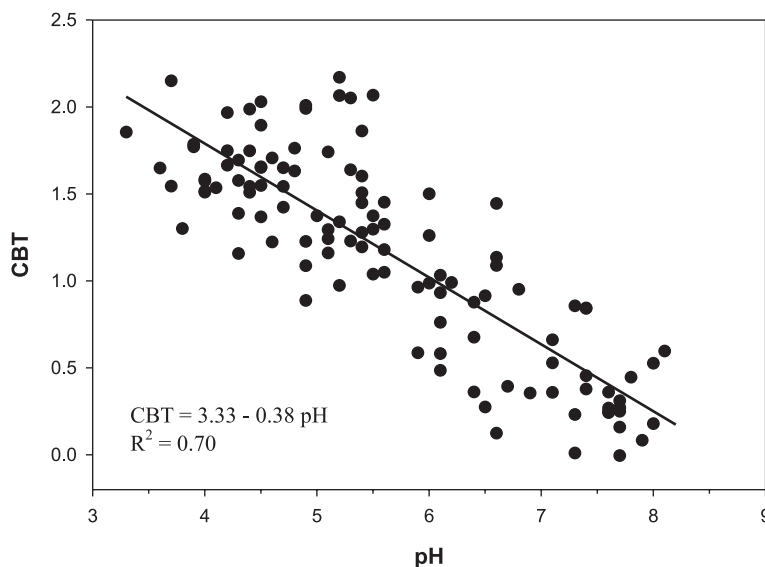
Figure 9.8: Calibration plot of the cyclisation ratio of branched tetraethers (CBT) in soils vs. soil pH.

MBT = 0.122 + 0.187 CBT + 0.020 MAT
R^2 = 0.77
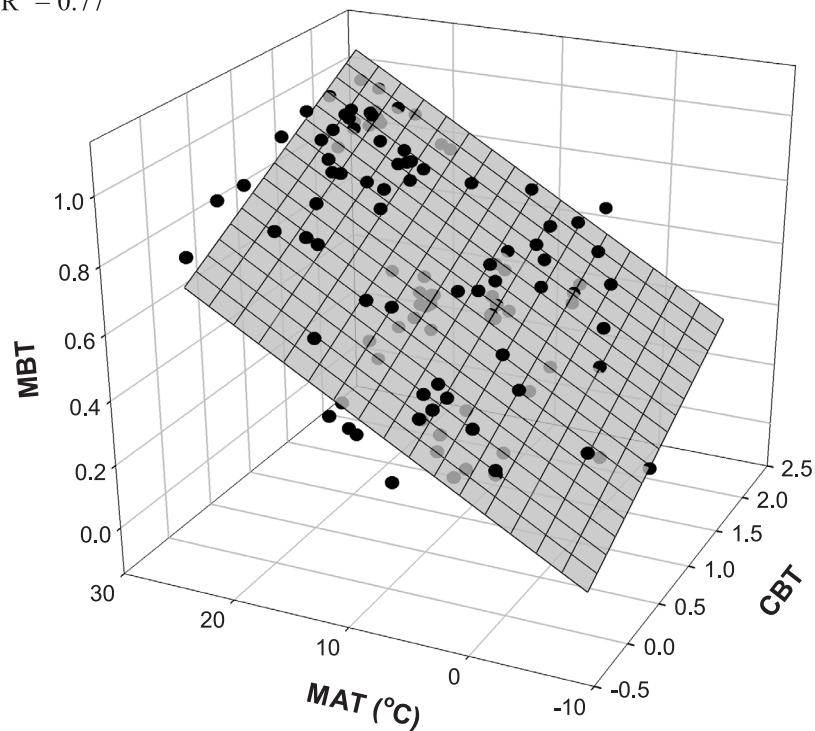
Figure 9.9: 3-D calibration plot of the methylation index of branched tetraethers (MBT) in soils vs. the cyclisation ratio of branched tetraethers (CBT) in soils and annual mean air temperature (MAT).

9.4. Conclusions

Our empirical study shows that branched GDGT-producing soil bacteria may adapt their core membrane lipid composition to both pH and temperature. The relative amount of cyclopentyl moieties in the alkyl chains seems to be related to pH, whereas the relative amount of additional methyl branches at the C-5 and C-5' positions may be related to both pH and temperature. These results fit well with current knowledge on mechanisms of temperature induced membrane lipid adaptation and with current ideas concerning pH adaptation mechanisms of cell membranes. The CBT ratio and MBT index, describing the degree of cyclisation and methylation of branched GDGTs, respectively, show great promise as new proxies in reconstructing palaeo soil pH and continental air temperatures.

Acknowledgements

Appendix
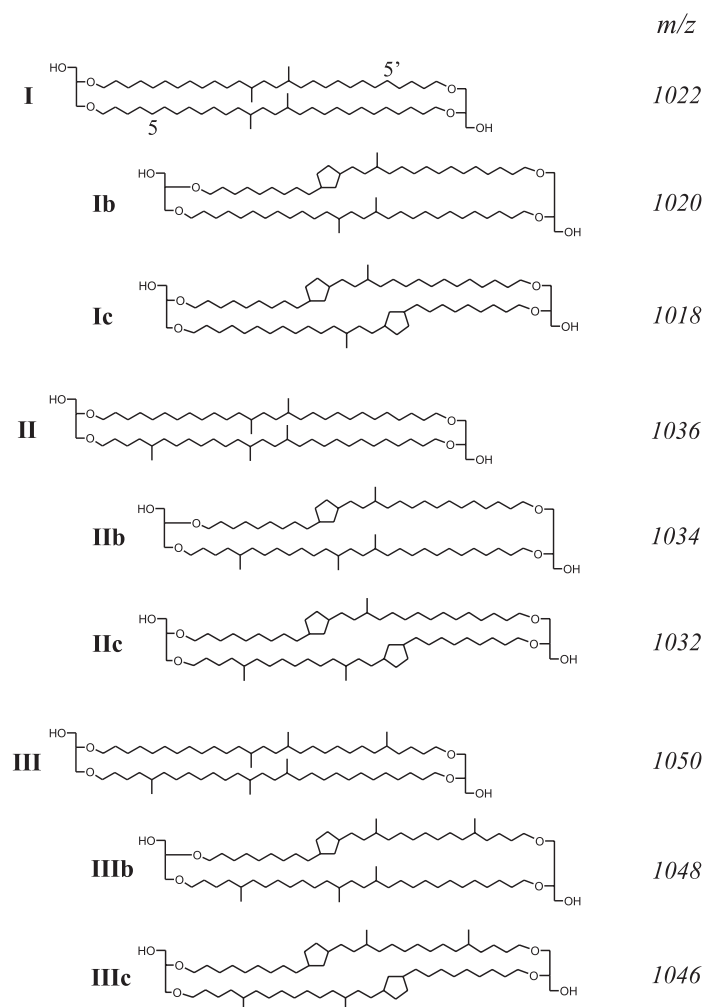
Figure A9.1: Chemical structures of the branched glycerol dialkyl glycerol tetraether (GDGT) membrane lipids discussed in the text.

Table A9,1: Overview of sample locations, soil characteristics and climate data

Sample [a]	LAT	LONG	ALT (m)	Depth (cm)	Landuse	pH	EC [b]	Sum Cat [b]	MBT	cycl. ratio [c]	CBT [c]	MAT (°C) [d]	P (mm) [d]	Weather station [e]	LAT	LONG	ALT (m)
Australia-4	26:43 S	150:36 E	304	0-10	semi-natural grassland, grazed	6.6	1.04	26.4	0.52	0.03	1.45	19	677	Dalby	27:18 S	151:19 E	344
Australia-9	34:58 S	138:39 E	134	0-10	pasture	6.0	-	-	0.33	0.09	0.99	17.3	450	Adelaide	34:56 S	138:31 E	6
				10-33		6.4	-	-	0.41	0.12	0.88	17.3	450				
Australia-17	34:43 S	148:20 E	472	0-12	cultivated pasture / woodland	6.4	-	-	0.57	0.17	0.68	13.9	624	Canberra	35:18 S	149:11 E	575
				12-25		6.9	-	-	0.65	0.31	0.36	13.9	624				
Australia-25	34:42 S	139:40 E	396	0-6	shrubland grazed / deciduous woodland	5.6	-	-	0.38	0.05	1.33	14.7	450	Adelaide	34:56 S	138:31 E	6
				6-22		5.5	-	-	0.48	0.04	1.37	14.7	450				
Brasil-1	22:45 S	43:41 E	45	0-14	semi-natural grassland, grazed	4.5	0.20	1.8	0.90	0.01	1.90	22.9	1021	Rio De Janeiro	22:55 S	43:10 W	3
Brasil-3	21:08 S	42:50 W	210	0-9	semi-natural grassland, grazed	5.1	0.04	1.3	0.96	0.02	1.74	22.8	1177	Itaperuna	21:12 S	41:53 W	123
				9-36		4.9	0.02	0.4	0.85	0.06	1.23	22.8	1177				
Brasil-6	22:33 S	50:19 W	562	0-28	semi-natural grassland, grazed	5.2	0.04	0.5	0.91	0.01	2.07	20.8	1194	Maringa	23:25 S	51:57 W	542
Cameroon-1	4:14 N	9:20 E	1200	0-15	coffee farm	6.4	0.14	13.8	0.81	0.30	0.36	21.7	1950	Koundja	5:39 N	10:45 E	1208
				38-55		6.1	0.03	3.6	0.92	0.08	1.03	21.7	1950				
Canada-14	45:25 N	63:25 W	~ 100	0-5	natural deciduous forest and woodland	4.0	-	-	0.61	0.03	1.57	6.1	1474	Halifax Int.A.	44:88 N	63:52 W	126
Canada-17	49:57 N	98:11 W	256	0-15	cropland (cleared forest)	7.7	-	-	0.22	0.36	0.25	2.4	505	Winnipeg	49:54 N	97:14 W	239
				15-22		7.6	-	-	0.23	0.36	0.25	2.4	505				
Canada-24	49:15 N	122:23 W	180	1-9	natural deciduous forest and woodland	5.0	-	-	0.51	0.04	1.37	9.5	2031	Vancouver	49:11 N	123:10 W	3
China-4	28:12 N	113:50 E	40	0-6	afforestation	4.9	0.04	0.7	0.83	0.01	2.01	17.2	1422	Changsha	28:15 N	112:50 E	48
				6-25		4.9	0.03	0.2	0.84	0.08	1.09	17.2	1422				
China-5	28:12 N	113:90 E	40	0-10	semi-natural grassland	8	0.22	37.4	0.55	0.40	0.18	17.2	1422	Changsha	28:15 N	112:50 E	48
China-6	24:49 N	110:31 E	150	0-7	semi-natural grassland	7.1	0.23	44.5	0.76	0.23	0.53	19.2	1876	Guilin	25:15 N	110:10 E	167
				7-20		6.7	0.07	19.7	0.80	0.29	0.39	19.2	1876				
China-7	23:13 N	113:28 E	45	0-5	semi-natural vegetation	4.9	-	0.8	0.94	0.01	1.99	21.9	1679	Guangzhou	23:00 N	113:13 E	18
				5-20		5.2	-	0.7	0.88	-	-	21.9	1679				
China-19	18:54 N	109:30 E	770	0-11	semi-natural deciduous forest	4.6	0.07	1.4	0.95	0.02	1.71	22.4	2006	Qiongzhong	19:20 N	109:50 E	250
China-20	18:46 N	110:20 E	40	0-6	fallow	3.9	0.16	0.8	0.92	0.02	1.77	24.7	-	Lingshui	18:30 N	110:2 E	10
				6-30		4	0.07	0.2	0.92	0.03	1.52	24.7	-				
China-23	28:13 N	116:55 E	50	0-5	fallow	4.5	0.03	1.5	0.85	0.03	1.55	18.2	-	Yujiang	- [f]	-	-
				5-30		4.4	0.02	1.2	0.82	-	-	18.2	-				
China-25	28:29 N	116:16 E	30	0-11	low level arable farming	5.5	0.08	6.6	0.79	0.08	1.04	17.2	1670	Jinxian	28:23 N	116:17 E	30
				11-50		5.4	0.04	7.9	0.68	-	-	17.2	1670				
China-27	27:52 N	117:45 E	700	2-10	semi-natural evergreen forest	4.7	0.07	2.4	0.86	0.03	1.54	17.8	-	Yanshan	28:19 N	117:33 E	100
				17-42		4.5	0.02	0.3	0.88	0.04	1.37	17.8	-				
China-31	24:23 N	114:17 E	250	0-5	semi-natural evergreen shrub	6.1	0.20	21.4	0.87	0.21	0.58	19.6	-	Wengyuan	24:22 N	114:29 E	215
				10-20		4.9	0.06	8.0	0.91	0.11	0.89	19.6	-				
China-32	23:39 N	113:39 E	250	8-20	semi-natural evergreen forest	4.3	0.04	0.5	0.90	0.03	1.58	20.8	-	Jiekou	23:52 N	113:32 E	68
China-49	26:23 N	106:26 E	1290	0-35	non-agricultural land / grassland	6.5	0.20	40.1	0.55	-	-	14	-	Pingba	26:25 N	106:16 E	1251
Finland-2	61:24 N	24:10 E	140	0-5	afforestation	3.7	0.01	10.9	0.69	0.01	2.15	3.9	547	Tampere	61:25 N	23:35 E	112
				5-8		4.2	0.09	0.5	0.51	0.02	1.75	3.9	547				
				9-20		4.7	0.04	0.0	0.50	0.02	1.65	3.9	547				
Finland-4	62:11 N	23:00 E	150	5-15	afforestation	4.3	0.05	0.7	0.72	0.02	1.69	3.9	547	Tampere	61:25 N	23:35 E	112
				15-25		4.8	0.05	0.4	0.47	0.02	1.63	3.9	547				
France-15	45:03 N	2:33 E	1080	0-8	semi-natural grassland, grazed	4.7	-	-	0.46	0.04	1.42	8.3	664	Le Puy-Chadrac	45:05 N	3:46 E	832
				8-32		5.1	-	-	0.51	0.05	1.24	8.3	664				
				32-50		4.3	-	-	0.50	0.07	1.16	8.3	664				
				50-90		5.2	-	-	0.60	0.10	0.97	8.3	664				

Table A9.1 continued

Sample [a]	LAT	LONG	ALT (m)	Depth (cm)	Landuse	pH	EC [b]	Sum Cat [b]	MBT	cycl. ratio [c]	CBT [c]	MAT (°C) [d]	P (mm) [e]	Weather station	LAT	LONG	ALT (m)
Gabon-1	0:31 N	12:48 E	530	0-7	tropical evergreen forest	3.3	0.60	0.8	0.89	0.01	1.86	23.7	1781	Makokou	0:34 N	12:52 E	509
				7-20		3.6	0.75	0.3	0.91	0.02	1.65	23.7	1781				
				50-65		4.2	0.08	0.3	0.90	0.01	1.97	23.7	1781				
Gabon-2	1:31 S	14:07 E	640	6-15	savannah with parts of forest	5.3	0.03	0.3	0.98	0.01	2.05	24.1	2007	Moanda	1:32 S	13:16 E	572
Gabon-3	1:41 S	13:35 E	350	0-10	herbs and grasses after burning	4.7	0.14	3.0	0.99	-	-	24.1	2007	Moanda	1:32 S	13:16 E	572
				10-25		4.8	0.04	0.8	0.98	-	-	24.1	2007				
Gabon-4	2:13 S	11:32 E	215	0-10	grassland	5.3	0.14	4.2	0.96	-	-	25.8	2158	Mouila	1:52 S	11:01 E	88
				10-19		5.2	0.03	0.6	0.98	-	-	25.8	2158				
Gabon-5	2:21 S	11:23 E	150	0-20	semi-deciduous shrub	5.1	0.05	0.9	0.98	-	-	26.3	2158	Mouila	1:52 S	11:01 E	88
Gabon-6	0:31 S	10:17 E	150	0-5	grassland	5.9	0.68	11.0	0.89	0.21	0.59	26	1969	Lambarene	0:43 S	10:14 E	27
				10-25		5.6	0.12	3.2	0.96	0.08	1.05	26	1969				
Ghana-2	5-7 N	~0	27	0-10	coastal savannah grassland	6.0	0.05	2.8	0.97	0.03	1.50	27.0	810.0	Accra	5:36 N	0:10 W	68
				10-24		5.7	0.04	2.2	0.99			27.0	810				
Greece-5	40:35 N	22:30 E	25	0-5	fallow / grassland	7.4		35.9	0.20	0.26	0.45	15.7	446	Larissa	39:38 N	22:25 E	73
				5-25		7.6		36.4	0.24	0.30	0.36	15.7	446				
Greece-13	40:30 N	23:33 E	600	0-3	deciduous forest	5.4		23.0	0.51	0.01	1.86	12.1	458	(Thes)Saloniki	40:31 N	22:58 E	8
Greenland-05	65:37 N	37:40 W	-[g]	0-5	tundra	5.5			0.36	0.05	1.30	-0.4	984	Angmagssalik	65:36 N	37:38 W	50
				5-35		5.2			0.48	0.04	1.34	-0.4	984				
Iceland-6	65:21 N	20:53 W	-[g]	5-15	heath and mosses, grazed	6.1			0.37	0.15	0.76	3.5	706	Stykkisholmur	65:05 N	22:44 W	8
				17-30		6.5			0.33	0.11	0.91	3.5	706				
Ireland-9	53:54 N	7:48 W	50	0-7	grazed shrubland	3.8			0.57	0.05	1.30	8.8	928	Clones	54:11 N	7:14 W	87
				7-40		4.6		0.1	0.64	0.06	1.22	8.8	928				
Italy-1	39:40 N	16:09 E	500	0-10	grazed woodland	6.2		13.9	0.48	0.09	0.99	14	811	Cosenza	39:17 N	16:15 E	256
Italy-2	39:12 N	16:90 E	680	10-25	semi-natural shrub	6.8		9.0	0.53	0.10	0.95	13.2	811	Cosenza	39:17 N	16:15 E	256
Italy-3	39:13 N	16:90 E	650	17-31	semi-natural grassland, grazed	6.6	0.16	14.0	0.51	0.08	1.09	13.2	811	Cosenza	39:17 N	16:15 E	256
Italy-11	41:29 N	13:31 E	315	0-7	semi-natural grassland, grazed	5.4	0.11	13.3	0.46	0.03	1.45	15.4	1007	Napels	40:51 N	14:18 E	88
				7-20		5.4	0.21	9.4	0.50	0.05	1.28	15.4	1007				
Italy-14	41:29 N	13:32 E	325	0-5	semi-natural grassland, grazed / shrub	5.6	0.21	20.5	0.48	0.06	1.18	14.2	928	Napels	40:51 N	14:18 E	88
				5-15		5.1	0.09	13.2	0.58	0.06	1.16	14.2	928				
Italy-17	41:27 N	13:37 E	100	0-7	non-agricultural land	7.6	0.27	49.2	0.35	0.36	0.24	15.4	1007	Napels	40:51 N	14:18 E	88
				7-29		7.9	0.24	50.7	0.34	0.45	0.08	15.4	1007				
Nigeria-015	5:18 N	6:38 E	2	0-12	grazed grassland in delta	4.4	0.04	0.5	0.99	-	1.76	26.7	2811	Warri	5:31 N	5:44 E	6
				12-25		4.8	0.02	0.1	0.99	0.02	0.01	26.7	2811				
Nigeria-019	6:37 N	3:30 E	35	0-25	semi deciduous forest	7.3	0.15	19.3	0.76	0.49	0.38	26.8	1507	Lagos	6:35 N	3:20 E	40
				25-60		7.4	0.05	7.7	0.87	0.30	0.27	26.8	1507				
Norway-1	63:49 N	9:41 E	5	0-8	grassland	7.6	0.17	8.7	0.21	0.35	0.36	5	1048	Orland	63:42 N	9:37 E	7
				8-14		7.1	0.21	15.7	0.32	0.30		5	1048				
Norway-3	63:26 N	10:41 E	30	3-13	forestry / semi decidious forest	4.3	0.10	0.5	0.56	0.04	1.39	5.3	892	Trondheim	63:28 N	10:56 E	17
South Africa-3	29:30 S	30:55 E	1067	0-15	afforestation / closed forest	4.4	0.06	1.2	0.89	0.03	1.54	18.4	759	Ladysmith	28:34 S	29:46 E	1078
South Africa-7	29:47 S	30:41 E	765	0-10	grassland with acia trees	5.5	0.08	3.0	0.92			18	1015	Durban	29:58 S	30:57 E	8
				10-20		5.3	0.06	2.0	0.95			18	1015	Pietermaritzburg	29:36 S	30:26 E	613
South Africa-12	29:31 S	30:16 E	1067	0-20	semi-natural grassland, grazed	5.5	0.11	7.7	0.83	0.01	2.07	18.4	759	Ladysmith	28:34 S	29:46 E	1078
South Africa-16	29:40 S	30:23 E	790	0-20	semi-natural grassland, grazed	6	0.08	17.5	0.82	0.05	1.26	19.9	759	Ladysmith	28:34 S	29:46 E	1078
Spain-6	38:54 N	6:16 W	280	1-12	cultivated pasture	6.6		22.8	0.41	0.07	1.14	16.4	486	Badajoz	38:53 N	6:58 W	198
Spain-7	38:59 N	6:20 W	260	0-2	semi-natural grassland, grazed	5.5		6.4	0.40			16.4	486	Badajoz	38:53 N	6:58 W	198
				2-15		5.1		0.5	0.43			16.4	486				
Sweden-4	55:49 N	14:04 E	80	0-15	grassland, cultivated pasture	7.7	0.11	5.3	0.24	0.33	0.31	7.7	578	Kristianstad	55:55 N	14:05 E	23
				17-35		7.8	0.06	3.2	0.38	0.26	0.45	7.7	578				

Table A9.1 continued

Sample[a]	LAT	LONG	ALT (m)	Depth (cm)	Landuse	pH	EC[b]	Sum Cat[b]	MBT	cycl. ratio[c]	CBT[c]	MAT (°C)[c]	P (mm)[e]	Weather station	LAT	LONG	ALT (m)
Sweden-15	64:11 N	19:34 E	270	0-10	semi decidious forest	4.5	0.07	0.3	0.55	0.02	1.65	0.7	569	Lycksele	64:35 N	18:39 E	234
Sweden-17	64:12 N	19:29 E	245	0-15	afforestation / evergreen forest	4.5	0.04	0.6	0.65	0.02	1.66	1.9	569	Lycksele	64:35 N	18:39 E	234
Turkey-8	37:44 N	33:34 E	1003	0-3	semi-natural grassland, grazed	8	0.27	28.4	0.21	-	-	10.5	340	Konya	37:58 N	32:33 E	1032
				3-33	semi-natural grassland, grazed	8.2	0.26	24.9	0.26	-	-	10.5	340				
Turkey-12	39:55 N	29:56 E	740	0-25	semi decidious woodland, grazed	8	0.32	29.4	0.27	0.23	0.53	10.4	547	Bolu	40:44 N	31:36 E	742
Uruguay-7	32:40 S	57:50 W	60	0-50	semi-natural grassland, grazed	5.6	0.08	1.6	0.81	0.03	1.45	17.3	1133	Mercedes	33:15 S	58.04 W	22
Uruguay-8	32:00 S	57:30 W	100	0-19	semi-natural grassland	5.3	0.24	16.6	0.82	0.02	1.64	17.3	1133	Mercedes	33:15 S	58.04 W	22
USA-10 (Hawaii)	22:4 N	159:24 W	180	0-35	semi-natural grassland, grazed	5.1	-	2.5	0.93	0.05	1.29	24.2	1093	Lihue	21:59 N	159:21 W	45
				35-64		5.4	-	1.5	0.87	0.03	1.51	24.2	1093				
USA-13	40:28 N	99:28 W	600	0-19	semi natural grassland, grazed	5.9	0.24	16.5	0.59	0.10	0.96	10.0	493	North platte	41:08 N	100:41 W	847
USA-17 (Alaska)	64:52 N	147:50 W	_[g]	0-20	cultivated test plot	7.1	0.90	37.8	0.24	0.18	0.66	-2.9	277	Fairbanks	64:49 N	147:52 W	132
				20-28		7.3	0.66	36.1	0.18	0.12	0.86	-2.9	277				
Zaire-1	0:52 N	24:28 E	440	0-15	evergreen forest	3.9	0.17	-	0.91	0.02	1.79	24.6	1871	Kissangani	0:31 N	25:11 E	415
				15-32		4.2	0.06	-	0.95	0.02	1.67	24.6	1871				
Zaire-2	0:46 N	24:26 E	460	0-8	rubber plantation	4.1	0.09	-	0.97	-	-	24.6	1871	Kissangani	0:31 N	25:11 E	415
				10-30		4.4	0.04	-	0.96	0.02	1.75	24.6	1871				
Netherlands-Texel-5	53:05 N	4:45 E	5	0-10	deciduous forest	4.0	-	-	0.62	0.03	1.58	9.4	752	Den Helder	52:55 N	4:47 E	0
Netherlands-Texel-7	53:05 N	4:45 E	5	0-10	deciduous forest	3.7	-	-	0.56	0.03	1.54	9.4	752	Den Helder	52:55 N	4:47 E	0
Scotland-Dornock	54:55 N	3:20 W	8	0-10	grazed pasture grassland	5.4	-	-	0.48	0.06	1.20	8.2	991	Glasgow	55:52 N	4:26 W	8
Iceland-Stykkis	65:05 N	22:45 W	8	5-15	grass patch	5.3	-	-	0.35	0.06	1.23	3.5	706	Stykkisholmur	65:05 N	22:44 W	8
Spitsbergen-S	78:20 N	15:80 E	20	0-5	tundra	5.4	-	-	0.19	-	-	-6.7	197	Adventdalen	78:20 N	15:83 E	20
Spitsbergen-C	78:20 N	15:80 E	20	0-5	tundra	6.1	-	-	0.16	0.10	0.93	-6.7	197	Adventdalen	78:20 N	15:83 E	20
Seychelles	4:40 S	55:31E	5	0-10	tropical evergreen forest	5.2	-	-	0.98	0.01	2.17	26.6	235	Victoria	4:40 S	55:31E	5
USA R-1	42:75 N	73:80 W	83	~0-15	forest	6.6	-	-	0.37	0.43	0.12	8	918	Albany, N.Y.	42:75 N	73:80 W	83
USA R-2	41:58 N	84:60 W	262	~0-15	forest	6.5	-	-	0.42	0.35	0.27	8.6	876	Montpelier, OHIO	41:58 N	84.60 W	262
USA R-3	43:31 N	89:25 W	243	~0-15	forest	7.7	-	-	0.40	0.41	0.16	7.1	815	Portage, WIS	43:51 N	89:43 W	243
USA R-4	44:53 N	93:13 W	256	~0-15	forest	7.7	-	-	0.30	0.35	0.27	7.2	719	Minneapolis, MINN	44:53 N	93:13 W	256
USA R-5	45:57 N	112:29 W	1692	~0-15	forest	8.1	-	-	0.20	0.20	0.60	3.8	307	Butte, MONT	45:95 N	112:50 W	1688
USA R-6	47:38 N	117:32 W	723	~0-15	forest	7.4	-	-	0.25	0.13	0.84	8.5	419	Spokane, WASH	47:63 N	117:53 W	718
Galapagos	0:85 S	89:45 W	~600	~0-5	volcanic	4.4	-	-	0.92	0.01	1.99	24	451	Puerto Baquerizo	0:90 S	89:60 W	118
Germany-Hamburg-1	53:38 N	9:59 E	30	0-10	peatland	6.1	-	-	0.40	0.25	0.49	8.7	768	Hamburg	53:38 N	9:59 E	16
Netherlands-Bunde	50:55 N	5:45 E	~100	3-10	forest	7.7	-	-	0.19	0.50	0.00	9.5	761	Maastricht	50:55 N	5:47 E	114
Germany-Geigerst-1	~48 N	~12 E	1200	0-10	forest	7.4	-	-	0.45	0.13	0.84	5.4	805	Munchen	48:21 N	11:47 E	527
Germany-Geigerst-2	~48 N	~12 E	900	0-10	grassland	7.3	-	-	0.19	0.37	0.23	5.8	805	Munchen	48:21 N	11:47 E	527
Sweden-Stockholm	59:21 N	17:57 E	15	0-5	forest	4.1	-	-	0.66	0.03	1.54	6.6	555	Stockholm	59:21 N	17:57 E	15
Finland-Pojo	66:70 N	24:70 E	-	5-10	forest	3.9	-	-	0.54	-	-	1.1	525	Kemi	65:78 N	24:50 E	18
USA-Woodshole	41:54 N	70:65 W	5	6-15	forest	4.5	-	-	0.74	0.01	2.03	9.9	1239	Woodshole	41:54 N	70.65 W	5
Sweden-Berghamra	59:38 N	18:26 E	~200	3-5	forest	4.0	-	-	0.73	0.03	1.51	5.3	641	Jonkoeping	57:46 N	14:05 E	226
Australia-Tasmania	42:50 N	147:30 W	5	0-5	forest	4.4	-	-	0.82	0.03	1.51	12.2	513	Hobart	42:50 S	147:30 W	4
Rarotonga	21:12 S	159:49 W	7	0-10	tropical evergreen forest	5.4	-	-	0.95	0.02	1.60	23.8	2112	Rarotonga	21:12 S	159:49 W	7

[a] the upper part of the table are soil samples derived from the ISRIC soil repository, the lower part represents soil samples gathered ourselves

[b] "_" indicates that data were not available in the ISIS database of ISRIC; these parameters are not determined in our own soil samples

[c] in cases peaks of GDGT IIb were too low for proper integration cyclisation ratios and CBT values are excluded in order not to introduce additional noise

[d] in cases of large altitudinal differences between soil sample site and weather station, the annual mean air temperature (MAT) is corrected for this (see methods section)

[e] for a few weather stations no data on precipitation were available

[f] coordinates of this weather station were missing in the ISIS database, however, the station is located at 12km from the sample site and the relevance of this station is qualified as 'very good'

[g] altitudes of these locations are missing in the ISIS database

Chapter 10

Coupled thermal and hydrological evolution of tropical Africa over the last deglaciation

Johan W.H. Weijers, Enno Schefuß, Stefan Schouten and Jaap S. Sinninghe Damsté

Abstract

We analyzed the distribution of branched tetraether membrane lipids derived from soil bacteria in a marine sediment record that was recovered close to the Congo River outflow, and the results enabled us to reconstruct large-scale continental temperature changes in tropical Africa that span the past 25,000 years. Tropical African temperatures gradually increased from ~21 to 25ºC over the last deglaciation, which is a larger warming than estimated for the tropical Atlantic Ocean. A direct comparison with sea-surface temperature estimates from the same core revealed that the land-sea temperature difference was, through the thermal pressure gradient, an important control on central African precipitation patterns.

Continental climate change during the last deglaciation, especially in the tropics, is not as well understood as it is for the oceans (Farrera et al., 1999; Bard, 1999; Schaefer et al., 2006). For Africa, consensus is emerging on past changes in humidity and their causes, based on lake level and pollen studies as well as the deuterium content of plant waxes (Bonnefille et al., 1990; Gasse, 2000; Schefuß et al., 2005), but temperature records for such tropical continental areas remain scarce and incomplete. In contrast to the marine environment, few quantitative temperature proxies exist for the terrestrial environment, and continuous long-term climate archives on land are limited. For instance, pollen-based vegetation studies, a widely used method for environmental reconstructions on land (Bonnefille et al., 1990), are complicated in the tropics because the effects of changes in temperature are difficult to distinguish from those of changes in precipitation. Temperature estimates based on another method, stable oxygen isotope contents of carbonates and silicates, are widely applied in lacustrine sediments and speleothems. However, although these methods are appropriate for high-resolution qualitative palaeoclimate reconstructions (Leng and Marshall, 2004; McDermott, 2004), quantification of climate change in terms of palaeotemperatures requires tenuous assumptions about the past changes in parameters that have influenced the source-water composition. The scant palaeotemperature data available for the African continent imply a temperature difference of ~3.5 to 6°C between the Last Glacial Maximum (LGM) and the present day (Bonnefille et al., 1990; Farrera et al., 1999; Kulongoski et al., 2004; Powers et al., 2005) but often represent a relatively local signal or are incomplete records. Thus, knowledge on African tropical temperature change over the last deglaciation is rather limited, especially for the vast tropical rainforest area of the Congo Basin. Continuous, high resolution long-term records of continental-scale temperature change are much needed to improve this knowledge and enable proper comparison with records of marine temperature changes.
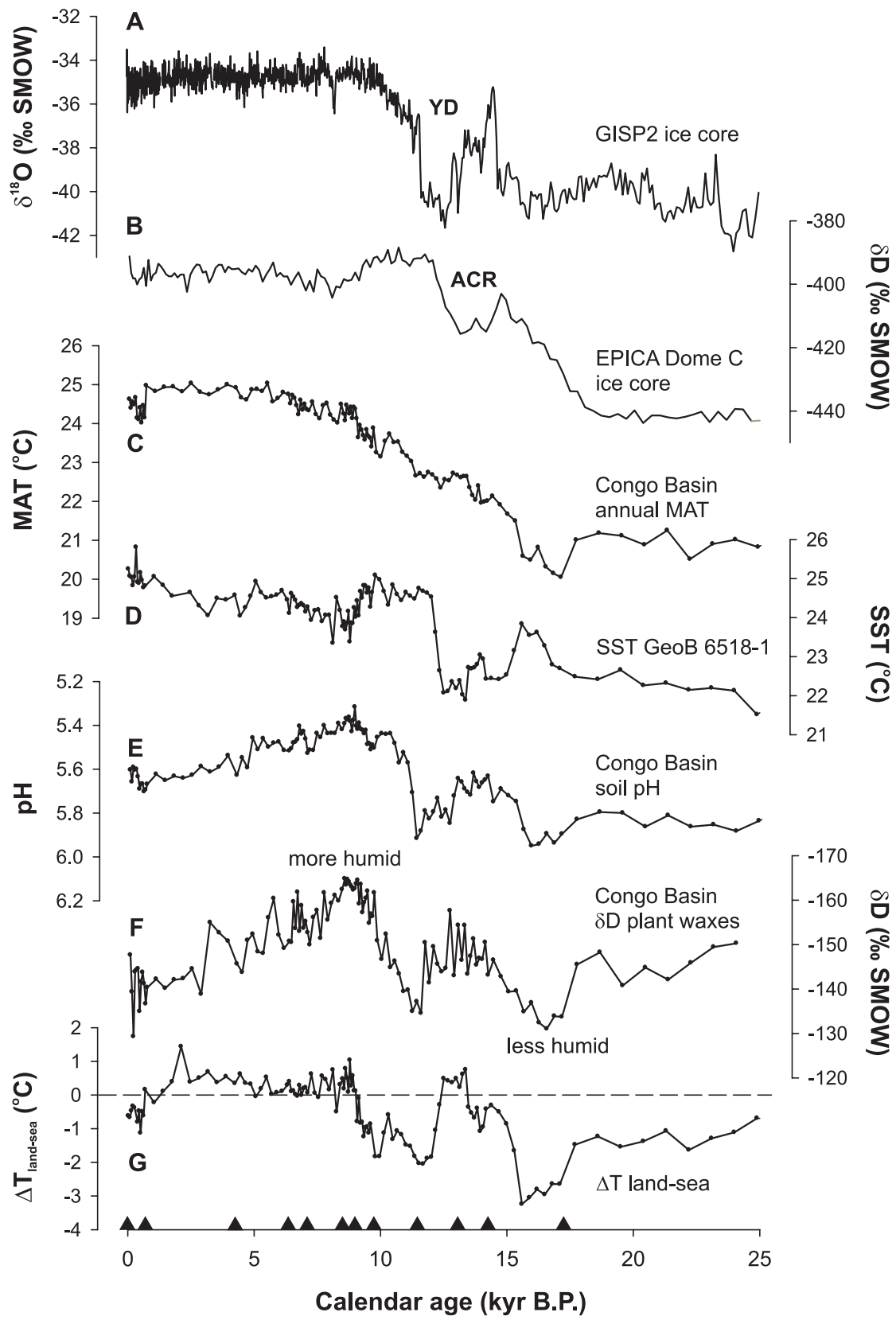
To gain better insight into the central African temperature development over the last deglaciation, its relation to global climatic changes, and its effect on the continental hydrological cycle, we used the Methylation index of Branched Tetraethers (MBT) and Cyclisation ratio of Branched Tetraethers (CBT) based on branched glycerol dialkyl glycerol tetraethers (GDGTs) (Weijers et al., 2007a) present in a marine core recovered close to the Congo River outflow (GeoB 6518-1, 05°35.3'S, 11°13.3'E, water depth of 962 m, Fig. 10.1). Using the MBT and CBT, we reconstructed the annual mean air temperature (MAT) of the Congo River basin (see supporting material at the end of this chapter) which could be compared with the sea surface temperature (SST) record obtained from the same core (Fig. 10.2). Branched GDGTs (Fig. S10.1; see supporting material at the end of this chapter) are abundant core membrane lipids from bacteria that thrive in soils (Hopmans et al., 2004; Weijers et al., 2006b, 2007a). As the soil erodes, the GDGTs are fluvially transported to the ocean. Indeed, they have been shown to be an excellent tracer of the fate of soil organic matter in the Congo deep-sea fan (Hopmans et al., 2004; Fig. S10.2) and in the Bay of Biscay (Ménot et al., 2006). The large catchment area of the Congo River (3.7×10^6 km^2) extends

from about 6ºN to 13ºS and from about 13 to 33ºE in central Africa (Fig. 10.1A) with elevations between 300 and 1200 m except for one small part, located at its eastern boundary, that rises above 2000 m (Kazadi and Kaoru, 1996). The temperature estimates obtained from our marine core, therefore, represent a catchment-integrated terrestrial temperature signal derived from land of low to intermediate elevation. Analysis of the stable carbon isotopic content (δ^{13}C) of plant-wax *n*-alkanes has shown that the Congo River mainly drained rainforest-vegetated areas over the past 20,000 years (Schefuß et al., 2005).
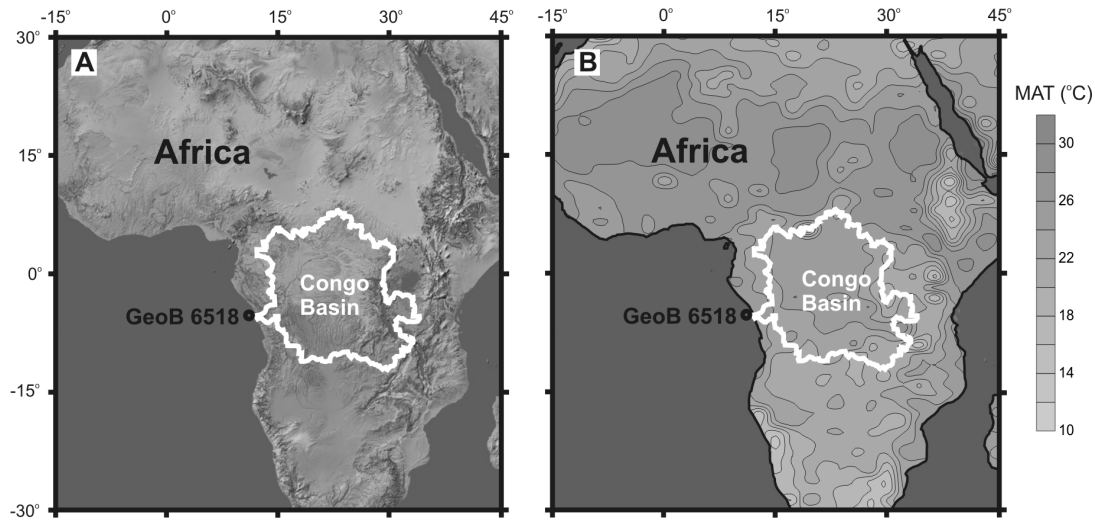
Figure 10.1: Overview maps of Africa. The position of core GeoB 6518, recovered close to the Congo River outflow from a water depth of 962 m, and the extent of the Congo River drainage basin (white outline) are plotted (**A**) on a digital elevation map of Africa (picture from NASA Jet Propulsion Laboratory, California Institute of Technology) and (**B**) on a map showing the annual MAT distribution in Africa [data in Willmott and Robeson (1995)]. See page 171 for color figure.

The main advantages of our record compared with previous climate records are its relatively high temporal resolution (~200 years), continuous nature, and large geographical coverage (i.e., central tropical Africa). The nature of our data allowed us to gain detailed insight into the general development of tropical African temperature over the last deglaciation. The annual MAT record of the Congo Basin reveals an overall warming since the LGM [~ 24,000 to 18,000 calibrated years before present (~24 to 18 cal kyr B.P.)] of 4 to 4.5°C (Fig. 10.2C). This is consistent with scant data on palaeotemperatures from a few other locations in tropical Africa outside the Congo Basin. Pollen-based temperature reconstructions suggest an LGM that had been 4 to 4.5°C cooler than today – that is, ~4°C cooler in the Burundi highlands (Bonnefille et al., 1990) and ~4.5°C cooler in the southern Lake Tanganyika basin (Chalie, 1995). Furthermore, LGM temperatures that were ~3.5°C lower than today have been reported based on TEX$_{86}$ lake surface temperature reconstructions for northern Lake Malawi (Powers et al., 2005). Larger differences between LGM and present-day temperatures have

A — δ¹⁸O (‰ SMOW) — GISP2 ice core — YD

B — δD (‰ SMOW) — EPICA Dome C ice core — ACR

C — MAT (°C) — Congo Basin annual MAT

D — SST (°C) — SST GeoB 6518-1

E — pH — Congo Basin soil pH — more humid

F — δD (‰ SMOW) — Congo Basin δD plant waxes — less humid

G — ΔT land-sea (°C) — ΔT land-sea

Calendar age (kyr B.P.)

been reported based on analyses of stalagmite stable isotope and groundwater noble gases. Such analyses indicated that temperatures were ~5.7°C cooler in a South African speleothem (Holmgren et al., 2003) and 5 to 6°C cooler in groundwater aquifers in Namibia and South Africa (Heaton et al., 1986; Kulongoski et al., 2004), but these data were derived from sites substantially farther south of the equatorial Congo Basin. Our record indicates that deglacial warming has been of similar magnitude for the whole of tropical Africa, from the western and central lowlands to the eastern highlands.

The onset of postglacial warming in our record at about 17 cal kyr B.P. (Fig. 10.2C) is in line with the Southern Hemispheric climate development, with the EPICA (European Project for Ice Coring in Antarctica) Dome C Deuterium record showing the onset of warming at about 17.5 cal kyr B.P. (Augustin et al., 2004) (Fig. 10.2B) and about 17 cal kyr B.P. in a stalagmite $\delta^{18}O$ record from South Africa (Holmgren et al., 2003). Recent work based on ^{10}Be exposure dating of moraines (Schaefer et al., 2006) has shown that in the mid-latitudes of both hemispheres the onset of the last deglaciation was near synchronous at about 17.2 cal kyr B.P.; a similar timing of 17.3 cal kyr B.P. was inferred for the onset of the last deglaciation in the South American tropics of Peru and Bolivia. Our tropical temperature record shows that the post-glacial warming in tropical central Africa started at the same time, after a short cooling episode between 18 and 17 cal kyr B.P., providing strong evidence for a globally synchronous onset of the last deglaciation.

Figure 10.2 (opposite page)**:** Temperature changes over the past 25,000 years in tropical central Africa compared with African humidity changes and Arctic and Antarctic climate signals. (**A**) The Greenland Ice Sheet Project 2 (GISP2) $\delta^{18}O$ record indicative of Greenland air-temperature fluctuations (Stuiver and Grootes, 2000). SMOW, standard mean ocean water. (**B**) The EPICA Dome C δD record indicative of Antarctic air-temperature changes (Augustin et al., 2004). (**C**) The annual MAT record of the Congo Basin based on the MBT index and CBT ratio of the branched GDGT lipids of soil bacteria in core GeoB 6518-1. (**D**) The SST changes in the equatorial Atlantic Ocean based on alkenone palaeothermometry at site GeoB 6518-1 (Schefuß et al., 2005). (**E**) A record of the average soil pH in the Congo Basin based on the CBT ratio of branched GDGT lipids of soil bacteria in core GeoB 6518-1. (**F**) The δD record of C_{29} *n*-alkane plant waxes in core GeoB 6518-1 reflecting humidity changes in tropical central Africa (Schefuß et al., 2005). (**G**) The land-sea temperature gradient between central tropical Africa and the tropical Atlantic Ocean based on records (**C**) and (**D**). Black triangles on the age scale indicate the ^{14}C-AMS (accelerator mass spectrometry) radiocarbon dates derived from mixed planktonic foraminifera used for establishing the chronology of core GeoB 6518-1 (Schefuß et al., 2005). YD, Younger Dryas; ACR, Antarctic Cold Reversal. See page 170 for color figure.

With values of 20.5 to 21°C, temperatures were rather constant during the LGM. The rate of subsequent deglacial warming was highest between 17 and 13.5 cal kyr B.P. and between 11.5 and 9 cal kyr B.P., with an average warming of ~0.7°C kyr^{-1}. During the intervening period from 13.5 to 11.5 cal kyr B.P., temperatures remained relatively stable at about 22.5°C and were, notably, not influenced by the Antarctic Cold Reversal in the Southern Hemisphere or by the Younger Dryas cold episode in the Northern Hemisphere, respectively. From 9 to 5.5 cal kyr B.P. temperatures only rose slowly by ~0.3°C kyr^{-1}, reaching maximum values of 25°C. During the second part of the Holocene, temperatures remained about 25°C, except for the last 0.7 kyr when the temperature decreased slightly again by 0.5 to 1°C. The 24.5°C reconstructed from the core-top sediment is similar to the present-day annual MAT of the Congo River basin, about 23.7°C, based on weather station data (KNMI, 1997) (Fig. 10.1B).

Our record also enables a more detailed comparison of tropical continental temperature change with global climate development and SST records, in particular from the tropical Atlantic Ocean. SST reconstructions based on alkenone palaeothermometry indicate ~1.7°C lower SSTs for the Indian Ocean and ~ 2.7°C lower SSTs for the tropical Atlantic Ocean during the LGM relative to Holocene temperatures (Rosell-Melé et al., 2004). This agrees well with the ~ 2.5°C alkenone-based LGM-Holocene SST range at this site (Fig. 10.2D), representative for the eastern tropical Atlantic Ocean (Schefuß et al., 2005). Thus, compared with the ocean, the reconstructed continental deglacial warming of 4 to 4.5°C is considerably stronger. This difference between continental and oceanic deglacial warming in the tropics is in agreement with climate model studies, which suggest that the average continental deglacial warming in the tropics was about 1.5 times stronger than the deglacial warming of the tropical oceans (Shin et al., 2003; Otto-Bliesner et al., 2006). This amplified continental warming may have been because the continents cool more during glacial times. At high and mid latitudes, the presence of a changed and often reduced vegetation cover during glacials results, through increased albedo, in enhanced cooling of the land surface. However, in tropical areas, this effect is counteracted by a negative feedback from reduced evaporation, which results from decreased tropical rainforest area. The reduced evaporation leads to a decreased loss of latent heat and thus relatively warmer surface temperatures. As a result, vegetation changes in tropical Africa are thought to result eventually in a negligible temperature effect (Wyputta and McAvaney, 2001). A more likely explanation for the enhanced glacial cooling of the continental tropics may thus be an increased pole-to-equator temperature gradient, resulting in a strengthened and enlarged Hadley Cell circulation (Ramstein et al., 1998) and, consequently, an increase in relatively cool air that flows from higher toward lower latitudes.

Because central Africa seasonally receives airflow from both the Northern Hemisphere, when the Intertropical Convergence Zone (ITCZ) is in its southernmost position, and the Southern Hemisphere, when the ITCZ is in its northernmost position (Gasse, 2000), its temperature evolution is likely related to climate changes in both hemispheres. This coupling to both hemispheres supports the idea that the onset of the deglacial warming in our record at

about 17 cal kyr B.P. is global in character. It also might explain the lack of clear temperature signals related to the Antarctic Cold Reversal and the Younger Dryas, which were asynchronous deglacial cold events in the Southern and Northern hemispheres, respectively (Blunier et al., 1997). Compensation of these cooling events by warmer air from the opposite hemisphere in the tropical realm apparently resulted in the observed period of relatively stable annual MAT over equatorial tropical Africa from 13.5 to 11.5 cal kyr B.P..

Notably, the difference in deglacial warming between the continent and the ocean should have had an impact on continental hydrology through the land-sea thermal gradient. Present-day African rainfall variability is in large part associated with SST distributions in the South Atlantic Ocean in that the thermal pressure gradient differs between the African continent and the ocean surface (Camberlin et al., 2001). A large negative land-sea temperature gradient – that is, relatively warm sea and cool continent – will result in a generally off-land air flow, preventing moist air from the ocean from flowing onto the continent. An advantage of reconstructing continental African temperatures from a marine core is the possibility of comparing the results with SSTs derived from the same core (Schefuß et al., 2005) (Fig. 10.2D); we used this comparison to reconstruct the thermal gradient between central Africa and the eastern equatorial Atlantic Ocean over the past 25,000 years ($\Delta T_{\text{land-sea}}$; Fig. 10.2G). During glacial times, the $\Delta T_{\text{land-sea}}$ record generally shows values of -1 to -3°C, which disappear rather quickly after the onset of the deglaciation. Negative values down to -2°C return at about 12 cal kyr B.P., coincident with a fast SST increase in the eastern equatorial Atlantic Ocean, and gradually disappear again at the start of the Holocene. During the Holocene, the land-sea temperature gradient was rather stable, with values just greater than 0°C.

The influence of the land-sea thermal gradient on continental hydrology can be evaluated by comparison with central African humidity changes reflected in the Deuterium content (δD) of plant wax *n*-alkanes from the same record (Schefuß et al., 2005) and with the soil pH record derived from the CBT ratio of the branched GDGT membrane lipids (Figs. 10.2E and F). Large-scale soil pH changes are assumed to reflect changes in precipitation intensity given that in the long term, soil-leaching processes result in either stronger or weaker soil acidification as precipitation increases or decreases, respectively (Johnson et al., 1998). Indeed, the large negative values in the $\Delta T_{\text{land-sea}}$ record correspond to relatively dry periods reflected in the δD record and relatively high soil pH values (Figs. 10.2E-G). Smaller negative or even positive values, indicating weak off-land or even on-land air flow, correspond to wetter conditions and lower soil pH values. Thus, the land-sea thermal gradient apparently exerts a strong control on central African precipitation patterns. The discrepancy between the $\Delta T_{\text{land-sea}}$ record and the humidity records during the second part of the Holocene might be due to a very weak land-sea temperature gradient in this time interval that allowed other forcing mechanisms to become predominant.

It has been suggested that the meridional tropical-subtropical SST gradient in the South Atlantic Ocean exerts a strong control on central African precipitation changes (Schefuß et al., 2005). This mechanism works in the same direction as the land-sea thermal gradient: A relatively warm tropical ocean will result in stronger meridional winds as well as off-land winds, both preventing moist air from flowing from the oceans onto the continent. Before the Holocene, the land-sea thermal gradient was large and apparently exerted a dominant control, whereas during the Holocene, when the land-sea thermal gradient remained weak, the meridional SST gradient increased and became dominant in controlling precipitation in central tropical Africa, thereby causing increasingly dry conditions (Schefuß et al., 2005). Hence, the combined evolution of land temperature and SST in different parts of the Atlantic Ocean controlled precipitation patterns in central Africa during the past 25,000 years.

Supporting Material

Materials and Methods

Age calibration of MBT record
Dating of core GeoB 6518-1 was carried out by means of fifteen ^{14}C-AMS dates on mixed planktonic foraminifera fractions containing *Globigerinoides ruber* (white), *Globigerinoides sacculifer* and *Orbulina universa*. Radiocarbon ages were converted to calendar ages using the program CALIB 4.4 (using the marine calibration and applying a reservoir effect of 400 years) and were linearly interpolated to provide the core chronology (Schefuß et al., 2005).

Lipid extraction and analysis
Lipid extractions and HPCL/MS analyses were performed as described previously (Hopmans et al., 2000) with minor modifications: Freeze-dried, powdered samples were extracted 3 times for 5 min with an accelerated solvent extractor (DIONEX2000) using a dichloromethane (DCM):methanol 9:1 (v/v) solvent mixture at 100ºC and 7.6×10^6 Pa. The obtained extracts were separated over an activated Al_2O_3 column, using hexane:DCM 1:1 (v/v) and DCM:methanol 1:1 (v/v), into apolar and polar fractions, respectively. The polar

fractions, containing the branched glycerol dialkyl glycerol tetraethers (GDGTs), were analyzed by high performance liquid chromatography / atmospheric pressure chemical ionization – mass spectrometry (HPLC/APCI-MS) using an Agilent 1100 series / Hewlett-Packard 1100 MSD. Separation was achieved in normal phase on an Alltech Prevail Cyano column (150 mm × 2.1 mm; 3 µm). The flow rate of the hexane:propanol 99:1 (v/v) eluent was 0.2 ml min^{-1}, isocratically for the first 5 min, thereafter with a linear gradient to 1.8% propanol in 45 min. GDGTs were detected and quantified by selective ion monitoring of the $[M+H]^+$ (protonated molecular ion) peaks.

MBT & CBT proxies

A detailed description of the definitions and characteristics of the Methylation index of Branched Tetraethers (MBT) and the Cyclisation ratio of Branched Tetraethers (CBT) is provided by Weijers et al. (2007a). Briefly, previous studies have shown the occurrence in soils and peat bogs of new types of GDGTs, the so-called branched GDGTs (Fig. S10.1), which differ in their amount of methyl and cyclopentanyl moieties (Schouten et al., 2000; Sinninghe Damsté et al., 2000; Weijers et al., 2006a, 2006b). A survey of 134 globally distributed soils showed that these GDGTs are ubiquitously present and that the average amount of cyclopentanyl moieties in these GDGT lipids, expressed in the CBT ratio is related to soil pH. In addition, the degree of methyl branching of the alkyl chains of the GDGT lipids, expressed in the MBT index, is related to the annual mean air temperature (MAT) and, to a lesser extent, also to soil pH. These relations reflect biological adaptations of the membranes of soil bacteria to ambient conditions, similar to what is observed for membrane lipids of other bacteria and archaea (e.g., Uda et al., 2001). Combining both relations, i.e. correcting the MBT index for changes in soil pH using the CBT ratio, enables the reconstruction of the annual MAT. The MBT index and CBT ratio were calculated as follows:

$$\text{MBT} = \frac{[\text{I} + \text{Ib} + \text{Ic}]}{[\text{I} + \text{Ib} + \text{Ic}] + [\text{II} + \text{IIb} + \text{IIc}] + [\text{III} + \text{IIIb} + \text{IIIc}]} \tag{1}$$

$$\text{CBT} = -\text{LOG}\left(\frac{([\text{Ib}] + [\text{IIb}])}{([\text{I}] + [\text{II}])}\right) \tag{2}$$

The Roman numerals correspond to those in Fig. S10.1. The calibration formulas used to transfer the CBT ratio into pH and the MBT and CBT values into annual MAT are (Weijers et al., 2007a):

$$\text{CBT} = 3.33 - 0.38 \, \text{pH} \quad (R^2 = 0.70) \tag{3}$$

$$\text{MBT} = 0.122 + 0.187 \, \text{CBT} + 0.020 \, \text{MAT} \quad (R^2 = 0.77) \tag{4}$$

The pH calibration range is from 3.3 to 8.2 and the temperature calibration range is from -6.7 to 27.0°C, which covers the entire range of pH and temperatures reconstructed from our core. The analytical reproducibility based on pooled standard deviations of duplicate measurements of samples is ≤ 0.01 units for the MBT index and ± 0.01 units for the CBT ratio, or ± 0.02 pH units and ± 0.2°C in the temperature estimates.
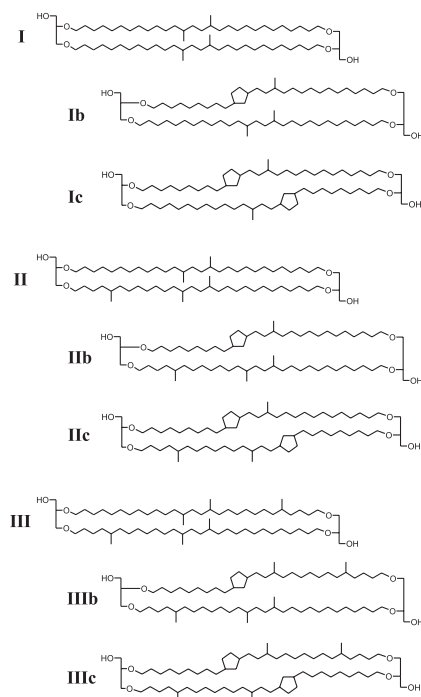

Figure S10.1: Chemical structures of the different branched glycerol dialkyl glycerol tetraethers (GDGTs).

Supporting text

Distribution and origin of branched GDGTs in surface sediments of the Congo deep-sea fan
In an earlier report (Hopmans et al., 2004) it has been shown that the abundance of branched GDGTs in surface sediments of the Congo deep-sea fan relative to the marine derived isoprenoid GDGT crenarchaeol [expressed in the Branched vs. Isoprenoid Tetraether (BIT) index] accurately traces the fluvial input of terrestrial organic matter (Fig. S10.2). High BIT indices, i.e., samples dominated by branched GDGTs, are found in the Congo River estuary and values decrease, i.e., marine derived crenarchaeol becomes more dominant, with increasing distance from the river mouth, indicating that the branched GDGTs are terrestrial in origin and transported adsorbed to suspended particulate matter (SPM) in river water. This has been confirmed by analysis of riverine suspended particulate matter (Kim et al., 2006; Herfort et al., 2006). Therefore, our annual MAT signal represents a continental temperature signal and not a marine signal. In addition to the annual MAT reconstructed from the core top sediment from core GeoB 6518-1 (24.5°C), the 'present-day' annual MAT for the Congo

Basin reconstructed based on these Congo deep-sea fan surface sediments (those with a BIT index ≥0.20, elsewhere the signal is too low for reliably determining MBT and CBT) is 23.5°C (± 1.5°C).
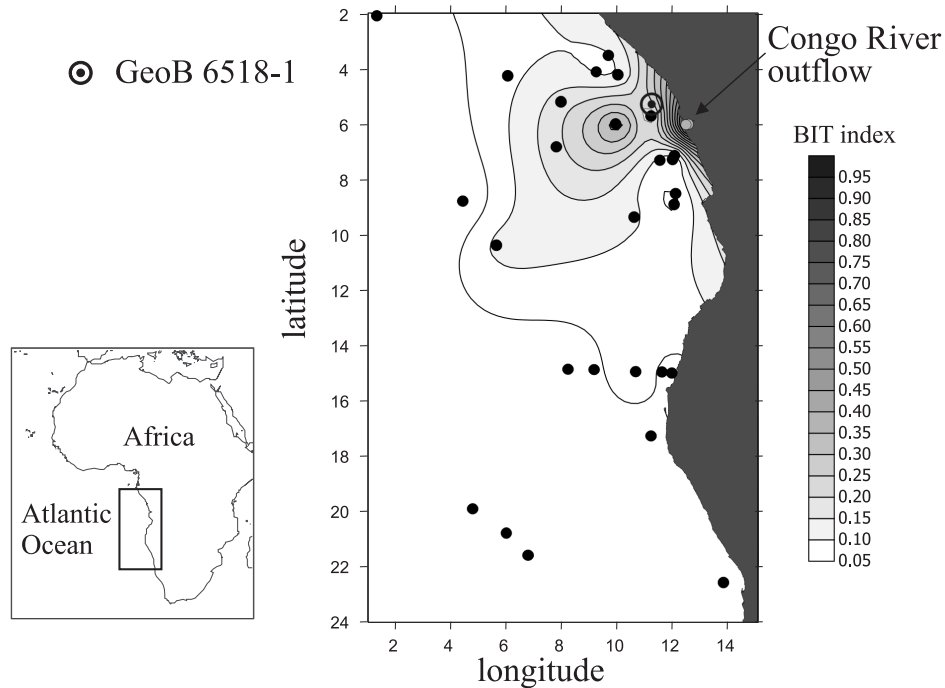
Figure S10.2: Contour plot of BIT index values of surface sediments in the eastern South Atlantic Ocean. Figure adapted from Hopmans et al. (2004).

We assume that the obtained annual MAT values represent a Congo Basin wide integrated signal. This is the best assumption that can presently be made, regarding the uncertainties that still remain about the exact temporal and spatial origin of sedimentary organic matter in large river systems (McKee et al., 2004). This potential bias is, however, unlikely to considerably affect our obtained MAT values, especially given the rather even distribution of temperatures in the Cong Basin (Fig. 10.1B).

Potential time lags between marine and terrestrial proxies
Potentially, there may be a time lag between the time of biosynthesis of the branched GDGT membrane lipids in the soils and the moment of their sedimentation on the sea floor as the GDGTs transported by the river may be derived from soils of various ages. This could result in a wrong dating of the onset of deglacial warming as the age-calibration of the MBT/CBT record is based on marine foraminifera. This time-lag effect, however, seems to be negligible in this record. The pattern of the CBT (= soil-pH) record matches very well with the independent record of foraminiferal residual $\delta^{18}O$, which reveals Congo River discharge

changes synchronous with known climate events like the YD (Schefuß et al., 2005). This can be explained by the fact that, at least on the long term, soil acidification slows down as a result of reduced precipitation (Johnson et al., 1998). The good match between the soil-pH and $\delta^{18}O_{seawater}$ records implies that the amount of 'fresh' GDGTs transported to the marine environment must be relatively large relative to the amount of 'fossil' GDGT lipids released from soils and the transport time must be minor. In addition to the YD humidity event, the onset of deglacial warming in our record is coincident with the global onset of deglacial warming. If there would have been a large age offset, then this should have resulted in a delay of the warming and YD signal, which is not observed.

Evidence for a small time lag comes from a radiocarbon study of soils from tropical areas which indicates that, despite the presence of refractory organic matter, the majority of the organic matter in the top 22 cm of tropical soils has residence times of less than 10 years (Trumbore, 1993). This young age of organic matter in tropical top-soils seems further supported by studies on the ^{14}C content of riverine organic matter which point to older ages in river systems from temperate regions (e.g., Raymond and Bauer, 2001) but younger ages in tropical river systems (e.g., Hedges et al., 1986; Mayorga et al., 2005). This is in strong support of our interpretation that no significant time lag is present between the continental climate record archived in the terrestrial GDGTs and the marine record contained in the alkenone distribution.

Chapter 11

High latitude subtropical continental temperatures during the Palaeocene-Eocene thermal maximum

Johan W.H. Weijers, Stefan Schouten, Henk Brinkhuis and Jaap S. Sinninghe Damsté

Abstract

The Palaeocene-Eocene thermal maximum (PETM; ~55.5 Ma) is a geologically relatively brief episode of extreme warmth. Both deep and surface ocean temperatures increased by up to 5°C in equatorial waters and up to 8°C in mid and high latitude waters. From the continents, the annual mean air temperature response during the PETM is still largely unknown, mainly due to a lack of quantitative temperature proxies and sufficient suitable, continuous high resolution records. In this study we reconstruct the annual mean air temperature for the PETM at high latitude continents by analysis of membrane lipids of soil bacteria from a marine central Arctic Ocean sediment core. The results indicate a warming of ~8°C above background values of ~17°C, coincident with a similar rise in sea surface temperatures documented earlier. Our results thus further confirm the initial studies, and point to a strongly reduced latitudinal temperature gradient during the PETM.

11.1. Introduction

Superimposed on the already warm climates of the early Cenozoic, the Palaeocene-Eocene thermal maximum (PETM) at ~55.5 million years ago represents a geologically relatively brief episode (~120 kyr) (Farley and Eltgroth, 2003) of extreme global warming. Sediments deposited during the PETM are also characterized by a strong negative excursion (2.5 to 6 ‰) in the stable carbon isotope ($\delta^{13}C$) records of carbonates and organic carbon in both the marine and terrestrial realms (e.g., Kennett and Stott, 1991; Koch et al., 1992; Sluijs et al., 2006; Wing et al., 2005). This excursion is considered to be associated with the release of massive amounts of ^{13}C-depleted carbon into the ocean and atmosphere system (Pagani et al., 2006a and references therein). Biotic responses to the climatic changes during the PETM include rapid floral range changes (Wing et al., 2005), large scale faunal dispersion (Koch et al., 1992; Smith et al., 2006), as well as massive benthic extinctions (Kennett and Stott, 1991) and proliferation of exotic foraminifera (Kelly et al., 1996) and certain dinoflagellates (Bujak and Brinkhuis, 1998; Crouch et al., 2001).

During the PETM, the deep oceans warmed globally by 4 to 6°C (e.g., Bralower et al., 1995; Kennett and Stott, 1991; Tripati and Elderfield, 2005). Sea surface temperatures (SST) in the tropics showed a warming of up to 5°C (Bralower et al., 1995; Thomas et al., 1999; Zachos et al., 2003) while stronger warming of 5 to 8°C has been reported for the mid and high latitude ocean surfaces (Kennett and Stott, 1991; Sluijs et al., 2006; Zachos et al., 2003, 2006). Compared to the marine realm relatively little is known about changes in the annual mean air temperature (MAT) on the continents during the PETM, due to a lack of quantitative temperature proxies in combination with the relative short duration of the PETM. Several qualitative climate reconstructions indicate generally warmer conditions throughout on the continents around the PETM, notably at higher latitudes (e.g., Francis and Poole, 2002; Markwick, 1998; Robert and Kennett, 1994). Based, for example, on leaf margin analysis and oxygen isotope analysis of fossil teeth enamel, temperatures of ~20°C and ~26°C have been estimated for the PETM in mid latitude North America (Fricke and Wing, 2004; Wing et al., 2005). Unfortunately, however, continuous high resolution records of annual MAT on the continents are not available for the PETM interval.

Recently, a new method for estimating terrestrial annual MAT has been developed based on the relative distribution of branched glycerol dialkyl glycerol tetraether (GDGT) membrane lipids derived from bacteria thriving in soils (Weijers et al., 2006a, 2007a). The analysis of a globally distributed set of soils shows that the degree of methylation and cyclisation of these branched GDGT membrane lipids, expressed in the Methylation index of Branched Tetraethers (MBT) and Cyclisation ratio of Branched Tetraethers (CBT), respectively, correlates well with annual MAT (Weijers et al., 2007a). Since these membrane lipids are fluvially transported to the oceans (Hopmans et al., 2004), analysing marine sedimentary records in front of large river outflows provides continuous high resolution

records of river basin integrated continental temperature signals (Weijers et al., 2007b). Here we apply this method to sediments obtained from a core from the Lomonosov Ridge in the Arctic Ocean, from Integrated Ocean Drilling Program (IODP) Expedition 302. During the PETM this site received considerable fluvial terrestrial organic matter input from surrounding continents (Sluijs et al., 2006). By analysing the distribution of the soil-derived GDGT lipids in this sediment core we aim to reconstruct annual MAT for the high latitude continents surrounding the Arctic Ocean during the PETM.
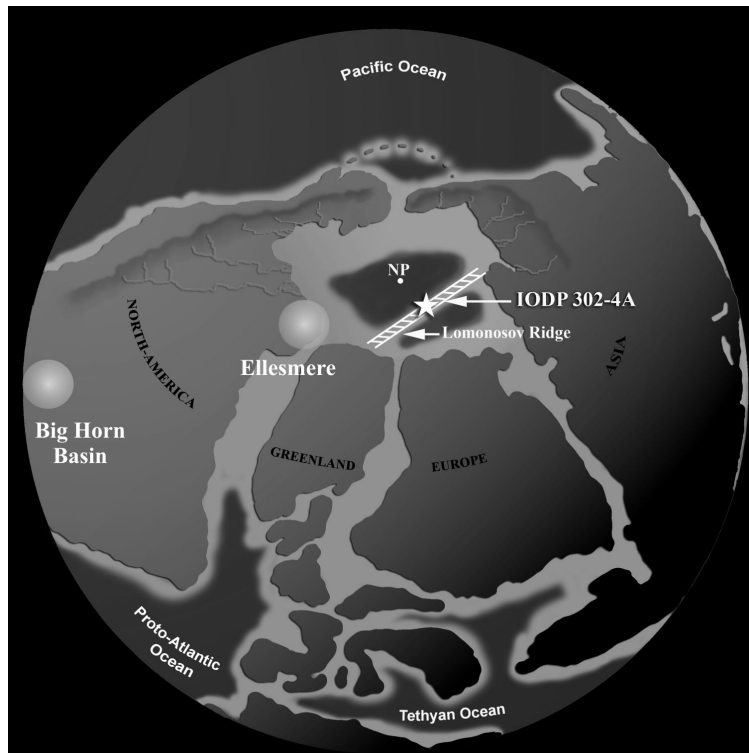
Figure 11.l: Location of IODP Hole 302-4A in the palaegeographical context of the late Palaeocene – early Eocene. Also indicated are the approximate palaeolocations of Ellesmere Island and the Bighorn Basin area, for which PETM (Fricke and Wing, 2004; Wing et al., 2005) and post PETM (Markwick, 1998) temperature estimates have been reported. This figure is modified from Sluijs et al. (2006). See page 172 for colour version of this picture.

11.2. Methods

11.2.1. Sample and site description

Marine sediment samples are derived from IODP Hole 302-4A (~ 87° 52.00' N; 136° 10.64' E; 1,288 m water depth), positioned on the Lomonosov Ridge in the central Arctic Ocean (Fig. 11.1), recovered during IODP Expedition 302 (or Arctic Coring Expedition; ACEX) in August 2004 (Backman et al., 2006). The Lomonosov Ridge represents a part of the Barentsz

Shelf that rifted from the Svalbard margin and subsequently drifted away towards the pole and submerged to its present depth during the Cenozoic (Jokat et al., 1992). During the late Palaeocene, this location was strongly influenced by fresh water input as evident from organic walled dinoflagellate cyst (dinocyst) assemblages and high proportions of terrestrial palynomorphs (Sluijs et al., 2006). The PETM section has been recognized on basis of the concomitant occurrence of a ~6‰ negative excursion in $\delta^{13}C_{org}$ values and the occurrence of the dinocyst species *Apectodinium augustum*, which is diagnostic of the PETM (Bujak and Brinkhuis, 1998; Sluijs et al., 2006).

11.2.2. Sample preparation and HPLC/MS analysis

Powdered and freeze dried sediments (1-3 g dry mass) were extracted with an accelerated solvent extractor (Dionex2000), using a dichloromethane (DCM):MeOH 9:1 (v/v) solvent mixture, 3 times for 5 min at a pressure of ca 7.6×10^6 Pa and a temperature of 100°C. The obtained total extracts were rotary evaporated and separated over an activated Al_2O_3 column using hexane:DCM 9:1 (v/v) and DCM:MeOH 1:1 (v/v) solvent mixtures into an apolar and polar fraction, respectively. The polar fraction, containing the branched GDGTs, was dried under a pure N_2 flow, dissolved ultrasonically in a hexane:propanol 99:1 (v/v) mixture at a concentration of 2 mg ml^{-1} and filtered over an 0.45 μm mesh PTFE filter (ø 4mm) prior to HPLC/MS analysis.
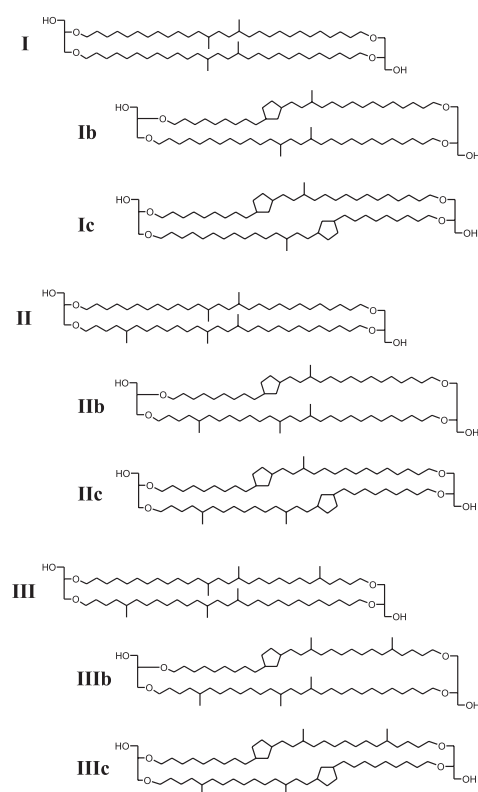
Figure 11.2: Chemical structures of the branched glycerol dialkyl glycerol tetraether (GDGT) membrane lipids of soil bacteria used in this study.

High performance liquid chromatography – atmospheric pressure chemical ionization / mass spectrometry (HPLC-APCI/MS) analyses were performed on an Agilent 1100 series / Hewlett-Packard 1100 MSD series machine equipped with auto-injector and HP Chemstation software as described previously (Hopmans et al., 2000) with minor modifications. Injection volume was usually 10 µl and separation of the compounds was achieved in normal phase on a Prevail Cyano column (150 x 2.1 mm; 3 µm; Alltech). The flow rate of the hexane:propanol 99:1 (v/v) eluent was 0.2 ml min^{-1}, isocratically for the first 5 min and thereafter with a linear gradient to 1.8% propanol in 45 min. Analyses were performed in selective ion monitoring mode in order to increase sensitivity and reproducibility. Branched GDGTs (see Fig. 11.2 for structures) were quantified by integrating the area of the $[M+H]^{+}$ peaks (protonated molecular ion) and comparing these with an external standard curve prepared with known amounts of the isoprenoid GDGT crenarchaeol. The Cyclisation ratio of Branched Tetraethers (CBT) and the Methylation index of Branched Tetraethers (MBT) were calculated as follows:

$$CBT = -LOG\left(\frac{([Ib]+[IIb])}{([I]+[II])}\right) \qquad (1)$$

$$MBT = \frac{([I]+[Ib]+[Ic])}{([I]+[Ib]+[Ic])+([II]+[IIb]+[IIc])+([III]+[IIIb]+[IIIc])} \qquad (2)$$

Roman numerals correspond to the GDGT structures drawn in Fig. 11.2. Annual MAT was then calculated from the CBT and MBT values using the calibration equation given by Weijers et al. (2007a):

$$MBT = 0.122 + 0.187*CBT + 0.020*MAT \qquad (3)$$

The analytical reproducibility is ± 0.01 unit for both the CBT and MBT, together accounting for an analytical reproducibility of ± 0.9°C in the temperature estimates.

11.3. Results and discussion

11.3.1. Temperature estimates based on soil derived branched GDGT lipids
Concentrations of the soil derived branched GDGT membrane lipids (see Fig. 11.2 for structures) are ~90 µg g^{-1} dry weight sediment (dws) during the PETM interval which is higher than the values of 10 and 60 µg g^{-1} dws obtained from the pre- and post-PETM sections of this core, respectively. Based on the rather constant and substantial TOC contents (~2%) in combination with well preserved palynomorphs both within and outside the PETM

section, this difference is unlikely to be the result of differences in preservation conditions (Sluijs et al., 2006). Instead, the higher concentrations of branched GDGTs during the PETM suggest enhanced river discharge during the PETM which is consistent with the more humid conditions on the nearby Arctic continents at that time (Pagani et al., 2006b).
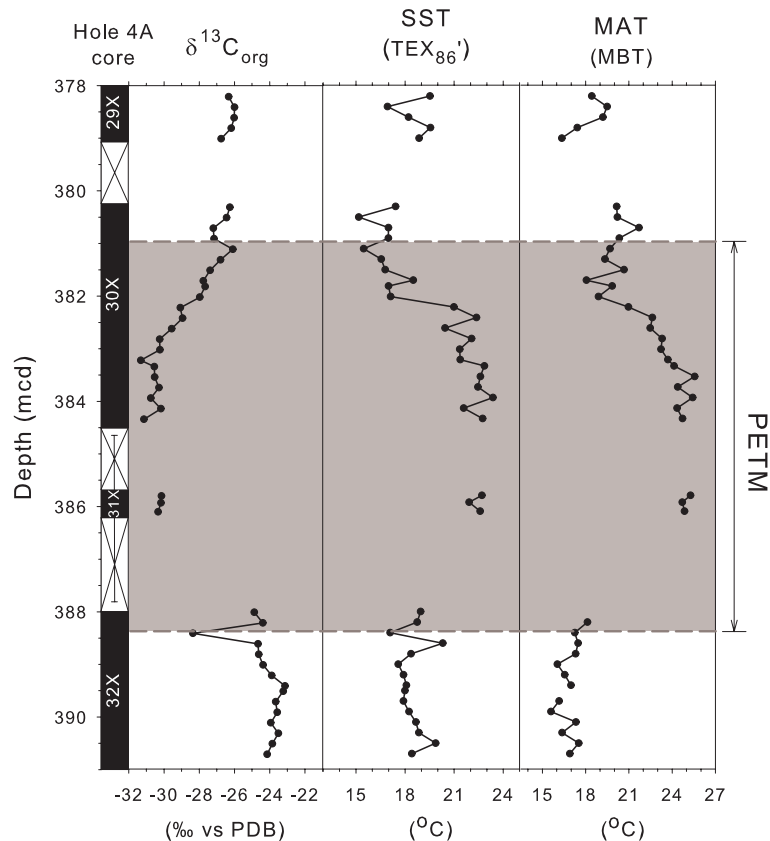
Figure 11.3: Annual mean air temperature (MAT) across the PETM for the high latitude continents surrounding the Arctic Ocean. Annual MAT is derived from branched GDGT lipids in IODP Hole 302-4A and plotted alongside the TEX_{86}' derived sea surface temperature (SST) and the ^{13}C content of TOC reported by Sluijs et al. (2006). Error bars in the core recovery column indicate the uncertain stratigraphic position of section 31X, see also Sluijs et al. (2006). mcd, meters composite depth.

Since fluvial input of terrestrial organic matter was high, it was possible to determine the degree of cyclisation (CBT) and methylation (MBT) of the terrestrial derived branched GDGTs in the sediments of this core and thus to reconstruct the continental annual MAT for the PETM interval. With respect to the palaeolocation of the core site during the late Palaeocene and early Eocene, at the edge of the high latitude continental margins, reconstructed annual MAT signals are probably derived for a substantial part from the high latitude Eurasian continent. Since the largest part of this continental region is assumed to have comprised lowland area, the obtained temperature record is expected to represent a lowland temperature signal and is, therefore, here assumed not to be influenced to a large extent by

soil material transported from high altitude sites. The reconstructed annual MAT shows values of 16 to 18°C for the latest Palaeocene and increases to values up to 25°C during the PETM (Fig. 11.3). Towards the end of the PETM, temperatures drop again to values of around 18 to 20°C. This transient temperature change runs parallel with the negative $\delta^{13}C_{org}$ excursion and the acme of the subtropical dinoflagellate *Apectodinium augustum* (Sluijs et al., 2006). Highest temperatures occur at the time of the lowest $\delta^{13}C_{org}$ values and the subsequent cooling mirrors the recovery pattern of $\delta^{13}C_{org}$ (Fig. 11.3).

11.3.2. Comparison with other Palaeocene-Eocene temperature estimates
The annual MAT record for the high latitude continents surrounding the Arctic Ocean compares well with the SST reconstruction for the Arctic Ocean at this location by Sluijs et al. (2006). On the basis of the TEX_{86}' proxy, their reconstruction shows SSTs of ~18°C for the latest Palaeocene, >23°C for the PETM, and a cooling towards ~17°C at the end of the PETM (Fig. 11.3). Thus, both proxies indicate a strong climatic warming in the Arctic region during the PETM, and a cooling towards the end of the PETM consistent with the recovery of the $\delta^{13}C_{org}$ signal. Remarkably, the absolute temperatures estimated by both proxies are also similar, particularly so when taking into account uncertainties like the exact temporal origin of the temperature signals in this high latitude area, i.e., annual mean or seasonal temperatures. It has to be emphasized that both organic proxies are based on different compounds and source organisms and are differently calibrated and hence totally independent of each other. Therefore, the fact that the absolute values of our continental temperature reconstruction for the Arctic region are very similar to the absolute temperatures reconstructed for the Arctic sea surface is a first and strong independent confirmation that temperatures in the Arctic during the PETM were indeed extremely high compared to the present-day situation.

As noted above, and in contrast to the marine realm, terrestrial temperature estimates for the PETM interval are very scarce. For high latitude regions only two semi-quantitative temperature estimates are available (Markwick, 1998; Robert and Kennett, 1994) (Table 11.1). In addition to the minimum temperature provided by the clay mineral assemblage derived from coastal Antarctica, its composition during the PETM interval compares to that found in modern tropical to subtropical Atlantic sediments, which even suggests subtropical conditions on coastal Antarctica during the PETM (Robert and Kennett, 1994). Absolute estimates of annual MAT for the PETM, based on leaf margin analysis are derived from the Big Horn Basin area, Wyoming USA, which was located towards considerably lower latitudes (Wing et al., 2000, 2005) (compare Table 11.1). These estimates are ~6°C lower than temperatures derived from oxygen isotope ratio analyses of phosphate in teeth from fossil mammals from the same area (Fricke and Wing, 2004) (Table 11.1). This could be explained by the fact that floras of predominantly wet-soil environments, as used in the Big Horn Basin study, generally show a greater proportion of toothed leaves, resulting in possible temperature underestimates of up to 10°C (Kowalski and Dilcher, 2003). Correction for this possible bias implies that

subtropical to tropical temperature conditions occurred at the mid-latitude North American continent during the PETM. Remarkably, these mid-latitude PETM temperature estimates are, even if taking into account the uncertainties accompanying the different methods, at most similar to the maximum PETM temperatures reconstructed for high the latitude continents surrounding the Arctic Ocean and likely not substantially higher. One possible explanation might be that the peak PETM warmth was missed in the Bighorn Basin section due to the relatively poor stratigraphic resolution of the samples. On the other hand, due to the strong seasonal difference at the high latitudes, our Arctic air temperature estimates might represent maximum (summer) estimates because the season of maximum growth occurs during the polar day (summer) season. However, given that branched GDGT membrane lipids are produced by ostensibly non-phototrophic bacteria thriving in the anoxic parts of soils and peat bogs (Weijers et al., 2006a), and thus likely not affected by polar night/day conditions, and the absence of permafrost at the PETM, recording maximum summer temperatures alone seems to be unlikely. Alternatively, our data are in support of the idea that the latitudinal thermal gradient between the high and mid latitudes was very small during the PETM, a feature which seems to be characteristic of greenhouse climates (e.g., Huber et al., 1995).

Table 11.1: Overview of Palaeocene-Eocene continental temperature estimates

Time interval	Location	Palaeo Lat.	Method	Temperature	Reference
Early Eocene	Arctic Eurasia	~75°N	MBT/CBT	~17°C	this study
	Ellesmere Island Canada	71°N	crocodile remains	>14°C [a]	Markwick, 1998
	Bighorn Basin Wyoming, USA	45°N	leaf margin analyses	~18°C [b]	Wing et al., 2000
PETM	Arctic Eurasia	~75°N	MBT/CBT	~25°C	this study
	Coastal continent Antarctica	65°S [c]	clay mineral composition	>15°C [d]	Robert & Kennett, 1994
	Bighorn Basin Wyoming, USA	45°N	leaf margin analyses	~20°C [b]	Wing et al., 2005
	Bighorn Basin Wyoming, USA	45°N	δ^{18}O composition of fossil teeth	~26°C	Fricke & Wing, 2004
Late Palaeocene	Arctic Eurasia	~75°N	MBT/CBT	~19°C	this study
	Bighorn Basin Wyoming, USA	45°N	leaf margin analyses	~15°C [b]	Wing et al., 2000

[a] minimum mean annual air temperature required for the presence of crocodiles

[b] underestimate; see text for discussion

[c] this represents the latitude of the ODP Site 690B at Maud Rise; Antarctic coastline is at 70°S

[d] formation temperature of kaolinite and thus minimum soil temperature; the overall clay mineral composition is indicative of sub-tropical conditions

11.3.3. Implications

Our record of high latitude continental PETM air temperatures, in conjunction with the few other available high latitude temperature estimates (Robert and Kennett, 1994; Sluijs et al., 2006), provide strong indications of subtropical conditions at the Earth's polar regions during the PETM. This has considerable implications for our knowledge of the Earth's climate state under elevated greenhouse gas levels in an ice free world. Several modelling studies have been conducted to simulate the response of Earth's climate to high greenhouse gas levels for the PETM (e.g., Renssen et al., 2004; Schmidt and Shindell, 2003; Shellito et al., 2003; Shellito and Sloan, 2006). Generally these models show, as expected, increased warming with increasing greenhouse gas conditions and, in addition, amplified warming at the high latitudes of ~5 to 8°C (e.g., Renssen et al., 2004), which is in agreement with proxy data (e.g., Kennett and Stott, 1991). However, the simulated absolute temperatures are, especially for the high latitudes, considerably lower than the indications from proxy data. Thus, proxy data indicate a latitudinal thermal gradient that is much flatter than simulated by climate models. These models, generally, yield gradients of ~30°C (e.g., Shellito et al., 2003; Shellito and Sloan, 2006), which is too large to support the subtropical temperature conditions in the polar region as that would result in unrealistically high equatorial temperatures of 50°C or so.

Apparently, current climate models lack one or more physical mechanisms that are able to warm the polar regions without substantially increasing temperatures in the tropics during the early Cenozoic. Several reasons have been suggested explaining this model-data discrepancy. The presence of sea ice in the initial conditions of the models might be a reason for the low simulated temperatures at the high latitudes. However, even specifying warm polar SSTs, thus excluding sea ice, in a global circulation model resulted in continental interior winter temperatures of less than -13°C (Huber and Sloan, 1999) and thus not necessarily in higher polar temperatures. Increased oceanic heat transport to the poles might be another mechanism preferentially warming the poles, but this then needs to be increased by a factor 2 to 3, a feature that coupled climate models are unable to simulate (Huber and Sloan, 2001). In addition to these proposed mechanisms, the lack of accurate SST boundary conditions and annual cycle definition together with the coarse spatial resolution of topography in the models is suggested to be a cause for the observed model-data discrepancy (Sloan et al., 2001).

One plausible mechanism that might (partly) explain the persistent polar warmth during the early Cenozoic is a higher abundance of polar stratospheric clouds due to increased atmospheric methane concentrations (Sloan and Pollard, 1998). The formation of these clouds is restricted to the relatively colder polar night regions and therefore provides a way to amplify polar warming relative to low and mid latitude warming. Due to the absence of permafrost in the polar regions during these times, increased rates of methanogenesis from soils (Jahren et al., 2004), and possibly also direct methane emissions from the vegetation itself (Keppler et al., 2006), could have led to elevated levels of methane in the atmosphere. Indeed, a model study focussing on aspects of stratospheric clouds yielded year round non-

freezing conditions in the Arctic (Peters and Sloan, 2000), a prerequisite for the observed faunal dispersion at the PETM (Koch et al., 1992; Smith et al., 2006) and reducing the latitudinal thermal gradient, and thus the discrepancy between model output and proxy data. Still, our reconstructed annual MAT for high latitude continents at the PETM is much higher than those obtained by these model studies. This suggests that there still might be additional, yet unknown mechanisms playing a role in warming the Earth's polar regions during the early Cenozoic in general and the PETM in particular.
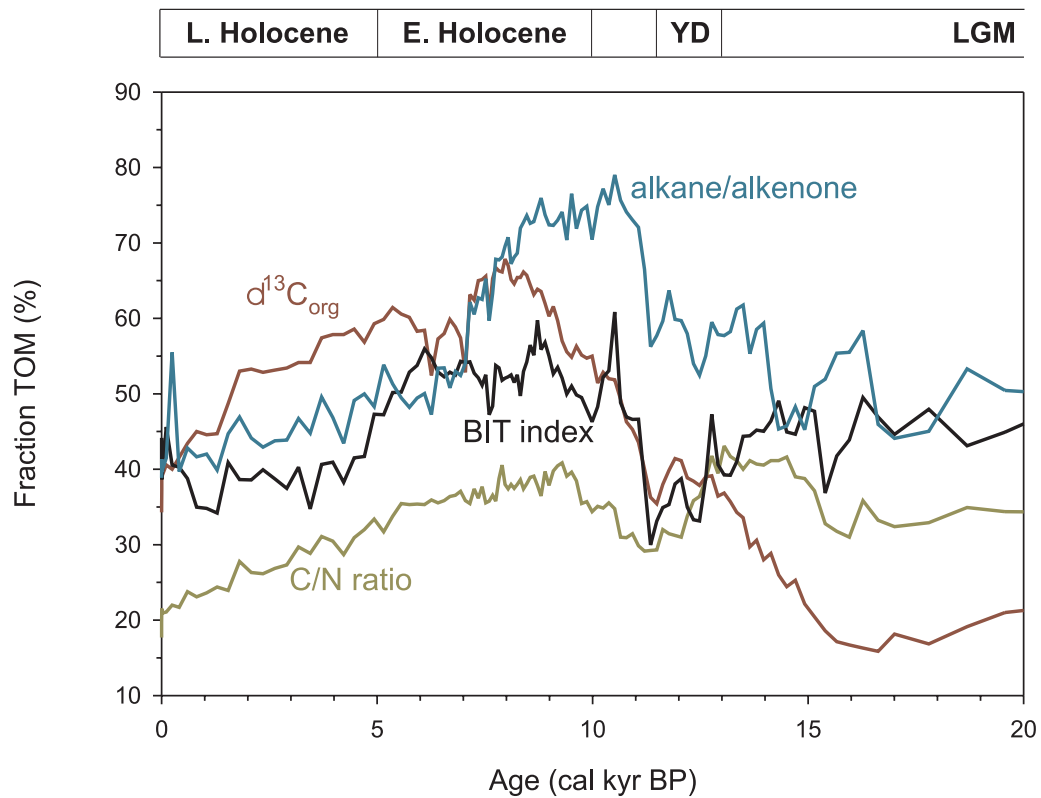
Finally, given the sub-tropical conditions at the poles (Robert and Kennett, 1994; Sluijs et al., 2006 and this study) and conservative temperature estimates in excess of 33°C for the mid latitudes (Zachos et al., 2006), there is the possibility that temperatures at the equator were as high as 40°C during the PETM. Published reconstructions of Cretaceous SSTs at low to mid latitudes using the TEX_{86} proxy (Forster et al., 2007; Schouten et al., 2003; Zachos et al., 2006) and Mg/Ca proxy (Bice et al., 2006; Forster et al., 2007) do suggest that tropical sea waters may have indeed been as high as 40°C. Thus, there may have been somewhat of a latitudinal thermal gradient, but much smaller than today, superimposed on temperatures that were globally substantially higher than currently assumed.
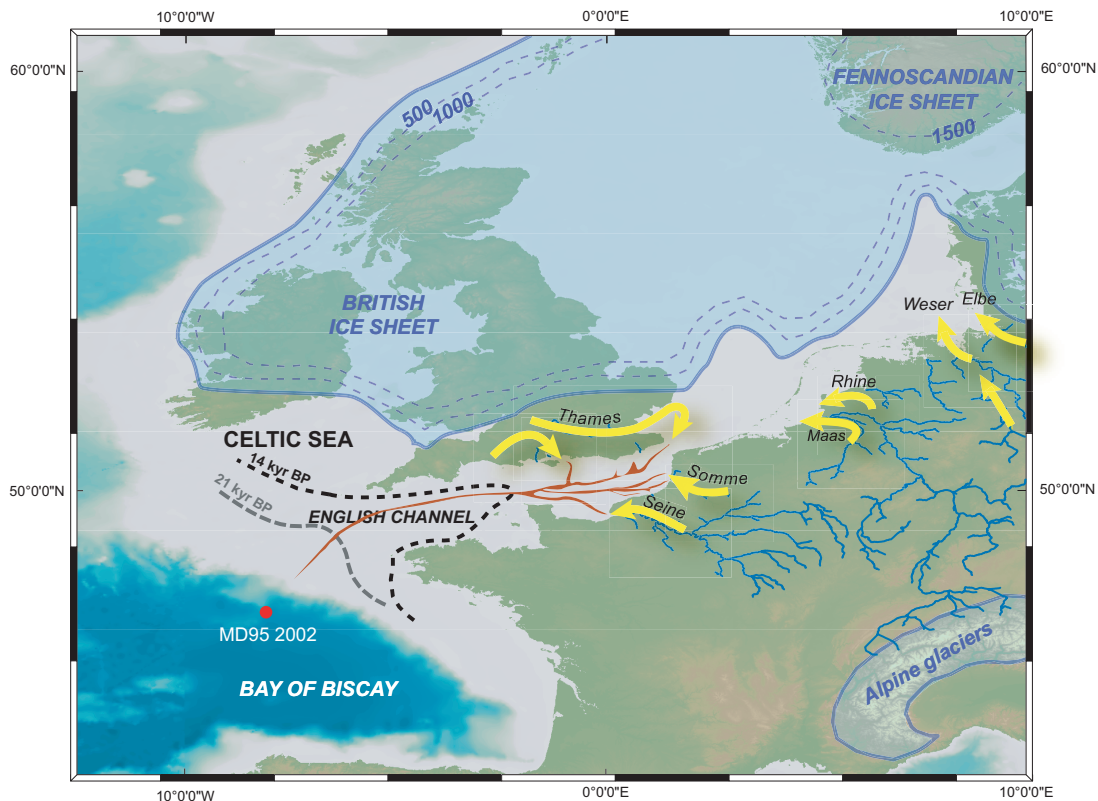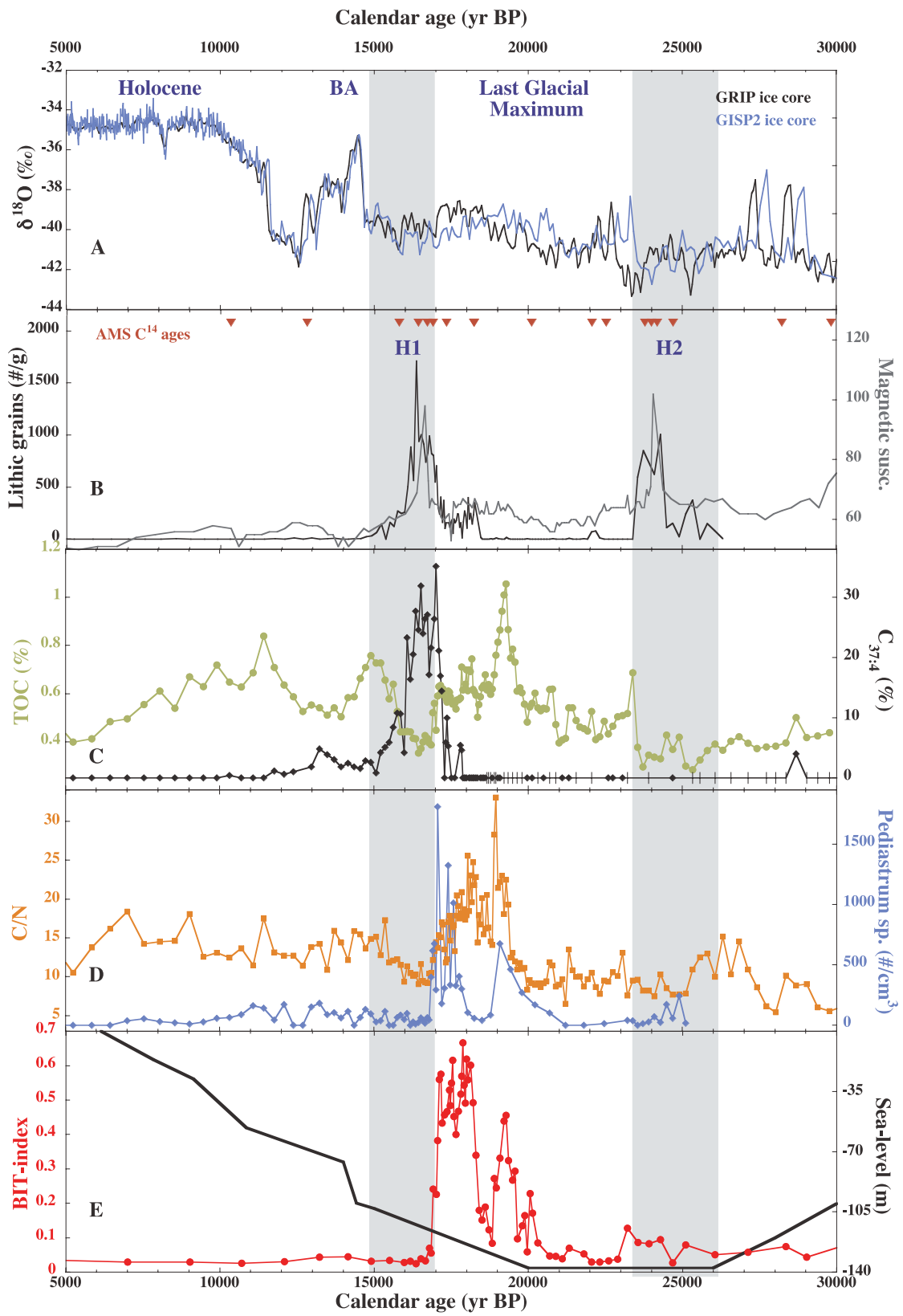
Colour figures

Figure 7.5: Estimates of the proportions of terrestrial organic matter (TOM) in the marine sediments at site GeoB 6518-1 over the past 20 kyr based on two end-member mixing models of the different proxies.
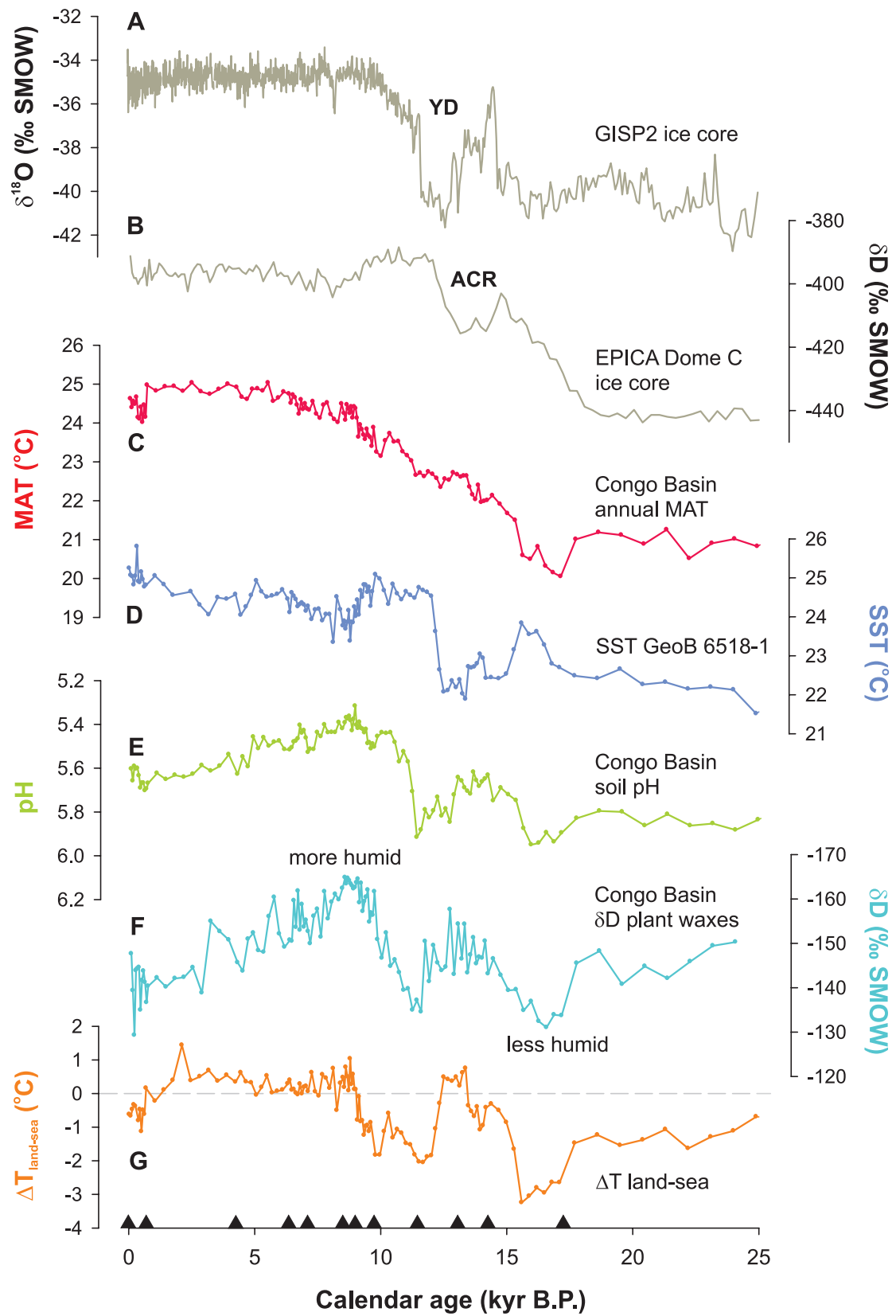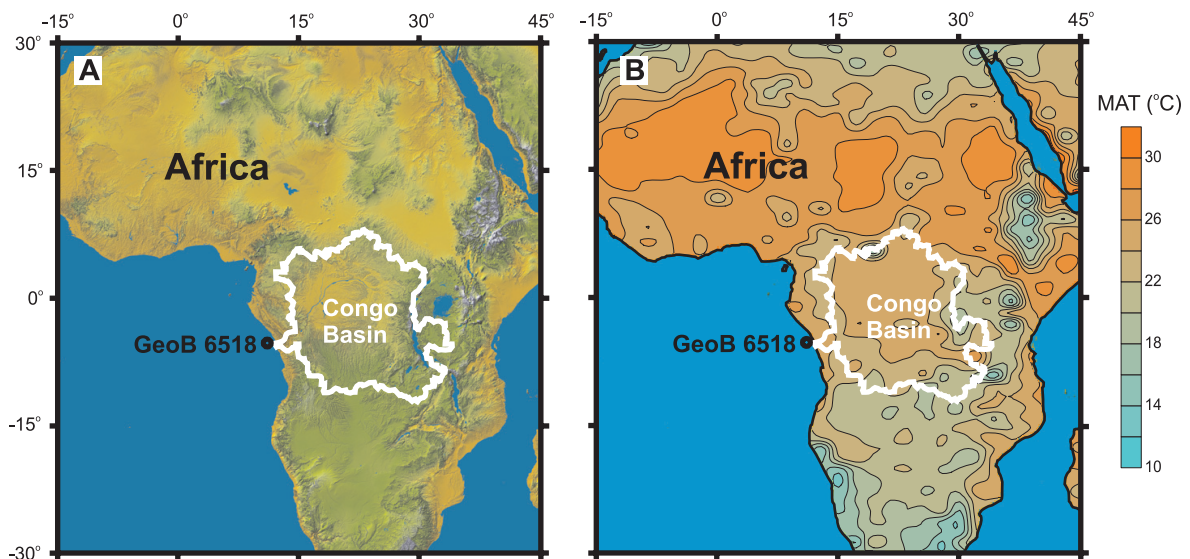
Figure 8.1: The palaeoenvironment of the LGM on the Eurasian continent was radically different from today. The Fennoscandian ice sheet was established on the northern part of Europe, extending west into the Norwegian Sea, south across the north German Plain into Poland, and eastward into North Poland and Russia (Bowen et al., 2002; Mangerud et al., 2004). A smaller dome was installed on the British Isles (Bowen et al., 2002). Recent geomorphological evidence indicates that the British-Irish ice sheet (BIS) and Fennoscandian ice sheet coalesced, and a huge ice dam extended over the present-day North Sea (Mangerud et al., 2004; Svendsen et al., 2004). The Alps were almost entirely covered by an ice dome formed by valley glaciers (Denton and Hughes, 1981). The maximum extent of ice sheets at the LGM is illustrated by the blue contours. A final ice-age sea-level lowstand led to emersion of the channel between England and France, with the coastlines at 14 and 21 kyr B.P. illustrated by the dashed lines (after Lambeck, 1997). A palaeoriver, known as the Channel River (in orange), extended across the emerged continental margin (Bourillet et al., 2003). It drained most of the major rivers in northwestern Europe, that is, the Rhine, Maas, Seine, Solent and Thames (yellow arrows on the map). In addition to these rivers, the Irish Sea drained a large part of the BIS meltwaters (McCabe and Clark, 1998). Furthermore, damming by the Fennoscandian ice sheet favored the development of southward-flowing meltwater valleys and ice-margin spillways running westward. These spillways collected proglacial waters from rivers even farther east than the Elbe basin and allowed drainage to the Channel River (Marks, 2002; Mangerud et al., 2004). Core MD952002 (red dot) was taken at a water depth of 2174 m in the axis of the English Channel, close to the LGM position of the Channel River outlet.

Figure 8.2 (opposite page)**:** Deglaciation-Holocene records of the past activity of the Channel River as a function of palaeoclimatic changes. The chronology is based on calibrated ^{14}C ages measured on planktonic foraminifera [shown as triangles in (B)] (see supporting material). Climatic events are abbreviated as follows: B-A, Bølling-Allerød; H1, Heinrich 1; and H2, Heinrich 2. The grey areas underline the H1 and H2 events. (**A**) δ^{18}O GRIP (black line) (Johnsen et al., 2001) and δ^{18}O GISP2 (light blue line) (Stuiver and Grootes, 2000) records reflecting Greenland air temperatures. (**B**) Black line shows the counting of grains identified as ice-rafted debris (IRD) per 10 g for the size fraction coarser than 150 μm, and the grey curve shows the magnetic susceptibility (MS) record measured on board Marion Dufresne (Auffret et al., 2002). (**C**) Green circles represent the total organic carbon contents, and the black diamonds the percentage of $C_{37:4}$ among C_{37} alkenones, i.e., $\%C_{37:4} = 100 \times [C_{37:4}]/[C_{37:2} + C_{37:3} + C_{37:4}]$. Beyond 19 kyr B.P., the relative percentage of $C_{37:4}$ could not be quantified because alkenones are very scarce in the sediments corresponding to the last glacial period (black ticks in Fig. 8.2C). (**D**) Orange squares indicate the total organic carbon-to-nitrogen ratios (C/N), and the blue symbols show the abundance of freshwater algae, *Pediastrum sp.* (counts from Zaragosi et al., 2001). (**E**) The BIT index is defined as follows: BIT = (I+II+III)/[(I+II+III)+(IV)] (the roman numbers refer to the glycerol dialkyl glycerol tetraethers in Figure 5.1, Hopmans et al., 2004), and is represented here by red dots. The black curve shows the sea-level curve (Lambeck et al., 2002).

Figure 10.1: Overview maps of Africa. Shown are the position of core GeoB 6518, recovered close to the Congo River outflow from a water depth of 962 m, and the extent of the Congo River drainage basin (white outline) plotted on a digital elevation map of Africa (picture from NASA Jet Propulsion Lab., California Institute of Technology) (**A**) and on a map showing the annual mean air temperature distribution in Africa [data based on Willmott and Robeson (1995)] (**B**).

Figure 10.2 (opposite page)**:** Temperature changes over the last 25 kyr in tropical central Africa compared with African humidity changes and Arctic and Antarctic climate signals. Shown are the GISP2 δ^{18}O record indicative of Greenland air temperature fluctuations (Stuiver and Grootes, 2000) (**A**); the EPICA Dome C δD record indicative of Antarctic air temperature changes (Augustin et al., 2004) (**B**); the annual mean air temperature (MAT) record of the Congo Basin based on the MBT index and CBT ratio of the branched GDGT lipids of soil bacteria in core GeoB 6518-1 (**C**); the SST changes in the equatorial Atlantic Ocean based on alkenone palaeo-thermometry at site GeoB 6518-1 (Schefuß et al., 2005) (**D**); a record of the average soil pH in the Congo Basin based on the CBT ratio of branched GDGT lipids of soil bacteria in core GeoB 6518-1 (**E**); the δD record of C_{29} *n*-alkane plant waxes in core GeoB 6518-1 reflecting humidity changes in tropical central Africa (Schefuß et al., 2005) (**F**) and the land-sea temperature gradient between central tropical Africa and the tropical Atlantic Ocean based on records c and d (**G**). Black triangles on the age scale indicate the ^{14}C-AMS radiocarbon dates derived from mixed planktonic foraminifera used for establishing the chronology of core GeoB 6518-1 (Schefuß et al., 2005). YD = Younger Dryas; ACR = Antarctic Cold Reversal.
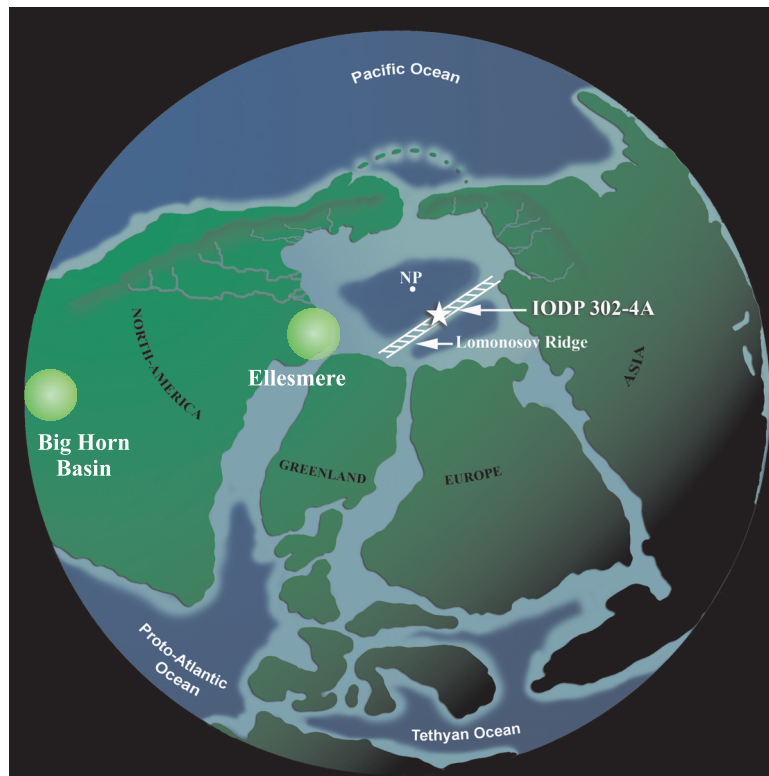
Figure 11.l: Location of IODP Hole 302-4A in the palaegeographical context of the late Palaeocene – early Eocene. Also indicated are the approximate palaeolocations of Ellesmere Island and the Bighorn Basin area, for which PETM (Fricke and Wing, 2004; Wing et al., 2005) and post PETM (Markwick, 1998) temperature estimates have been reported. This figure is modified from Sluijs et al. (2006).

References

Adegbie, A.T., Schneider, R.R., Rohl, U., Wefer, G., 2003. Glacial millennial-scale fluctuations in central African precipitation recorded in terrigenous sediment supply and freshwater signals offshore Cameroon. Palaeogeography Palaeoclimatology Palaeoecology 197, 323-333.

Aislabie, J.M., Chhour, K.L., Saul, D.J., Miyauchi, S., Ayton, J., Paetzold, R.F., Balks, M.R., 2006. Dominant bacteria in soils of Marble Point and Wright Valley, Victoria Land, Antarctica. Soil Biology & Biochemistry 38, 3041-3056.

Allen, J.R.M., Brandt, U., Brauer, A., Hubberten, H.W., Huntley, B., Keller, J., Kraml, M., Mackensen, A., Mingram, J., Negendank, J.F.W., Nowaczyk, N.R., Oberhansli, H., Watts, W.A., Wulf, S., Zolitschka, B., 1999. Rapid environmental changes in southern Europe during the last glacial period. Nature 400, 740-743.

Alley, R.B., Brook, E.J., Anandakrishnan, S., 2002. A northern lead in the orbital band: north-south phasing of Ice-Age events. Quaternary Science Reviews 21, 431-441.

Amann, R.I., Zarda, B., Stahl, D.A., Schleifer, K.H., 1992. Identification of individual prokaryotic cells by using enzyme-labeled, ribosomal-RNA-targeted oligonucleotide probes. Applied and Environmental Microbiology 58, 3007-3011.

Anka, Z., Seranne, M., 2004. Reconnaissance study of the ancient Zaire (Congo) deep-sea fan (ZaiAngo Project). Marine Geology 209, 223-244.

Antoine, P., Coutard, J.P., Gibbard, P., Hallegouet, B., Lautridou, J.P., Ozouf, J.C., 2003. The pleistocene rivers of the English channel region. Journal of Quaternary Science 18, 227-243.

Arens, N.C., Jahren, A.H., Amundson, R., 2000. Can C3 plants faithfully record the carbon isotopic composition of atmospheric carbon dioxide? Paleobiology 26, 137-164.

Auffret, G., Zaragosi, S., Dennielou, B., Cortijo, E., Van Rooij, D., Grousset, F., Pujol, C., Eynaud, F., Siegert, M., 2002. Terrigenous fluxes at the Celtic margin during the last glacial cycle. Marine Geology 188, 79-108.

Augustin, L., Barbante, C., Barnes, P.R.F., Barnola, J.M., Bigler, M., Castellano, E., Cattani, O., Chappellaz, J., DahlJensen, D., Delmonte, B., Dreyfus, G., Durand, G., Falourd, S., Fischer, H., Fluckiger, J., Hansson, M.E., Huybrechts, P., Jugie, R., Johnsen, S.J., Jouzel, J., Kaufmann, P., Kipfstuhl, J., Lambert, F., Lipenkov, V.Y., Littot, G.V.C., Longinelli, A., Lorrain, R., Maggi, V., Masson-Delmotte, V., Miller, H., Mulvaney, R., Oerlemans, J., Oerter, H., Orombelli, G., Parrenin, F., Peel, D.A., Petit, J.R., Raynaud, D., Ritz, C., Ruth, U., Schwander, J., Siegenthaler, U., Souchez, R., Stauffer, B., Steffensen, J.P., Stenni, B., Stocker, T.F., Tabacco, I.E., Udisti, R., van de Wal, R.S.W., van den Broeke, M., Weiss, J., Wilhelms, F., Winther, J.G., Wolff, E.W., Zucchelli, M., 2004. Eight glacial cycles from an Antarctic ice core. Nature 429, 623-628.

Backman, J., Moran, K., McInroy, D.B., Mayer, L.A., the Expedition 302 Scientists, 2006. Arctic Coring Expedition (ACEX). Proc. IODP 302, doi:10.2204/iodp.proc.302.2006-(Integrated Ocean Drilling Program Management International, College Station, Texas, 2006).

Bard, E., Arnold, M., Hamelin, B., Tisnerat-Laborde, N., Cabioch, G., 1998. Radiocarbon calibration by means of mass spectrometric Th-230/U-234 and C-14 ages of corals: An updated database including samples from Barbados, Mururoa and Tahiti. Radiocarbon 40, 1085-1092.

Bard, E., 1999. Paleoclimate - Ice age temperatures and geochemistry. Science 284, 1133-1134.

Bard, E., Rostek, F., Turon, J.L., Gendreau, S., 2000. Hydrological impact of Heinrich events in the subtropical northeast Atlantic. Science 289, 1321-1324.

Bard, E., Ménot-Combes, G., Rostek, F., 2004. Present status of radiocarbon calibration and comparison records based on Polynesian corals and Iberian Margin sediments. Radiocarbon 46, 1189-1202.

Barns, S.M., Takala, S.L., Kuske, C.R., 1999. Wide distribution and diversity of members of the bacterial kingdom Acidobacterium in the environment. Applied and Environmental Microbiology 65, 1731-1737.

Bartlett, K.B., Harriss, R.C., 1993. Review and assessment of methane emissions from wetlands. Chemosphere 26, 261-320.

Beales, N., 2004. Adaptation of microorganisms to cold temperatures, weak acid preservatives, low pH, and osmotic stress: A review. Comprehensive Reviews in Food Science and Food Safety 3, 1-20.

References

Benson, D.A., Karsch-Mizrachi, I., Lipman, D.J., Ostell, J., Rapp, B.A., Wheeler, D.L., 2000. GenBank. Nucleic Acids Research 28, 15-18.

Benthien, A., Andersen, N., Schulte, S., Muller, P.J., Schneider, R.R., Wefer, G., 2005. The carbon isotopic record of the C-37 : 2 alkenone in the South Atlantic: Last Glacial Maximum (LGM) vs. Holocene. Palaeogeography, Palaeoclimatology, Palaeoecology 221, 123-140.

Berner, R.A., 1989. Biogeochemical cycles of carbon and sulfur and their effect on atmospheric oxygen over Phanerozoic time. Global and Planetary Change 75, 97-122.

Bianchi, T.S., Mitra, S., McKee, B.A., 2002. Sources of terrestrially-derived organic carbon in lower Mississippi River and Louisiana shelf sediments: implications for differential sedimentation and transport at the coastal margin. Marine Chemistry 77, 211-223.

Bice, K.L., Birgel, D., Meyers, P.A., Dahl, K.A., Hinrichs, K.U., Norris, R.D., 2006. A multiple proxy and model study of Cretaceous upper ocean temperatures and atmospheric CO_2 concentrations. Paleoceanography 21, doi:10.1029/2005PA001203.

Bintrim, S.B., Donohue, T.J., Handelsman, J., Roberts, G.P., Goodman, R.M., 1997. Molecular phylogeny of Archaea from soil. Proceedings of the National Academy of Sciences of the United States of America 94, 277-282.

Blunier, T., Schwander, J., Stauffer, B., Stocker, T., Dallenbach, A., Indermuhle, A., Tschumi, J., Chappellaz, J., Raynaud, D., Barnola, J.M., 1997. Timing of the Antarctic cold reversal and the atmospheric CO_2 increase with respect to the Younger Dryas event. Geophysical Research Letters 24, 2683-2686.

Bonnefille, R., Roeland, J.C., Guiot, J., 1990. Temperature and rainfall estimates for the past 40,000 years in equatorial Africa. Nature 346, 347-349.

Booth, I.R., 1985. Regulation of Cytoplasmic pH in Bacteria. Microbiological Reviews 49, 359-378.

Boucher, Y., Kamekura, M., Doolittle, W.F., 2004. Origins and evolution of isoprenoid lipid biosynthesis in archaea. Molecular Microbiology 52, 515-527.

Bourillet, J.F., Reynaud, J.Y., Baltzer, A., Zaragosi, S., 2003. The 'Fleuve Manche': the submarine sedimentary features from the outer shelf to the deep-sea fans. Journal of Quaternary Science 18, 261-282.

Bowen, D.Q., Phillips, F.M., McCabe, A.M., Knutz, P.C., Sykes, G.A., 2002. New data for the Last Glacial Maximum in Great Britain and Ireland. Quaternary Science Reviews 21, 89-101.

Bralower, T.J., Zachos, J.C., Thomas, E., Parrow, M., Paull, C.K., Kelly, D.C., Silva, I.P., Sliter, W.v., Lohmann, K.C., 1995. Late Paleocene to Eocene paleoceanography of the equatorial Pacific-Ocean - Stable isotopes recorded at Ocean Drilling Program Site-865, Allison-Guyot. Paleoceanography 10, 841-865.

Brassell, S.C., Eglinton, G., Marlowe, I.T., Pflaumann, U., Sarnthein, M., 1986. Molecular stratigraphy - A new tool for climatic assessment. Nature 320, 129-133.

Brauer, S.L., Yashiro, E., Ueno, N.G., Yavitt, J.B., Zinder, S.H., 2006. Characterization of acid-tolerant H-2/CO_2-utilizing methanogenic enrichment cultures from an acidic peat bog in New York State. FEMS Microbiology Ecology 57, 206-216.

Broecker, W.S., Kennett, J.P., Flower, B.P., Teller, J.T., Trumbore, S., Bonani, G., Wolfli, W., 1989. Routing of meltwater from the Laurentide ice-sheet during the Younger Dryas cold episode. Nature 341, 318-321.

Brofft, J.E., McArthur, J.V., Shimkets, L.J., 2002. Recovery of novel bacterial diversity from a forested wetland impacted by reject coal. Environmental Microbiology 4, 764-769.

Buckley, D.H., Graber, J.R., Schmidt, T.M., 1998. Phylogenetic analysis of nonthermophilic members of the kingdom Crenarchaeota and their diversity and abundance in soils. Applied and Environmental Microbiology 64, 4333-4339.

Bujak, J.P., Brinkhuis, H., 1998. Global warming and dinocyst changes across the Paleocene/Eocene Epoch boundary. In: Aubry, M.-P., Lucas, S.G., Berggren, W.A. (Eds.), Late Paleocene-early Eocene climatic and biotic events in the marine and terrestrial records. Columbia University Press, New York, pp. 277-295.

Burdige, D.J., 2005. Burial of terrestrial organic matter in marine sediments: A re-assessment. Global Biogeochemical Cycles 19, doi:10.1029/2004GB002368.

Camberlin, P., Janicot, S., Poccard, I., 2001. Seasonality and atmospheric dynamics of the teleconnection between African rainfall and tropical sea-surface temperature: Atlantic vs. ENSO. International Journal of Climatology 21, 973-1005.

Carballeira, N.M., Reyes, M., Sostre, A., Huang, H., Verhagen, M.F.J.M., Adams, M.W.W., 1997. Unusual fatty acid composition of the hyperthermophilic archaeon *Pyrococcus furiosus* and the bacterium *Thermotoga maritima*. Journal of Bacteriology 179, 2766-2768.

Chalie, F., 1995. Paleoclimates of the southern Tanganyika Basin over the last 25-thousand years - Quantitative reconstruction from the statistical treatment of pollen data. Comptes Rendus de l Academie des Sciences Serie II 320, 205-210.

Chan, O.C., Yang, X.D., Fu, Y., Feng, Z.L., Sha, L.Q., Casper, P., Zou, X.M., 2006. 16S rRNA gene analyses of bacterial community structures in the soils of evergreen broad-leaved forests in south-west China. FEMS Microbiology Ecology 58, 247-259.

Chanal, A., Chapon, V., Benzerara, K., Barakat, M., Christen, R., Achouak, W., Barras, F., Heulin, T., 2006. The desert of Tataouine: an extreme environment that hosts a wide diversity of microorganisms and radiotolerant bacteria. Environmental Microbiology 8, 514-525.

Chikaraishi, Y., Naraoka, H., Poulson, S.R., 2004. Hydrogen and carbon isotopic fractionations of lipid biosynthesis among terrestrial (C3, C4 and CAM) and aquatic plants. Phytochemistry 65, 1369-1381.

Chin, K.-J., Lukow, T., Conrad, R., 1999. Effect of temperature on structure and function of the methanogenic archaeal community in an anoxic rice field soil. Applied and Environmental Microbiology 65, 2341-2349.

Coates, J.D., Ellis, D.J., Gaw, C.V., Lovley, D.R., 1999. Geothrix fermentans gen. nov., sp nov., a novel Fe(III)-reducing bacterium from a hydrocarbon-contaminated aquifer. International Journal of Systematic Bacteriology 49, 1615-1622.

Combourieu Nebout, N., Turon, J.L., Zahn, R., Capotondi, L., Londeix, L., Pahnke, K., 2002. Enhanced aridity and atmospheric high-pressure stability over the western Mediterranean during the North Atlantic cold events of the past 50 k.y. Geology 30, 863-866.

Cowie, G.L., Hedges, J.I., Calvert, S.E., 1992. Sources and relative reactivities of amino-acids, neutral sugars, and lignin in an intermittently anoxic marine-environment. Geochimica et Cosmochimica Acta 56, 1963-1978.

Coynel, A., Seyler, P., Etcheber, H., Meybeck, M., Orange, D., 2005. Spatial and seasonal dynamics of total suspended sediment and organic carbon species in the Congo River. Global Biogeochemical Cycles 19, doi:10.1029/2004GB002335.

Crouch, E.M., Heilmann-Clausen, C., Brinkhuis, H., Morgans, H.E.G., Rogers, K.M., Egger, H., Schmitz, B., 2001. Global dinoflagellate event associated with the late Paleocene thermal maximum. Geology 29, 315-318.

Dale, J.A., Mosher, H.S., 1973. Nuclear magnetic-resonance enantiomer reagents - configurational correlations via nuclear magnetic-resonance chemical-shifts of diastereomeric mandelate, O-methylmandelate, and alpha-methoxy-alpha-trifluoromethylphenylacetate (Mtpa) esters. Journal of the American Chemical Society 95, 512-519.

de Leeuw, J.W., van de Meer, F.W., Rijpstra, W.I.C., Schenck, P.A., 1980. On the occurrence and structural identification of long chain unsaturated ketones and hydrocarbons in sediments. In: Douglas, A.G., Maxwell , J.R. (Eds.), Advances in Organic Geochemistry 1979. Pergamon Press, Oxford, pp. 211-217.

de Leeuw, J.W., Largeau, C., 1993. A review of macromolecular organic compounds that comprise living organisms and their role in kerogen, coal and petroleum formation. In: Engel, M.H., Macko, S.A. (Eds.), Organic Geochemistry. Plenum Press, pp. 23-72.

de Leeuw, J.W., Frewin, N.L., van Bergen, P.F., Sinninghe Damsté, J.S., Collinson, M.E., 1995. Organic carbon as a palaeoenvironmental indicator in the marine realm. In: Bosence, D.W.J., Allison, P.A. (Eds.), Marine Palaeoenvironmental Analysis from Fossils. Geological Society, London, pp. 43-71.

de Leeuw, J.W., Versteegh, G.J.M., van Bergen, P.F., 2006. Biomacromolecules of algae and plants and their fossil analogues. Plant Ecology 182, 209-233.

de Rosa, M., de Rosa, S., Gambacorta, A., 1977. ^{13}C-NMR assignments and biosynthetic data for the ether lipids of *Caldariella*. Phytochemistry 16, 1909-1912.

de Rosa, M., Gambacorta, A., Huber, R., Lanzotti, V., Nicolaus, B., Stetter, K.O., Trincone, A., 1988. A new 15,16-dimethyl-30-glyceryloxytriacontanoic acid from lipids of *Thermotoga maritima*. Chemical Communications, 1300-1301.

References

de Ruijter, W.M.P., Postma, L., de Kok, J.M., 1987. Transport Atlas of the Southern North Sea. Rijkswaterstaat, 's Gravenhage.

Dedysh, S.N., Pankratov, T.A., Belova, S.E., Kulichevskaya, I.S., Liesack, W., 2006. Phylogenetic analysis and in situ identification of Bacteria community composition in an acidic Sphagnum peat bog. Applied and Environmental Microbiology 72, 2110-2117.

Deines, P., 1980. The isotopic composition of reduced organic carbon. In: Fritz, P., Fontes, J.Ch. (Eds.), Handbook of environmental isotope geochemistry. Elsevier Scientific Publishing Company, Amsterdam, pp. 329-406.

Delègue, M.A., Fuhr, M., Schwartz, D., Mariotti, A., Nasi, R., 2001. Recent origin of a large part of the forest cover in the Gabon coastal area based on stable carbon isotope data. Oecologia 129, 106-113.

DeLong, E.F., 1992. Archaea in coastal marine environments. Proceedings of the National Academy of Sciences of the United States of America 89, 5685-5689.

DeLong, E.F., 1998. Everything in moderation: Archaea as 'non-extremophiles'. Current Opinion in Genetics & Development 8, 649-654.

DeLong, E.F., Wu, K.Y., Prézelin, B.B., Jovine, R.V.M., 1994. High abundance of Archaea in Antarctic marine picoplankton. Nature 371, 695-697.

DeLong, E.F., King, L.L., Massana, R., Cittone, H., Murray, A., Schleper, C., Wakeham, S.G., 1998. Dibiphytanyl ether lipids in nonthermophilic Crenarchaeotes. Applied and Environmental Microbiology 64, 1133-1138.

Denton, G.H., Hughes, T.J., 1981. The last great ice sheets. Wiley, New York.

Driessen, A.J.M., van de Vossenberg, J.L.C.M., Konings, W.N., 1996. Membrane composition and ion-permeability in extremophiles. FEMS Microbiology Reviews 18, 139-148.

Dunbar, J., Ticknor, L.O., Kuske, C.R., 2000. Assessment of microbial diversity in four southwestern United States soils by 16S rRNA gene terminal restriction fragment analysis. Applied and Environmental Microbiology 66, 2943-2950.

Eglinton, G., Gonzalez, A.G., Hamilton, R.J., Raphael, R.A., 1962. Hydrocarbon constituents of the wax coatings of plant leaves - a taxonomic survey. Phytochemistry 1, 89-102.

Eglinton, G., Hamilton, R.J., 1963. The distribution of alkanes. In: Swain, T. (Ed.), Chemical plant taxonomy. Academic Press, London, pp. 187-208.

Eguchi, T., Nishimura, Y., Kakinuma, K., 2003. Importance of the isopropylidene terminal of geranylgeranyl group for the formation of tetraether lipid in methanogenic archaea. Tetrahedron Letters 44, 3275-3279.

Eisma, D., Kalf, J., van der Gaast, S.J., 1978. Suspended matter in the Zaire estuary and the adjacent Atlantic Ocean. Netherlands Journal of Sea Research 12, 382-406.

Elferink, M.G.L., Dewit, J.G., Driessen, A.J.M., Konings, W.N., 1994. Stability and proton-permeability of liposomes composed of archaeal tetraether lipids. Biochimica et Biophysica Acta-Biomembranes 1193, 247-254.

Farley, K.A., Eltgroth, S.F., 2003. An alternative age model for the Paleocene-Eocene thermal maximum using extraterrestrial He-3. Earth and Planetary Science Letters 208, 135-148.

Farrera, I., Harrison, S.P., Prentice, I.C., Ramstein, G., Guiot, J., Bartlein, P.J., Bonnefille, R., Bush, M., Cramer, W., Von Grafenstein, U., Holmgren, K., Hooghiemstra, H., Hope, G., Jolly, D., Lauritzen, S.E., Ono, Y., Pinot, S., Stute, M., Yu, G., 1999. Tropical climates at the Last Glacial Maximum: a new synthesis of terrestrial palaeoclimate data. I. Vegetation, lake levels and geochemistry. Climate Dynamics 15, 823-856.

Farrington, J.W., Davis, A.C., Sulanowski, J., McCaffrey, M.A., McCarthy, M., Clifford, C.H., Dickinson, P., Volkman, J.K., 1988. Biogeochemistry of lipids in surface sediments of the Peru upwelling area at 15-Degrees-S. Organic Geochemistry 13, 607-617.

Felske, A., Wolterink, A., Van Lis, R., Akkermans, A.D.L., 1998. Phylogeny of the main bacterial 16S rRNA sequences in Drentse A grassland soils (The Netherlands). Applied and Environmental Microbiology 64, 871-879.

Forster, A., Schouten, S., Moriya, K., Wilson, P.A., Sinninghe Damsté, J.S., 2007. Tropical warming and intermittent cooling during the Cenomanian/Turonian Oceanic Anoxic Event (OAE 2): Sea surface temperature records from the equatorial Atlantic. Paleoceanography 22, doi:10.1029/2006PA001349.

Francis, J.E., Poole, I., 2002. Cretaceous and early Tertiary climates of Antarctica: evidence from fossil wood. Palaeogeography, Palaeoclimatology, Palaeoecology 182, 47-64.

Fricke, H.C., Wing, S.L., 2004. Oxygen isotope and paleobotanical estimates of temperature and δ^{18}O-latitude gradients over North America during the early Eocene. American Journal of Science 304, 612-635.

Fry, B., Sherr, E.B., 1984. Delta-C-13 measurements as indicators of carbon flow in marine and fresh-water ecosystems. Contributions in Marine Science 27, 13-47.

Fuhrman, J.A., McCallum, K., Davis, A.A., 1992. Novel major archaebacterial group from marine plankton. Nature 356, 148-149.

Gagosian, R.B., Peltzer, E.T., Zafiriou, O.C., 1981. Atmospheric transport of continentally derived lipids to the tropical north Pacific. Nature 291, 312-315.

Galand, P.E., Saarnio, S., Fritze, H., Yrjälä, K., 2002. Depth related diversity of methanogen Archaea in Finnish oligotrophic fen. FEMS Microbiology Ecology 42, 441-449.

Ganopolski, A., Rahmstorf, S., 2001. Rapid changes of glacial climate simulated in a coupled climate model. Nature 409, 153-158.

Gasse, F., 2000. Hydrological changes in the African tropics since the Last Glacial Maximum. Quaternary Science Reviews 19, 189-211.

Gattinger, A., Günthner, A., Schloter, M., Munch, J.C., 2003. Characterisation of *Archaea* in soils by polar lipid analysis. Acta Biotechnol. 23, 21-28.

Gliozzi, A., Paoli, G., DeRosa, M., Gambacorta, A., 1983. Effect of isoprenoid cyclization on the transition-temperature of lipids in thermophilic archaebacteria. Biochimica et Biophysica Acta 735, 234-242.

Goñi, M.A., Ruttenberg, K.C., Eglinton, T.I., 1997. Source and contribution of terrigenous organic carbon to surface sediments in the Gulf of Mexico. Nature 389, 275-278.

Goñi, M.A., Monacci, N., Gisewhite, R., Ogston, A., Crockett, J., Nittrouer, C., 2006. Distribution and sources of particulate organic matter in the water column and sediments of the Fly River Delta, Gulf of Papua (Papua New Guinea). Estuarine Coastal and Shelf Science 69, 225-245.

Gordon, E.S., Goñi, M.A., 2003. Sources and distribution of terrigenous organic matter delivered by the Atchafalaya River to sediments in the northern Gulf of Mexico. Geochimica et Cosmochimica Acta 67, 2359-2375.

Großkopf, R., Stubner, S., Liesack, W., 1998. Novel euryarchaeotal lineages detected on rice roots and in the anoxic bulk soil of flooded rice microcosms. Applied and Environmental Microbiology 64, 4983-4989.

Grousset, F.E., Pujol, C., Labeyrie, L., Auffret, G., Boelaert, A., 2000. Were the North Atlantic Heinrich events triggered by the behavior of the European ice sheets? Geology 28, 123-126.

Hackl, E., Zechmeister-Boltenstern, S., Bodrossy, L., Sessitsch, A., 2004. Comparison of diversities and compositions of bacterial populations inhabiting natural forest soils. Applied and Environmental Microbiology 70, 5057-5065.

Heaton, T.H.E., Talma, A.S., Vogel, J.C., 1986. Dissolved-gas paleotemperatures and O-18 variations derived from groundwater near Uitenhage, South-Africa. Quaternary Research 25, 79-88.

Hedges, J.I., Clark, W.A., Quay, P.D., Richey, J.E., Devol, A.H., Santos, U.D., 1986a. Compositions and fluxes of particulate organic material in the Amazon River. Limnology and Oceanography 31, 717-738.

Hedges, J.I., Ertel, J.R., Quay, P.D., Grootes, P.M., Richey, J.E., Devol, A.H., Farwell, G.W., Schmidt, F.W., Salati, E., 1986b. Organic C-14 in the Amazon River system. Science 231, 1129-1131.

Hedges, J.I., Keil, R.G., 1995. Sedimentary organic-matter preservation - an assessment and speculative synthesis. Marine Chemistry 49, 81-115.

Hedges, J.I., Oades, J.M., 1997. Comparative organic geochemistries of soils and marine sediments. Organic Geochemistry 27, 319-361.

Hedges, J.I., Keil, R.G., Benner, R., 1997. What happens to terrestrial organic matter in the ocean? Organic Geochemistry 27, 195-212.

Herfort, L., Schouten, S., Boon, J.P., Woltering, M., Baas, M., Weijers, J.W.H., Sinninghe Damsté, J.S., 2006. Characterization of transport and deposition of terrestrial organic matter in the southern North Sea using the BIT index. Limnology and Oceanography 51, 2196-2205.

References

Hiraishi, A., Kishimoto, N., Kosako, Y., Wakao, N., Tano, T., 1995. Phylogenetic position of the menaquinone-containing acidophilic chemo-organotroph *Acidobacterium capsulatum*. FEMS Microbiology Letters 132, 91-94.

Hoefs, M.J.L., Schouten, S., de Leeuw, J.W., King, L.L., Wakeham, S.G., Sinninghe Damsté, J.S., 1997. Ether lipids of planktonic archaea in the marine water column. Applied and Environmental Microbiology 63, 3090-3095.

Hoefs, M.J.L., Rijpstra, W.I.C., Sinninghe Damsté, J.S., 2002. The influence of oxic degradation on the sedimentary biomarker record I: Evidence from Madeira Abyssal Plain turbidites. Geochimica et Cosmochimica Acta 66, 2719-2735.

Høj, L., Olsen, R.A., Torsvik, V.L., 2005. Archaeal communities in High Arctic wetlands at Spitsbergen, Norway (78 degrees N) as characterized by 16S rRNA gene fingerprinting. FEMS Microbiology Ecology 53, 89-101.

Holmgren, K., Lee-Thorp, J.A., Cooper, G.R.J., Lundblad, K., Partridge, T.C., Scott, L., Sithaldeen, R., Talma, A.S., Tyson, P.D., 2003. Persistent millennial-scale climatic variability over the past 25,000 years in Southern Africa. Quaternary Science Reviews 22, 2311-2326.

Holtvoeth, J., Kolonic, S., Wagner, T., 2005. Soil organic matter as an important contributor to late Quaternary sediments of the tropical West African continental margin. Geochimica et Cosmochimica Acta 69, 2031-2041.

Hopmans, E.C., Schouten, S., Pancost, R.D., van der Meer, M.T.J., Sinninghe Damsté, J.S., 2000. Analysis of intact tetraether lipids in archaeal cell material and sediments by high performance liquid chromatography/atmospheric pressure chemical ionization mass spectrometry. Rapid Communications in Mass Spectrometry 14, 585-589.

Hopmans, E.C., Weijers, J.W.H., Schefuß, E., Herfort, L., Sinninghe Damsté, J.S., Schouten, S., 2004. A novel proxy for terrestrial organic matter in sediments based on branched and isoprenoid tetraether lipids. Earth and Planetary Science Letters 224, 107-116.

Horn, M.A., Matthies, C., Kusel, K., Schramm, A., Drake, H.L., 2003. Hydrogenotrophic methanogenesis by moderately acid-tolerant methanogens of a methane-emitting acidic peat. Applied and Environmental Microbiology 69, 74-83.

Huang, W.Y., Meinschein, W.G., 1976. Sterols as source indicators of organic materials in sediments. Geochimica et Cosmochimica Acta 40, 323-330.

Huber, B.T., Hodell, D.A., Hamilton, C.P., 1995. Middle-Late Cretaceous climate of the Southern high-latitudes - Stable isotopic evidence for minimal equator-to-pole thermal-gradients. Geological Society of America Bulletin 107, 1164-1191.

Huber, M., Sloan, L.C., 1999. Warm climate transitions: A general circulation modeling study of the Late Paleocene thermal maximum (about 56 Ma). Journal of Geophysical Research-Atmospheres 104, 16633-16655.

Huber, M., Sloan, L.C., 2001. Heat transport, deep waters, and thermal gradients: Coupled simulation of an Eocene greenhouse climate. Geophysical Research Letters 28, 3481-3484.

Huber, R., Wilharm, T., Huber, D., Trincone, A., Burggraf, S., König, H., Rachel, R., Rockinger, I., Fricke, H., Stetter, K.O., 1992. *Aquifex pyrophilus* gen. nov. sp. nov., represents a novel group of marine hyperthermophilic hydrogen-oxidizing bacteria. Systematic and Applied Microbiology 15, 340-351.

Huber, R., Rossnagel, P., Woese, C.R., Rachel, R., Langworthy, T.A., Stetter, K.O., 1996. Formation of ammonium from nitrate during chemolithoautotrophic growth of the extremely thermophilic bacterium *Ammonifex degensii* gen.nov.sp.nov. Systematic and Applied Microbiology 19, 40-49.

Hugenholtz, P., Goebel, B.M., Pace, N.R., 1998. Impact of culture-independent studies on the emerging phylogenetic view of bacterial diversity. Journal of Bacteriology 180, 4765-4774.

Hughen, K.A., Baillie, M.G.L., Bard, E., Beck, J.W., Bertrand, C.J.H., Blackwell, P.G., Buck, C.E., Burr, G.S., Cutler, K.B., Damon, P.E., Edwards, R.L., Fairbanks, R.G., Friedrich, M., Guilderson, T.P., Kromer, B., McCormac, G., Manning, S., Ramsey, C.B., Reimer, P.J., Reimer, R.W., Remmele, S., Southon, J.R., Stuiver, M., Talamo, S., Taylor, F.W., Van der Plicht, J., Weyhenmeyer, C.E., 2004. Marine04 marine radiocarbon age calibration, 0-26 cal kyr BP. Radiocarbon 46, 1059-1086.

Ivy-Ochs, S., Kerschner, H., Kubik, P.W., Schluchter, C., 2006. Glacier response in the European Alps to Heinrich Event 1 cooling: the Gschnitz stadial. Journal of Quaternary Science 21, 115-130.

Jahren, A.H., Lepage, B.A., Werts, S.P., 2004. Methanogenesis in Eocene Arctic soils inferred from delta C-13 of tree fossil carbonates. Palaeogeography, Palaeoclimatology, Palaeoecology 214, 347-358.

Jansen, J.H.F., de Lange, G.J., van Bennekom, A.J., 1990. (Pale)oceanography and geochemistry of the Angola Basin (South Atlantic Ocean); cruise report RV Tyro. Netherlands Institute for Sea Research Report, Texel.

Janssen, P.H., 2006. Identifying the dominant soil bacterial taxa in libraries of 16S rRNA and 16S rRNA genes. Applied and Environmental Microbiology 72, 1719-1728.

Jennerjahn, T.C., Ittekkot, V., Arz, H.W., Behling, H., Patzold, J., Wefer, G., 2004. Asynchronous terrestrial and marine signals of climate change during Heinrich events. Science 306, 2236-2239.

Johnsen, S.J., DahlJensen, D., Gundestrup, N., Steffensen, J.P., Clausen, H.B., Miller, H., Masson-Delmotte, V., Sveinbjornsdottir, A.E., White, J., 2001. Oxygen isotope and palaeotemperature records from six Greenland ice-core stations: Camp Century, Dye-3, GRIP, GISP2, Renland and NorthGRIP. Journal of Quaternary Science 16, 299-307.

Johnson, D.W., Hanson, P.J., Todd, D.E., Susfalk, R.B., Trettin, C.F., 1998. Precipitation change and soil leaching: Field results and simulations from Walker Branch Watershed, Tennessee. Water Air and Soil Pollution 105, 251-262.

Jokat, W., Uenzelmannneben, G., Kristoffersen, Y., Rasmussen, T.M., 1992. Lomonosov Ridge - A double-sided continental-margin. Geology 20, 887-890.

Jones, G.A., Keigwin, L.D., 1988. Evidence from Fram Strait (78-Degrees-N) for early deglaciation. Nature 336, 56-59.

Jung, S., Zeikus, J.G., Hollingsworth, R.I., 1994. A new family of very long chain α,ω-dicarboxylic acids is a major structural fatty acyl component of the membrane lipids of *Thermoanaerobacter ethanolicus* 39E. Journal of Lipid Research 35, 1057-1065.

Juottonen, H., Galand, P.E., Tuittila, E.S., Laine, J., Fritze, H., Yrjala, K., 2005. Methanogen communities and Bacteria along an ecohydrological gradient in a northern raised bog complex. Environmental Microbiology 7, 1547-1557.

Jurgens, G., Lindström, K., Saano, A., 1997. Novel group within the kingdom of *Crenarchaeota* from boreal forest soil. Applied and Environmental Microbiology 63, 803-805.

Jurgens, G., Glöckner, F.-O., Amann, R., Saano, A., Montonen, l., Likolammi, M., Münster, U., 2000. Identification of novel Archaea in bacterioplankton of a boreal forest lake by phylogenetic analysis and fluorescent in situ hybridization. FEMS Microbiology Ecology 34, 45-56.

Karner, M.B., DeLong, E.F., Karl, D.M., 2001. Archaeal dominance in the mesopelagic zone of the Pacific Ocean. Nature 409, 507-510.

Kates, M., 1978. The phytanyl ether-linked polar lipids and isoprenoid neutral lipids of extremely halophilic bacteria. Progress in the Chemistry of Fats and other Lipids 15, 301-342.

Kates, M., Kushner, D.J., Matheson, A.T., 1993. The biochemistry of Archaea (Archaebacteria). Elsevier Science Publishers, Amsterdam.

Kazadi, S.N., Kaoru, F., 1996. Interannual and long-term climate variability over the Zaire River Basin during the last 30 years. Journal of Geophysical Research-Atmospheres 101, 21351-21360.

Kelly, D.C., Bralower, T.J., Zachos, J.C., Silva, I.P., Thomas, E., 1996. Rapid diversification of planktonic foraminifera in the tropical Pacific (ODP Site 865) during the late Paleocene thermal maximum. Geology 24, 423-426.

Kemnitz, D., Chin, K.J., Bodelier, P., Conrad, R., 2004. Community analysis of methanogenic archaea within a riparian flooding gradient. Environmental Microbiology 6, 449-461.

Kennett, J.P., Stott, L.D., 1991. Abrupt deep-Sea warming, palaeoceanographic changes and benthic extinctions at the end of the Paleocene. Nature 353, 225-229.

Keough, B.P., Schmidt, T.M., Hicks, R.E., 2003. Archaeal nucleic acids in picoplankton from great lakes on three continents. Microbial Ecology 46, 238-248.

Keppler, F., Hamilton, J.T.G., Brass, M., Rockmann, T., 2006. Methane emissions from terrestrial plants under aerobic conditions. Nature 439, 187-191.

References

Killops, S.D., Frewin, N.L., 1994. Triterpenoid diagenesis and cuticular preservation. Organic Geochemistry 21, 1193-1209.

Kim, J.-H., Schouten, S., Buscail, R., Ludwig, W., Bonnin, J., Sinninghe Damsté, J.S., Bourrin, F., 2006. Origin and distribution of terrestrial organic matter in the NW Mediterranean (Gulf of Lion): application of the newly developed BIT index. Geochemistry Geophysics Geosystems 7, Q11017-doi:10.1029/2006GC001306.

King, L.L., Pease, T.K., Wakeham, S.G., 1998. Archaea in Black Sea water column particulate matter and sediments -- evidence from ether lipids derivatives. Organic Geochemistry 28, 677-688.

Kishimoto, N., Kosako, Y., Tano, T., 1991. *Acidobacterium-capsulatum* gen-nov, sp-nov - an acidophilic chemoorganotrophic bacterium containing menaquinone from acidic mineral environment. Current Microbiology 22, 1-7.

Kito, M., Pizer, L.I., 1969. Purification and regulatory properties of biosynthetic L-glycerol 3-phosphate dehydrogenase from *Escherichia coli*. Journal of Biological Chemistry 244, 3316-3323.

KNMI, 1997. Royal Netherlands Meteorological Institute (KNMI), World Climate Information (WKI 2.0), available online at: http://www.knmi.nl/klimatologie/normalen1971-2000/wki.html.

Koch, P.L., Zachos, J.C., Gingerich, P.D., 1992. Correlation between isotope records in marine and continental carbon reservoirs near the Paleocene Eocene boundary. Nature 358, 319-322.

Koga, Y., Nishihara, M., Morii, H., Akagawa-Matsushita, M., 1993. Ether polar lipids of methanogenic bacteria: structures, comparative aspects, and biosyntheses. Microbiological Reviews 57, 164-182.

Koga, Y., Kyuragi, T., Nishihara, M., Sone, N., 1998a. Did archaeal and bacterial cells arise independently from noncellular precursors? A hypothesis stating that the advent of membrane phospholipid with enantiomeric glycerophosphate backbones caused the separation of the two lines of descent. Journal of Moleculair Evolution 46, 54-63.

Koga, Y., Morii, H., kagawa-Matsushita, M., Ohga, I., 1998b. Correlation of polar lipid composition with 16S rRNA phylogeny in methanogens. Further analysis of lipid component parts. Bioscience Biotechnology and Biochemistry 62, 230-236.

Könneke, M., Bernhard, A.E., de la Torre, J.R., Walker, C.B., Waterbury, J.B., Stahl, D.A., 2005. Isolation of an autotrophic ammonia-oxidizing marine archaeon. Nature 437, 543-546.

Koopmans, M.P., Koster, J., van Kaam-Peters, H.M.E., Kenig, F., Schouten, S., Hartgers, W.A., de Leeuw, J.W., Sinninghe Damsté, J.S., 1996. Diagenetic and catagenetic products of isorenieratene: Molecular indicators for photic zone anoxia. Geochimica et Cosmochimica Acta 60, 4467-4496.

Kotsyurbenko, O.R., Chin, K.J., Glagolev, M.V., Stubner, S., Simankova, M.V., Nozhevnikova, A.N., Conrad, R., 2004. Acetoclastic and hydrogenotrophic methane production and methanogenic populations in an acidic West-Siberian peat bog. Environmental Microbiology 6, 1159-1173.

Kowalski, E.A., Dilcher, D.L., 2003. Warmer paleotemperatures for terrestrial ecosystems. Proceedings of the National Academy of Sciences of the United States of America 100, 167-170.

Kraigher, B., Stres, B., Hacin, J., Ausec, L., Mahne, I., van Elsas, J.D., Mandic-Mulec, I., 2006. Microbial activity and community structure in two drained fen soils in the Ljubljana Marsh. Soil Biology & Biochemistry 38, 2762-2771.

Kuhner, C.H., Matthies, C., Acker, G., Schmittroth, M., Gossner, A.S., Drake, H.L., 2000. *Clostridium akagii* sp nov and *Clostridium acidisoli* sp nov.: acid-tolerant, N-2-fixing clostridia isolated from acidic forest soil and litter. International Journal of Systematic and Evolutionary Microbiology 50, 873-881.

Kulongoski, J.T., Hilton, D.R., Selaolo, E.T., 2004. Climate variability in the Botswana Kalahari from the late Pleistocene to the present day. Geophysical Research Letters 31, L10204-doi:10.1029/2003GL019238.

Kuske, C.R., Barns, S.M., Busch, J.D., 1997. Diverse uncultivated bacterial groups from soils of the arid southwestern United States that are present in many geographic regions. Applied and Environmental Microbiology 63, 3614-3621.

Kuypers, M.M.M., Pancost, R.D., Sinninghe Damsté, J.S., 1999. A large and abrupt fall in atmospheric CO_2 concentration during Cretaceous times. Nature 399, 342-345.

Kuypers, M.M.M., Blokker, P., Erbacher, J., Kinkel, H., Pancost, R.D., Schouten, S., Sinninghe Damsté, J.S., 2001. Massive expansion of marine archaea during a mid-Cretaceous oceanic anoxic event. Science 293, 92-94.

Lambeck, K., 1997. Sea-level change along the French Atlantic and channel coasts since the time of the last glacial maximum. Palaeogeography Palaeoclimatology Palaeoecology 129, 1-22.

Lambeck, K., Yokoyama, Y., Purcell, T., 2002. Into and out of the Last Glacial Maximum: sea-level change during Oxygen Isotope Stages 3 and 2. Quaternary Science Reviews 21, 343-360.

Langworthy, T.A., 1977. Long-chain diglycerol tetraethers from *Thermoplasma acidophilum*. Biochimica et Biophysica Acta 487, 37-50.

Langworthy, T.A., Holzer, G., Zeikus, J.G., Tornabene, T.G., 1983. Iso- and anteiso- branched glycerol diethers of the thermophilic anaerobe *Thermodesulfotobacterium commune*. Systematic and Applied Microbiology 4, 1-17.

Laraque, A., Mahe, G., Orange, D., Marieu, B., 2001. Spatiotemporal variations in hydrological regimes within Central Africa during the XXth century. Journal of Hydrology 245, 104-117.

Laws, E.A., Popp, B.N., Bidigare, R.R., Kennicutt, M.C., Macko, S.A., 1995. Dependence of phytoplankton carbon isotopic composition on growth-rate and $[CO_2](aq)$ - Theoretical considerations and experimental results. Geochimica et Cosmochimica Acta 59, 1131-1138.

Lee, S., Kang, S., Kim, J.N., Jung, S., 2002. Structural analyses of the novel phosphoglycolipids containing the unusual very long bifunctional acyl chain, α,ω-13,16-dimethyloctacosanedioate in *Thermoanaerobacter ethanolicus*. Bull. Korean Chem. Soc. 23, 1778-1784.

Leng, M.J., Marshall, J.D., 2004. Palaeoclimate interpretation of stable isotope data from lake sediment archives. Quaternary Science Reviews 23, 811-831.

Liaaen-Jensen, S., 1978. Marine carotenoids. In: Faulkner, D.J., Fenical, W.H. (Eds.), Marine natural products. Academic Press, New York, pp. 1-73.

Liesack, W., Bak, F., Kreft, J.U., Stackebrandt, E., 1994. *Holophaga foetida* gen-nov, sp-nov, a new, homoacetogenic bacterium degrading methoxylated aromatic compounds. Archives of Microbiology 162, 85-90.

Lonergan, D.J., Jenter, H.L., Coates, J.D., Phillips, E.J.P., Schmidt, T.M., Lovley, D.R., 1996. Phylogenetic analysis of dissimilatory Fe(III)-reducing bacteria. Journal of Bacteriology 178, 2402-2408.

Ludwig, W., Strunk, O., Westram, R., Richter, L., Meier, H., Yadhukumar, Buchner, A., Lai, T., Steppi, S., Jobb, G., Forster, W., Brettske, I., Gerber, S., Ginhart, A.W., Gross, O., Grumann, S., Hermann, S., Jost, R., Konig, A., Liss, T., Lussmann, R., May, M., Nonhoff, B., Reichel, B., Strehlow, R., Stamatakis, A., Stuckmann, N., Vilbig, A., Lenke, M., Ludwig, T., Bode, A., Schleifer, K.H., 2004. ARB: a software environment for sequence data. Nucleic Acids Research 32, 1363-1371.

Macalady, J.L., Vestling, M.M., Baumler, D., Boekelheide, N., Kaspar, C.W., Banfield, J.F., 2004. Tetraether-linked membrane monolayers in *Ferroplasma* spp: a key to survival in acid. Extremophiles 8, 411-419.

MacGregor, B.J., Moser, D.P., Wheeler-Alm, E., Nealson, K.H., Stahl, D.A., 1997. Crenarchaeota in Lake Michigan sediment. Applied and Environmental Microbiology 63, 1178-1181.

Manabe, S., Stouffer, R.J., 1997. Coupled ocean-atmosphere model response to freshwater input: Comparison to Younger Dryas event. Paleoceanography 12, 321-336.

Mangerud, J., Jakobsson, M., Alexanderson, H., Astakhov, V., Clarke, G.K.C., Henriksen, M., Hjort, C., Krinner, G., Lunkka, J.P., Moller, P., Murray, A., Nikolskaya, O., Saarnisto, M., Svendsen, J.I., 2004. Ice-dammed lakes and rerouting of the drainage of northern Eurasia during the Last Glaciation. Quaternary Science Reviews 23, 1313-1332.

Mariotti, A., Gadel, F., Giresse, P., Mouzeo, K., 1991. Carbon isotope composition and geochemistry of particulate organic-matter in the Congo River (Central-Africa) - Application to the study of Quaternary sediments off the mouth of the river. Chemical Geology 86, 345-357.

Marks, L., 2002. Last Glacial Maximum in Poland. Quaternary Science Reviews 21, 103-110.

Markwick, P.J., 1998. Fossil crocodilians as indicators of Late Cretaceous and Cenozoic climates: implications for using palaeontological data in reconstructing palaeoclimate. Palaeogeography, Palaeoclimatology, Palaeoecology 137, 205-271.

Marret, F., Scourse, J.D., Versteegh, G., Jansen, J.H.F., Schneider, R., 2001. Integrated marine and terrestrial evidence for abrupt Congo River palaeodischarge fluctuations during the last deglaciation. Journal of Quaternary Science 16, 761-766.

References

Mayorga, E., Aufdenkampe, A.K., Masiello, C.A., Krusche, A.V., Hedges, J.I., Quay, P.D., Richey, J.E., Brown, T.A., 2005. Young organic matter as a source of carbon dioxide outgassing from Amazonian rivers. Nature 436, 538-541.

McCabe, A.M., Clark, P.U., 1998. Ice-sheet variability around the north Atlantic Ocean during the last deglaciation. Nature 392, 373-377.

McCaffrey, M.A., Farrington, J.W., Repeta, D.J., 1991. The organic geochemistry of Peru Margin surface sediments II. Paleoenvironmental implications of hydrocarbon and alcohol profiles. Geochimica et Cosmochimica Acta 55, 483-498.

McDermott, F., 2004. Palaeo-climate reconstruction from stable isotope variations in speleothems: a review. Quaternary Science Reviews 23, 901-918.

McDonald, I.R., Upton, M., Hall, G., Pickup, R.W., Edwards, C., Saunders, J.R., Ritchie, D.A., Murrell, J.C., 1999. Molecular ecological analysis of methanogens and methanotrophs in blanket bog peat. Microbial Ecology 38, 225-233.

McKee, B.A., Aller, R.C., Allison, M.A., Bianchi, T.S., Kineke, G.C., 2004. Transport and transformation of dissolved and particulate materials on continental margins influenced by major rivers: benthic boundary layer and seabed processes. Continental Shelf Research 24, 899-926.

McQuoid, M.R., Whiticar, M.J., Calvert, S.E., Pedersen, T.F., 2001. A post-glacial isotope record of primary production and accumulation in the organic sediments of Saanich Inlet, ODP Leg 169S. Marine Geology 174, 273-286.

Ménot, G., Bard, E., Rostek, F., Weijers, J.W.H., Hopmans, E.C., Schouten, S., Sinninghe Damsté, J.S., 2006. Early reactivation of European rivers during the last deglaciation. Science 313, 1623-1625.

Meyers, P.A., 2003. Applications of organic geochemistry to paleolimnological reconstructions: a summary of examples from the Laurentian Great Lakes. Organic Geochemistry 34, 261-289.

Middelburg, J.J., Baas, M., Ten Haven, H.L., de Leeuw, J.W., 1993. Organic geochemical characteristics of sediments from Kau Bay. In: Øygard, K. (Ed.), Organic Geochemistry. Falch Hurtigtrykk, Oslo, pp. 413-417.

Mitchell, P., 1966. Chemiosmotic coupling in oxidative and photosynthetic phosphorylation. Biological Reviews of the Cambridge Philosophical Society 41, 445-&.

Monnin, E., Indermuhle, A., Dallenbach, A., Fluckiger, J., Stauffer, B., Stocker, T.F., Raynaud, D., Barnola, J.M., 2001. Atmospheric CO_2 concentrations over the last glacial termination. Science 291, 112-114.

Morales, S.E., Mouser, P.J., Ward, N., Hudman, S.P., Gotelli, N.J., Ross, D.S., Lewis, T.A., 2006. Comparison of bacterial communities in New England Sphagnum bogs using terminal restriction fragment length polymorphism (T-RFLP). Microbial Ecology 52, 34-44.

Morrison, D.F., 1976. Multivariate statistical methods. McGraw-Hill, New York.

Müller, P.J., Kirst, G., Ruhland, G., von Storch, I., Rosell-Melé, A., 1998. Calibration of the alkenone paleotemperature index U^k_{37} based on core-tops from the eastern South Atlantic and the global ocean (60^oN-60^oS). Geochimica et Cosmochimica Acta 62, 1757-1772.

Muyzer, G., de Waal, E.C., Uitterlinden, A.G., 1993. Profiling of complex microbial populations by denaturing gradient gel electrophoresis analysis of polymerase chain reaction-amplified genes coding for 16S ribosomal RNA. Applied and Environmental Microbiology 59, 695-700.

Nagle, J.F., Morowitz, H.J., 1978. Molecular mechanisms for proton transport in membranes. Proceedings of the National Academy of Sciences of the United States of America 75, 298-302.

Nelson, K.E., Clayton, R.A., Gill, S.R., Gwinn, M.L., Dodson, R.J., Haft, D.H., Hickey, E.K., Peterson, L.D., Nelson, W.C., Ketchum, K.A., McDonald, L., Utterback, T.R., Malek, J.A., Linher, K.D., Garrett, M.M., Stewart, A.M., Cotton, M.D., Pratt, M.S., Phillips, C.A., Richardson, D., Heidelberg, J., Sutton, G.G., Fleischmann, R.D., Eisen, J.A., White, O., Salzberg, S.L., Smith, H.O., Venter, J.C., Fraser, C.M., 1999. Evidence for lateral gene transfer between Archaea and Bacteria from genome sequence of *Thermotoga maritima*. Nature 399, 323-329.

Nemoto, N., Shida, Y., Shimada, H., Oshima, T., Yamagishi, A., 2003. Characterization of the precursor of tetraether lipid biosynthesis in the thermoacidophilic archaeon *Thermoplasma acidophilum*. Extremophiles 7, 235-243.

Nes, W.R., McKean, M.L., 1977. Biochemistry of steroids and other isopentenoids. University Park Press, Baltimore.

Nicol, G.W., Glover, L.A., Prosser, J.I., 2003a. Molecular analysis of methanogenic archaeal communities in managed and natural upland pasture soils. Global Change Biology 9, 1451-1457.

Nicol, G.W., Glover, L.A., Prosser, J.I., 2003b. The impact of grassland management on archaeal community structure in upland pasture rhizosphere soil. Environmental Microbiology 5, 152-162.

Nishihara, M., Koga, Y., 1995. Sn-glycerol-1-phosphate dehydrogenase in *Methanobacterium thermoautotrophicum* - key enzyme in biosynthesis of the enantiomeric glycerophosphate backbone of ether phospholipids of Archaebacteria. Journal of Biochemistry 117, 933-935.

Ochsenreiter, T., Selezi, D., Quaiser, A., Bonch-Osmolovskaya, L., Schleper, C., 2003. Diversity and abundance of Crenarchaeota in terrestrial habitats studied by 16S RNA surveys and real time PCR. Environmental Microbiology 5, 787-797.

Opsahl, S., Benner, R., 1997. Distribution and cycling of terrigenous dissolved organic matter in the ocean. Nature 386, 480-482.

Otto-Bliesner, B.L., Brady, E.C., Clauzet, G., Tomas, R., Levis, S., Kothavala, Z., 2006. Last Glacial Maximum and Holocene climate in CCSM3. Journal of Climate 19, 2526-2544.

Øvreås, L., Forney, L., Daae, F.L., Torsvik, V., 1997. Distribution of bacterioplankton in meromictic Lake Saelenvannet, as determined by denaturing gradient gel electrophoresis of PCR-amplified gene fragments coding for 16S rRNA. Applied and Environmental Microbiology 63, 3367-3373.

Pace, N.R., 1997. A molecular view of microbial diversity and the biosphere. Science 276, 734-740.

Pagani, M., Caldeira, K., Archer, D., Zachos, J.C., 2006a. An ancient carbon mystery. Science 314, 1556-1557.

Pagani, M., Pedentchouk, N., Huber, M., Sluijs, A., Schouten, S., Brinkhuis, H., Sinninghe Damsté, J.S., Dickens, G.R., 2006b. Arctic hydrology during global warming at the Palaeocene/Eocene thermal maximum. Nature 442, 671-675.

Pailler, D., Bard, E., 2002. High frequency palaeoceanographic changes during the past 140 000 yr recorded by the organic matter in sediments of the Iberian Margin. Palaeogeography Palaeoclimatology Palaeoecology 181, 431-452.

Pancost, R.D., van Geel, B., Baas, M., Sinninghe Damsté, J.S., 2000. $\delta^{13}C$ values and radiocarbon dates of microbial biomarkers as tracers for carbon recycling in peat deposits. Geology 28, 663-666.

Pancost, R.D., Bouloubassi, I., Aloisi, G., Sinninghe Damsté, J.S., the Medinaut Shipboard Scientific Party, 2001a. Three series of non-isoprenoidal dialkyl glycerol diethers in cold-seep carbonate crusts. Organic Geochemistry 32, 695-707.

Pancost, R.D., Hopmans, E.C., Sinninghe Damsté, J.S., the Medinaut Shipboard Scientific Party, 2001b. Archaeal lipids in Mediterranean cold seeps: Molecular proxies for anaerobic methane oxidation. Geochimica et Cosmochimica Acta 65, 1611-1627.

Pancost, R.D., Sinninghe Damsté, J.S., 2003. Carbon isotopic compositions of prokaryotic lipids as tracers of carbon cycling in diverse settings. Chemical Geology 195, 29-58.

Pancost, R.D., Baas, M., van Geel, B., Sinninghe Damsté, J.S., 2003. Response of an ombrotrophic bog to a regional climate event revealed by macrofossil, molecular and carbon isotopic data. The Holocene 13, 921-932.

Pankratov, T.A., Belova, S.E., Dedysh, S.N., 2005. Evaluation of the phylogenetic diversity of prokaryotic microorganisms in Sphagnum peat bogs by means of fluorescence in situ hybridization (FISH). Microbiology 74, 722-728.

Pauly, G.G., van Vleet, E.S., 1986. Acyclic archaebacterial ether lipids in swamp sediments. Geochimica et Cosmochimica Acta 50, 1117-1125.

Pearson, A., Huang, Z., Ingalls, A.E., Romanek, C.S., Wiegel, J., Freeman, K.H., Smittenberg, R.H., Zhang, C.L., 2004. Nonmarine crenarchaeol in Nevada hot springs. Applied and Environmental Microbiology 70, 5229-5237.

Pedros-Alio, C., 2007. Dipping into the rare biosphere. Science 315, 192-193.

Pesaro, M., Widmer, F., 2002. Identification of novel Crenarchaeota and Euryarchaeota clusters associated with different depth layers of a forest soil. FEMS Microbiology Ecology 42, 89-98.

References

Peters, R.B., Sloan, L.C., 2000. High concentrations of greenhouse gases and polar stratospheric clouds: A possible solution to high-latitude faunal migration at the latest Paleocene thermal maximum. Geology 28, 979-982.

Popp, B.N., Laws, E.A., Bidigare, R.R., Dore, J.E., Hanson, K.L., Wakeham, S.G., 1998. Effect of phytoplankton cell geometry on carbon isotopic fractionation. Geochimica et Cosmochimica Acta 62, 69-77.

Powers, J.S., Schlesinger, W.H., 2002. Geographic and vertical patterns of stable carbon isotopes in tropical rain forest soils of Costa Rica. Geoderma 109, 141-160.

Powers, L.A., Werne, J.P., Johnson, T.C., Hopmans, E.C., Sinninghe Damsté, J.S., Schouten, S., 2004. Crenarchaeotal membrane lipids in lake sediments: A new paleotemperature proxy for continental paleoclimate reconstruction? Geology 32, 613-616.

Powers, L.A., Johnson, T.C., Werne, J.P., Castañeda, I.S., Hopmans, E.C., Sinninghe Damsté, J.S., Schouten, S., 2005. Large temperature variability in the southern African tropics since the Last Glacial Maximum. Geophysical Research Letters 32, L08706-doi:10.1029/2004GL022014.

Poynter, J.G., Farrimond, P., Robinson, N., Eglinton, G., 1989. Aeolian-derived higher plant lipids in the marine sedimentary record: links with palaeoclimate. In: Leinen, M., Sarnthein, M. (Eds.), Paleoclimatology and paleometeorology : modern and past patterns of global atmospheric transport. Kluwer Academic Publishing, Dordrecht, pp. 435-463.

Prado, A., Dacosta, M.S., Madeira, V.M.C., 1988. Effect of Growth Temperature on the Lipid-Composition of 2 Strains of Thermus Sp. Journal of General Microbiology 134, 1653-1660.

Prahl, F.G., Wakeham, S.G., 1987. Calibration of unsaturation patterns in long-chain ketone compositions for palaeotemperature assessment. Nature 330, 367-369.

Prahl, F.G., Hayes, J.M., Xie, T.M., 1992. Diploptene - An indicator of terrigenous organic carbon in Washington coastal sediments. Limnology and Oceanography 37, 1290-1300.

Prahl, F.G., de Lange, G.J., Scholten, S., Cowie, G.L., 1997. A case of post-depositional aerobic degradation of terrestrial organic matter in turbidite deposits from the Madeira Abyssal Plain. Organic Geochemistry 27, 141-152.

Preston, M.P., Wu, K.Y., Molinski, T.F., DeLong, E.F., 1996. A psychrophilic crenarchaeon inhabits a marine sponge: *Cenarchaeum symbiosum* gen. nov., sp. nov. Proceedings of the National Academy of Sciences of the United States of America 93, 6241-6246.

Quaiser, A., Ochsenreiter, T., Lanz, C., Schuster, S.C., Treusch, A.H., Eck, J., Schleper, C., 2003. Acidobacteria form a coherent but highly diverse group within the bacterial domain: evidence from environmental genomics. Molecular Microbiology 50, 563-575.

Ramstein, G., Serafini-Le Treut, Y., Le Treut, H., Forichon, M., Joussaume, S., 1998. Cloud processes associated with past and future climate changes. Climate Dynamics 14, 233-247.

Raymond, P.A., Bauer, J.E., 2001. Riverine export of aged terrestrial organic matter to the North Atlantic Ocean. Nature 409, 497-500.

Reizer, J., Grossowicz, N., Barenholz, Y., 1985. The effect of growth temperature on the thermotropic behavior of the membranes of a thermophilic Bacillus - composition-structure-function relationships. Biochimica et Biophysica Acta 815, 268-280.

Renssen, H., Vandenberghe, J., 2003. Investigation of the relationship between permafrost distribution in NW Europe and extensive winter sea-ice cover in the North Atlantic Ocean during the cold phases of the Last Glaciation. Quaternary Science Reviews 22, 209-223.

Renssen, H., Beets, C.J., Fichefet, T., Goosse, H., Kroon, D., 2004. Modeling the climate response to a massive methane release from gas hydrates. Paleoceanography 19, doi:10.1029/2003PA000968.

Rinterknecht, V.R., Clark, P.U., Raisbeck, G.M., Yiou, F., Bitinas, A., Brook, E.J., Marks, L., Zelcs, V., Lunkka, J.P., Pavlovskaya, I.E., Piotrowski, J.A., Raukas, A., 2006. The last deglaciation of the southeastern sector of the Scandinavian Ice Sheet. Science 311, 1449-1452.

Robert, C., Kennett, J.P., 1994. Antarctic subtropical humid episode at the Paleocene-Eocene boundary - Clay-mineral evidence. Geology 22, 211-214.

Rohmer, M., Bouviernave, P., Ourisson, G., 1984. Distribution of hopanoid triterpenes in Prokaryotes. Journal of General Microbiology 130, 1137-1150.

Rosell-Melé, A., 1998. Interhemispheric appraisal of the value of alkenone indices as temperature and salinity proxies in high-latitude locations. Paleoceanography 13, 694-703.

Rosell-Melé, A., Bard, E., Emeis, K.C., Grieger, B., Hewitt, C., Müller, P.J., Schneider, R.R., 2004. Sea surface temperature anomalies in the oceans at the LGM estimated from the alkenone-$U^{K}_{37'}$ index: comparison with GCMs. Geophysical Research Letters 31, 1-4.

Russell, N.J., Fukunaga, N., 1990. A comparison of thermal adaptation of membrane-lipids in psychrophilic and thermophilic bacteria. FEMS Microbiology Reviews 75, 171-182.

Rütters, H., Sass, H., Cypionka, H., Rullkotter, J., 2001. Monoalkylether phospholipids in the sulfate-reducing bacteria *Desulfosarcina variabilis* and *Desulforhabdus amnigenus*. Archives of Microbiology 176, 435-442.

Sait, M., Hugenholtz, P., Janssen, P.H., 2002. Cultivation of globally distributed soil bacteria from phylogenetic lineages previously only detected in cultivation-independent surveys. Environmental Microbiology 4, 654-666.

Sanchez Goñi, M.F., Turon, J.L., Eynaud, F., Gendreau, S., 2000. European climatic response to millennial-scale changes in the atmosphere-ocean system during the last glacial period. Quaternary Research 54, 394-403.

Sauer, P.E., Eglinton, T.I., Hayes, J.M., Schimmelmann, A., Sessions, A.L., 2001. Compound-specific D/H ratios of lipid biomarkers from sediments as a proxy for environmental and climatic conditions. Geochimica et Cosmochimica Acta 65, 213-222.

Schaefer, J.M., Denton, G.H., Barrell, D.J.A., Ivy-Ochs, S., Kubik, P.W., Andersen, B.G., Phillips, F.M., Lowell, T.V., Schluchter, C., 2006. Near-synchronous interhemispheric termination of the last glacial maximum in mid-latitudes. Science 312, 1510-1513.

Schafer, H., Muyzer, G., 2001. Denaturing gradient gel electrophoresis in marine microbial ecology. Methods in Microbiology 30, 425-468.

Schefuß, E., Ratmeyer, V., Stuut, J.-B.W., Jansen, J.H.F., Sinninghe Damsté, J.S., 2003. Carbon isotope analyses of n-alkanes in dust from the lower atmosphere over the central eastern Atlantic. Geochimica et Cosmochimica Acta 67, 1757-1767.

Schefuß, E., Sinninghe Damsté, J.S., Jansen, J.H.F., 2004a. Forcing of tropical Atlantic sea surface temperatures during the mid-Pleistocene transition. Paleoceanography 19, doi:10.1029/2003PA000892.

Schefuß, E., Versteegh, G.J.M., Jansen, J.H.F., Sinninghe Damsté, J.S., 2004b. Lipid biomarkers as major source and preservation indicators in SE Atlantic surface sediments. Deep-Sea Research Part I-Oceanographic Research Papers 51, 1199-1228.

Schefuß, E., Schouten, S., Schneider, R.R., 2005. Climatic controls on central African hydrology during the past 20,000 years. Nature 437, 1003-1006.

Schleper, C., Holben, W., Klenk, H.P., 1997. Recovery of Crenarchaeotal ribosomal DNA sequences from freshwater-lake sediments. Applied and Environmental Microbiology 63, 321-323.

Schlesinger, W.H., Melack, J.M., 1981. Transport of organic carbon in the world's rivers. Tellus 33, 172-187.

Schlünz, B., Schneider, R.R., Muller, P.J., Showers, W.J., Wefer, G., 1999. Terrestrial organic carbon accumulation on the Amazon deep sea fan during the last glacial sea level low stand. Chemical Geology 159, 263-281.

Schlünz, B., Schneider, R.R., 2000. Transport of terrestrial organic carbon to the oceans by rivers: re-estimating flux- and burial rates. International Journal of Earth Sciences 88, 599-606.

Schmidt, G.A., Shindell, D.T., 2003. Atmospheric composition, radiative forcing, and climate change as a consequence of a massive methane release from gas hydrates. Paleoceanography 18, doi:10.1029/2002PA000757.

Schouten, S., Hopmans, E.C., Pancost, R.D., Sinninghe Damsté, J.S., 2000. Widespread occurrence of structurally diverse tetraether membrane lipids: Evidence for the ubiquitous presence of low-temperature relatives of hyperthermophiles. Proceedings of the National Academy of Sciences of the United States of America 97, 14421-14426.

Schouten, S., Hopmans, E.C., Schefuß, E., Sinninghe Damsté, J.S., 2002. Distributional variations in marine crenarchaeotal membrane lipids: a new tool for reconstructing ancient sea water temperatures? Earth and Planetary Science Letters 204, 265-274.

References

Schouten, S., Hopmans, E.C., Forster, A., van Breugel, Y., Kuypers, M.M.M., Sinninghe Damsté, J.S., 2003. Extremely high sea-surface temperatures at low latitudes during the middle Cretaceous as revealed by archaeal membrane lipids. Geology 31, 1069-1072.

Scourse, J.D., Hall, I.R., McCave, I.N., Young, J.R., Sugdon, C., 2000. The origin of Heinrich layers: evidence from H2 for European precursor events. Earth and Planetary Science Letters 182, 187-195.

Shellito, C.J., Sloan, L.C., Huber, M., 2003. Climate model sensitivity to atmospheric CO2 levels in the Early-Middle Paleogene. Palaeogeography, Palaeoclimatology, Palaeoecology 193, 113-123.

Shellito, C.J., Sloan, L.C., 2006. Reconstructing a lost Eocene paradise: Part I. Simulating the change in global floral distribution at the initial Eocene thermal maximum. Global and Planetary Change 50, 1-17.

Shin, S.I., Liu, Z., Otto-Bliesner, B., Brady, E.C., Kutzbach, J.E., Harrison, S.P., 2003. A simulation of the last glacial maximum climate using the NCAR-CCSM. Climate Dynamics 20, 127-151.

Showers, W.J., Angle, D.G., 1986. Stable isotopic characterization of organic-carbon accumulation on the Amazon continental-shelf. Continental Shelf Research 6, 227-244.

Simoneit, B.R.T., 1977. Organic matter in eolian dusts over the Atlantic Ocean. Marine Chemistry 5, 443-464.

Sinensky, M., 1974. Homeoviscous adaptation - a homeostatic process that regulates the viscosity of membrane lipids in *Escherichia coli*. Proceedings of the National Academy of Sciences of the United States of America 71, 522-525.

Sinninghe Damsté, J.S., de Leeuw, J.W., 1990. Analysis, structure and geochemical significance of organically-bound sulphur in the geosphere: State of the art and future research. Organic Geochemistry 16, 1077-1101.

Sinninghe Damsté, J.S., Wakeham, S.G., Kohnen, M.E.L., Hayes, J.M., de Leeuw, J.W., 1993. A 6,000-year sedimentary molecular record of chemocline excursions in the Black Sea. Nature 362, 827-829.

Sinninghe Damsté, J.S., Hopmans, E.C., Pancost, R.D., Schouten, S., Geenevasen, J.A.J., 2000. Newly discovered non-isoprenoid glycerol dialkyl glycerol tetraether lipids in sediments. Chemical Communications, 1683-1684.

Sinninghe Damsté, J.S., Rijpstra, W.I.C., Hopmans, E.C., Prahl, F., Wakeham, S.G., Schouten, S., 2002a. Distribution of membrane lipids of planktonic *Crenarchaeota* in the Arabian Sea. Applied and Environmental Microbiology 68, 2997-3002.

Sinninghe Damsté, J.S., Rijpstra, W.I.C., Reichart, G.J., 2002b. The influence of oxic degradation on the sedimentary biomarker record II. Evidence from Arabian Sea sediments. Geochimica et Cosmochimica Acta 66, 2737-2754.

Sinninghe Damsté, J.S., Schouten, S., Hopmans, E.C., van Duin, A.C.T., Geenevasen, J.A.J., 2002c. Crenarchaeol: the characteristic core glycerol dibiphytanyl glycerol tetraether membrane lipid of cosmopolitan pelagic crenarchaeota. Journal of Lipid Research 43, 1641-1651.

Sinninghe Damsté, J.S., Strous, M., Rijpstra, W.I.C., Hopmans, E.C., Geenevasen, J.A.J., van Duin, A.C.T., Van Niftrik, L.A., Jetten, M.S.M., 2002d. Linearly concatenated cyclobutane lipids from a dense bacterial membrane. Nature 419, 708-712.

Sinninghe Damsté, J.S., Rijpstra, W.I.C., Schouten, S., Fuerst, J.A., Jetten, M.S.M., Strous, M., 2004a. The occurrence of hopanoids in planctomycetes: implications for the sedimentary biomarker record. Organic Geochemistry 35, 561-566.

Sinninghe Damsté, J.S., Rijpstra, W.I.C., Strous, M., Jetten, M.S.M., David, O.R.P., Geenevasen, J.A.J., Van Maarseveen, J.H., 2004b. A mixed ladderane/n-alkyl glycerol diether membrane lipid in an anaerobic ammonium-oxidizing bacterium. Chemical Communications, 2590-2591.

Sizova, M.V., Panikov, N.S., Tourova, T.P., Flanagan, P.W., 2003. Isolation and characterization of oligotrophic acido-tolerant methanogenic consortia from a *Sphagnum* peat bog. FEMS Microbiology Ecology 45, 301-315.

Sloan, L.C., Pollard, D., 1998. Polar stratospheric clouds: A high latitude warming mechanism in an ancient greenhouse world. Geophysical Research Letters 25, 3517-3520.

Sloan, L.C., Huber, M., Crowley, T.J., Sewall, J.O., Baum, S., 2001. Effect of sea surface temperature configuration on model simulations of "equable" climate in the Early Eocene. Palaeogeography, Palaeoclimatology, Palaeoecology 167, 321-335.

Sluijs, A., Schouten, S., Pagani, M., Woltering, M., Brinkhuis, H., Sinninghe Damsté, J.S., Dickens, G.R., Huber, M., Reichart, G.J., Stein, R., Matthiessen, J., Lourens, L.J., Pedentchouk, N., Backman, J., Moran, K., 2006.

Subtropical Arctic Ocean temperatures during the Palaeocene/Eocene thermal maximum. Nature 441, 610-613.

Smith, T., Rose, K.D., Gingerich, P.D., 2006. Rapid Asia-Europe-North America geographic dispersal of earliest Eocene primate Teilhardina during the Paleocene-Eocene Thermal Maximum. Proceedings of the National Academy of Sciences of the United States of America 103, 11223-11227.

Smittenberg, R.H., Hopmans, E.C., Schouten, S., Sinninghe Damsté, J.S., 2002. Rapid isolation of biomarkers for compound specific radiocarbon dating using high-performance liquid chromatography and flow injection analysis-atmospheric pressure chemical ionisation mass spectrometry. Journal of Chromatography A 978, 129-140.

Sogin, M.L., Morrison, H.G., Huber, J.A., Welch, D.M., Huse, S.M., Neal, P.R., Arrieta, J.M., Herndl, G.J., 2006. Microbial diversity in the deep sea and the underexplored "rare biosphere". Proceedings of the National Academy of Sciences of the United States of America 103, 12115-12120.

Sonzogni, C., Bard, E., Rostek, F., Lafont, R., Rosell-Mele, A., Eglinton, G., 1997. Core-top calibration of the alkenone index vs sea surface temperature in the Indian Ocean. Deep-Sea Research II 44, 1445-1460.

Spiess,V. and Cruise Participants. METEOR Cruise No. 47, Leg 3, 1 June - 3 July 2000, Libreville - Walvis Bay. METEOR - Berichte 02-1, Leitstelle METEOR. 2002. Institut für Meereskunde der Universitaet Hamburg.

Stahl, D.A., Amann, R.I., 1991. Development and application of nucleic acid probes. In: Stackebrandt, E., Goodfellow, M. (Eds.), Nucleic acid techniques in bacterial systematics. John Wiley & Sons, Inc., New York, N.Y., pp. 205-248.

Steinmann, P., Shotyk, W., 1997. Geochemistry, mineralogy, and geochemical mass balance on major elements in two peat bog profiles (Jura Mountains: Switzerland). Chemical Geology 138, 25-53.

Stern, J., Freisleben, H.J., Janku, S., Ring, K., 1992. Black lipid-membranes of tetraether lipids from *Thermoplasma acidophilum*. Biochimica et Biophysica Acta 1128, 227-236.

Stocker, T.F., Wright, D.G., 1991. Rapid transitions of the ocean's deep circulation induced by changes in surface-water fluxes. Nature 351, 729-732.

Stuiver, M., Reimer, P.J., 1993. Extended C-14 data-base and revised Calib 3.0 C-14 age calibration program. Radiocarbon 35, 215-230.

Stuiver, M., Reimer, P.J., Braziunas, T.F., 1998. High-precision radiocarbon age calibration for terrestrial and marine samples. Radiocarbon 40, 1127-1151.

Stuiver, M., Grootes, P.M., 2000. GISP2 oxygen isotope ratios. Quaternary Research 53, 277-283.

Summons, R.E., Powell, T.G., 1986. Chlorobiaceae in Paleozoic seas revealed by biological markers, isotopes and geology. Nature 319, 763-765.

Suutari, M., Laakso, S., 1992. Changes in fatty-acid branching and unsaturation of *Streptomyces griseus* and *Brevibacterium fermentans* as a response to growth remperature. Applied and Environmental Microbiology 58, 2338-2340.

Svendsen, J.I., Alexanderson, H., Astakhov, V.I., Demidov, I., Dowdeswell, J.A., Funder, S., Gataullin, V., Henriksen, M., Hjort, C., Houmark-Nielsen, M., Hubberten, H.W., Ingolfsson, O., Jakobsson, M., Kjaer, K.H., Larsen, E., Lokrantz, H., Lunkka, J.P., Lysa, A., Mangerud, J., Matiouchkov, A., Murray, A., Moller, P., Niessen, F., Nikolskaya, O., Polyak, L., Saarnisto, M., Siegert, C., Siegert, M.J., Spielhagen, R.F., Stein, R., 2004. Late quaternary ice sheet history of northern Eurasia. Quaternary Science Reviews 23, 1229-1271.

Takai, K., Moser, D.P., DeFlaun, M., Onstott, T.C., Fredrickson, J.K., 2001. Archaeal diversity in waters from deep South African gold mines. Applied and Environmental Microbiology 67, 5750-5760.

Thomas, D.J., Bralower, T.J., Zachos, J.C., 1999. New evidence for subtropical warming during the late Paleocene thermal maximum: Stable isotopes from Deep Sea Drilling Project Site 527, Walvis Ridge. Paleoceanography 14, 561-570.

Tindal, B.J., 1992. The archaebacteria. In: Balows, A., Truper, H.G., Dworkin, M., Harder, K., Schleifer, K.H. (Eds.), The prokaryotes. Springer-Verlag, New York, pp. 677-808.

Tissot, B.P., Welte, D.H., 1984. Petroleum formation and occurrence. Springer Verlag, Berlin.

Tornabene, T.G., Langworthy, T.A., 1979. Diphytanyl and dibiphytanyl glycerol ether lipids of methanogenic archaebacteria. Science 203, 51-53.

References

Torsvik, V., Øvreås, L., Thingstad, T.F., 2002. Prokaryotic diversity - Magnitude, dynamics, and controlling factors. Science 296, 1064-1066.

Tripati, A., Elderfield, H., 2005. Deep-sea temperature and circulation changes at the Paleocene-Eocene thermal maximum. Science 308, 1894-1898.

Trumbore, S.E., 1993. Comparison of carbon dynamics in tropical and temperate soils using radiocarbon measurements. Global Biogeochemical Cycles 7, 275-290.

Tu, T.T.N., Kurschner, W.A., Schouten, S., van Bergen, P.F., 2004. Leaf carbon isotope composition of fossil and extant oaks grown under differing atmospheric CO_2 levels. Palaeogeography, Palaeoclimatology, Palaeoecology 212, 199-213.

Tyson, R.V., 1995. Sedimentary OM: Organic facies and palynofacies. Chapman and Hall, London.

Tzedakis, P.C., Lawson, I.T., Frogley, M.R., Hewitt, G.M., Preece, R.C., 2002. Buffered tree population changes in a quaternary refugium: Evolutionary implications. Science 297, 2044-2047.

Uda, I., Sugai, A., Itoh, Y.H., Itoh, T., 2001. Variation in molecular species of polar lipids from *Thermoplasma acidophilum* depends on growth temperature. Lipids 36, 103-105.

van de Vossenberg, J.L.C.M., UbbinkKok, T., Elferink, M.G.L., Driessen, A.J.M., Konings, W.N., 1995. Ion permeability of the cytoplasmic membrane limits the maximum growth temperature of bacteria and archaea. Molecular Microbiology 18, 925-932.

van de Vossenberg, J.L.C.M., Driessen, A.J.M., Konings, W.N., 1998. The essence of being extremophilic: the role of the unique archaeal membrane lipids. Extremophiles 2, 163-170.

van de Vossenberg, J.L.C.M., Driessen, A.J.M., Da Costa, M.S., Konings, W.N., 1999. Homeostasis of the membrane proton permeability in Bacillus subtilis grown at different temperatures. Biochimica et Biophysica Acta-Biomembranes 1419, 97-104.

van Dongen, B.E., Rijpstra, W.I.C., Philippart, C.J.M., de Leeuw, J.W., Sinninghe Damsté, J.S., 2000. Biomarkers in upper Holocene eastern North Sea and Wadden Sea sediments. Organic Geochemistry 31, 1533-1543.

Versteegh, G.J.M., Blokker, P., Wood, G.D., Collinson, M.E., Sinninghe Damsté, J.S., de Leeuw, J.W., 2004a. An example of oxidative polymerization of unsaturated fatty acids as a preservation pathway for dinoflagellate organic matter. Organic Geochemistry 35, 1129-1139.

Versteegh, G.J.M., Schefuß, E., Dupont, L., Marret, F., Sinninghe Damsté, J.S., Jansen, J.H.F., 2004b. Taraxerol and Rhizophora pollen as proxies for tracking past mangrove ecosystems. Geochimica et Cosmochimica Acta 68, 411-422.

Vetriani, C., Jannasch, H.W., MacGregor, B.J., Stahl, D.A., Reysenbach, A.-L., 1999. Population structure and phylogenetic characterization of marine benthic Archaea in deep-sea sediments. Applied and Environmental Microbiology 65, 4375-4384.

Volkman, J.K., Eglinton, G., Corner, E.D.S., Forsberg, T.E.V., 1980. Long-chain alkenes and alkenones in the marine coccolithophorid *Emiliania huxleyi*. Phytochemistry 19, 2619-2622.

Volkman, J.K., 1986. A review of sterol markers for marine and terrigenous organic-matter. Organic Geochemistry 9, 83-99.

Wakeham, S.G., Lewis, C.M., Hopmans, E.C., Schouten, S., Sinninghe Damsté, J.S., 2003. Archaea mediate anaerobic oxidation of methane in deep euxinic waters of the Black Sea. Geochimica et Cosmochimica Acta 67, 1359-1374.

Weijers, J.W.H., Schouten, S., van der Linden, M., van Geel, B., Sinninghe Damsté, J.S., 2004. Water table related variations in the abundance of intact archaeal membrane lipids in a Swedish peat bog. FEMS Microbiology Letters 239, 51-56.

Weijers, J.W.H., Schouten, S., Hopmans, E.C., Geenevasen, J.A.J., David, O.R.P., Coleman, J.M., Pancost, R.D., Sinninghe Damsté, J.S., 2006a. Membrane lipids of mesophilic anaerobic bacteria thriving in peats have typical archaeal traits. Environmental Microbiology 8, 648-657.

Weijers, J.W.H., Schouten, S., Spaargaren, O.C., Sinninghe Damsté, J.S., 2006b. Occurrence and distribution of tetraether membrane lipids in soils: Implications for the use of the TEX_{86} proxy and the BIT index. Organic Geochemistry 37, 1680-1693.

188

Weijers, J.W.H., Schouten, S., van den Donker, J.C., Hopmans, E.C., Sinninghe Damsté, J.S., 2007a. Environmental controls on bacterial tetraether membrane lipid distribution in soils. Geochimica et Cosmochimica Acta 71, 703-713.

Weijers, J.W.H., Schefuß, E., Schouten, S., Sinninghe Damsté, J.S., 2007b. Coupled thermal and hydrological evolution of tropical Africa over the last deglaciation. Science 315, ppp-ppp.

West, A.E., Schmidt, S.K., 2002. Endogenous methanogenesis stimulates oxidation of atmospheric CH4 in alpine tundra soil. Microbial Ecology 43, 408-415.

Williams, M., Shimabukuro, Y.E., Herbert, D.A., Lacruz, S.P., Renno, C., Rastetter, E.B., 2002. Heterogeneity of soils and vegetation in an eastern Amazonian rain forest: Implications for scaling up biomass and production. Ecosystems 5, 692-704.

Willmott, C.J., Robeson, S.M., 1995. Climatologically aided interpolation (CAI) of terrestrial air-temperature. International Journal of Climatology 15, 221-229.

Wing, S.L., Bao, H., Koch, P.L., 2000. An early Eocene cool period? Evidence for continental cooling during the warmest part of the Cenozoic. In: Huber, B.T., MacLeod, K.G., Wing, S.L. (Eds.), Warm climates in Earth history. Cambridge University Press, Cambridge UK, pp. 197-237.

Wing, S.L., Harrington, G.J., Smith, F.A., Bloch, J.I., Boyer, D.M., Freeman, K.H., 2005. Transient floral change and rapid global warming at the Paleocene-Eocene boundary. Science 310, 993-996.

Woese, C.R., Kandler, O., Wheels, M.L., 1990. Towards a natural system of organisms: proposal for the domains Archaea, Bacteria, and Eucarya. Proceedings of the National Academy of Sciences of the United States of America 87, 4576-4579.

Wuchter, C., Schouten, S., Coolen, M.J.L., Sinninghe Damsté, J.S., 2004. Temperature-dependent variation in the distribution of tetraether membrane lipids of marine Crenarchaeota: Implications for TEX_{86} paleothermometry. Paleoceanography 19, doi:10.1029/2004PA001041.

Wyputta, U., McAvaney, B.J., 2001. Influence of vegetation changes during the Last Glacial Maximum using the BMRC atmospheric general circulation model. Climate Dynamics 17, 923-932.

Xie, S., Nott, C.J., Avsejs, L.A., Maddy, D., Chambers, F.M., Evershed, R.P., 2004. Molecular and isotopic stratigraphy in an ombrotrophic mire for paleoclimate recontruction. Geochimica et Cosmochimica Acta 68, 2849-2862.

Yuk, H.G., Marshall, D.L., 2004. Adaptation of Escherichia coli O157 : H7 to pH alters membrane lipid composition, verotoxin secretion, and resistance to simulated gastric fluid acid. Applied and Environmental Microbiology 70, 3500-3505.

Zachos, J.C., Wara, M.W., Bohaty, S., Delaney, M.L., Petrizzo, M.R., Brill, A., Bralower, T.J., Premoli-Silva, I., 2003. A transient rise in tropical sea surface temperature during the Paleocene-Eocene Thermal Maximum. Science 302, 1551-1554.

Zachos, J.C., Schouten, S., Bohaty, S., Quattlebaum, T., Sluijs, A., Brinkhuis, H., Gibbs, S.J., Bralower, T.J., 2006. Extreme warming of mid-latitude coastal ocean during the Paleocene-Eocene Thermal Maximum: Inferences from TEX86 and isotope data. Geology 34, 737-740.

Zaragosi, S., Eynaud, F., Pujol, C., Auffret, G.A., Turon, J.L., Garlan, T., 2001. Initiation of the European deglaciation as recorded in the northwestern Bay of Biscay slope environments (Meriadzek Terrace and Trevelyan Escarpment): a multi-proxy approach. Earth and Planetary Science Letters 188, 493-507.

Zaragosi, S., Bourillet, J.F., Eynaud, F., Toucanne, S., Denhard, B., Van Toer, A., Lanfumey, V., 2006. The impact of the last European deglaciation on the deep-sea turbidite systems of the Celtic-Armorican margin (Bay of Biscay). Geo-Marine Letters 26, 317-329.

Zhang, C.L., Pancost, R.D., Sassen, R., Qian, Y., Macko, S.A., 2003. Archaeal lipid biomarkers and isotopic evidence of anaerobic methane oxidation associated with gas hydrates in the Gulf of Mexico. Organic Geochemistry 34, 827-836.

190

Summary

This thesis describes the structure and the occurrence of branched tetraether membrane lipids, their potential biological origin, and shows their application in reconstructions of past continental climate and soil organic matter fluxes to the ocean. The membrane spanning alkyl chains of branched glycerol dialkyl glycerol tetraether (GDGT) membrane lipids are not composed of isoprene units, that are typical for GDGTs synthesised by Archaea, but of straight carbon chains. These possess a different degree of methyl branching and sometimes one or two cyclopentanyl moieties. Based on the branched nature of the alkyl chains, but foremost on the stereo configuration of the glycerol backbone, it was concluded that these lipids are synthesised by Bacteria. Branched GDGTs were detected in high amounts in several peat bogs, especially in the anoxic deeper layer, and in variable amounts in soils world wide. It was, therefore, suggested that the bacteria synthesising branched GDGTs are anaerobic soil bacteria. The exact origin is as yet unclear, but based on molecular ecological analysis using rDNA of peat bog samples, it was concluded that the large phylum of Acidobacteria might encompass the GDGT-producing bacteria, especially as Acidobacteria occur widespread in soils as well.

Besides in soils and peat bogs, branched GDGTs were also detected in lake sediments and near coastal marine sediments. Analysis of marine surface sediments from the Angola Basin off West Africa showed a decrease in the amount of branched GDGTs relative to an isoprenoid GDGT (crenarchaeol), produced by ubiquitous marine Crenarchaeota, with increasing distance from the Congo river-mouth. This indicated a dominant fluvial transport of branched GDGTs from land to the marine environment. Moreover, it implied that this relative abundance, expressed in the Branched vs. Isoprenoid Tetraether (BIT) index, is a proxy to trace the relative fluvial input of soil organic matter in marine sediments. However, small amounts of crenarchaeol were also detected in soils and peat bogs, likely derived from freshwater or soil Crenarchaeota, but these amounts were small relative to the amount of branched GDGTs in soils and peat bogs and do not considerably affect the BIT index measured in marine sediments. Other isoprenoid GDGTs, derived from methane-producing Euryarchaeota and from Crenarchaeota, were detected in soils and peat bogs in more substantial amounts than crenarchaeol. It was shown that a high input of soil organic matter, therefore, could bias sea surface temperatures reconstructed with the TEX_{86} proxy near large river outflows since the TEX_{86} proxy is based on the relative abundance of isoprenoid GDGTs derived from marine Crenarchaeota. To assess a potential bias, it is, therefore, recommended to always analyse the BIT index in conjunction with the TEX_{86} in these settings.

Application of the BIT index, in conjunction with other proxies, in a marine sediment core in front of the Congo River outflow showed that terrestrial organic matter accounts for ~45% of the total organic matter in these marine sediments over the period of the last deglaciation. The results also indicated, however, that the accumulation of absolute amounts of terrestrial

Summary

organic matter was likely not constant over glacial-interglacial times, but has varied considerably in relation to alternating drier and wetter conditions on land. The BIT index was also applied in a sediment core from the Bay of Biscay. During the last glacial period, when the North Sea and Channel were emerged as a result of the sea-level low-stand, this core location was situated in front of the Channel River, a large river draining all major river drainage basins and ice sheets of north-western Europe. The BIT index revealed an abrupt and early reactivation of this river at the onset of the deglaciation. The substantial increase of freshwater discharge to the Bay of Biscay, together with melt water from floating icebergs associated with Heinrich event 1, created a kind of 'lid' of fresh cold water on the Bay of Biscay which hindered evaporation of seawater and thus cloud formation. As a consequence, climate on land shifted back to drier conditions resulting in lower Channel River discharge, which, subsequently, was recorded again as an abrupt fall in the BIT index in this core.

Although branched GDGTs occur ubiquitously, the relative abundance of the different branched GDGTs, i.e. degree of methylation and cyclisation, varied from place to place. In order to study the environmental factors controlling this distribution, 134 soil samples from 90 globally distributed locations were analysed for their branched GDGT content. Principal component analysis showed that the degree of cyclisation, expressed in the Cyclisation ratio of Branched Tetraethers (CBT) is related to soil pH ($R^2 = 0.70$) and not to temperature. The degree of methylation, expressed in the Methylation index of Branched Tetraethers (MBT), showed a positive correlation with the annual mean air temperature (MAT) ($R^2 = 0.62$) and a weaker negative correlation with soil pH ($R^2 = 0.37$). If both parameters are combined, however, it appeared that a strong correlation exists between the MBT index and both annual MAT and soil pH ($R^2 = 0.82$). These results indicated that the relative distribution of soil-derived branched GDGTs is primarily determined by temperature and pH. This feature can be explained by the fact that many micro-organisms adapt the molecular composition of their cell membrane to ambient conditions (like temperature and pH) in order to keep the membrane functioning well.

The correlation between relative branched GDGT distribution and soil pH can be used to determine (past) soil pH from the GDGT distribution. Using this relation, soil pH could be exchanged with the CBT ratio in the correlation of MBT with annual MAT and soil pH (resulting $R^2 = 0.77$). This enables the determination of (past) temperatures from the branched GDGT distribution as well. Analysis of this MBT index and CBT ratio in a marine sediment core in front of the Congo River outflow yielded records of annual MAT and soil pH changes spanning the last deglaciation, integrated over the whole Congo River drainage basin. These records showed that soil pH values in the Congo Basin decreased upon increases in central African precipitation and that annual MAT in central tropical Africa gradually increased by ~4°C since the last glacial. As an advantage of reconstructing continental temperatures in a marine core, it was possible to directly compare these temperature changes with changes of sea surface temperature over the same period at the same location. This comparison revealed

that the temperature differences between land and sea in equatorial Africa exerted a strong control, through the thermal pressure gradient, on African precipitation patterns during the past 25,000 years.

The relative distribution of branched GDGTs was also determined in a sediment core obtained from the Arctic Ocean, which covers the Palaeocene-Eocene thermal maximum (PETM). The PETM was a relatively short interval in Earth history, ~55 million years ago, characterised by both extremely high atmospheric greenhouse gas concentrations and temperatures. The reconstructed annual MAT for the Arctic continents indicated a warming during the PETM interval of ~8°C above background values, reaching subtropical temperatures of 25°C. This continental temperature increase was concurrent with a similar rise in sea surface temperature for the Arctic Ocean during the PETM, documented earlier. In addition, these results pointed to a strongly reduced latitudinal temperature gradient during the PETM.

In conclusion, this thesis shows that branched GDGT membrane lipids comprise an interesting new group of biomarkers with a high potential to serve as proxy for terrestrial organic matter input, soil pH and continental temperature in palaeo-climate studies.

Samenvatting

Dit proefschrift beschrijft de structuur en het voorkomen van vertakte tetraether membraanlipiden, hun potentiële biologische oorsprong en hun toepassing in de reconstructie van het verleden continentale klimaat en van de aanvoer van terrestrisch organisch materiaal naar de oceaan. De membraan-overspannende alkylketens van de vertakte glycerol dialkyl glycerol tetraether (GDGT) membraanlipiden zijn niet opgebouwd uit isoprene eenheden, welke typisch zijn voor GDGT's gesynthetiseerd door Archaea, maar uit rechte koolstofketens. Deze koolstofketens bezitten een verschillende gradatie van methylering en soms één of twee cyclopentaan-eenheden. Op basis van de vertakte structuur, maar met name op basis van de stereoconfiguratie van de glyceroleenheid, is geconcludeerd dat deze lipiden gesynthetiseerd worden door bacteriën. Vertakte GDGT's zijn in relatief grote hoeveelheden gedetecteerd in verschillende veenkussens, met name in de anoxische diepere laag, en in variabele hoeveelheden in bodems over de hele wereld. Het wordt daarom aangenomen dat de bacteriën welke de vertakte GDGT's synthetiseren anaërobe bodembacteriën zijn. De exacte oorsprong is vooralsnog niet bekend, maar gebaseerd op moleculair ecologische analyse van het in veen aanwezige rDNA is gesuggereerd dat het grote phylum van de Acidobacteriën de vertakte GDGT-producerende bacteriën zou kunnen bevatten, bovenal omdat Acidobacteriën ook wereldwijd voorkomen in bodems.

Behalve in bodems en veenkussens zijn vertakte GDGT's ook gedetecteerd in meersedimenten en kustnabije mariene sedimenten. Analyse van oppervlaktesedimenten uit het Angolabekken, voor de kust van West Afrika, liet een afname in de hoeveelheid vertakte GDGT's zien ten opzichte van een isoprenoïde GDGT (crenarchaeol), geproduceerd door de alomtegenwoordige mariene Crenarchaeota, met toenemende afstand van de monding van de Congo Rivier. Dit duidt op een voornamelijk fluviatiele aanvoer van vertakte GDGT's naar zee. Bovendien impliceert deze observatie dat de relatieve hoeveelheid vertakte GDGT's, uitgedrukt in de 'Branched versus Isoprenoid Tetraether (BIT) index', gebruikt kan worden als palaeo-indicator voor de relatieve fluviatiele aanvoer van terrestrisch organisch bodemmateriaal naar het mariene milieu. Echter, crenarchaeol werd ook aangetroffen in bodems en veenkussens, waarschijnlijk afkomstig van zoetwater- en/of bodem-Crenarchaeota, maar deze hoeveelheden waren over het algemeen erg klein ten opzichte van de hoeveelheid vertakte GDGT's in bodems en veenkussens en hebben daardoor geen noemenswaardige invloed op de BIT-index gemeten in mariene sedimenten. Isoprenoïde GDGT's daarentegen, afkomstig van methaangas-producerende Euryarchaeota en van Crenarchaeota, werden in meer substantiële hoeveelheden dan crenarchaeol gedetecteerd in bodems en veenkussens. Het is aangetoond dat een grote aanvoer van terrestrisch organisch materiaal daarom een afwijking kan veroorzaken in zeewatertemperaturen welke gereconstrueerd zijn met de TEX_{86}-proxy, omdat deze indicator voor zeewatertemperatuur gebaseerd is op de verhouding van isoprenoïde GDGT's afkomstig van mariene Crenarchaeota. Dit effect is voornamelijk

merkbaar in de buurt van grote riviermondingen. Om de kans op een mogelijke afwijking te bepalen, wordt aanbevolen om naast de TEX_{86} ook altijd de BIT index te analyseren op deze locaties.

Toepassing van de BIT index in een mariene sedimentkern voor de monding van de Congo Rivier heeft, in combinatie met andere proxies, laten zien dat sinds de laatste ijstijd ongeveer 45% van het totaal aanwezige organisch materiaal in deze mariene sedimenten bestaat uit terrestrisch organisch materiaal. Diezelfde resultaten laten echter ook zien dat de accumulatie van absolute hoeveelheden terrestrisch organisch materiaal zeer waarschijnlijk niet constant was maar juist sterk varieerde in relatie tot de afwisselend drogere en nattere perioden in centraal Afrika.

De BIT index is vervolgens ook geanalyseerd in een mariene sedimentkern uit de Golf van Biskaje. Gedurende de laatste ijstijd, toen de Noordzee en het Kanaal als gevolg van een lage zeespiegel droog stonden, was deze locatie gesitueerd vlak voor de monding van de Kanaal Rivier. Dit was één van Europa's grootste rivieren ooit die vrijwel alle noordwest Europese stroomgebieden, alsmede het smeltwater van de ijskappen draineerde. De BIT index in deze kern laat een vroege en abrupte reactivatie van deze rivier zien bij aanvang van de laatste deglaciatie. De substantiële toename van de rivierwaterafvoer naar de Golf van Biskaje, samen met smeltwater van drijvende ijsbergen die samenhangen met 'Heinrich event I', resulteerden in een soort deksel van koud, zoet water op de golf van Biskaje. Deze afsluiting verhinderde de verdamping van zeewater en daarmee de vorming van wolken wat leidde tot een terugkeer naar drogere condities op het land. De hiermee samenhangende afname van de waterafvoer door de Kanaal Rivier was duidelijk zichtbaar als een abrupte daling van de BIT index in deze kern.

Alhoewel was gebleken dat vertakte GDGT's wijd verspreid voorkomen, bleek de verhouding tussen de verschillende individuele vertakte GDGT's, d.w.z. de mate van methylering en de mate van cyclisering, verschillend te zijn op verschillende plaatsen. Om te onderzoeken welke natuurlijke parameters dit verschil bepalen, zijn 134 bodemmonsters van 90 verschillende locaties onderzocht op vertakte GDGT's. 'Principal Component Analysis' liet vervolgens zien dat de mate van cyclisatie, uitgedrukt in de 'Cyclisation ratio of Branched Tetraethers' (CBT), gerelateerd is aan de pH van de bodem ($R^2 = 0.70$) en niet aan temperatuur. De mate van methylering, uitgedrukt in de 'Methylation index of Branched Tetraehters' (MBT), liet een positieve correlatie zien met de jaargemiddelde luchttemperatuur ($R^2 = 0.62$) en een zwakkere negatieve correlatie met de pH waarden van de bodems ($R^2 = 0.37$). Wanneer beide parameters worden gecombineerd, blijkt dat er een sterke correlatie bestaat tussen de MBT-index en zowel de luchttemperatuur als de pH van de bodem ($R^2 = 0.82$). Deze resultaten impliceren dat de verhouding van vertakte GDGT's in bodems voornamelijk wordt bepaald door temperatuur en pH. Dit gegeven kan worden verklaard met het feit dat veel micro-organismen de moleculaire samenstelling van hun celmembraan

aanpassen aan de omringende milieucondities (zoals temperatuur en pH) om zodoende het membraan goed te kunnen laten functioneren.

De correlatie tussen de verhouding van vertakte GDGT's en de pH waarde van de bodem kan gebruikt worden om de (verleden) bodem-pH te bepalen uit de GDGT verhouding. Daarnaast kan met behulp van deze correlatie de bodem pH worden vervangen door de CBT-ratio in de correlatie tussen de MBT-index en de temperatuur en pH (resulterende R^2 = 0.77). Dit maakt het mogelijk ook (verleden) luchttemperaturen te bepalen aan de hand van de vertakte GDGT verhouding. De MBT-index en CBT-ratio zijn vervolgens geanalyseerd in een mariene sedimentkern voor de riviermonding van de Congo Rivier. Dit leverde reconstructies op van veranderingen in de jaargemiddelde temperatuur en de pH van de bodem gedurende de laatste deglaciatie, geïntegreerd over het gehele Congo rivierbekken. Deze reconstructies laten zien dat pH waarden van de bodems in het Congo bekken daalden als reactie op een toename in neerslag in centraal Afrika en dat de jaargemiddelde temperatuur in centraal tropisch Afrika geleidelijk is toegenomen met ongeveer 4°C sinds de laatste ijstijd. Een voordeel van het analyseren van continentale temperatuurveranderingen in een mariene kern is dat deze direct vergeleken kunnen worden met veranderingen in zeewatertemperatuur gereconstrueerd uit dezelfde kern. Deze vergelijking laat zien dat de temperatuurverschillen tussen land en zee in equatoriaal Afrika een sterke invloed hebben gehad, via de thermale drukgradiënt, op neerslagpatronen in centraal Afrika gedurende de afgelopen 25.000 jaar.

De verhouding van vertakte GDGT's is ook gemeten in een kern uit de Arctische Oceaan, welke de tijdsperiode van het Palaeoceen-Eoceen thermale maximum (PETM) beslaat. Het PETM was een relatief kort interval in de geologische geschiedenis, circa 55 miljoen jaar geleden, gekarakteriseerd door zeer hoge concentraties broeikasgassen in de atmosfeer en door hoge temperaturen. De gereconstrueerde jaargemiddelde temperatuur voor de Arctische continenten toont een opwarming aan van 8°C boven achtergrondwaarden, waardoor in deze periode subtropische temperaturen van rond de 25°C bereikt werden. Deze continentale temperatuurstijging heeft gelijktijdig plaatsgevonden met een stijging van de zeewatertemperatuur. Naast deze temperatuurstijging wijzen deze resultaten op een sterk afgenomen meridionale temperatuurgradiënt gedurende het PETM.

Samengenomen laat dit proefschrift zien dat de vertakte GDGT membraanlipiden een nieuwe, interessante groep biomarkers vormen met een hoge potentie om als palaeo-indicator voor continentale temperatuur, bodem pH en aanvoer van terrestrisch organisch materiaal te dienen in palaeo-klimaat studies.

Dankwoord

Jawel, ook in dit proefschrift het stukje tekst dat altijd als laatste geschreven maar als eerste gelezen wordt. Zonder de hulp, inzet en een lach van velen was ik nooit bij het punt aangeland dat je überhaupt een dankwoord mag schrijven. Deze velen zijn er echt een heleboel en dus helaas teveel om allemaal de revue te laten passeren; misschien waag ik aan het eind nog een poging. Enkele personen vielen echter zodanig op dat ze wel genoemd moeten worden:

Uiteraard als eerste mijn promotor Jaap – "JA!" – Sinninghe Damsté, een briljant wetenschapper die ook zeker het gevoel voor humor niet mist en altijd in is voor een potje tafelvoetbal, bier, golf of een uitgesproken rol in een sketch. Een congres had altijd net een beetje meer als jij ook acte de présence gaf. Vooral de reis naar de Gordon Conference in Amerika, toen we vanwege verloren bagage met (of was het voor...) Marco onderbroeken op de markt moesten uitzoeken, was hilarisch. Deze combi van goed en efficiënt werk en de fun maken MBT absoluut tot een goed geoliede machine.

Ook als eerste te noemen..... co-promotor Stefan – "dusssssssssss...." – Schouten. Ik weet niet wat er precies in de NIOZ-chocomel zit, maar soms ziet hij dingen in de data die er eigenlijk niet zijn.....dacht ik..., maar die dan toch in een publicatie terecht komen. De cynische opmerkingen 's ochtends bij de koffie, absoluut opgestookt door Michiel, waren ook zeker niet van de lucht. Samen met de andere mensen van de vroege-vogel koffieclub leverde dit altijd een prettig begin van de dag op! Ik zal jullie een timer cadeau doen om te zorgen dat ook de komende tijd 's ochtends de koffie klaar staat...

Een ander persoon zeker te noemen is 'mijn projectleidster' Ellen (Catharina; ja, je wilde graag met toenaam genoemd worden...) Hopmans die zich goed 'van haar taak heeft gekweten'. Ook met de nodige hoeveelheid cynisme (hoe kan het anders...) kwam jij altijd even informeren hoe het ermee stond en je was altijd in voor enig niet-wetenschappelijk gesprek. Jij bent absoluut een excellent technician c.q. manager van de MBT-LC-'renstal', de apparatuur die de meeste data voor dit proefschrift heeft uitgespuugd (zo rond de 2000 runs moeten het geweest zijn). Maar bijna was ik niet aan dat aantal gekomen toen een analyse-verbod voor een jaar dreigde vanwege het feit dat ik je toch één keer op de kast had weten te jagen; je weet wel... van de quantum/kwantum en de gordijnen...

Dan natuurlijk mijn huisgenoten/collega's in Den Hoorn; Jayne en Arjan. Arjan is gewoon Arjan; nuchter, een echte Hollander, altijd in voor een spelletje, feestje, praatje of gewoon een biertje! En dan Jayne, onze Nederlandse Schotse; met jou heb ik ook wat gelachen de afgelopen jaren en over jou kan ik heel wat vertellen..... dus 'maak je borst maar nat'... Maar dat doe ik niet; gewoon in je eigen woorden: You're just a Star!!

Not to forget Lydie, my French office mate for the first three years; many good conversations we had, both about science and non-science, over the always growing piles of papers on your desk. I've seen many tears, but fortunately they were always from laughing! Then I was very lucky to share the office with Angela for the last year, which has actually been too short or went too fast. Maybe it's the secret of the Canadian maple syrup, but I have never seen so much enthusiasm gathered into one single person. That even Stefan came looking around the corner to see what's going on, does say enough. Angela, you were the sunshine in the office and I'm certainly going to miss your enthusiasm.

Ook dank aan alle analytische en technische ondersteuning op het lab (en natuurlijk de fun); Jort, Sebastiaan, Martijn, Marianne, Irene, Michiel en Marielle. Die hulp kon deze jongen zeker gebruiken, al kan ik me voorstellen dat enkele van deze mensen er ook wel moedeloos van werden; zeker Jort wanneer ik kwam vragen om de gouden tip voor het open krijgen van de jerry-can met DCM waarvan ik na 10 min de dop helemaal kapot gedraaid had met de dekselopener; Jort's tip: gewoon de andere kant op draaien....

Ook iemand die even apart genoemd dient te worden is Jurgen. Als master-student uit Utrecht was jouw hulp zeer welkom om de set bodemmonsters door te werken en ik mocht mij gelukkig prijzen met jouw inzet. Daarnaast was jij ook een zeer enthousiaste en ondernemende student die uiteindelijk bekend was op het gehele NIOZ alsook in de horeca-wereld van De Koog. Niet in de laatste plaats ook vanwege je kookkunsten, welke indruk gemaakt hebben bij de kerstlunch 2005.

Tot slot dan natuurlijk alle andere, nog niet genoemde collega's bij MBT die het werken op het Instituut absoluut niet tot een straf maakten. Hartelijk dank daarvoor! Op het gevaar af iemand te vergeten...dan toch een poging.... Yvonne, Cornelia, Antje, Thorsten, Rienk, Bart, Alina, Joost, Astrid, Marco, Marcel (vooral ook voor de nodige microbiologische info!), Henry, Margot, Rianne, Andrea, Carme, Kim, Jan, Ben, Elda, Francien (voor jou nu het stokje...), Adam, Angelique, Ronald en Kees. En natuurlijk ook dank aan de mensen van andere afdelingen met wie ik goed contact had en de collega's bij de ondersteunende afdelingen die altijd beschikbaar waren voor vragen van administratieve of (computer)technische aard. De medewerking en flexibiliteit van Bert Aggenbach bij het print- en inbindwerk van posters, foto's en documenten mag hier zeker ook genoemd worden.

Van buiten het NIOZ is uiteraard niet te vergeten 'Der Enno' die net zijn promotie had afgerond bij MBT toen ik begon. In zekere zin had ik wel het idee dat ik het stokje van jou – 'King of the Congo' – overnam, vooral vanwege het werk aan de kern uit de Congo delta. De vaak humoristische en soms in 'straattaal Nederlands' geschreven e-mails en aanmerkingen bij manuscripten vanuit Woods Hole en Bremen werkten zeker motiverend.

Van voor mijn NIOZ-tijdperk moeten ook genoemd worden Kees Kasse en Wim Hoek, twee docenten die mij op de VU absoluut hebben gemotiveerd voor de wetenschap. Veldwerken met jullie waren altijd een feest, zowel op wetenschappelijk als sociaal vlak. Van jullie heb ik geleerd dat je met een gezond portie enhousiasme (daar is het woord weer) al een heel eind kunt komen. En aan jullie sketch van de operatie van een veenkern voor een door ons georganiseerde ouderdag wordt ik nog regelmatig herinnerd!

Dan echt als laatste, maar zeker niet minste, enkele goede vrienden voor de 'weekendjes Texel', 'Pension Ruijpers' te Nuth voor de altijd gastvrije ontvangst, mijn paranimfen Aniska en Reinoud, mijn zus Mariska en mijn ouders voor alle geboden steun en (keuze)vrijheid. En dan natuurlijk Linda, die mij de nodige uurtjes, dagen en weken heeft moeten missen, voor haar niet aflatende steun, geduld en liefde. Ik hoop dat ik, ondanks mijn aanstelling in Bristol, de komende tijd iets terug kan geven!

Curriculum Vitae

Johannes Wilhelmus Hendrikus (Johan) Weijers werd geboren op 27 oktober 1978 te Heemstede en is opgegroeid te Hillegom. In 1997 behaalde hij zijn VWO-atheneum diploma aan het r.k. College Hageveld te Heemstede. Vervolgens is hij Aardwetenschappen gaan studeren aan de Vrije Universiteit Amsterdam. In de loop van deze studie heeft hij zich gespecialiseerd op de gebieden van de geomorfologie en sedimentologie van riviersystemen en van de palaeo-klimatologie. Na in 2002 afgestudeerd te zijn in de specialisatie Toegepaste Fysische Geografie heeft hij een promotiestudie uitgevoerd aan het Koninklijk Nederlands Instituut voor Onderzoek der Zee bij de afdeling Mariene Biogeochemie en Toxicologie onder begeleiding van prof. dr. ir. Jaap S. Sinninghe Damsté en dr. ir. Stefan Schouten, wat heeft geresulteerd in dit proefschrift. Per april 2007 is hij met een Rubicon stipendium van de Nederlandse Organisatie voor Wetenschappelijk Onderzoek (NWO) werkzaam als post-doctorale onderzoeker binnen de 'Organic Geochemistry Unit' aan de 'University of Bristol' in Engeland.

Scientific assessment committee

Prof. Dr. J.W. de Leeuw
Department of Marine Biogeochemistry and Toxicology,
Royal Netherlands Institute for Sea Research, the Netherlands
and
Department of Earth Sciences – Geochemistry, Faculty of Geosciences,
University of Utrecht, the Netherlands

Prof. Dr. E. Bard
Department of Organic Geochemistry and Stable Isotopes, CEREGE,
Aix-en-Provence, France

Prof Dr. T. Wagner
School of Civil Engineering and Geosciences,
University of Newcastle upon Tyne, United Kingdom

Prof. Dr. H. Hooghiemstra
Research Group Palaeo-Ecology and Landscape Ecology, Institute of Biodiversity and Ecosystem
Dynamics, University of Amsterdam, the Netherlands